ADVANCES IN THE STRUCTURAL ELUCIDATION AND UTILIZATION OF LIGNINS

EDITED BY: Li Shuai, Chang Geun Yoo, Fengxia Yue and Arthur Jonas Ragauskas

PUBLISHED IN: Frontiers in Energy Research

frontiers Research Topics

frontiers

ISSN 1664-8714
ISBN 978-2-88971-326-4
DOI 10.3389/978-2-88971-326-4

About Frontiers

Frontiers is more than just an open-access publisher of scholarly articles: it is a pioneering approach to the world of academia, radically improving the way scholarly research is managed. The grand vision of Frontiers is a world where all people have an equal opportunity to seek, share and generate knowledge. Frontiers provides immediate and permanent online open access to all its publications, but this alone is not enough to realize our grand goals.

Frontiers Journal Series

The Frontiers Journal Series is a multi-tier and interdisciplinary set of open-access, online journals, promising a paradigm shift from the current review, selection and dissemination processes in academic publishing. All Frontiers journals are driven by researchers for researchers; therefore, they constitute a service to the scholarly community. At the same time, the Frontiers Journal Series operates on a revolutionary invention, the tiered publishing system, initially addressing specific communities of scholars, and gradually climbing up to broader public understanding, thus serving the interests of the lay society, too.

Dedication to Quality

Each Frontiers article is a landmark of the highest quality, thanks to genuinely collaborative interactions between authors and review editors, who include some of the world's best academicians. Research must be certified by peers before entering a stream of knowledge that may eventually reach the public - and shape society; therefore, Frontiers only applies the most rigorous and unbiased reviews.
Frontiers revolutionizes research publishing by freely delivering the most outstanding research, evaluated with no bias from both the academic and social point of view. By applying the most advanced information technologies, Frontiers is catapulting scholarly publishing into a new generation.

What are Frontiers Research Topics?

Frontiers Research Topics are very popular trademarks of the Frontiers Journals Series: they are collections of at least ten articles, all centered on a particular subject. With their unique mix of varied contributions from Original Research to Review Articles, Frontiers Research Topics unify the most influential researchers, the latest key findings and historical advances in a hot research area! Find out more on how to host your own Frontiers Research Topic or contribute to one as an author by contacting the Frontiers Editorial Office: frontiersin.org/about/contact

ADVANCES IN THE STRUCTURAL ELUCIDATION AND UTILIZATION OF LIGNINS

Topic Editors:
Li Shuai, Fujian Agriculture and Forestry University, China
Chang Geun Yoo, Suny College of Environmental Science and Forestry, United States
Fengxia Yue, South China University of Technology, China
Arthur Jonas Ragauskas, The University of Tennessee, Knoxville, United States

Citation: Shuai, L., Yoo, C. G., Yue, F., Ragauskas, A. J., eds. (2021). Advances in the Structural Elucidation and Utilization of Lignins. Lausanne: Frontiers Media SA. doi: 10.3389/978-2-88971-326-4

Table of Contents

04 ***Editorial: Advances in the Structural Elucidation and Utilization of Lignins***
Fengxia Yue and Li Shuai

06 ***Unraveling the Structural Transformation of Wood Lignin During Deep Eutectic Solvent Treatment***
Shuizhong Wang, Helong Li, Ling-Ping Xiao and Guoyong Song

16 ***Accelerated Aging Process of Bio-Oil Model Compounds: A Mechanism Study***
Rui Wang and Haoxi Ben

28 ***Structural Features of Lignin Fractionated From Industrial Furfural Residue Using Alkaline Cooking Technology and Its Antioxidant Performance***
Rui Li, Xiaohui Wang, Qixuan Lin, Fengxia Yue, Chuanfu Liu, Xiaoying Wang and Junli Ren

42 ***An Investigation Into the Upgrading Process of Lignin Model Dimer—Phenethyl Phenyl Ether by* in situ *2H NMR and GC-MS***
Yunyi Yang, Zhihong Wu, Ying Luo, Guangting Han, Wei Jiang, Maorong Wang and Haoxi Ben

52 ***Effects of CELF Pretreatment Severity on Lignin Structure and the Lignin-Based Polyurethane Properties***
Yun-Yan Wang, Priya Sengupta, Brent Scheidemantle, Yunqiao Pu, Charles E. Wyman, Charles M. Cai and Arthur J. Ragauskas

64 ***Preparation of Graphene-Like Porous Carbons With Enhanced Thermal Conductivities From Lignin Nano-particles by Combining Hydrothermal Carbonization and Pyrolysis***
Huiling Dong, Min Li, Yongcan Jin, Yan Wu, Caoxing Huang and Jinlai Yang

74 ***Understanding the Structural Changes of Lignin Macromolecules From Balsa Wood at Different Growth Stages***
Chen Zhang, Ling-Hua Xu, Cheng-Ye Ma, Han-Min Wang, Yuan-Yuan Zhao, Yu-Ying Wu and Jia-Long Wen

83 ***Insights Into Structural Transformations of Lignin Toward High Reactivity During Choline Chloride/Formic Acid Deep Eutectic Solvents Pretreatment***
Si Hong, Xiao-Jun Shen, Zhuohua Sun and Tong-Qi Yuan

90 ***Efficient Synthesis of Pinoresinol, an Important Lignin Dimeric Model Compound***
Fengxia Yue, Wu Lan, Liming Zhang, Fachuang Lu, Runcang Sun and John Ralph

frontiers in Energy Research

EDITORIAL
published: 16 July 2021
doi: 10.3389/fenrg.2021.724825

Editorial: Advances in the Structural Elucidation and Utilization of Lignins

Fengxia Yue[1]* *and Li Shuai*[2]

[1]State Key Laboratory of Pulp and Paper Engineering, School of Light Industry and Engineering, South China University of Technology, Guangzhou, China, [2]College of Material Engineering, Fujian Agriculture and Forestry University, Fuzhou, China

Keywords: lignin, structural characterization, valorization, aromatic resource, fractionation

Editorial on the Research Topic

Advances in the Structural Elucidation and Utilization of Lignins

As one of the most abundant plant-derived aromatic resources on the planet, lignin has drawn increasing attention in the past few decades. Although remarkable progress has been made in lignin structural elucidation and utilization in recent years, lignin valorization remains the most changing topic due to the complexity and inherent heterogeneity of lignin. As an irregular and non-repeated polymer, lignin has long been recognized as the major recalcitrant that hinders the utilization of cellulose.

Normally, native lignin is a highly complex natural polymer formed primarily from three typical monolignol precursors, including *p*-coumaryl alcohol, coniferyl alcohol, and sinapyl alcohol, that differ in the methoxyl degree of the aromatic ring via a combinatorial radical coupling process. The monoligniols are then displayed as *p*-hydroxyphenyl (H), guaiacyl (G), and syringyl (S) units, so called lignin structural units, that linked by several types of C–O and C–C linkages, including β–O–4, β–5, β–β, 5–5, β–1, and 4–O–5 linkages formed during lignin biosynthesis (**Figure 1**). Among these linkages, β–O–4 alkyl aryl ethers, accounting for 50–80% of the total linkages in native lignins, are the most predominant interunit linkages in lignin polymer. However, selective fractionation of biomass into different constituents (i.e., carbohydrates and lignin) will cause significant structural changes due to degradation and condensation reactions. The resultant condensed lignin increases the difficulty for its valorization. Therefore, efficient fractionation and characterization are two essential prerequisites of valorizing lignin. Understanding reaction mechanisms involved during lignin isolation and revealing the structure of lignin are crucial for development of new methods for lignin fractionation and valorization, especially for the full valorization of lignocellulosic biomass.

The topic "Advances in the structural elucidation and utilization of lignins" covers isolation, characterization and utilization of lignin. Here we heartily acknowledge all the contributors for their amazing works on this topic. Following are the highlights drawn from the contributions to this special topic. Understanding the structural changes during lignin isolation is important for optimizing the separation or pretreatment processes. Zhang et al. investigated the structural changes of lignin macromolecules of balsa wood during the growth stages by using double enzymatic lignin (DEL) that was isolated from balsa grown for different lengths of time. They found that the balsa lignin was a typical hardwood lignin overwhelmingly composed of C–O bonds (i.e., β–O–4 linkages, 66.33–68.81/100Ar) and elevated with increasing tree-age, which is beneficial for the production of aromatic chemicals from lignin depolymerization. Li et al. reported the structural features and antioxidant performance of lignin fractionated from industrial furfural residue by an alkaline cooking process. They found that such lignin has appropriate radical scavenging capability and could be a promising antioxidant. Wang et al. examined the structural transformation during deep eutectic solvent (DES) treatments of enzymatic mild acidolysis lignin (EMAL) and a series of β–O–4 lignin model compounds. They demonstrated that β–O–4 linkages, existing in either real lignin or model compounds, could be cleaved by DES (ChCl/LA). The cleavage of β–O–4 linkages of EMAL led to the decrease of molecular weights and the rise of hydroxyl groups, which would be beneficial for developing an efficient fractionation process. Hong et al. investigated the structural changes of alkali lignin under choline chloride/formic acid (ChCl/FA) DES pretreatment, and revealed the lignin structural transformation during the DES

OPEN ACCESS

Edited and reviewed by:
Uw Schröder,
Technische Universitat Braunschweig, Germany

***Correspondence:**
Fengxia Yue
yuefx@scut.edu.cn

Specialty section:
This article was submitted to Bioenergy and Biofuels, a section of the journal Frontiers in Energy Research

Received: *14 June 2021*
Accepted: *28 June 2021*
Published: *16 July 2021*

Citation:
Yue F and Shuai L (2021) Editorial: Advances in the Structural Elucidation and Utilization of Lignins. Front. Energy Res. 9:724825. doi: 10.3389/fenrg.2021.724825

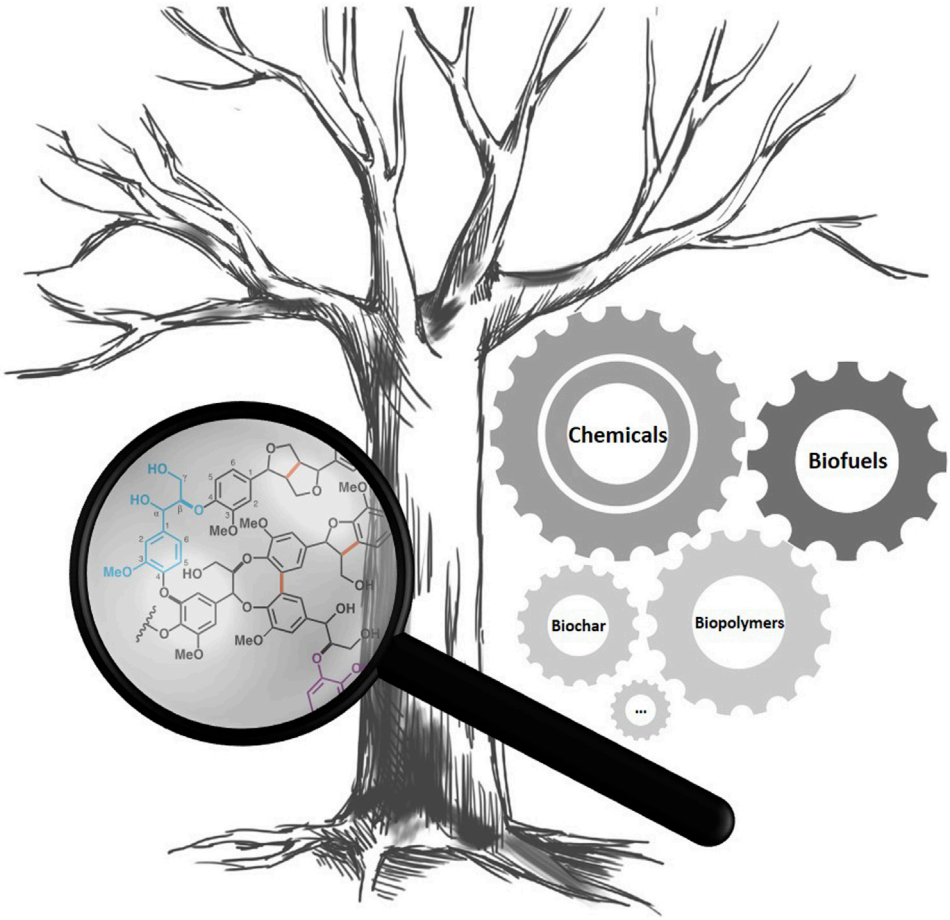

FIGURE 1 | Lignin structure and valorization.

pretreatment process, which provided new insights into preparation of homogeneous lignin with low molecular weights. Lignin model compounds always play an essential role in lignin characterization and mechanism studies. Yue et al. developed an efficient synthesis method for pinoresinol, an important lignin dimeric model compound and a high-value monolignol-derived lignan, by using 5-bromoconiferyl alcohol to suppress the undesired side-reactions by substitution at the C-5 position. Yang et al. examined the hydrognolysis of phenethyl phenyl ether (PPE) catalyzed by Pd, Ru, and Pt supported on carbon or γ-Al_2O_3 and proposed a novel strategy to monitor the ongoing reactions with *in situ* ^{1}H NMR and GC-MS. Wang and Ben evaluated the aging mechanism of bio-oils by model compound studies. They found that small acids, aldehydes, and HMF were the most active molecules and acidity was an important factor affecting the aging process of the bio-oils. Incorporating lignin into polymers is one of the most promising way of utilizing lignin, and the properties of the lignin-based polymers highly depend on the structural features of lignin. Wang et al. examined the effects of co-solvent-enhanced lignocellulosic fractionation (CELF) pretreatment severity on lignin structure of CELF-extracted lignin, and analyzed the influence of the structure on the mechanical properties of CELF lignin-based polyurethane. Finally, Dong et al. described the performance of porous carbons produced from lignin nanoparticles (LNPs) by two different protocols, and found the combination of hydrothermal carbonization and pyrolysis would improve the specific surface areas and total pore volumes of LNPs derived graphene-like porous carbons.

AUTHOR CONTRIBUTIONS

All authors listed have made a substantial, direct, and intellectual contribution to the work and approved it for publication.

Conflict of Interest: The authors declare that the research was conducted in the absence of any commercial or financial relationships that could be construed as a potential conflict of interest.

frontiers in Energy Research

ORIGINAL RESEARCH
published: 14 April 2020
doi: 10.3389/fenrg.2020.00048

Unraveling the Structural Transformation of Wood Lignin During Deep Eutectic Solvent Treatment

Shuizhong Wang[1†], *Helong Li*[1†], *Ling-Ping Xiao*[2,3*] *and Guoyong Song*[1*]

[1] *Beijing Key Laboratory of Lignocellulosic Chemistry, Beijing Advanced Innovation Center for Tree Breeding by Molecular Design, Beijing Forestry University, Beijing, China,* [2] *Liaoning Key Laboratory of Pulp and Paper Engineering, Center for Lignocellulose Chemistry and Biomaterials, School of Light Industry and Chemical Engineering, Dalian Polytechnic University, Dalian, China,* [3] *Guangxi Key Laboratory of Clean Pulp and Papermaking and Pollution Control, College of Light Industry and Food Engineering, Guangxi University, Nanning, China*

OPEN ACCESS

Edited by:
Chang Geun Yoo,
SUNY College of Environmental Science and Forestry, United States

Reviewed by:
Wen Wang,
Guangzhou Institute of Energy Conversion (CAS), China
Qiong Wang,
Guangzhou Institute of Energy Conversion (CAS), China

***Correspondence:**
Ling-Ping Xiao
lpxiao@dlpu.edu.cn
Guoyong Song
songg@bjfu.edu.cn

[†] *These authors have contributed equally to this work*

Specialty section:
This article was submitted to Bioenergy and Biofuels, a section of the journal Frontiers in Energy Research

Received: *12 February 2020*
Accepted: *10 March 2020*
Published: *14 April 2020*

Citation:
Wang S, Li H, Xiao L-P and Song G (2020) Unraveling the Structural Transformation of Wood Lignin During Deep Eutectic Solvent Treatment. Front. Energy Res. 8:48. doi: 10.3389/fenrg.2020.00048

Deep eutectic solvents (DESs) can efficiently promote the efficiency of cellulose enzymatic hydrolysis through the removal of lignin component in lignocellulosic biomass pretreatment. Unraveling the fundamental structural variant of lignin during DES treatment would facilitate to understand the DES-based biomass pretreatment in a clear perspective. Herein, an enzymatic mild acidolysis lignin (EMAL) and a series of β-O-4 lignin model compounds were employed to be treated with choline chloride (ChCl)/lactic acid (LA) (1:2) DES, from which the structural variant of all lignin fractions can be realized in a detailed version. The β-O-4 linkages, existing in either realistic lignin or model compounds, could be cleaved by ChCl/LA, thus leading to the decrease of molecular weight and the rise of hydroxyl groups. The influence of reaction temperature and time was also examined in view of some key structural parameters. Experimental evidences from model compounds confirmed that the repolymerization occurs with the depolymerization of lignin, which may account for the low production of monomeric products during DES treatment.

Keywords: lignin, deep eutectic solvents (DESs), β-O-4 mimics, repolymerization, depolymerization

INTRODUCTION

Lignocellulosic biomass, which possesses cellulose (*ca.* 30–50 wt%), hemicellulose (*ca.* 20–30 wt%), and lignin (*ca.* 15–30 wt%), is recognized as a complementary and alternative hydrocarbon resource to fossil feedstocks (Tuck et al., 2012; Galkin and Samec, 2016). In current biorefineries, the pretreatment of biomass, which aims to remove the lignin and promote the efficiency of cellulose enzymatic hydrolysis, remains an essential step (Behera et al., 2014; Rastogi and Shrivastava, 2017). The efforts at developing novel and efficient pretreatment technologies still stay an important one. Recently, deep eutectic solvents (DESs) have gained considerable attention as a new medium for biomass pretreatment due to their significant merits, including ease to prepare, stable chemical property, low cost, recyclability, and environment amity (Mbous et al., 2017; Satlewal et al., 2018). DESs are a mixture of a hydrogen bonding donor (HBD) and a hydrogen bonding acceptor (HBA), which present analogous solvent characteristics with ionic liquids (ILs) (Zhang et al., 2012; Smith et al., 2014). In DESs, the lignin and hemicellulose components can be deconstructed and removed

from biomass matrix, while cellulose component can survive because of strong hydrogen bonding networks and stable cohesive energy (Vigier et al., 2015). Pioneering works have indicated that DES pretreatment can significantly promote the efficacy of residue cellulose enzymatic hydrolysis. The plant species, which on the pretreatment with different DESs, have been extended to gramineae [corncob (Procentese et al., 2015; Zhang et al., 2016), wheat straw (Jeong et al., 2015), sorghum (Das et al., 2018), and switchgrass (Chen et al., 2018; Kim et al., 2018)], hardwood [eucalyptus (Shen et al., 2019), willow (Lyu et al., 2018; Song et al., 2019), and poplar (Alvarez-Vasco et al., 2016; Liu et al., 2017)], softwood [pine (Lynam et al., 2017), spruce (Wahlström et al., 2016), and fir (Alvarez-Vasco et al., 2016)], and endocarp (Li et al., 2018).

Lignin is the only renewable aromatic hydrocarbon resource, and biorefinery industries have pursued efficient means for lignin valorization for more than a century (Ragauskas et al., 2014; Sun et al., 2018; Song, 2019; Wu et al., 2019; Zhang et al., 2019). Upon the treatment of biomass with DESs, lignin in lignocellulosic biomass matrix can be cleaved and solubilized (Satlewal et al., 2018). In such a process, more structural complexity has been added to chemical properties of DES-extracted lignin compared to its native version, and this would influence the subsequent upgrading of lignin remarkably. Zhang et al. illustrated that choline chloride (ChCl)/lactic acid (LA) (1:2 molar ratio) DES was capable of extracting lignin with low molecular weight (M_w) from poplar and Douglas fir trees, and they suggested that DES served as an acidic catalyst to rupture β-O-4 lignin linkages without subsequent condensation reactions (Alvarez-Vasco et al., 2016). Shi et al. reported that all ether linkages in sorghum straw lignin were ruptured with ChCl/LA DES, and the resulting lignin could be depolymerized into monophenols with Ru/C catalyst efficiently (Das et al., 2018). Singh et al. used the DESs from lignin-derived monophenols to treat switchgrass; instead, they found that major ether linkages still remained intact in the residual lignin after pretreatment/saccharification (Kim et al., 2018). Wan et al. used ternary DESs to treat switchgrass, which led to the removal of lignin and hemicellulose efficiently; depolymerization and repolymerization of lignin were corroborated on the analysis of NMR spectra (Chen et al., 2019). Obviously, different views on whether repolymerization reaction of lignin occurs or not in DES-pretreated biomass were both taken on in the past. Moreover, it is worthy to point out that only partial lignin fraction could be recovered and characterized in DES biomass pretreatment, thus leaving other lignin fractions in an unknown state. From the pretreatment of biomass and valorization of lignin viewpoints, the deep insight into lignin structural transformation with DES is great of interest and importance.

Herein, we used enzymatic mild acidolysis lignin (EMAL), derived from *Eucalyptus* tree, as well as dimeric and polymeric β-O-4 lignin models to undergo the treatment of ChCl/LA DES. The whole lignin fractions (i.e., regenerated and fragmented lignin) derived from DES treatment could be retrieved for investigation. Based on the NMR, gel permeation chromatography (GPC), gas chromatography (GC)–mass spectrometry (MS), liquid chromatography (LC)–mass spectrometry (MS), and biomass compositional analysis, the variations of lignin with reaction temperature and time were established in terms of M_w, monomeric products, as well as the abundance linkages and hydroxyl group. The profound comprehension on lignin structural transformation unraveled the depolymerization and repolymerization pathways of lignin during the treatment of DES.

MATERIALS AND METHODS

Materials

Eucalyptus grandis (5 years old) were obtained from Guangxi Province, China. *Eucalyptus* EMAL was isolated according to the procedure developed by Wu and Argyropoulos (2003). The lignin chemical composition was measured according to NREL/TP-510-42618 protocol described previously (Sluiter et al., 2008). Polymeric and dimeric model compounds were synthesized according to our previous report (Li and Song, 2019), such as: dimeric model compound **1a** had a complete β-O-4 structure and a phenolic group, dimeric model compound **1b** had a complete β-O-4 structure but lacked a non-phenolic group, dimeric model compound **1c** was a phenolic model but was lacking γ-CH_2OH in the β-O-4 structure, dimeric model compounds phenethoxybenzene and 2-phenoxy-1-phenylethanol had no complete β-O-4 structure and methoxyl group on aromatic ring. ChCl and LA, purchased from Energy Chemical, were used for the preparation of DES in a 1:2 ratio without further purification. Commercial cellulase and xylanase were obtained from Shandong Longcott Enzyme Preparation Co., Ltd., China.

Treatment of Lignin With Deep Eutectic Solvent

EMAL (0.2 g) and ChCl/LA DES (2.0 g) were loaded in a 20-ml reactor, which was heated to the desired reaction temperature for a certain time with magnetic stirring (500 rpm). After the reaction, the reactor was cooled, and the thick reaction mixture was diluted with ethanol (5 ml). The addition of HCl solution (pH = 2) led to a precipitate, which was on the treatment of centrifugation, washing with ethanol/water (v/v, 1:9), and freeze-drying to afford regenerated lignin (**RL**). The liquid fraction from centrifugation was extracted with dichloromethane to obtain fragmented lignin samples (**FL**) in organic phase. The detailed post-processing flowchart of lignin treatment with DES was shown in **Figure 1**. The obtained regenerated and fragmented lignin samples were characterized by NMR [two-dimensional (2D) heteronuclear single quantum coherence spectroscopy (HSQC) and ^{31}P], GPC, and GC-MS analysis. The used DES existed in the water phase after dichloromethane extraction, which could be recycled by the removal of water under vacuum conditions.

Analytic Methods

The NMR spectra were acquired on a Bruker AVANCE 400 MHz spectrometer by using a lignin sample (50 mg) dissolved in DMSO-d_6 (0.5 ml). HSQC cross peaks and ^{31}P signals were assigned by comparing the spectra with the literatures (Brosse et al., 2010; Mansfield et al., 2012; Wang et al., 2017; Xiao et al.,

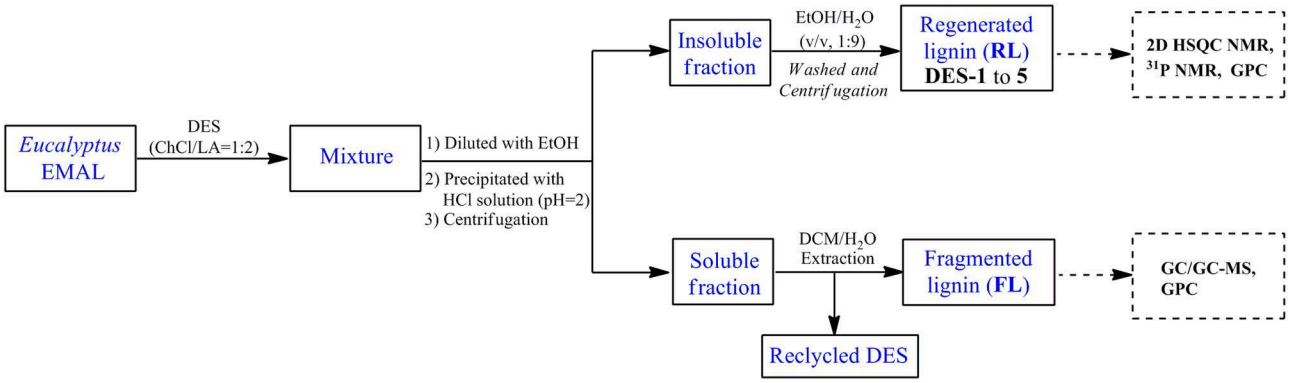

FIGURE 1 | The post-processing flowchart of lignin treatment with deep eutectic solvent (DES).

2017; Meng et al., 2019; Yang et al., 2020). GPC analysis of lignin samples [tetrahydrofuran (THF) solution, *ca.* 2 mg/ml] was performed on Shimadzu LC-20AD equipped with a PL-gel 10 μm Mixed-B 7.5 mm ID column (mixed) and UV detection detector (254 nm) at 50°C, using THF as the solvent (1 ml/min), which was calibrated with polystyrene standards (peak average M_w values of 96, 500, 1,320, 9,200, 66,000 g/mol; Polymer Laboratories Ltd.). GC-MS analysis of fragmented lignin samples was performed on Shimadzu GC-MS-QP2010SE equipped with an HP-5 MS (30 m × 250 mm × 0.25; Agilent) capillary column and a mass spectroscopy detector. LC-MS analysis of DES-treated dimeric compound was performed on Agilent 1290-6460 equipped with SB-C18 and electrospray ionization (ESI). The column oven was held at 30°C during analysis process. The mobile phase was a gradient methanol/water (with 0.1% formic acid and 5 mM ammonium acetate) at 0.2 ml/min flow rate.

RESULTS AND DISCUSSION

The Treatment of Enzymatic Mild Acidolysis Lignin With Choline Chloride/Lactic Acid Deep Eutectic Solvent

An EMAL isolated from *Eucalyptus* was selected as a substrate (Guerra et al., 2006; Xiao et al., 2017; Wang et al., 2018). The total lignin and carbohydrate contents were measured as about 87 wt% and 7 wt% based on biomass compositional analysis (**Table S1**). 2D HSQC NMR spectra analysis indicated this EMAL featured abundant β-O-4 linkages (64%), as well as less β-β (3%) and β-5 (10%) substructures, being kin to native lignin in biomass (**Figure 2A**). Thereby, this EMAL is a suitable substrate to unravel the lignin structural variation. After the treatment of EMAL with ChCl/LA DES (1:2 of molar ratio), the reaction mixture was diluted with EtOH and HCl solution (pH = 2), thus leading to obtain regenerated lignin (**RL**, **DES-1** to **DES-5**) as a precipitate. The leftover soluble fraction contained fragmented lignin (**FL**) species and DES, which could be separated by dichloromethane/water extraction (**Figure 1**). The analysis of ^{1}H NMR spectra indicated no changing on the recycled DES (90%) (**Figure S1**). The detailed yields of **RL** and **FL** obtained at different reaction temperatures and times were presented in **Table 1**. With 80°C and 1 h treatment, 86% of **RL** (**DES-1**) and 10% of **FL** were obtained, respectively (**Table 1**, entry 2). The high mass balance (96%) indicated that all lignin fractions could be basically recovered for characterization. Thereby, the utilization of isolated EMAL can overcome the limitation in the biomass pretreatment by DES, wherein the illustration of the lignin variation is incomplete. With the rise of reaction temperature, the decreasing of **RL** and increasing of **FL** were observed simultaneously, as seen in the case of 100°C (83% and 16%; **Table 1**, entry 3), 120°C (73% and 23%; **Table 1**, entry 4) and 140°C (71% and 20%; **Table 1**, entry 5). This scenario may be because the harsher reaction condition enhances the fragmentation of lignin into small and soluble pieces. A similar trend was also observed at variable reaction times at 100°C, that is, prolonging the treatment time led to the low yield of **RL** and high yield of **FL** (**Table 1**, entries 6 and 7). The detailed structural changes to the EMAL were then assessed by GC-MS, GPC, and NMR spectroscopy.

NMR Analysis

The abundance of hydroxyl group (OH) plays a critical role in future lignin valorization (Li and Song, 2019), which would be alternated with the cleavage of β-O-4 linkages and condensation reaction. To assess the variations of OH after DES treatment, regenerated lignin samples were treated with a phosphorylation reagent [2-chloro-4,4,5,5-tetramethyl-1,3,2-dioxaphospholate (TMDP)] and analyzed by typical ^{31}P NMR technology (Brosse et al., 2010; Wang et al., 2017; Meng et al., 2019; Yang et al., 2020). The aliphatic OH (145.5–149.5 ppm), condensed phenolic OH (S unit, 143.5–144.5 ppm; G unit, 140.8–141.2), uncondensed phenolic OH (S unit, 141.8–143.5 ppm; G unit, 138.5–140.5) from syringyl and guaiacyl units, as well as carboxylic group (134.5–135.5 ppm) were all measured (**Table 1**; see also **Figure S2**). The abundance of aliphatic OH tapered off with the increasing of reaction temperature and time because the cleavage of β-O-4 linkages resulted in the loss of C_α-OH moiety. On the contrary, the total phenolic OH gradually increased with higher reaction temperature or longer time, which derived from the exposing of phenolic OH after the cleavage of β-O-4 linkages. The non-condensed OH for **DES-1** (80°C,

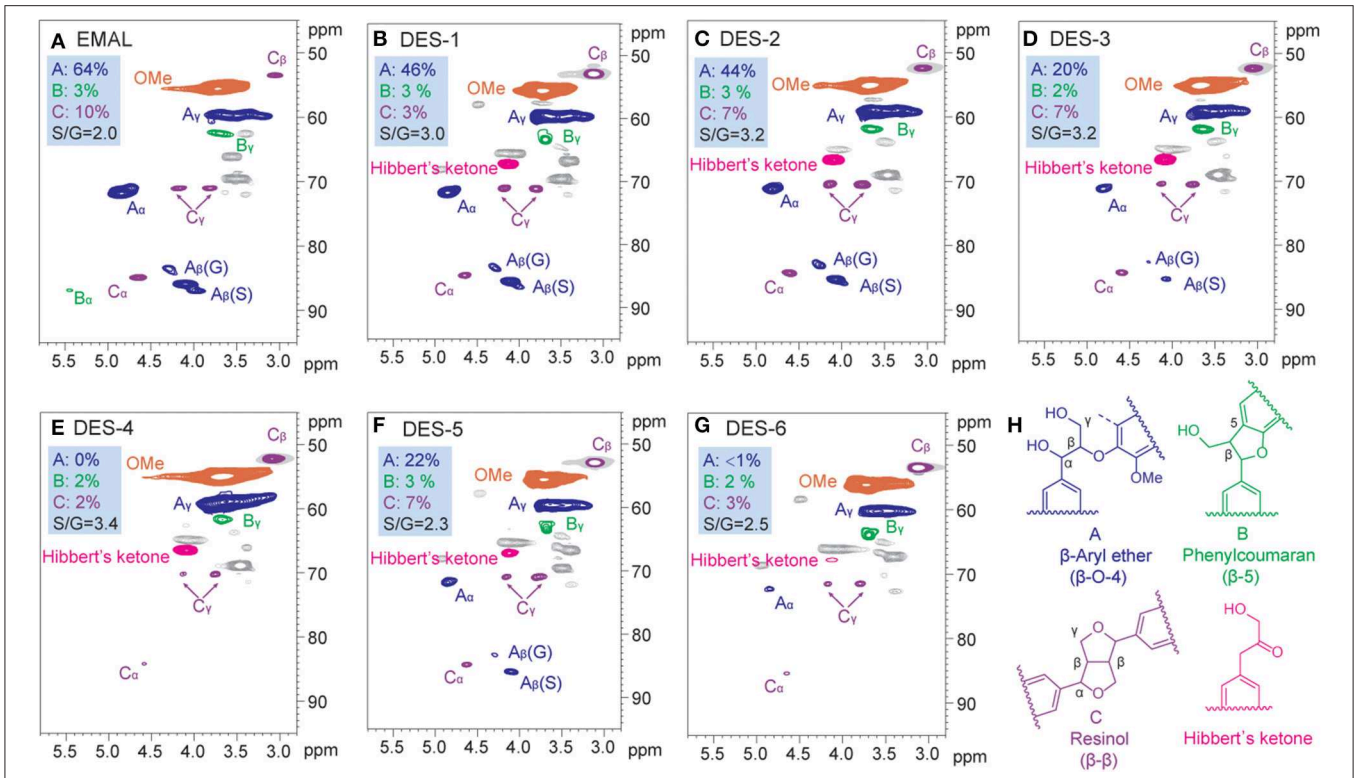

FIGURE 2 | Side chain (δ_C/δ_H 45–100/2.8–5.3 ppm) in the two-dimensional (2D) heteronuclear single quantum coherence spectroscopy (HSQC) NMR spectra of regenerated lignin (**RL**) after deep eutectic solvent (DES) treatment. **(A)** Enzymatic Mild Acidolysis Lignin (EMAL), **(B)** DES-1 (**Table 1**, entry 2), **(C)** DES-2 (**Table 1**, entry 3), **(D)** DES-3 (**Table 1**, entry 4), **(E)** DES-4 (**Table 1**, entry 5), **(F)** DES-5 (**Table 1**, entry 6), **(G)** DES-6 (**Table 1**, entry 7), **(H)** main classical substructures and Hibbert's ketone structure in 2D HSQC NMR of the lignins.

TABLE 1 | ChCl/LA DES-treated *Eucalyptus* EMAL under various reaction conditions (the unit of hydroxyl and carboxylic group: mmol/g)[a].

Entry	Samples	T (°C)	t (h)	Yield[b] (wt%)		Aliphatic OH	Syringyl OH	Guaiacyl OH	Total phenolic OH	Carboxylic group
				RL[c]	FL[c]		NC/C	NC/C		
1	EMAL	–	–	–	–	4.40	0.26/0.08	0.40/0.06	0.80	0.04
2	DES-1	80	1	86	10	3.90	0.22/0.09	0.31/0.07	0.69	0.08
3	DES-2	100	1	83	16	3.02	0.26/0.09	0.34/0.07	0.76	0.13
4	DES-3	120	1	73	23	2.76	0.53/0.18	0.48/0.15	1.34	0.19
5	DES-4	140	1	71	25	1.29	0.92/0.39	0.54/0.25	2.10	0.15
6	DES-5	100	2	74	11	3.20	0.30/0.10	0.34/0.12	0.86	0.26
7	DES-6	100	4	65	18	3.00	0.31/0.13	0.36/0.19	0.99	0.23

[a] *Reaction condition: EMAL (0.2 g), DES (2.0 g).*

[b] *The yield was calculated based on the mass ratio of **RL** or **FL** to corresponding EMAL.*

[c] *The **RL** (regenerated lignin) was obtained from precipitation with acid water (pH = 2) after DES treatment; **FL** (fragmented lignin) was extracted with dichloromethane from soluble fraction after DES treatment.*

C, condensed; ChCl, choline chloride; DES, deep eutectic solvent; EMAL, enzymatic mild acidolysis lignin; LA, lactic acid; NC, non-condensed.

0.53 mmol/g) and **DES-2** (100°C, 0.60 mmol/g) at a relative low reaction temperature were comparable to initial EMAL (0.66 mmol/g), while significant increase of non-condensed OH was observed in **DES-3** (120°C, 1.01 mmol/g) and **DES-4** (140°C, 1.46 mmol/g) at high temperatures. In the case of condensed OH, a similar variation trend was also observed, and a maximum value of condensed OH was obtained in **DES-4** (140°C, 0.64 mmol/g). These results suggested that the lignin experiences depolymerization and repolymerization upon the cleavage of β-O-4 linkages in a synchronous manner, and both of them would be enhanced under harsh conditions, being in line with a previous report (Chen et al., 2019). Similar variation trends occurred in DES treatment time (**DES-5** and **DES-6**). The carboxylic group, probably generated from oxidation reaction with DES, was also increased, especially with longer reaction time (**DES-5**, 0.26 mmol/g; **DES-6**, 0.23 mmol/g).

To elaborate the changes of inter-unit linkages, 2D HSQC NMR analysis for regenerated lignin samples **DES-1** to **DES-6** were performed (**Figure 2**; see also **Figure S3**). The detailed signal peaks were assigned according to previous reports (Mansfield et al., 2012; Xiao et al., 2017). A decline of β-O-4 linkage (46%) was observed after DES treatment 80°C for 1 h, being lower than that from EMAL (64%). This decline was intensified with the rise of reaction temperature and/or time until almost all cross signals for β-O-4 units disappeared in **DES-4** and **DES-6**. The lessening of β-O-4 linkage corresponded to the rise of phenolic hydroxyl groups. In the case of carbon–carbon linkages (β-β and β-5), partial degradation was detected by comparison with those from EMAL. Thereby, the cleavage of β-O-4 linkage occurred preferentially in the DES treatment process. Of note, cross signals for Hibbert's ketone (labeled in red) were also detected in the regenerated lignin samples, which kept consistent in the conclusion that DES treatment process is an acid-catalyzed process (Brandt et al., 2015; Alvarez-Vasco et al., 2016; Das et al., 2018). Further analysis of HSQC NMR spectra showed that the signal intensity of Hibbert's ketone gradually decreased with prolonging reaction time until disappearance in **DES-6** (**Figure 2G**) probably because Hibbert's ketone moiety could be released or retransformed.

The ratios of S/G subunits of regenerated lignin were also measured by semiquantitative integration of cross signals at aromatic/unsaturated region (δ_C/δ_H 100–135/5.9–8.0 ppm) (**Figure 2** and **Figure S3**). The increased S/G ratio values were detected after DES treatment by comparison with unreacted EMAL. The high ratios of S/G in regenerated lignin indicated that more guaiacyl subunits have been solubilized in fragmented lignin.

Gel Permeation Chromatography and Gas Chromatography–Mass Spectrometry Analysis

To address changes in lignin polymerization degree during DES treatment, analysis of the resulting samples by GPC was performed, as shown in **Figure 3**. The average M_w slightly decreased from 8,590 g/mol for initial EMAL to 6,110 g/mol for regenerated lignin sample **DES-1**, in line with the observation in 2D NMR spectra, where most β-O-4 linkages still remained. The corresponding fragmented lignin recovered from soluble fraction showed a low M_w of 1,890 g/mol. With the elevation of reaction temperature or time, the degree of lignin polymerization declined continuously. **DES-4**, obtained at 140°C and 1 h, exhibited the lowest M_w values of regenerated lignin (2,350 g/mol) and fragmented lignin (780 g/mol). Under such a condition, GPC corroborated the prevalence of full dissociation of lignin biopolymer, in alignment with NMR analysis, wherein highest abundance of hydroxyl groups and lowest content of β-O-4 moiety were both detected. In addition, the polydispersity values (M_w/M_n) for regenerated lignin (1.35–1.57) and fragmented lignin (1.12–1.38) were both decreased compared to initial EMAL (2.08), indicating that the resulted lignin samples have a narrow distribution.

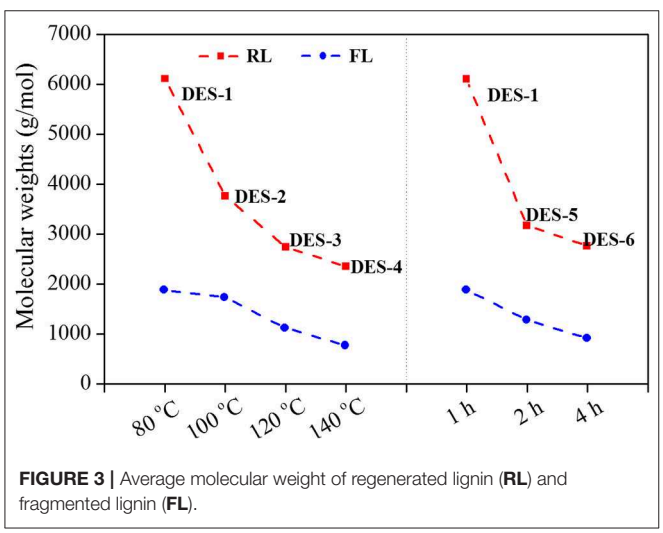

FIGURE 3 | Average molecular weight of regenerated lignin (**RL**) and fragmented lignin (**FL**).

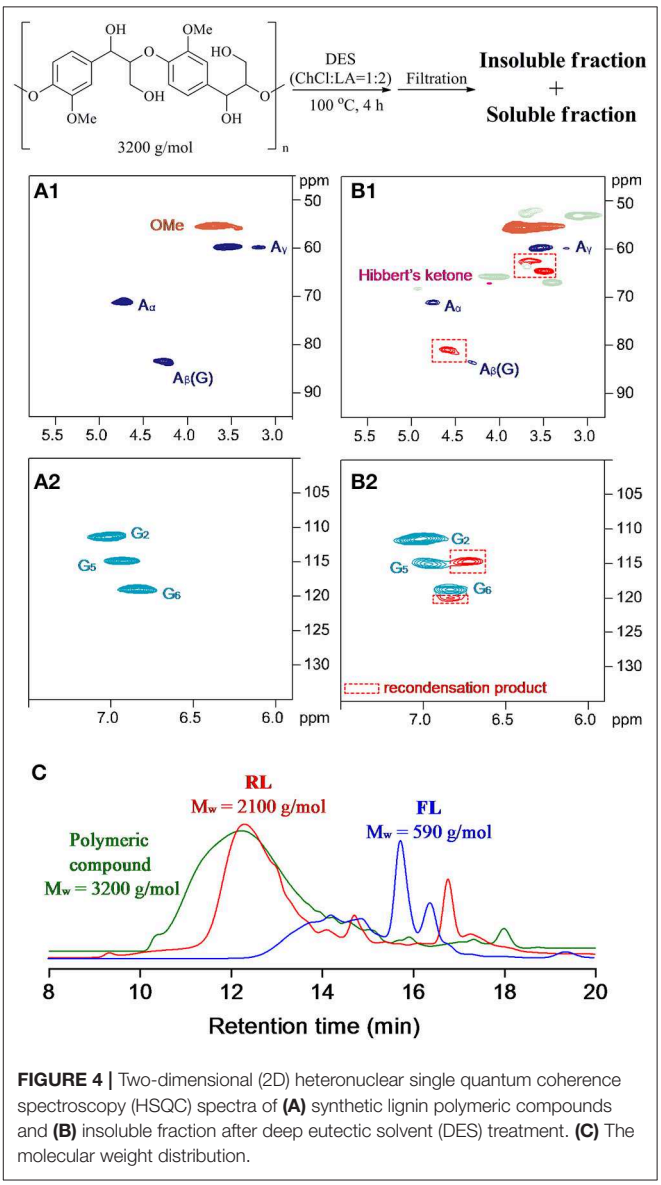

FIGURE 4 | Two-dimensional (2D) heteronuclear single quantum coherence spectroscopy (HSQC) spectra of **(A)** synthetic lignin polymeric compounds and **(B)** insoluble fraction after deep eutectic solvent (DES) treatment. **(C)** The molecular weight distribution.

In view of the low polymerization degree in fragmented lignin, we speculated that some monomeric products have been generated. Product distributions based on GC-MS analysis showed that vanillin and syringaldehyde were produced as the major monomeric phenols in all cases. Interestingly, syringyl- and guaiacyl-derived monoketones and diketones were also detected (**Figure S4**), which were promoted with the rise of reaction temperature. It should be noted that either aldehyde or diketone derivatives from lignin depolymerization proceeded through an acid-catalyzed reaction according to previous reports (Lundquist and Hedlund, 1967; Deuss et al., 2015). Unfortunately, the combined yield of total monomers is less than 3 wt% by comparison with the authentic samples, which is rather lower than that from metal-catalyzed hydrogenolysis of EMAL (Xiao et al., 2017). The severe recondensation, which accompanies the depolymerization of lignin, may account for this scenario.

Treatment of β-O-4 Mimics With Deep Eutectic Solvent

Currently used EMAL contained 7 wt% carbohydrate, which, together with β-β and β-5 linkages, will exhibit in the 2D NMR spectra after DES treatment and will disturb the distinction of lignin structure changes. To recognize the lignin-derived signals in a clear version, a synthetic polymer composed exclusively of the β-O-4 substructure was treated with ChCl/LA DES at 100°C for 4 h (**Figure 4A**). The detailed workup procedure to acquire the soluble and insoluble fractions is similar with realistic lignin sample. For the case of insoluble fraction, the changes in 2D NMR spectra proceeded in a fashion akin to EMAL, that is, the sharp decline of β-O-4 signals and the emergence of Hibbert's ketone specie (Alvarez-Vasco et al., 2016; Das et al., 2018). Additionally, the cross peaks at aliphatic area (62.1/3.6 ppm, 64.3/3.5 ppm, 80.6/4.6 ppm), as well as at aromatic (114.6/6.7 ppm, 120.0/6.8 ppm), were emerged and detected (**Figure 4B**). Some of these signals could be found in NMR spectra of DES-treated EMAL (**Figure 2**). Taking into consideration the decline of β-O-4 moiety, together with current polymeric state, these new signals may be ascribed to the recondensation product (Shuai et al., 2010). This observation is different with previous report by using lignocellulosic biomass as substrates, where no condensation structures were distinguished probably because of the overlapping of signals (Alvarez-Vasco et al., 2016). The DES-treated β-O-4 polymeric mimics also led to a decrease in M_w from 3,200 g/mol to 2,100 g/mol (insoluble fraction) and 590 g/mol

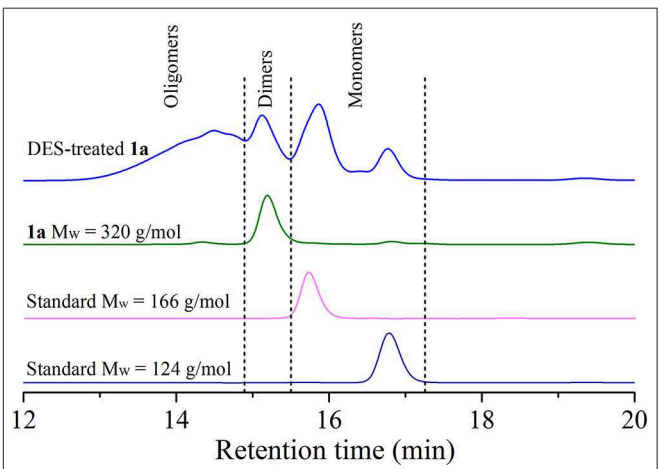

FIGURE 5 | Gel permeation chromatography (GPC) spectra of deep eutectic solvent (DES)-treated **1a**, compound **1a** and standard compounds [guaiacol: molecular weight (M_w) = 124 g/mol and dihydroeugenol: M_w = 166 g/mol].

TABLE 2 | Product distribution of lignin β-O-4 dimeric compounds treatment with DES (ChCl/LA)[a].

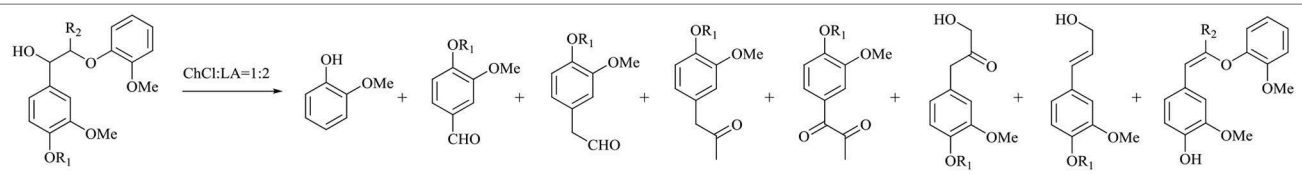

1 2 3 4 5 6 7 8 9

Entry	Substrate	R_1	R_2	Yield (%)[b]							
				2	3	4	5	6	7	8	9
1	**1a**	H	CH_2OH	10	0.1 (**3a**)	n.d.	Trace (**5a**)	Trace (**6a**)	2 (**7a**)	1 (**8a**)	1 (**9a**)
2	**1b**	OMe	CH_2OH	4	0.3 (**3b**)	n.d.	n.d.	Trace (**6b**)	4 (**7b**)	n.d.	2 (**9b**)
3	**1c**	H	H	17	2 (**3c**)	6 (**4c**)	n.d.	n.d.	n.d.	n.d.	4 (**9c**)

[a] *Reaction condition: substrate (0.1 g), DES (1.0 g), 100°C, 2 h; Compound **1a** has a complete β-O-4 structure and a phenolic group; Compound **1b** has a complete β-O-4 structure but lacks a non-phenolic group; Compound **1c** is a phenolic model but is lacking γ-CH_2OH in the β-O-4 structure.*

[b] *The yield was calculated based on the mole ratio of products to corresponding substrate by gas chromatography (GC)–mass spectrometry (MS).*

ChCl, choline chloride; DES, deep eutectic solvent; LA, lactic acid; n.d., not detected.

(soluble fraction) (**Figure 4C**). Further analysis of the soluble fraction suggested the vanillin, guaiacyl-derived monoketones, and diketone were all generated, being in line with scenario of realistic lignin (**Figure S5**).

A series of dimeric lignin mimics were also tested in DES at 100°C for 2 h, and some representative results were summarized in **Table 2** and **Figure S6**. Compound **1a**, having a complete β-O-4 structure and a phenolic group, underwent a full conversion after DES treatment. By comparison with authentic samples on GC-MS, some monophenols, such as vanillin (**3a**, 0.1%), guaiacyl-derived and Hibbert's ketone (**7a**, 2%), coniferol (**8a**, 1%), and guaiacol (**2**, 10%), were identified. It is worth mentioning that an enol ether derivative from dehydration reaction of **1a**, which is often generated through an acid-catalyzed hydrolysis reaction and considered as intermediates toward Hibbert's ketone or aldehyde, was also observed in DES treatment (**Table 2**, entry 1) (Lundquist and Lundgren, 1972; Lundquist, 1976). Compared to metal catalysis systems (Hossain et al., 2019; Li and Song, 2019), the rather low mass balance from monomeric and dimeric products suggested that a severe repolymerization has occurred in DES treatment. The analysis of resulted mixture on LC-MS showed that trimers, tetramers, and oligomers with corresponding mass values have been generated, despite that the exact structures of the resulting products were hard to identify (**Figure S7**). GPC analysis of the resulting mixture indicated a broader polydispersity after compound **1a** was treated with DES (**Figure 5**). A broad peak with a longer retention time (from 13.22 to 14.51 min) appeared, which is assigned to oligomers in accordance with their larger molecular structure by comparison with compound **1a**. The peak also having two shorter retention times (15.86 and 16.79 min) corresponded to the monophenols. The above results confirmed that the depolymerization of β-O-4 units and the repolymerization reactions occurred concurrently during DES treatment, being in accordance with realistic lignin and synthetic polymer. Given that few free phenolic groups exit in lignin before the cleavage of β-O-4 unit, a non-phenolic model compound **1b** with β-O-4 structure was also tested by DES. This reaction gave similar monomeric products in lower yields (**Table 2**, entry 2), albeit a full conversion of **1b** was observed. In the case of another phenolic lignin model **1c**, which lacks γ-CH_2OH in β-O-4 structure, aldehyde derivatives were generated as dominated monomers (**Table 2**, entry 3). Dimeric compounds

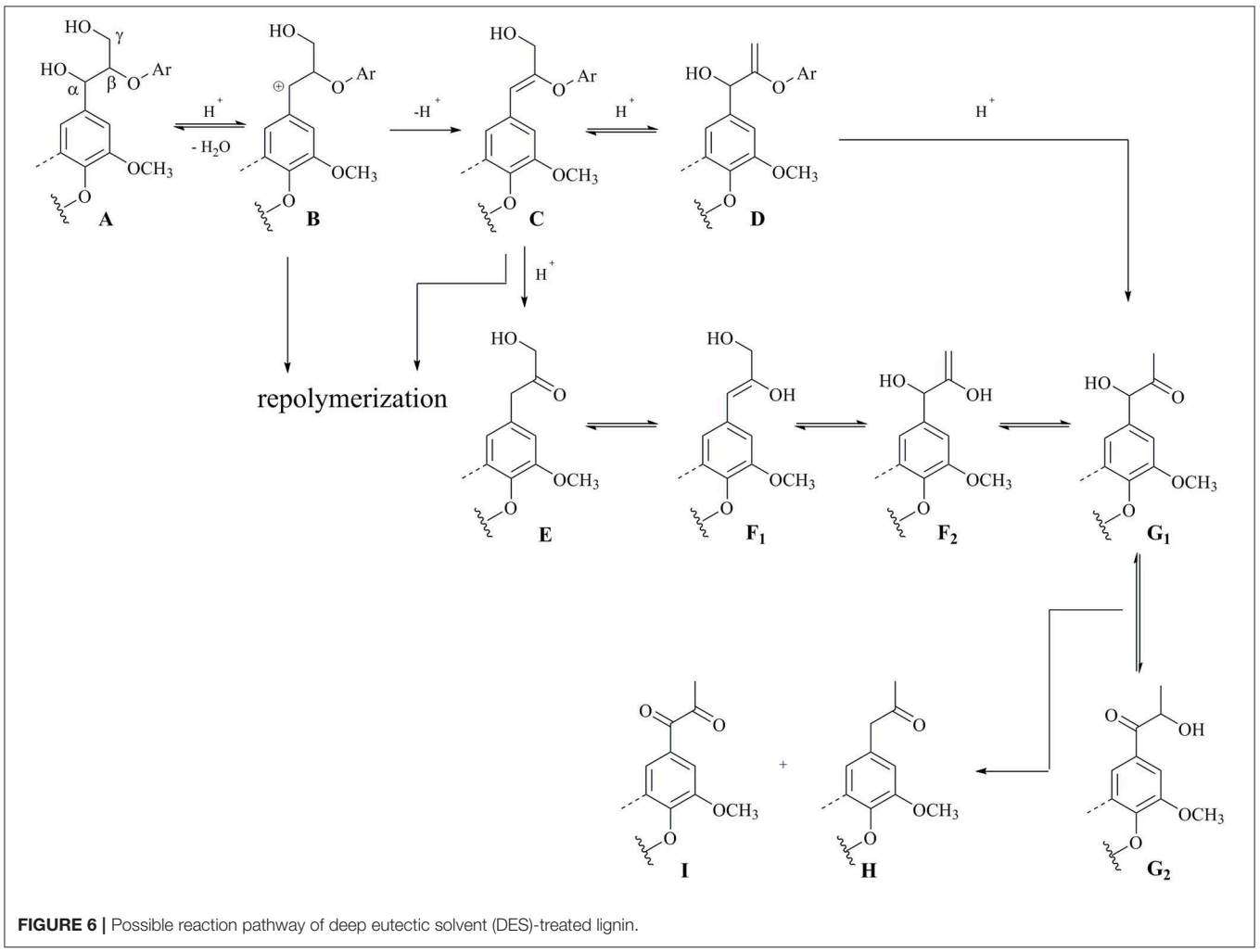

FIGURE 6 | Possible reaction pathway of deep eutectic solvent (DES)-treated lignin.

that do not contain complete β-O-4 structure and methoxyl group on aromatic ring, i.e., phenethoxybenzene and 2-phenoxy-1-phenylethanol, were also treated with ChCl/LA DES, while no obvious conversion was detected (**Figure S8**).

Plausible Reaction Pathway

Based on the above results acquired from realistic lignin and model compounds, a plausible reaction pathway for the DES-treated lignin was proposed in **Figure 6**. β-O-4 units in lignin should be efficiently cleaved probably through an acid-catalyzed process during DES. The reaction starts from a hydrogen ion attack on the α-hydroxyl group in **A**, which gives a carbocation species **B** *via* the release of one molecular unit of H_2O (Lundquist and Lundgren, 1972; Lundquist, 1976; Ito et al., 2011; Sturgeon et al., 2014). The elimination reaction between α positive charge and β-H results in an enol ether intermediate **C**, together with regeneration of a hydrogen ion. Following hydrolysis of **C** leads to the cleavage of C-O bond, thus affording Hibbert's ketone moiety **E** (Lundquist and Lundgren, 1972; Lundquist, 1976; Ito et al., 2011; Sturgeon et al., 2014). Alternatively, allylic rearrangement of **C** forms isomeric enol ether **G1** through **D**, and **G1** can also be generated from the rearrangement reaction of **E** and **F** under acidic conditions (Lundquist and Hedlund, 1967). The isomerization of **G1** intermediate gives **G2** probably *via* an enediol, and an equilibrium is proposed between **G1** and **G2** (Lundquist and Hedlund, 1967; Lundquist and Lundgren, 1972). Finally, an oxidoreduction of the mixture **G1** and **G2** leads to the formation of monoketone **H** and diketone **I** (Lundquist and Hedlund, 1967; Lundquist and Lundgren, 1972). Experimental evidences have substantiated the formation of oligomers rapidly during DES treatment, which may derive from the fact that the carbocation **B** or enol ether **C** is most likely responsible for the repolymerization rather than depolymerization (Lohr et al., 2015; Li and Song, 2019).

CONCLUSION

The detailed structural transformation of lignin during DES (ChCl:LA, 1:2) treatment was systematically unraveled by means of experiments using isolated lignin and a series of β-O-4 lignin model compounds. Entire fractions derived from lignin which were recovered from DES-treated EMAL showed different characteristics. The cleavage of β-O-4 linkages of EMAL is exacerbated with the increasing of reaction temperature and/or time, which leads to a sustained fall of insoluble lignin fraction and average M_w values, as well as a sustained rise of hydroxyl groups. The monomeric phenols derived from EMAL, polymeric and dimeric β-O-4 mimics were also identified, albeit in low combined yields. Experimental evidences from the reactions of β-O-4 models substantiated that the repolymerization reaction is accompanied by the depolymerization process. Mechanistic study suggested the main steps during DES-treated wood lignin, such as the cleavage of β-O-4, the repolymerization of active species, the production and derivation of mono products, should involve acid-catalyzed processes. This contribution provided a clear and beneficial information on lignin variation during DES treatment, which would be beneficial to design new DES-based pretreatment tailored for biorefinery and biotransformation.

DATA AVAILABILITY STATEMENT

All datasets generated for this study are included in the article/**Supplementary Material**.

AUTHOR CONTRIBUTIONS

SW carried out all experiments and wrote the manuscript. HL performed the lignin model compounds analysis. L-PX and GS designed the work and revised the manuscript. All authors discussed the results.

FUNDING

This work was supported by the National Natural Science Foundation of China (21776020, 31971607, 51961125207), the Natural Science Foundation of Liaoning Province (No. 2019-MS-019), the Opening Project of Guangxi Key Laboratory of Clean Pulp & Papermaking and Pollution Control (No. 2019KF14), and Youth Technology Talents of Dalian (No. 2019RQ035).

SUPPLEMENTARY MATERIAL

The Supplementary Material for this article can be found online at: https://www.frontiersin.org/articles/10.3389/fenrg.2020.00048/full#supplementary-material

REFERENCES

Alvarez-Vasco, C., Ma, R., Quintero, M., Guo, M., Geleynse, S., Ramasamy, K. K., et al. (2016). Unique low-molecular-weight lignin with high purity extracted from wood by deep eutectic solvents (DES): a source of lignin for valorization. *Green Chem.* 18, 5133–5141. doi: 10.1039/C6GC01007E

Behera, S., Arora, R., Nandhagopal, N., and Kumar, S. (2014). Importance of chemical pretreatment for bioconversion of lignocellulosic biomass. *Renew. Sust. Energy Rev.* 36, 91–106. doi: 10.1016/j.rser.2014.04.047

Brandt, A., Chen, L., van Dongen, B. E., Welton, T., and Hallett, J. P. (2015). Structural changes in lignins isolated using an acidic ionic liquid water mixture. *Green Chem.* 17, 5019–5034. doi: 10.1039/C5GC01314C

Brosse, N., El Hage, R., Chaouch, M., Pétrissans, M., Dumarçay, S., and Gérardin, P. (2010). Investigation of the chemical modifications of beech wood lignin during heat treatment. *Polym. Degrad. Stab.* 95, 1721–1726. doi: 10.1016/j.polymdegradstab.2010.05.018

Chen, Z., Jacoby, W. A., and Wan, C. (2019). Ternary deep eutectic solvents for effective biomass deconstruction at high solids and low enzyme loadings. *Bioresour. Technol.* 279, 281–286. doi: 10.1016/j.biortech.2019.01.126

Chen, Z., Reznicek, W. D., and Wan, C. (2018). Aqueous choline chloride: a novel solvent for switchgrass fractionation and subsequent hemicellulose conversion into furfural. *ACS Sust. Chem. Eng.* 6, 6910–6919. doi: 10.1021/acssuschemeng.8b00728

Das, L., Li, M., Stevens, J., Li, W., Pu, Y., Ragauskas, A. J., et al. (2018). Characterization and catalytic transfer hydrogenolysis of deep eutectic solvent

extracted sorghum lignin to phenolic compounds. *ACS Sust. Chem. Eng.* 6, 10408–10420. doi: 10.1021/acssuschemeng.8b01763

Deuss, P. J., Scott, M., Tran, F., Westwood, N. J., de Vries, J. G., and Barta, K. (2015). Aromatic monomers by in situ conversion of reactive intermediates in the acid-catalyzed depolymerization of lignin. *J. Am. Chem. Soc.* 137, 7456–7467. doi: 10.1021/jacs.5b03693

Galkin, M. V., and Samec, J. S. M. (2016). Lignin valorization through catalytic lignocellulose fractionation: a fundamental platform for the future biorefinery. *ChemSusChem* 9, 1544–1558. doi: 10.1002/cssc.201600237

Guerra, A., Filpponen, I., Lucia, L. A., Saquing, C., Baumberger, S., and Argyropoulos, D. S. (2006). Toward a better understanding of the lignin isolation process from wood. *J. Agric. Food Chem.* 54, 5939–5947. doi: 10.1021/jf060722v

Hossain, M. A., Phung, T. K., Rahaman, M. S., Tulaphol, S., Jasinski, J. B., and Sathitsuksanoh, N. (2019). Catalytic cleavage of the β-O-4 aryl ether bonds of lignin model compounds by Ru/C catalyst. *Appl. Catal. A* 582, 117100–117106. doi: 10.1016/j.apcata.2019.05.034

Ito, H., Imai, T., Lundquist, K., Yokoyama, T., and Matsumoto, Y. (2011). Revisiting the mechanism of β-O-4 bond cleavage during acidolysis of lignin. Part 3: search for the rate-determining step of a non-phenolic C_6-C_3 type model compound. *J. Wood Chem. Technol.* 31, 172–182. doi: 10.1080/02773813.2010.515050

Jeong, K. M., Lee, M. S., Nam, M. W., Zhao, J., Jin, Y., Lee, D.-K., et al. (2015). Tailoring and recycling of deep eutectic solvents as sustainable and efficient extraction media. *J. Chromatogr. A* 1424, 10–17. doi: 10.1016/j.chroma.2015.10.083

Kim, K. H., Dutta, T., Sun, J., Simmons, B., and Singh, S. (2018). Biomass pretreatment using deep eutectic solvents from lignin derived phenols. *Green Chem.* 20, 809–815. doi: 10.1039/C7GC03029K

Li, H., and Song, G. (2019). Ru-catalyzed hydrogenolysis of lignin: base-dependent tunability of monomeric phenols and mechanistic study. *ACS Catal.* 9, 4054–4064. doi: 10.1021/acscatal.9b00556

Li, W., Amos, K., Li, M., Pu, Y., Debolt, S., Ragauskas, A. J., et al. (2018). Fractionation and characterization of lignin streams from unique high-lignin content endocarp feedstocks. *Biotechnol. Biofuels* 11, 304–317. doi: 10.1186/s13068-018-1305-7

Liu, Y., Chen, W., Xia, Q., Guo, B., Wang, Q., Liu, S., et al. (2017). Efficient cleavage of lignin-carbohydrate complexes and ultrafast extraction of lignin oligomers from wood biomass by microwave-assisted treatment with deep eutectic solvent. *ChemSusChem* 10, 1692–1700. doi: 10.1002/cssc.201601795

Lohr, T. L., Li, Z., and Marks, T. J. (2015). Selective ether/ester C-O cleavage of an acetylated lignin model via tandem catalysis. *ACS Catal.* 5, 7004–7007. doi: 10.1021/acscatal.5b01972

Lundquist, K. (1976). Low-molecular weight lignin hydrolysis products. *Appl. Polym. Symp.* 28, 1393–1407

Lundquist, K., and Hedlund, K. (1967). Acid degradation of lignin I. the formation of ketones of the guaiacylpropane series. *Acta Chem. Scand.* 21, 1750–1754. doi: 10.3891/acta.chem.scand.21-1750

Lundquist, K., and Lundgren, R. (1972). Acid degradation of lignin part VII.* the cleavage of ether bonds. *Acta Chem. Scand.* 26, 2005–2023. doi: 10.3891/acta.chem.scand.26-2005

Lynam, J. G., Kumar, N., and Wong, M. J. (2017). Deep eutectic solvents' ability to solubilize lignin, cellulose, and hemicellulose; thermal stability; and density. *Bioresour. Technol.* 238, 684–689. doi: 10.1016/j.biortech.2017.04.079

Lyu, G., Li, T., Ji, X., Yang, G., Liu, Y., Lucia, A. L., et al. (2018). Characterization of lignin extracted from willow by deep eutectic solvent treatments. *Polymers* 10, 869–879. doi: 10.3390/polym10080869

Mansfield, S. D., Kim, H., Lu, F., and Ralph, J. (2012). Whole plant cell wall characterization using solution-state 2D NMR. *Nat. Protoc.* 7, 1579–1589. doi: 10.1038/nprot.2012.064

Mbous, Y. P., Hayyan, M., Hayyan, A., Wong, W. F., Hashim, M. A., and Looi, C. Y. (2017). Applications of deep eutectic solvents in biotechnology and bioengineering-promises and challenges. *Biotechnol. Adv.* 35, 105–134. doi: 10.1016/j.biotechadv.2016.11.006

Meng, X., Crestini, C., Ben, H., Hao, N., Pu, Y., Ragauskas, A. J., et al. (2019). Determination of hydroxyl groups in biorefinery resources via quantitative ^{31}P NMR spectroscopy. *Nat. Protoc.* 14, 2627–2647. doi: 10.1038/s41596-019-0191-1

Procentese, A., Johnson, E., Orr, V., Garruto Campanile, A., Wood, J. A., Marzocchella, A., et al. (2015). Deep eutectic solvent pretreatment and subsequent saccharification of corncob. *Bioresour. Technol.* 192, 31–36. doi: 10.1016/j.biortech.2015.05.053

Ragauskas, A. J., Beckham, G. T., Biddy, M. J., Chandra, R., Chen, F., Davis, M. F., et al. (2014). Lignin valorization: improving lignin processing in the biorefinery. *Science* 344:1246843. doi: 10.1126/science.1246843

Rastogi, M., and Shrivastava, S. (2017). Recent advances in second generation bioethanol production: An insight to pretreatment, saccharification and fermentation processes. *Renew. Sust. Energy Rev.* 80, 330–340. doi: 10.1016/j.rser.2017.05.225

Satlewal, A., Agrawal, R., Bhagia, S., Sangoro, J., and Ragauskas, A. J. (2018). Natural deep eutectic solvents for lignocellulosic biomass pretreatment: recent developments, challenges and novel opportunities. *Biotechnol. Adv.* 36, 2032–2050. doi: 10.1016/j.biotechadv.2018.08.009

Shen, X.-J., Wen, J.-L., Mei, Q.-Q., Chen, X., Sun, D., Yuan, T.-Q., et al. (2019). Facile fractionation of lignocelluloses by biomass-derived deep eutectic solvent (DES) pretreatment for cellulose enzymatic hydrolysis and lignin valorization. *Green Chem.* 21, 275–283. doi: 10.1039/C8GC03064B

Shuai, L., Yang, Q., Zhu, J. Y., Lu, F. C., Weimer, P. J., Ralph, J., et al. (2010). Comparative study of SPORL and dilute-acid pretreatments of spruce for cellulosic ethanol production. *Bioresour. Technol.* 101, 3106–3114. doi: 10.1016/j.biortech.2009.12.044

Sluiter, A., Hames, B., Ruiz, R., Scarlata, C., Sluiter, J., Templeton, D., et al. (2008). *Determination of Structural Carbohydrates and Lignin in Biomass*. Golden, CO: National Renewable Energy Laboratory (NREL).

Smith, E. L., Abbott, A. P., and Ryder, K. S. (2014). Deep eutectic solvents (DESs) and their applications. *Chem. Rev.* 114, 11060–11082. doi: 10.1021/cr300162p

Song, G. (2019). The development of catalytic fractionation and conversion of lignocellulosic biomass under lignin-first strategy. *J. For. Eng.* 4, 1–10. doi: 10.13360 /j.issn.2096-1359.2019.05.001

Song, Y., Chandra, R. P., Zhang, X., Tan, T., and Saddler, J. N. (2019). Comparing a deep eutectic solvent (DES) to a hydrotrope for their ability to enhance the fractionation and enzymatic hydrolysis of willow and corn stover. *Sust. Energy Fuels* 3, 1329–1337. doi: 10.1039/C8SE00617B

Sturgeon, M. R., Kim, S., Lawrence, K., Paton, R. S., Chmely, S. C., Nimlos, M., et al. (2014). A mechanistic investigation of acid-catalyzed cleavage of aryl-ether linkages: implications for lignin depolymerization in acidic environments. *ACS Sust. Chem. Eng.* 2, 472–485. doi: 10.1021/sc400384w

Sun, Z., Fridrich, B., de Santi, A., Elangovan, S., and Barta, K. (2018). Bright side of lignin depolymerization: toward new platform chemicals. *Chem. Rev.* 118, 614–678. doi: 10.1021/acs.chemrev.7b00588

Tuck, C. O., Pérez, E., Horváth, I. T., Sheldon, R. A., and Poliakoff, M. (2012). Valorization of biomass: deriving more value from waste. *Science* 337, 695–699. doi: 10.1126/science.1218930

Vigier, K. D. O., Chatel, G., and Jérôme, F. (2015). Contribution of deep eutectic solvents for biomass processing: opportunities, challenges, and limitations. *ChemCatChem* 7, 1250–1260. doi: 10.1002/cctc.201500134

Wahlström, R., Hiltunen, J., Pitaluga de Souza Nascente Sirkka, M., Vuoti, S., and Kruus, K. (2016). Comparison of three deep eutectic solvents and 1-ethyl-3-methylimidazolium acetate in the pretreatment of lignocellulose: effect on enzyme stability, lignocellulose digestibility and one-pot hydrolysis. *RSC Adv.* 6, 68100–68110. doi: 10.1039/C6RA11719H

Wang, H.-M., Wang, B., Wen, J.-L., Yuan, T.-Q., and Sun, R.-C. (2017). Structural characteristics of lignin macromolecules from different eucalyptus species. *ACS Sust. Chem. Eng.* 5, 11618–11627. doi: 10.1021/acssuschemeng.7b02970

Wang, S., Gao, W., Li, H., Xiao, L.-P., Sun, R.-C., and Song, G. (2018). Selective fragmentation of biorefinery corncob lignin into *p*-hydroxycinnamic esters with a supported zinc molybdate catalyst. *ChemSusChem* 11, 2114–2123. doi: 10.1002/cssc.201800455

Wu, S., and Argyropoulos, D. S. (2003). An improved method for isolating lignin in high yield and purity. *J. Pulp Pap. Sci.* 29, 235–240.

Wu, Y., Qian, Y., Lou, H., Yang, D., and Qiu, X. (2019). Enhancing the broad-spectrum adsorption of lignin through methoxyl activation, grafting modification, and reverse self-assembly. *ACS Sust. Chem. Eng.* 7, 15966–15973. doi: 10.1021/acssuschemeng.9b02317

Xiao, L.-P., Wang, S., Li, H., Li, Z., Shi, Z.-J., Xiao, L., et al. (2017). Catalytic hydrogenolysis of lignins into phenolic compounds over carbon

nanotube supported molybdenum oxide. *ACS Catal.* 7, 7535–7542. doi: 10.1021/acscatal.7b02563

Yang, H., Yoo, C. G., Meng, X., Pu, Y., Muchero, W., Tuskan, G. A., et al. (2020). Structural changes of lignins in natural populus variants during different pretreatments. *Bioresour. Technol.* 295, 122240–122246. doi: 10.1016/j.biortech.2019.122240

Zhang, C.-W., Xia, S.-Q., and Ma, P.-S. (2016). Facile pretreatment of lignocellulosic biomass using deep eutectic solvents. *Bioresour. Technol.* 219, 1–5. doi: 10.1016/j.biortech.2016.07.026

Zhang, Q., De Oliveira Vigier, K., Royer, S., and Jérôme, F. (2012). Deep eutectic solvents: syntheses, properties and applications. *Chem. Soc. Rev.* 41, 7108–7146. doi: 10.1039/C2CS35178A

Zhang, Y., Ni, S., Wang, X., Zhang, W., Lagerquist, L., Qin, M., et al. (2019). Ultrafast adsorption of heavy metal ions onto functionalized lignin-based hybrid magnetic nanoparticles. *Chem. Eng. J.* 372, 82–91. doi: 10.1016/j.cej.2019.04.111

Conflict of Interest: The authors declare that the research was conducted in the absence of any commercial or financial relationships that could be construed as a potential conflict of interest.

frontiers in Energy Research

ORIGINAL RESEARCH
published: 27 May 2020
doi: 10.3389/fenrg.2020.00079

Accelerated Aging Process of Bio-Oil Model Compounds: A Mechanism Study

Rui Wang[1,2] *and Haoxi Ben*[1,2*]

[1] School of Energy and Environment, Southeast University, Nanjing, China, [2] Key Laboratory of Energy Thermal Conversion and Control, Ministry of Education, Nanjing, China

Bio-oil, obtained from the pyrolysis of biomass, is identified as a potential material for producing transportation fuels and value-added chemicals. However, the physical and chemical properties of bio-oil change with time, known as "aging," and the instability of bio-oil brings a critical hurdle to the commercial application of bio-oil. Therefore, expanding and deepening the understanding of the aging mechanism of bio-oil is the key to later efficient application of bio-oil. In addition, the extreme complexity of pyrolysis bio-oil composition brings great difficulties in studying the aging mechanism. Thus, this study tries to better understand the aging mechanism by evaluating the aging performance for 39 model compound aging tests performed at 80°C for 72 h. Four kinds of reactions (self-condensation, esterification, aldol condensation, and phenol, and aldehyde reaction) were investigated to understand the contribution of various compounds and reactions during the aging process. It has been found that acids played an important role in the aging process, as these acted as the reactant in the esterification reaction and acted as the catalyst for aldol condensation and phenol and aldehyde reaction. Acids and alcohols reacted *via* the esterification reaction, resulting in the decline of aliphatic C-O bonds. Due to the absence of acids, aromatic compounds were relatively stable in these tests. In comparison, aldehydes and HMF were active since self-condensation reactions for these chemicals were observed in the absence of acids. Moreover, with the aid of acids, HMF showed high tendency toward polymerization during the accelerated aging process.

Keywords: bio-oil, aging mechanism, model compounds, ^{1}H NMR, accelerated aging process

OPEN ACCESS

Edited by:
Li Shuai,
Fujian Agriculture and Forestry University, China

Reviewed by:
Xun Hu,
University of Jinan, China
Kwang Ho Kim,
Korea Institute of Science and Technology (KIST), South Korea
Yuan Xue,
Shanghai Jiao Tong University, China

***Correspondence:**
Haoxi Ben
benhaoxi@gmail.com

Specialty section:
This article was submitted to Bioenergy and Biofuels, a section of the journal Frontiers in Energy Research

Received: *04 March 2020*
Accepted: *14 April 2020*
Published: *27 May 2020*

Citation:
Wang R and Ben H (2020) Accelerated Aging Process of Bio-Oil Model Compounds: A Mechanism Study. Front. Energy Res. 8:79. doi: 10.3389/fenrg.2020.00079

INTRODUCTION

Biomass is viewed as a promising renewable energy source, which can produce various forms of biofuels and biomaterials without contributing to new CO_2 in the atmosphere (Ragauskas, 2006; Yang et al., 2015). Among different types of conversion methods for biomass, pyrolysis, performed in an anaerobic environment, is one of the most effective and convenient strategies to convert biomass feedstock into useful products (Zhang et al., 2018). Bio-oil, derived from the thermal breakdown of cellulose, hemicellulose, tannin, and lignin, is a mixture of multiple organic substances. Moreover, bio-oil, with characteristics of low sulfur and nitrogen, is considered the precursor of biofuel, owing to its relatively high energy density and ease of transportation and storage.

However, the application of bio-oil is limited due to a number of undesirable properties; one is its aging problem, which results in chemical and physical changes of bio-oil such as high and changing water content, acidity, and molecular weight. Due to the dehydration reaction during the pyrolysis process, typically, pyrolysis bio-oil contains relatively high levels of water content, and the water content increases during bio-oil storage as water is produced by bio-oil aging reactions (Chaala et al., 2004). Chemically, bio-oil has high acidity (pH ∼2–3) (Alsbou and Helleur, 2014), and this acidic environment and the various organic compounds present in bio-oil play an important role in the bio-oil aging process. Therefore, several upgrading processes have been applied to optimize the deleterious properties of pyrolysis oil. The upgrading technologies, including hydrodeoxygenation (HDO), catalytic cracking, hydrogenation (HYD), and selective ring opening (SRO), show strong abilities to improve the quality of raw bio-oil, since these technologies can convert oxygen-enriched pyrolysis oil into renewable fuels and increase the content of valuable chemicals in bio-oil (Ma et al., 2018; Ben et al., 2019). However, it was found that during the hydrodeoxygenation process, polymerization, and hydrogenation have comparative reaction rates and even the polymerization process is relatively faster than the hydrogenation process, which could result in the deactivation of catalysts and bring more difficulties in the upgrading process (Hu et al., 2013; Luo et al., 2018). Therefore, expanding the knowledge of the bio-oil aging process, which brings changes in the physical and chemical properties of bio-oil and bring more problems in the upgrading process, is important for later application of bio-oil and the upgrading process. The study of the aging process of raw bio-oil can help understand how and why aging occurs, which later is crucial in taking any possible actions to plan for the upgrading process of bio-oil. To reveal the underlying mechanism of the aging process, great efforts have been made. Meng et al. (2014) proposed that the increasing temperature and presence of acids are responsible for the increase in the molecular weight of bio-oil. Increasing water content is observed during the aging process, as water is a by-product of the condensation reaction (Joseph et al., 2016). Reactive substances such as aldehydes, alcohols, and olefins reacting *via* the condensation reaction result in chemical changes of bio-oil (Alsbou and Helleur, 2014). This knowledge plays a very important role in expanding our understanding of aging and studying the aging process of bio-oil. However, the extreme complexity of bio-oil has brought great difficulties in studying the aging of bio-oil since there are more than 300 chemicals in bio-oil, and the aging mechanism of bio-oil is still not totally understood. Compared with the complex environment of bio-oil, the model compound simplifies the aging process of bio-oil, which is beneficial in analyzing the changes of single substances. Therefore, applying model compounds in bio-oil aging study helps provide more insights into the bio-oil aging mechanism at the molecular level, which few studies focused on.

In this work, an investigation on bio-oil aging reactions at a specified temperature has been performed to reveal the contribution of main reactive compounds and main reactions that cause bio-oil aging. To simplify and get specific information about the bio-oil aging mechanism, a number of model compounds representing the bio-oil derived from the cellulose and hemicellulose part and bio-oil derived from the lignin and tannin part were applied in this study. The use of these model compounds offer advantages for elucidating the role of each compound during the aging process. Additionally, deepening the understanding of this is essential in stabilizing bio-oil and optimizing the desirable properties of bio-oil.

EXPERIMENTAL SECTION

Materials

Hundreds of ingredients, produced from major components of biomass—lignin, tannin, cellulose, and hemicellulose—are found in bio-oil, which complicates the aging mechanism of bio-oils. Cellulose and hemicellulose make a significant contribution to sugar and sugar derivative formation, and lignin, and tannin are the main sources of aromatics (Wu et al., 2009; Ben and Ragauskas, 2011; Qu et al., 2011; Kibet et al., 2012; Vinu and Broadbelt, 2012; Mu et al., 2013; Huang et al., 2014). Therefore, a series of typical bio-oil model compounds, which are divided into two categories, cellulose and hemicellulose part (**Figure 1A**) and lignin and tannin part (**Figure 1B**), was chosen to simplify and get specific information about the bio-oil aging mechanism. 5-Hydroxymethylfurfuraldehyde (HMF), 2-furaldehyde (furfural), hydroxyacetone, glycolaldehyde dimer, and 4-allyl-2-hydroxybenzaldehyde contain more than one oxygen-containing functional group, which activates these compounds during the aging process. Therefore, these substances are individually heated for aging experiments named self-condensation test. Ben and Ragauskas (2012) observed a decrease in aliphatic C-O bonds and aromatic C-H bonds and an increase in aliphatic C-C bonds and aromatic C-C and C-O bonds during the accelerated aging process for various types of bio-oils at 80°C. Alcohols and acids, present in large quantities in bio-oil, can react *via* the esterification reaction, which consumes C-O bonds. It is well known that bio-oil has high acidity, and novolak resin and water could be formed since aldehyde hydrates can react with phenols and substituted phenols under acidic conditions (Yu et al., 2018). This reaction leads to increases in C-C bonds and water content, which affect the aging performance of bio-oil. Moreover, aldol condensation is catalyzed by acids, during which the number of C=O bonds declines and the number of C-C bonds increases (Patil and Lund, 2011; Patil et al., 2012; Hu et al., 2013). Therefore, four kinds of reactions (**Figure 2**), self-condensation, esterification, aldol condensation, and phenol and aldehyde reaction, were employed to study the bio-oil aging mechanism and the roles of all these reactions. All experimental materials used in this study were bought from Sigma-Aldrich and were used directly without further processing.

Experimental Procedure

The experiment was performed in a 2 ml threaded brown sample vial (11.6*32 mm). Typically, model compounds (0.001 mole for each model compound) were mixed 1: 1 (by mole) and loaded in the sample vial at room temperature. The mouth of the sample vial was sealed to ensure that the internal materials would not

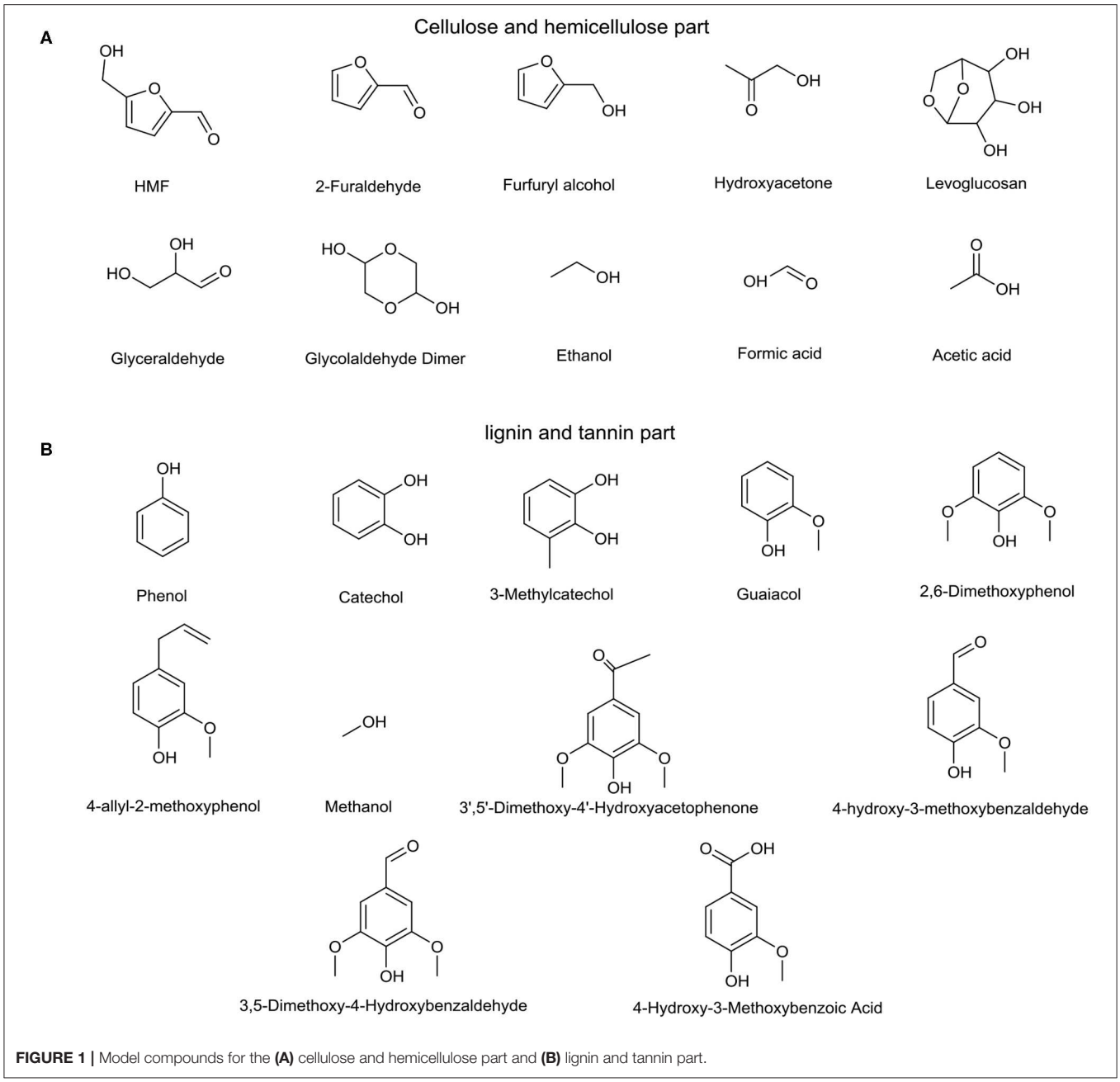

FIGURE 1 | Model compounds for the **(A)** cellulose and hemicellulose part and **(B)** lignin and tannin part.

overflow during the experiment process and the external gas would not affect the reaction. Then, the vial was placed in an oil pan and heated at 80°C for 72 h (Diebold and Czernik, 1997; Oasmaa and Kuoppala, 2003; Elliott et al., 2012; Meng et al., 2014). All model compound aging tests were repeated three times to ensure accuracy.

Analytical Method

^{1}H NMR Analysis

The products were analyzed by using a Bruker Avance/DMX 400 MHz NMR spectrometer. Quantitative ^{1}H NMR results were acquired with eight transients and a 5-s pulse delay. The MestReNova software was used to analyze the results of the experiments. In addition, the MestReNova software has the capacity to predict the ^{1}H NMR results of model compounds, which allows us to compare the changes in the model compounds before and after aging to clarify the aging mechanism. However, during the data analysis process, the inaccuracy of some ^{1}H NMR predictions of model compounds was found. In order to correct these errors, additional quantitative ^{1}H NMR tests of HMF, glycolaldehyde dimer, furfural, hydroxyacetone, levoglucosan, furfuryl alcohol, 4-allyl-2-hydroxybenzaldehyde, and glyceraldehyde were performed.

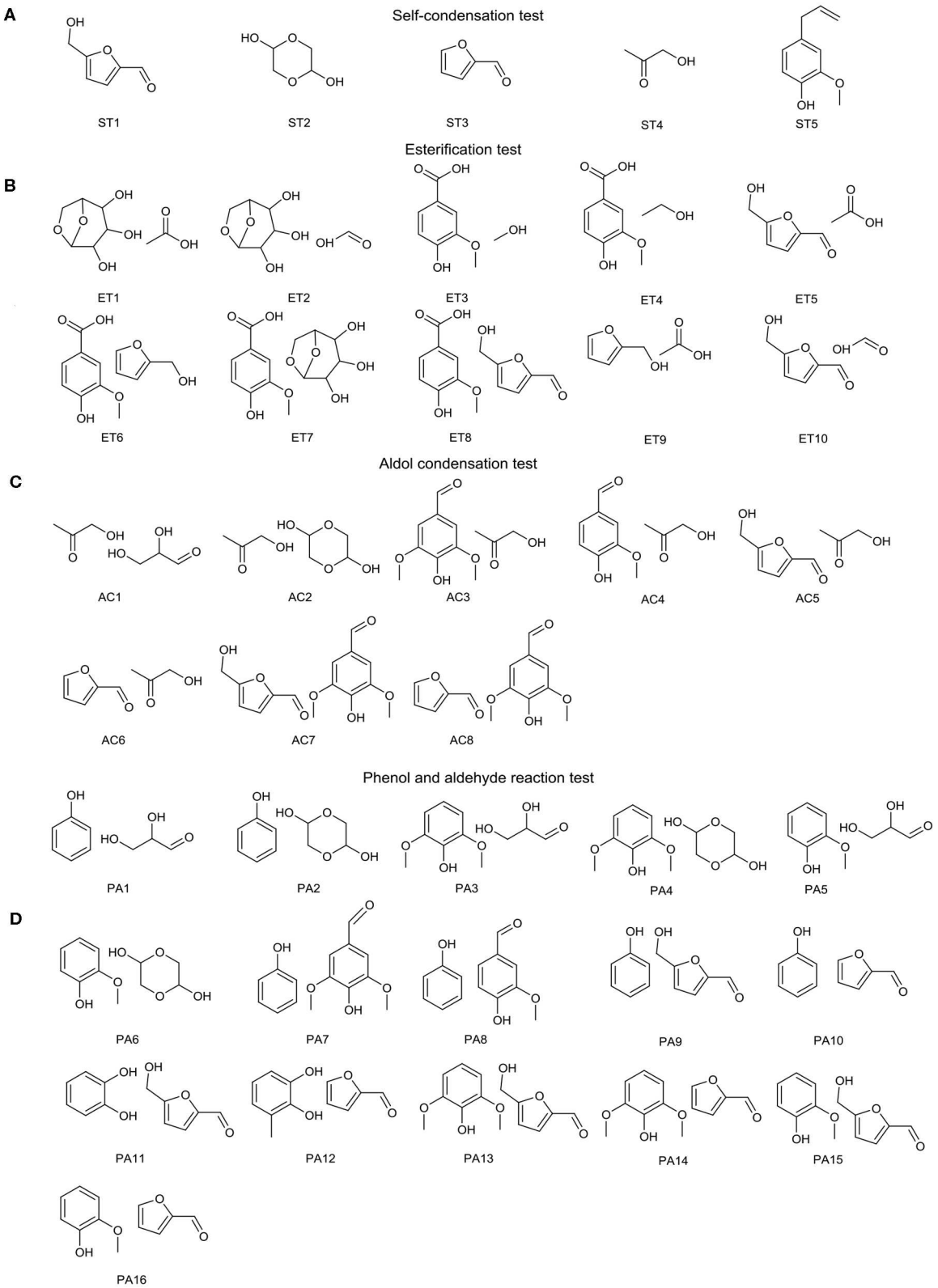

FIGURE 2 | Specific details of the **(A)** self-condensation test, **(B)** esterification test, **(C)** aldol condensation test, and **(D)** phenol and aldehyde reaction test (all experiments were heated at 80°C for 72 h).

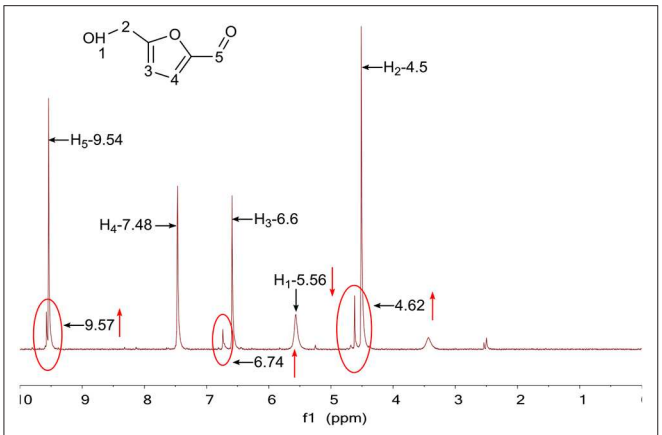

FIGURE 3 | ^{1}H NMR results for HMF after the aging process.

GC-MS Analysis

A Shimadzu GC-MS (GCMS-QP2010 SE) spectrometer was used to analyze the products. During the analysis process, the initial temperature was set as 40°C, and this temperature was maintained for 4 min. Later, the temperature was increased to 250°C at a heating rate of 25°C/min. Each compound was identified by comparing its mass spectrum with the standard mass spectrum in the spectral library.

RESULTS AND DISCUSSION

Self-Condensation Test

^{1}H NMR results for HMF before and after the accelerated aging process for 72 h are provided in **Figure S1** and **Figure 3**. Different from HMF that did not undergo aging processing, the aged HMF had three more peaks (4.62, 6.74, and 9.57 ppm) in the ^{1}H NMR spectrum, which were slightly shifted to the left compared with the original peaks (4.51, 6.59, and 9.54 ppm). These left-shifted peaks indicate that the overall structure of HMF did not change a lot, and only a part of the structures reacted. In addition, a decrease of the peak at 5.56 ppm, representing the hydroxyl functional groups of HMF, was observed after the aging process. This reduced functional group content is evidence that the hydroxyl functional group was chemically active and reacted with other parts of HMF. **Table S1** lists the identified compounds in HMF aging; it could be found that HMF decreased in abundance with aging. In contrast, 2,5-furandicarboxaldehyde and cirsiumaldehyde had an increase in abundance, and cirsiumaldehyde was the dehydration product of HMF, which is consistent with the observation of a decrease in hydroxyl groups found in ^{1}H NMR results.

For the glycolaldehyde dimer, significant changes have taken place in this chemical after the aging process. When comparing the spectra of the glycolaldehyde dimer before (**Figure 4A**) and after (**Figure 4B**) the aging process, it can be seem that all hydrogen signals for the glycolaldehyde dimer greatly decreased. In addition, after careful comparison of the ^{1}H NMR results before and after the aging process, it can be observed that the peaks of the aged glycolaldehyde dimer coincided with the peaks of the original impurities in the glycolaldehyde dimer (**Figure 4C** depicts an enlarged view of the bottom of the glycolaldehyde dimer spectrum, showing the peaks for impurities in the glycolaldehyde dimer), which suggests that almost no glycolaldehyde dimer was left after the aging process and polymerization may occur between glycolaldehyde dimers.

Interestingly, different from HMF and the glycolaldehyde dimer, although furfural, hydroxyacetone, and 4-allyl-2-hydroxybenzaldehyde have many active functional groups such as hydroxyl and carbonyl, these substances were stable after the aging process. ^{1}H NMR results before and after the aging process for furfural, hydroxyacetone, and 4-allyl-2-hydroxybenzaldehyde are listed in **Figures S2–S7**.

Esterification Test

In the case of ET1 (**Figure 5A**) and ET2 (**Figure 5B**), levoglucosan (^{1}H NMR result for levoglucosan without the aging process is shown in **Figure S8**) was mixed with acetic acid or formic acid; the disappearance of hydroxyl groups (4.77, 4.83, and 4.90 ppm) was observed and a number of new peaks appeared. Although hydrolysis was the main reaction for levoglucosan to form glucose, this product appeared only when the temperature exceeded 90°C (Hu et al., 2013), which suggests that levoglucosan reacted with acids as the alcohol at 80°C. Therefore, these three disappearing peaks and new peaks represent the occurrence of the esterification reaction. The number of aliphatic C-O bonds was greatly reduced due to the esterification reaction of levoglucosan, present in high abundance in pyrolysis (Helle et al., 2007; Yu et al., 2016).

ET5 examined the aging performance of the mixture of HMF and acetic acid, and the result is depicted in **Figure 5C**. It is shown in the spectrum that parts of the peak at 2.08 ppm for acetic acid and the peak at 9.54 ppm for HMF were shifted to the left side of their original peaks, meaning that both these substances were involved in the reaction. Moreover, these left-shifted peaks coincided with the peaks of the methyl (2.14 ppm) and carbonyl groups (9.61 ppm) on the esterification products of HMF and acetic acid, which was the evidence of the occurrence of the esterification reaction between these two reactants. Interestingly, in the case of ET8 (**Figure 5D**), although 4-hydroxy-3-methoxybenzoic acid contains a carboxyl group, no esterification reaction was observed between this substance and HMF. In this case, 4-hydroxy-3-methoxybenzoic acid was stable and the change of HMF was the same as the change of HMF aged alone, representing that the addition of 4-hydroxy-3-methoxybenzoic acid had no effect on HMF. In the presence of acetic acid, furfuryl alcohol (the ^{1}H NMR result for furfuryl alcohol without aging processing is shown in **Figure S9**, and the result for ET9 is shown in **Figure 5E**) was catalyzed to polymerize, as all signals for furfuryl alcohol greatly declined compared with the signals for acetic acid. Under the catalysis of acids, a carbocation would be formed from furfuryl alcohol, attaching another furfuryl alcohol *via* the electrophilic substitution reaction, as presented in **Figure 6A** (Hu et al., 2013). HMF was catalyzed by formic acid toward polymerization since no HMF was left after aging treatment

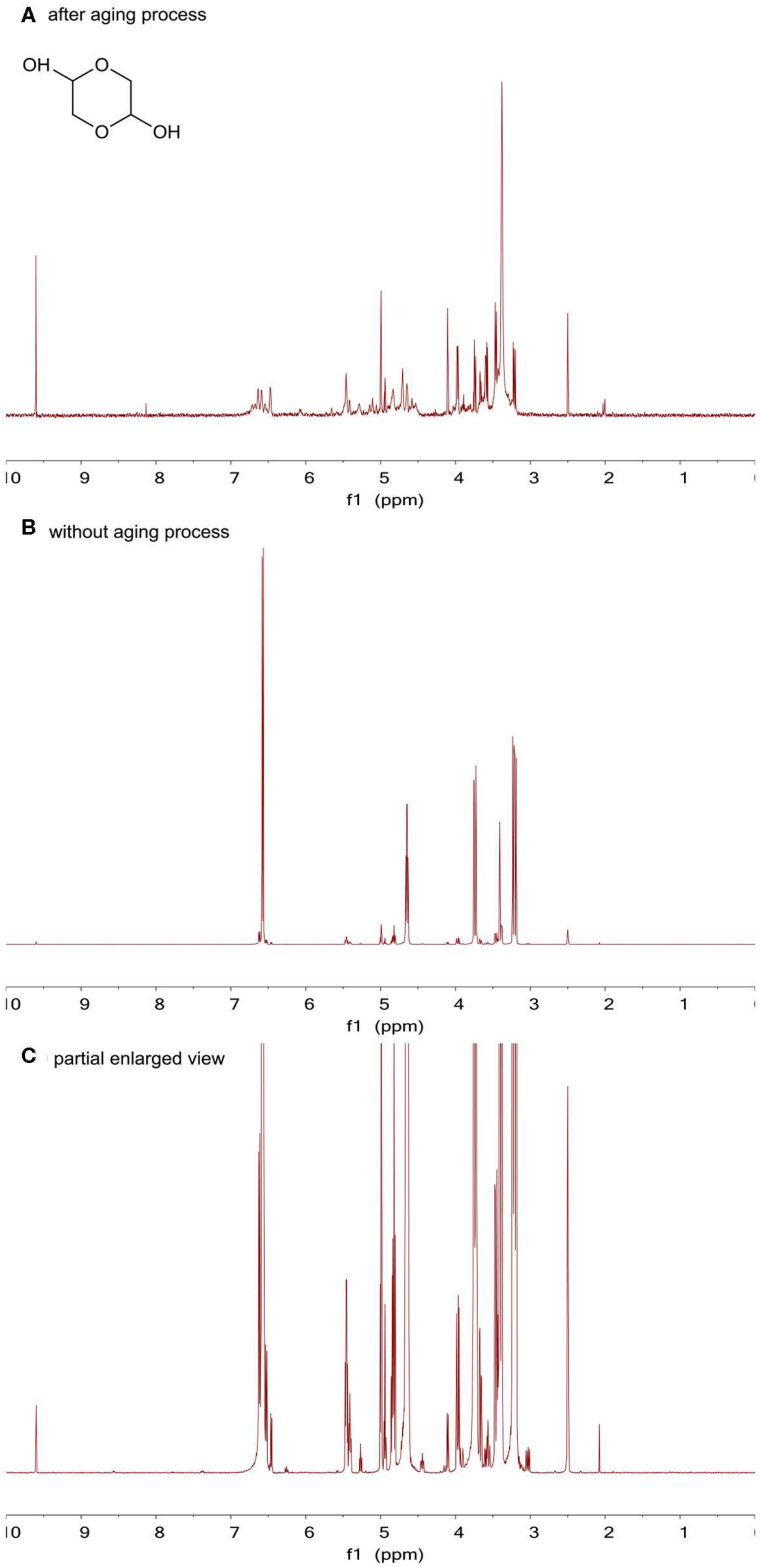

FIGURE 4 | (A) ^{1}H NMR results for the glycolaldehyde dimer after the aging process, **(B)** ^{1}H NMR results for the glycolaldehyde dimer without the aging process, and **(C)** an enlarged view of the bottom of the glycolaldehyde dimer spectrum.

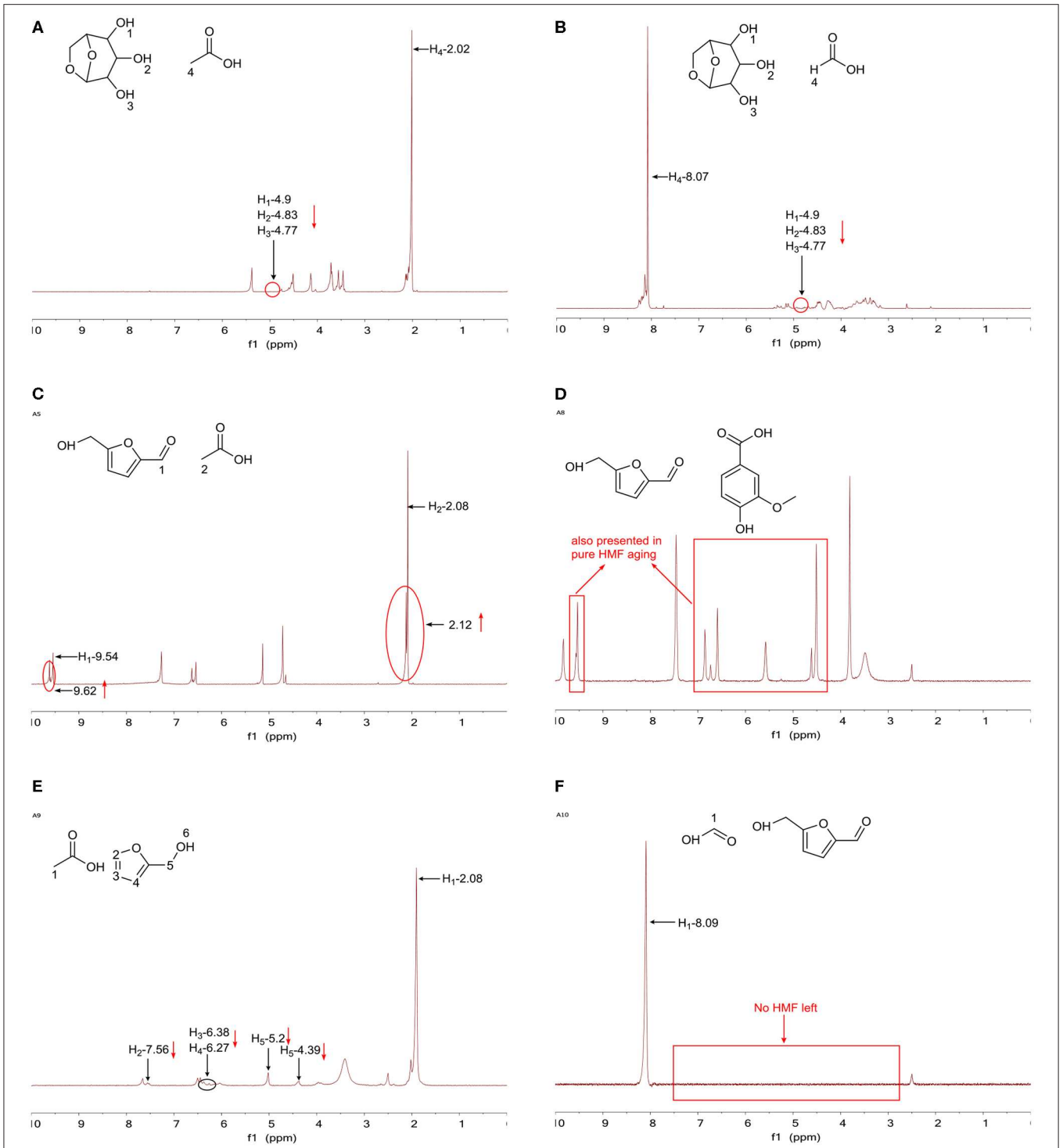

FIGURE 5 | ^{1}H NMR results for **(A)** ET1 after the aging process, **(B)** ET2 after the aging process, **(C)** ET5 after the aging process, **(D)** ET8 after the aging process, **(E)** ET9 after the aging process, and **(F)** ET10 after the aging process.

(**Figure 5F**). In addition, the formation of humins, a kind of dark-colored and tarry solids, was observed during the aging process. Patil et al. (2012) discovered the most likely pathway for humin formation, which showed that under acid catalysis, HMF formed 2,5-dioxo-6-hydroxyhexanal (DHH), an important intermediate for humin growth, and later *via* aldol addition/condensation, polymerization between DHH and HMF occurred (**Figure 6B**). In addition, the acid only played the role of a catalyst and did

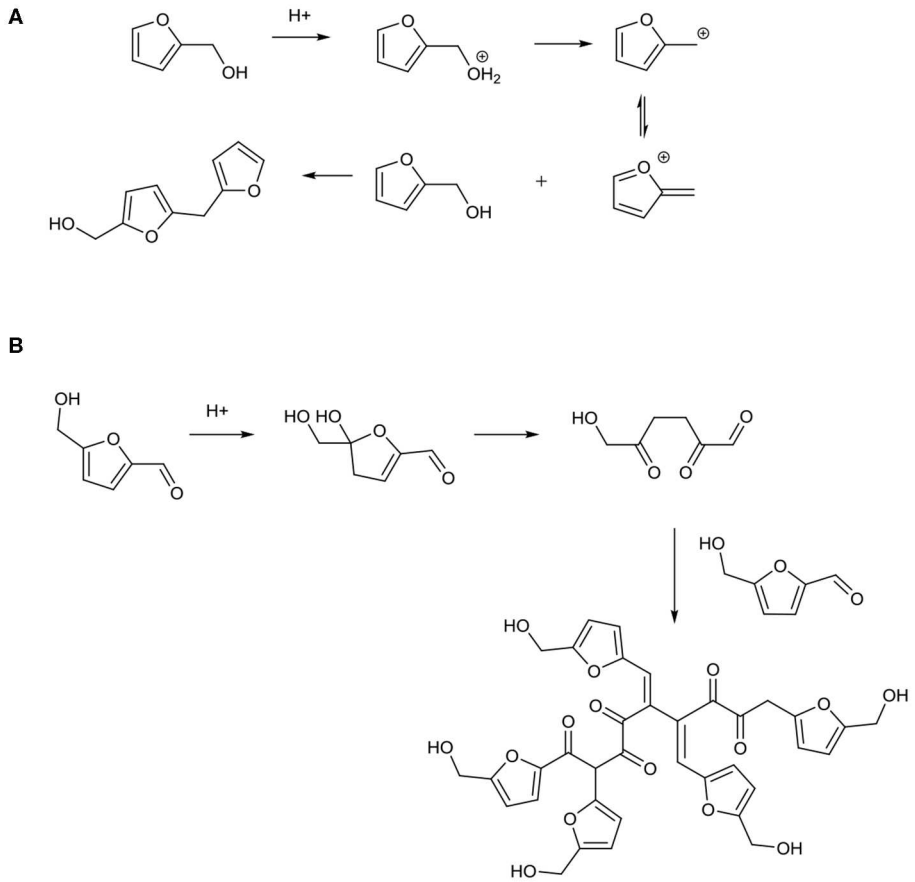

FIGURE 6 | Reaction mechanism of **(A)** furfuryl alcohol in the presence of acetic acid and **(B)** HMF in the presence of formic acid.

not participate in the reaction since no reduction in formic acid hydrogen signals was observed. Almost no reaction occurred in the case of ET3, ET4, ET6, and ET7, and these results are presented in **Figures S10–S13**.

Comparing ET5, ET8, and ET10, it can be found that the reaction mechanisms of HMF with different acids were different. 4-Hydroxy-3-methoxybenzoic acid, formic acid, and acetic acid have different pKa values (acidity), which may be the reason for the different reaction mechanisms (Hu et al., 2013; Meng et al., 2014). Compared with formic acid and acetic acid, 4-hydroxy-3-methoxybenzoic acid is so weak that it will not react with HMF. The acidity of acetic acid is stronger than that of 4-hydroxy-3-methoxybenzoic acid but weaker than that of formic acid, and it undergoes esterification with HMF. Moreover, formic acid shows high acidity; it can catalyze HMF toward polymerization. A similar situation can be observed in ET6 and ET9. Thus, it can be hypothesized that furan derivatives containing hydroxyl groups such as HMF and furfuryl alcohol are active compounds in bio-oil and the reaction mechanism of these substances with acid changes with the acidity of the acid. With increasing acidity, the following reactions occur in order: no reaction, esterification (consume aliphatic C-O bond and form water), and condensation reaction (tend to polymerize and form water).

Aldol Condensation Test

As shown in **Figure 7**, reactions between glyceraldehyde (**Figure S14**) and hydroxyacetone were observed, as almost all peaks for glyceraldehyde disappeared and a decrease in the methyl peak of hydroxyacetone was observed (the integration of the peak at 4.03 ppm: the integration of the peak at 2.03 ppm = 1: 1.27). These changes also suggest that a condensation reaction may occur in the mixture *via* aldol condensation reaction since the dual functionality of glyceraldehyde and hydroxyacetone (aldehyde and alcohol) made these chemicals active toward condensation reactions. Hydroxyacetone and the glycolaldehyde dimer contain various active functional groups such as hydroxyl and carbonyl, and it seems that the reaction between these two chemicals is very easy. However, the ^{1}H NMR result (**Figure S15**) showed that these two substances did not react with each other after the 72-h aging process. Although the hydroxyacetone and the glycolaldehyde dimer were mixed together, these two substances did not react with each other, and the spectrum of AC2 was like combining the spectra of aged hydroxyacetone and aged glycolaldehyde dimer together. ^{1}H NMR results for AC3, AC4, AC5, AC6, AC7, and AC8 are presented in **Figures S16–S21**, which show that these mixtures were stable after aging. Although phenolic compounds can be

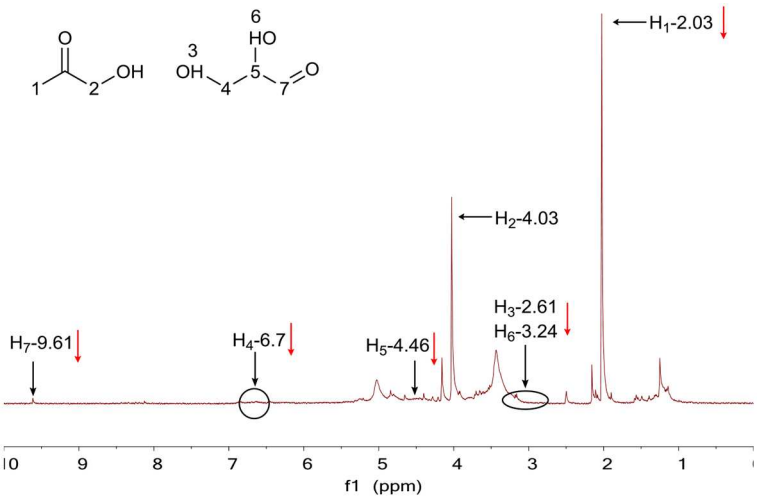

FIGURE 7 | ^{1}H NMR result for AC1 after the aging process.

regarded as weak acids, they are too weak to catalyze the aldol condensation reaction as shown in AC3, AC4, AC7, and AC8, suggesting that the presence of carboxylic acids may be the key to aldol condensation reactions (Patil and Lund, 2011; Patil et al., 2012). Interestingly, in AC5 and AC7 tests, no left-shifted peaks were discovered for HMF and almost no reaction occurred for it, indicating that HMF was relatively stable in these mixtures. The mechanism of this phenomenon is still unclear, and further research is needed.

Almost no obvious aldol condensation reaction was observed in these chosen tests; it seems that the acidic environment was very important during the reaction. The original low pH value of bio-oil and increasing acidity during the bio-oil aging process provided good reaction conditions for aldol condensation (Joseph et al., 2016; Jo et al., 2018), during which the number of C=O bonds decreased. It was found that benzaldehyde could be added to HMF *via* aldol condensation during acid-catalyzed conversion, which demonstrates the possibility of increasing the values of humins (Patil and Lund, 2011). In addition, water was formed as a by-product of aldol condensation or other condensation reactions of aldehydes and ketones, explaining the increase in water during the aging process (Naske et al., 2012).

Phenol and Aldehyde Reaction Test

After the 72-h aging process, phenol was found to be stable in the PA1 test since the hydrogen signals for it did not change after aging treatment, which evidently meant that phenol did not react with glyceraldehyde, as shown in **Figure 8A**. Furthermore, the reaction for glyceraldehyde itself is observed in **Figure 8A**, but to a limited extent, as the peaks for glyceraldehyde (2.50, 3.23, 4.52, and 9.63 ppm) decreased and a few small new peaks (1.0–5.5 ppm) appeared in the spectrum. Due to the dual functionality of glyceraldehyde (alcohol and aldehyde), different kinds of reactions would occur, which could explain the appearance of these new peaks. Moreover, although phenol could play the role of a weak acid, no cross-linking reaction was found in the PA1 test, indicating that phenol was too weak to catalyze the reaction. The same phenomenon was also found in PA3 (**Figure 8B**) and PA5 tests (**Figure 8C**), where phenolic compounds were stable and glyceraldehyde had the same peak distribution as that of glyceraldehyde in PA1. Thus, all these three tests indicated that the reaction between phenol and aldehyde required strong acids or a higher temperature (>80°C). From the ^{1}H NMR results of PA2 (**Figure S22**), PA4 (**Figure S23**) and PA6 (**Figure S24**), it could be concluded that phenolic components would not react with the glycolaldehyde dimer and they have no catalytic effect on the glycolaldehyde dimer, as the spectra of these three tests, after removing the hydrogen signals for phenolic compounds from the spectra, were basically consistent with the spectrum of the glycolaldehyde dimer self-condensation test. No more reaction was found in PA7-16, presented in **Figures S25–S34**. However, the stability of HMF was also discovered in PA9, PA11, PA13, and PA15, which was the same as the observation in AC5 and AC7. To examine whether HMF is stable in phenolic mixtures, an additional GC-MS test has been done for the aging test of the mixture of HMF and guaiacol. **Table S2** lists the identified compounds in PA15 aging; from the analysis, it can be seen that HMF is stable in guaiacol, a typical model compound for lignin pyrolysis bio-oil. Therefore, it can be suggested that it is easy for HMF to maintain stability in phenolic mixtures.

Same as the aldol1 condensation test part, due to the absence of an acid catalyst, no obvious reaction between phenol and aldehyde was found in this section. It is well known that with the aid of an acid, the formation of phenolic resins could be observed from the reaction between phenol and formaldehyde, furfural, or HMF, and this could be the reason for the increase in C-C bonds and the decrease in C=O bonds. In addition, under the catalysis of a proper acid, glycolaldehyde was found to react with phenol to a limited extent (Meng et al., 2014). All this existing knowledge indicates that in the acidic environment of bio-oil, the phenol and aldehyde selected in this section are likely to react with each other, which could explain the increase in C-C bonds and the decrease in C=O bonds during the aging process.

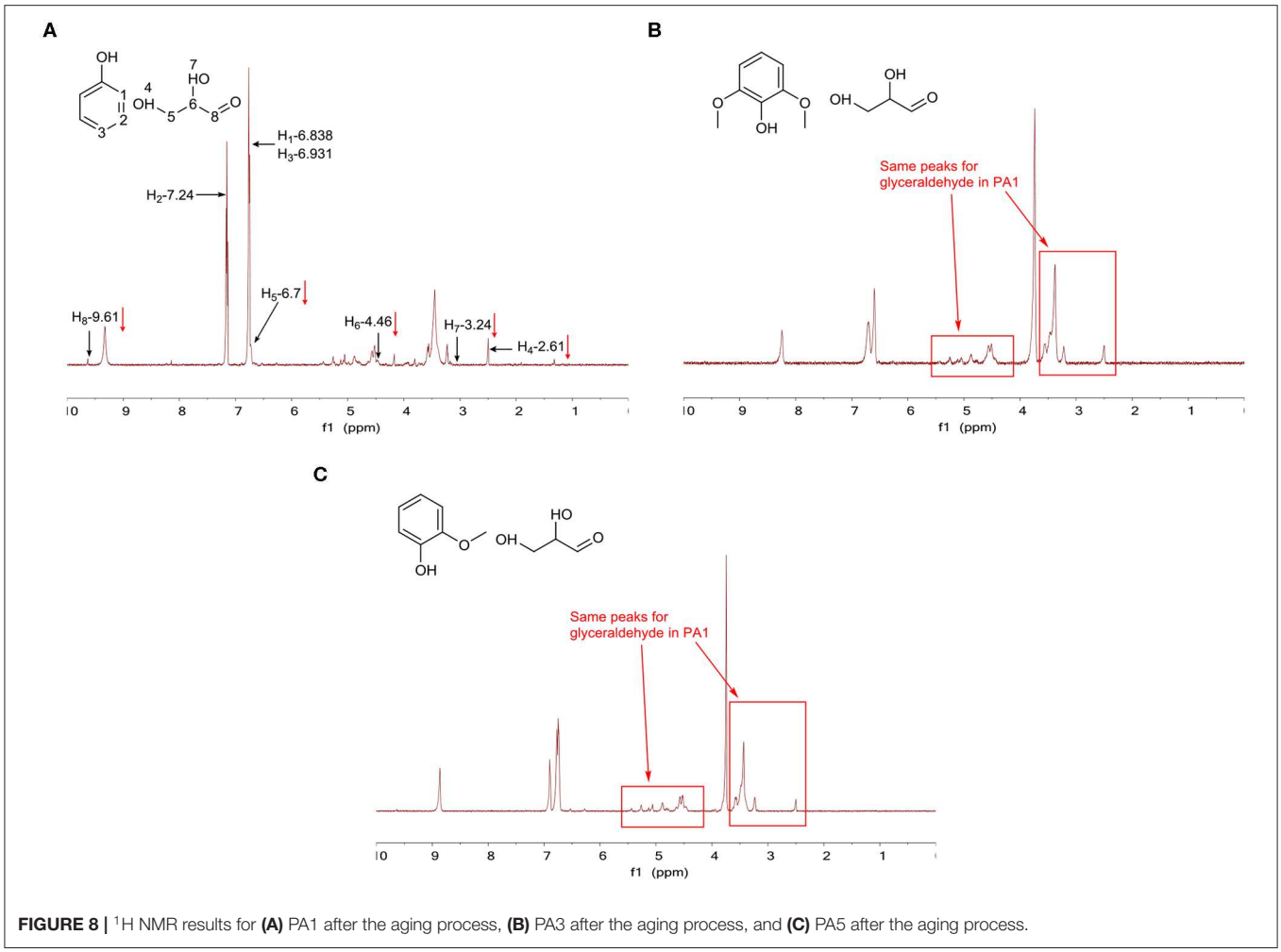

FIGURE 8 | ^{1}H NMR results for **(A)** PA1 after the aging process, **(B)** PA3 after the aging process, and **(C)** PA5 after the aging process.

The Role of Different Model Compounds

Different kinds of model compounds played significantly different roles in various reactions. Acids, especially formic acid and acetic acid, were the most reactive compounds in bio-oil, as acids could act as both reactants and catalysts in various reactions. For example, at a low temperature (80°C), formic acid can react with levoglucosan *via* esterification (**Figure 6**). In comparison, at a high temperature (>90°C), it is well known that with the aid of formic acid, levoglucosan tends to undergo hydrolysis to form glucose and glucose further reacts to form small molecules (Hu et al., 2013). Due to the different acidities of different acids, their catalytic abilities present in reactions are also different. The ^{1}H NMR results of HMF in the presence of acetic acid, 4-hydroxy-3-methoxybenzoic acid, or formic acid are presented in **Figures 5C,D,F**. In addition, phenolic compounds, as a kind of weak acid, show little catalytic effect at a low temperature (80°C). It can be concluded that removing acids from bio-oil and increasing the pH value of bio-oil would effectively slow the aging rate of bio-oil.

Aldehydes, sugars, and their derivatives, with different kinds of oxygen-containing functional groups, are the main components of bio-oils produced by pyrolysis of cellulose and hemicellulose, which contribute a lot to the aging of bio-oil. From the experiments above, HMF and the glycolaldehyde dimer are found to be highly reactive compounds in bio-oil, since reactions can be observed when these two substances are heated alone. Moreover, for furan and furan derivatives, with the presence of proper acids, these chemicals showed high tendency toward polymerization, which is closely related to the furan ring that they have. Moreover, under the catalysis of acid, a condensation reaction such as aldol condensation reaction can be observed for aldehyde, resulting in a decrease in C=O bonds and increases in the water content and molecular weight of bio-oil.

Aromatic compounds are found to relatively stable at a low temperature (80°C). Although phenolic compounds can be viewed as weak acids, the catalytic effect of phenolic compounds is not obvious, which indicates that a higher temperature may be needed. Even aromatic compounds containing carboxyl groups do not show significant catalytic effect. However, with the proper treatment of acids, new C-C bonds formed between phenolic compounds and aldehydes can be found and this reaction would significantly accelerate the aging of bio-oil.

In the case of model compound aging tests, the aging mechanism of bio-oil was investigated at the molecular level,

which was rarely studied. Due to the use of model compounds, reactive substances have been identified and some possible reaction pathways have been proposed. However, there are still shortcomings of this study since none of these aging reactions can be verified in bio-oil or a similar environment. For example, aldol condensation and phenol and aldehyde reaction are expected to occur in bio-oil during the aging process, but due to the absence of acids, no obvious reactions are found in this work. If acids are added in these two kinds of reactions, it can be expected that the number of C=O bonds will decrease, as both of these two reactions consume C=O bonds. Therefore, considering that bio-oil contains hundreds of compounds, more aging tests related to bio-oil should be examined in future research to gain more insights into the bio-oil aging mechanism.

CONCLUSION

To elucidate the roles of different components of bio-oil and various reactions that may occur in the bio-oil aging process, pyrolysis model compounds have been employed to explore more information about the aging process. Thirty-nine model compound aging tests have been chosen to deepen the understanding of aging mechanism, which were divided into four parts, self-condensation, esterification, aldol condensation, and phenol and aldehyde reaction, and these tests were performed at 80°C for 72 h. It can be concluded from the experiments that small acids, aldehydes, and HMF are the most active molecules in the model compound study. Acids play an important role in aging process, as these can be used not only as a reactant but also as a catalyst for the reaction. Therefore, it can be concluded that acidity is an important factor affecting the aging process of bio-oil. In the esterification test section, a decrease in the number of aliphatic C-O bonds was observed since acids and alcohols reacted *via* the esterification reaction. Although in this study, due to the absence of acids, no obvious reaction was observed in the aldol condensation reaction section and phenol and aldehyde reaction section; the reactions for aldehydes were observed. Sugar and sugar derivatives showed high tendency toward condensation reaction in the presence of acids. Especially for HMF, this chemical presented totally different reaction mechanisms with the aid of different acids due to the multiple functional groups of HMF.

DATA AVAILABILITY STATEMENT

The original contributions presented in the study are included in the article/supplementary materials, further inquiries can be directed to the corresponding author/s.

AUTHOR CONTRIBUTIONS

RW and HB contributed to the conception and design of the study. RW performed the statistical analysis and wrote the first draft of the manuscript. All authors contributed to manuscript revision and read and approved the submitted version.

FUNDING

The authors would like to acknowledge the financial support from the National Science Foundation of China [51706044], the Natural Science Foundation of the Jiangsu of China [BK20170666], and the Recruitment Program for Young Professionals in China.

SUPPLEMENTARY MATERIAL

The Supplementary Material for this article can be found online at: https://www.frontiersin.org/articles/10.3389/fenrg.2020.00079/full#supplementary-material

REFERENCES

Alsbou, E., and Helleur, B. (2014). Accelerated aging of bio-oil from fast pyrolysis of hardwood. *Energ. Fuel.* 28, 3224–3235. doi: 10.1021/ef500399n

Ben, H., and Ragauskas, A. J. (2011). Heteronuclear single-quantum correlation–nuclear magnetic resonance (HSQC–NMR) fingerprint analysis of pyrolysis oils. *Energ. Fuel.* 25, 5791–5801. doi: 10.1021/ef201376w

Ben, H., and Ragauskas, A. J. (2012). *In situ* NMR characterization of pyrolysis oil during accelerated aging. *ChemSusChem* 5, 1687–1693. doi: 10.1002/cssc.201200429

Ben, H., Wu, Z., Han, G., Jiang, W., and Ragauskas, A. (2019). *In-situ* evaluation for upgrading of biomass model compounds over noble metal catalysts by isotopic tracing and NMR monitoring. *J. Anal. Appl. Pyrol.* 137, 253–258. doi: 10.1016/j.jaap.2019.05.005

Chaala, A., Ba, T., Garcia-Perez, M., and Roy, C. (2004). Colloidal properties of bio-oils obtained by vacuum pyrolysis of softwood bark: aging and thermal stability. *Energ. Fuel.* 18, 1535–1542. doi: 10.1021/ef030156v

Diebold, J. P., and Czernik, S. (1997). Additives to lower and stabilize the viscosity of pyrolysis oils during storage. *Energ. Fuel.* 11, 1081–1091. doi: 10.1021/ef9700339

Elliott, D. C., Oasmaa, A., Preto, F., Meier, D., and Bridgwater, A. V. (2012). Results of the IEA round robin on viscosity and stability of fast pyrolysis bio-oils. *Energ. Fuel.* 26, 3769–3776. doi: 10.1021/ef300384t

Helle, S., Bennett, N. M., Lau, K., Matsui, J. H., and Duff, S. J. B. (2007). A kinetic model for production of glucose by hydrolysis of levoglucosan and cellobiosan from pyrolysis oil. *Carbohyd. Res.* 342, 2365–2370. doi: 10.1016/j.carres.2007.07.016

Hu, X., Wang, Y., Mourant, D., Gunawan, R., Lievens, C., Chaiwat, W., et al. (2013). Polymerization on heating up of bio-oil: a model compound study. *AIChE J.* 59, 888–900. doi: 10.1002/aic.13857

Huang, X., Korányi, T. I., Boot, M. D., and Hensen, E. J. M. (2014). Catalytic depolymerization of lignin in supercritical ethanol. *ChemSusChem* 7, 2276–2288. doi: 10.1002/cssc.201402094

Jo, H., Verma, D., and Kim, J. (2018). Excellent aging stability of upgraded fast pyrolysis bio-oil in supercritical ethanol. *Fuel* 232, 610–619. doi: 10.1016/j.fuel.2018.06.005

Joseph, J., Rasmussen, M. J., Fecteau, J. P., Kim, S., Lee, H., Tracy, K. A., et al. (2016). Compositional changes to low water content bio-oils during aging: an NMR, GC/MS, and LC/MS study. *Energ. Fuel.* 30, 4825–4840. doi: 10.1021/acs.energyfuels.6b00238

Kibet, J., Khachatryan, L., and Dellinger, B. (2012). Molecular products and radicals from pyrolysis of lignin. *Environ. Sci. Technol.* 46, 12994–13001. doi: 10.1021/es302942c

Luo, D., Yin, W., Liu, S., Yang, N., Xia, S., and Ma, P. (2018). Pyrolysis oil polymerization of water-soluble fraction during accelerated aging. *Fuel* 230, 368–375. doi: 10.1016/j.fuel.2018.05.017

Ma, W., Liu, B., Zhang, R., Gu, T., Ji, X., Zhong, L., et al. (2018). Co-upgrading of raw bio-oil with kitchen waste oil through fluid catalytic cracking (FCC). *Appl. Energ.* 217, 233–240. doi: 10.1016/j.apenergy.2018.02.036

Meng, J., Moore, A., Tilotta, D., Kelley, S., and Park, S. (2014). Toward understanding of bio-oil aging: accelerated aging of bio-oil fractions. *ACS Sustain. Chem. Eng.* 2, 2011–2018. doi: 10.1021/sc500223e

Mu, W., Ben, H., Ragauskas, A., and Deng, Y. (2013). Lignin pyrolysis components and upgrading—technology review. *Bioenerg. Res.* 6, 1183–1204. doi: 10.1007/s12155-013-9314-7

Naske, C. D., Polk, P., Wynne, P. Z., Speed, J., Holmes, W. E., and Walters, K. B. (2012). Postcondensation filtration of pine and cottonwood pyrolysis oil and impacts on accelerated aging reactions. *Energ. Fuel.* 26, 1284–1297. doi: 10.1021/ef200541d

Oasmaa, A., and Kuoppala, E. (2003). Fast pyrolysis of forestry residue. 3. storage stability of liquid fuel. *Energ. Fuel.* 17, 1075–1084. doi: 10.1021/ef030011o

Patil, S. K. R., Heltzel, J., and Lund, C. R. F. (2012). Comparison of structural features of humins formed catalytically from glucose, fructose, and 5-hydroxymethylfurfuraldehyde. *Energ. Fuel.* 26, 5281–5293. doi: 10.1021/ef3007454

Patil, S. K. R., and Lund, C. R. F. (2011). Formation and growth of humins via aldol addition and condensation during acid-catalyzed conversion of 5-hydroxymethylfurfural. *Energ. Fuel.* 25, 4745–4755. doi: 10.1021/ef2010157

Qu, T., Guo, W., Shen, L., Xiao, J., and Zhao, K. (2011). Experimental study of biomass pyrolysis based on three major components: hemicellulose, cellulose, and lignin. *Ind. Eng. Chem. Res.* 50, 10424–10433. doi: 10.1021/ie1025453

Ragauskas, A. J. (2006). The path forward for biofuels and biomaterials. *Science* 311, 484–489. doi: 10.1126/science.1114736

Vinu, R., and Broadbelt, L. J. (2012). *A mechanistic model of fast pyrolysis of glucose-based carbohydrates to predict bio-oil composition. Energy Environ. Sci.* 5, 9808–9826.

Wu, Y-m., Zhao, Z-L., Li, H-b. (2009). Low temperature pyrolysis characteristics of major components of biomass. *J. Fuel Chem. Technol.* 37, 427–432. doi: 10.1016/S1872-5813(10)60002-3

Yang, Z., Kumar, A., and Huhnke, R. L. (2015). Review of recent developments to improve storage and transportation stability of bio-oil. *Renew. Sust. Energy Rev.* 50, 859–870. doi: 10.1016/j.rser.2015.05.025

Yu, Y., Chua, Y. W., and Wu, H. (2016). Characterization of pyrolytic sugars in bio-oil produced from biomass fast pyrolysis. *Energ. Fuel.* 30, 4145–4149. doi: 10.1021/acs.energyfuels.6b00464

Yu, Y., Xu, P., Xing, J., Li, L., and Chang, J. (2018). Investigation of aging performance of bio-oil phenol-formaldehyde resin with the treatment of artificial accelerated aging method. *Polym. Eng. Sci.* 58, 1810–1816. doi: 10.1002/pen.24785

Zhang, S., Zhang, H., Liu, X., Zhu, S., Hu, L., and Zhang, Q. (2018). Upgrading of bio-oil from catalytic pyrolysis of pretreated rice husk over Fe-modified ZSM-5 zeolite catalyst. *Fuel Process. Technol.* 175, 17–25. doi: 10.1016/j.fuproc.2018.03.002

Conflict of Interest: The authors declare that the research was conducted in the absence of any commercial or financial relationships that could be construed as a potential conflict of interest.

frontiers in Energy Research

ORIGINAL RESEARCH
published: 05 June 2020
doi: 10.3389/fenrg.2020.00083

Structural Features of Lignin Fractionated From Industrial Furfural Residue Using Alkaline Cooking Technology and Its Antioxidant Performance

*Rui Li†, Xiaohui Wang†, Qixuan Lin, Fengxia Yue, Chuanfu Liu, Xiaoying Wang and Junli Ren**

State Key Laboratory of Pulp and Paper Engineering, School of Light Industry Science and Engineering, South China University of Technology, Guangzhou, China

OPEN ACCESS

Edited by:
Ao Xia,
Chongqing University, China

Reviewed by:
Jorge Rencoret,
Consejo Superior de Investigaciones Científicas (CSIC), Spain
Jixiang Zhang,
China University of Petroleum, China

***Correspondence:**
Junli Ren
renjunli@scut.edu.cn

†These authors have contributed equally to this work

Specialty section:
This article was submitted to Bioenergy and Biofuels, a section of the journal Frontiers in Energy Research

Received: *16 February 2020*
Accepted: *22 April 2020*
Published: *05 June 2020*

Citation:
Li R, Wang X, Lin Q, Yue F, Liu C, Wang X and Ren J (2020) Structural Features of Lignin Fractionated From Industrial Furfural Residue Using Alkaline Cooking Technology and Its Antioxidant Performance. Front. Energy Res. 8:83. doi: 10.3389/fenrg.2020.00083

Furfural, a versatile platform compound, is produced from the hydrolysis of pentose (hemicellulose) in lignocellulosic biomass. The manufacturing of furfural results in the production and accumulation of cellulose- and lignin-rich furfural residue, simultaneously. Reasonable and effective utilization of furfural residue would provide both environmental and economic benefits. In this work, alkali cooking technology was applied to extract lignin from industrial furfural residue. The effects of different alkali treatment conditions on the composition and chemical structure of extracted lignin and solid residue were studied. The results showed that extracted lignin contained abundant guaiacyl (G), syringyl (S), and *p*-hydroxyphenyl (H) structural units, among which the G-type lignin structural unit accounted for the main proportion. The extracted lignin samples were rich in hydroxyl, and the highest content of hydroxyl was 4.02 mM/g under the condition of T3 (135°C−0.35 M). An oxidize resistance test showed that extracted lignin showed a high inhibition effect on DPPH. The increase of lignin content in solid residue was due to the carbonization of cellulose into a lignin-like substance under the condition of a high temperature alkali treatment. This alkali cooking technology is suitable for extracting lignin from furfural residue, which has a promising application as a potential antioxidant in the food and cosmetic industry.

Keywords: furfural residue, alkali treatment, lignin, cellulose, chemical structure

INTRODUCTION

Furfural, a versatile industrial chemical, is regarded as a renewable, indispensable platform compound that is used for organic synthesis, solvents, petroleum refining, and pharmaceuticals. In general, furfural is derived from the dehydration of pentose (hemicellulose) in corncob, bagasse, rice husk, and other agricultural waste (Sun et al., 2008). The demand of market and industrial development drives the huge production of furfural, as about 12–15 t of furfural residue is produced for each ton of furfural production (Sun et al., 2008; Wang et al., 2019). At present, furfural residue is mostly used in the fields of heat generation, soil improvement, plant cultivation, and activated carbon synthesis (Ren et al., 2009; Wang et al., 2017), which is based on the overall utilization of

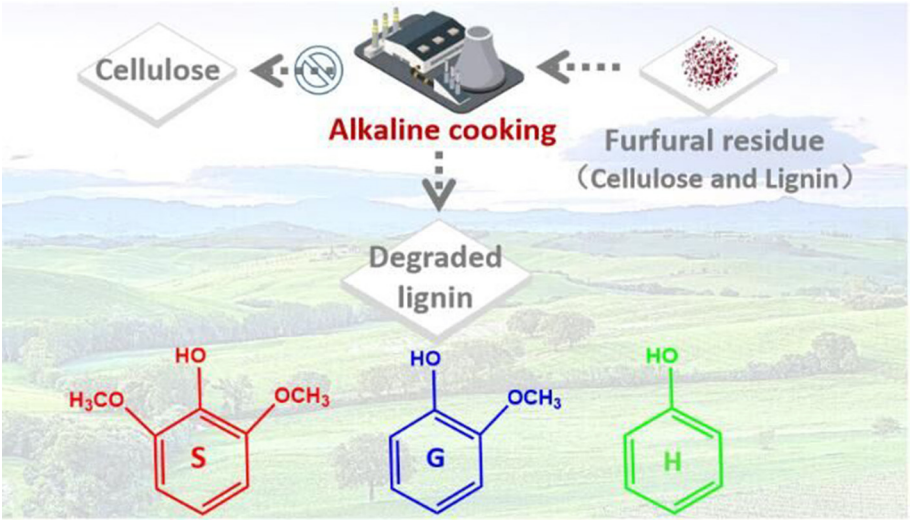

GRAPHICAL ABSTRACT | Extraction of lignin from industrial furfural residue by alkali cooking technology.

furfural residue solid waste, regardless of its composition and content. However, furfural residue is rich in cellulose (30 wt%) and lignin (63 wt%), each component having promising applications for the production of biofuels, chemicals, and materials (Wang et al., 2019). Furthermore, industrial furfural residue is a kind of organic waste with a high salt content and acidity, while the massive accumulation and unreasonable use would result in serious environmental pollution. Therefore, the reasonable and effective utilization of furfural residue would provide both environmental and economic benefits.

Most research has focused on the physical, chemical, and biological treatment of furfural residue to obtain cellulose for further utilization. However, the separation and utilization of lignin from furfural residue is scarce because of its complex structure. Lignin is a biopolymer with a three-dimensional network structure formed by three phenylpropane units, including *p*-hydroxyphenyl (H), guaiacyl (G), and syringyl (S). Lignin in furfural residue has the potential to be used as a reinforcing agent, antioxidants, a mineral powder binder, scale inhibitor, corrosion inhibitor, and in pharmaceuticals. At present, the main industrial methods to obtain lignin are dilute acid pretreatment, alkali pretreatment, ionic liquid treatment, and organosolv methods. The G and S-type lignin is extracted and purified by citric acid treatment from pulping black liquor (Liu Z. et al., 2009). Structural changes of corn stover lignin were studied during acid pretreatment, and the results showed that the condensation reaction became the main reaction of lignin at high temperature, which limited the depolymerization and subsequent utilization of lignin (Moxley et al., 2012). Olive residue lignin was extracted by ionic liquid triethylammonium hydrogen sulfate in Cequier's report, and the recovery yield of lignin reached 40% (Cequier et al., 2019). Two organosolv methods involving formic acid/acetic acid and sulfuric acid/ethanol solvent mixtures were investigated for lignin extraction from banana rachis biomass residue, and the obtained lignin fraction had a higher purity of 76.5 and 71.0% (Tiappi et al., 2019). Nitsos explored the characteristics of lignin isolated from spruce and birch with the use of alkaline or ethanol organosolv pretreatment, and the result showed that the molecular weight of alkaline lignin was higher than that of organosolv lignin (Nitsos et al., 2016). In summary, the cleavage of the C–O bond of lignin occurred in dilute acid treatment, and then the C–C bond was formed, which is more difficult to depolymerize. This phenomenon poses a huge challenge to the subsequent depolymerization and high value utilization of lignin. Although the higher yield and purity of lignin could be obtained by ionic liquid and organic solvent methods, the two methods are difficult to adapt to industrial production. In addition, in recent years, the acid-free pretreatment has attracted more interest to further improve lignin properties for high-value utilization (Tao et al., 2012). The condensation of lignin in raw materials could be avoided and high-performance lignin products could be obtained using alkali treatment technology, which is conducive to the utilization and development of lignin downstream industries. As an effective and simple way of lignin depolymerization, homogeneous alkaline catalysis technology has attracted the attention of researchers. Among them, alkaline cooking is a pulping method with NaOH as the catalyst and anthraquinone as the auxiliary catalyst to depolymerize lignin through the whole lignocellulosic biomass (Karp et al., 2014). Thring et al. proposed that up to 30% of small phenolic molecules could be achieved by the depolymerization of Alcell lignin with NaOH (Thring, 1994). Shabtai, Chornet, and Johnson reported that abundant small molecules were obtained by alkali depolymerization of lignin, and then the aromatics fuels such as gasoline were prepared by catalytic hydrogenation, realizing the high value utilization of lignin in the field of biofuel (Vigneault et al., 2007). Miller et al. reported the effect of alkaline strength on the depolymerization of lignin, and the results showed that strong alkali (NaOH, KOH) could produce more small molecular, than weak alkali (LiOH) (Miller

et al., 1999, 2002). Katahira et al. systematically studied the structure and properties of lignins obtained from the alkali extraction residue derived after the acid and enzyme hydrolysis, deacetylation disk mill treatment, and deacetylation twin-screw treatment. Different raw materials and alkali treatment methods would lead to different depolymerization degrees and small molecule types of lignin (Katahira et al., 2016). High quality lignin could be obtained through alkali treatment technology, which is conducive to the utilization and development of downstream industries.

In this work, alkali cooking technology was applied to extract lignin from industrial furfural residue (**Graphical Abstract**). The treatment condition was investigated as follows: 165°C−0.35 M NaOH-60 min (T1), 135°C−0.35 M NaOH-60 min (T2) and 135°C−0.20 M NaOH-60 min (T3). The structure and properties of lignin were comparatively studied under different alkaline cooking methods to examine the impact of alkali severity, and the treated solid residues were also investigated. The structural properties of extracted lignins and treated solid residues were determined using elemental analysis, gel permeation chromatography (GPC), fourier transform infrared (FTIR) spectroscopy, 2D HSQC NMR spectra, quantitative phosphorus spectrum (^{31}P NMR), gas chromatography-mass spectrometry (GC-MS), and oxidation resistance test.

MATERIALS AND METHODS

Materials

Furfural residue was obtained from the Henan biotechnology company (Henan, China), a solid residue was produced in the preparation of furfural from corncob by sulfuric acid hydrolysis. Furfural residue was washed to neutral, with a large amount of deionized water before being used, and then dried in an oven at 60°C for 12 h. The component content of the dried furfural residue was measured by NREL method (Zhang et al., 2010). The furfural residue contains 29.56% cellulose, 62.97% lignin, and 7.47% others. Deuterium pyridine, cyclohexanol, deuterium chloroform, 2-chloro-4,4,5,5-tetramethyl-1,3,2-dioxaphospholane (TMDP), 1,1-diphenyl-2-trinitrophenylhydrazine (DPPH), and 2,6-di-tert-butyl-4-methylphenol (BHT) were purchased from Mecklin Reagent Co., Ltd. (Shanghai, China). Sodium hydroxide, sulfuric acid and tetrahydrofuran were purchased from Guangzhou Chemical Reagent Co., Ltd. (Guangzhou, China). All reagents were of analytical pure grade, without any treatment before being used.

Separation and Recovery of Lignin From Furfural Residue

Furfural residue and a certain concentration of NaOH aqueous solution were fully stirred according to the solid-liquid ratio of 1:20 g/mL, and then transferred to a 100 mL Parr reactor (YZPR-100, Shanghai Yanzheng Instrument Co., Ltd.). The mixture was treated at a certain temperature for 60 min. After the reaction, the mixture was filtered. The filtrate was added to acid to precipitate lignin. The solid residue was washed repeatedly to neutral by a large amount of deionized water, and then dried in an oven at 60°C for 12 h. Based on the previous work and the screening of experimental data (Moghaddam et al., 2017), the alkali treatment conditions were determined with the yield of three components as the goal. In order to investigate the impact of the severity of alkali treatment on the extraction of lignin, three different reaction conditions were selected: 165°C−0.35 M NaOH-60 min (T1), 135°C−0.35 M NaOH-60 min (T2), and 135°C−0.20 M NaOH-60 min (T3). At the same time, in order to compare the structure of lignin in the black liquor during the pulping process, soda lignin was also extracted from corncob. Corncob was mixed with an aqueous sodium hydroxide (1 M NaOH) solution and the mixture was reacted at 170°C for 90 min in a 100 mL Parr reactor according to the solid-liquid ratio of 1:20 g/mL.

The precipitation process of lignin by adding acid was as follows (**Figure S1**): the pH value of the reaction liquid was adjusted by 2 M H_2SO_4 solution to precipitate the alkali extracted lignin. The steps were as follows: 2 M H_2SO_4 solution was added to the alkali treatment solution until the pH value was about 4.5, and stirred at room temperature for 15 min. Then 2 M H_2SO_4 solution was added until the pH value was about 3, and the alkali treatment solution was vibrated in an air constant temperature oscillator (THZ-C, Jiangsu Taicang experimental equipment factory) at 65°C for 30 min. The solid and liquid mixture were filtered and separated after the vibration was completed. The solid mixture was washed to neutral with deionized water and then dried in a vacuum drying oven at 40°C for 24 h. The dried solid was the precipitated lignin.

Characterization of Lignin

Component Analysis

The contents of the cellulose, hemicellulose, and lignin in the sample were measured by the standard method (NREL) of American Renewable Energy Laboratory (Zhang et al., 2010). 0.3 g of the sample was mixed with 3 mL of 72 wt% H_2SO_4 solution and reacted at 30°C for 60 min. Eighty four milliliter of deionized water was then added to the mixture. The mixture was transferred to a high-temperature autoclave (DSX-280kb24, Shanghai Shenan medical instrument factory) and reacted at 121°C for 60 min. After the reaction, the solid mixture and liquid were separated by G3 filter. The sugar content of liquid was detected after being filtered by a 0.22 μm aqueous filter membrane. The solid was dried to a constant weight and calcined in a muffle furnace at 575°C for 6 h. The reduced mass was the content of acid insoluble lignin. The acid soluble lignin was calculated by the absorption value of ultraviolet spectrophotometer at 205 nm. The total amount of lignin was the sum of acid soluble lignin and acid insoluble lignin. Cellulose and hemicellulose were calculated according to the following formula:

$$\text{Cellulose (\%)} = \frac{C_{Glu} \times 86.73\ \text{L} \times 0.90}{1000 \times \text{Sample weight (g)}} \times 100\% \quad (1)$$

$$\text{Hemicellulose (\%)} = \frac{C_{Xyl+Ara} \times 86.73\ \text{L} \times 0.88}{1000 \times \text{Sample weight (g)}} \times 100\% \quad (2)$$

C_{Glu} and $C_{Xyl+Ara}$ represent the concentrations of glucose, xylose, and arabinose, mg/L, respectively; 0.90 and 0.88 are the

coefficients of the conversion of cellulose and hemicellulose into glucose, xylose, and arabinose, respectively (Zhang et al., 2010).

The yield of extracted lignin samples was calculated according to the following formula (3):

$$\text{Yield}_{\text{Lignin}}\ (\%) = \frac{W_{\text{Lignin}}}{W_{\text{FR}}} \times 100\% \quad (3)$$

$\text{Yield}_{\text{Lignin}}$, W_{Lignin}, and W_{FR} represent the yield of extracted lignin, the mass of extracted lignin, the mass of furfural residue.

Molecular Weight Analysis

The 10 mg lignin sample was dissolved in 10 mL tetrahydrofuran and the mixture was filtered by an 0.22 μm organic filter membrane. The filtered liquid was injected into the gel chromatograph (Agilent 1260, USA) to determine sample molecular weight. The column was PL-gel 5 μm 10^3 Å and PL-gel 3 μm Mixed-3 (Series connection), the mobile phase was tetrahydrofuran, the flow rate was 1 mL/min, and the standard sample was 800–49,400 g/mol polystyrene.

Functional Group and Element Analysis

The infrared spectrum was determined by TENSOR27 (Bruker company Germany). A certain amount of sample was mixed with potassium bromide according to the mass ratio of 1:100. The scanning range was 4,000–400 cm^{-1}. The contents of carbon (C), hydrogen (H), nitrogen (N), sulfur (S), and oxygen (O) in the lignin samples were determined by element analyzer (Vario EL cube, Germany). At the same time, according to the alkane formula C_nH_{2n+2} and the relative content of elements, the C_9 expression of lignin samples were calculated (Moghaddam et al., 2017).

2D HSQC NMR Spectra Analysis

More detailed chemical structure information for lignin samples could be provided by 2D HSQC NMR spectra. The lignin samples were analyzed on a 600 MHz Bruker AVANCE III (Karlsruhe, Germany) spectrometer. Thirty milligram of lignin was dissolved in 1-mL DMSO-d_6, and then transferred to an NMR tube for testing. The spectrum width of the hydrogen spectrum and carbon spectrum were 5,000 and 20,000 kHz, respectively. The total number of samples collected in the one-dimensional hydrogen spectrum was 1,024, and the relaxation time was 1.5 s. The total number of acquisition points of one-dimensional carbon spectrum was 256 and the cumulative number is 64 times. The software used for data processing was mestrenova 6.1.1. It should be noted that the 2D HSQC NMR spectra of corncob and the furfural residue were tested according to the reference (Kim et al., 2008a). Eighty milligram of the sample, after full milling, was swelled in 0.75 mL DMSO-d_6. The data was measured according to the above set parameters.

Quantitative Phosphorus Spectra Analysis

According to the reference (Granata and Argropouls, 1995; Akim et al., 2001), the content of hydroxyl in lignin samples were determined by quantitative phosphorus spectroscopy (^{31}P-NMR). Twenty milligram of the lignin sample, 100 μL solution B, and 0.5 mL solution A were mixed. After full dissolution, 0.1 mL solution C was added, and then 0.1 mL of phosphating agent (TMDP) was added until the above mixture mixed well. The mixture was measured immediately after 15 min. Solution A was a mixture of deuterium pyridine and deuterium chloroform with the volume ratio of 1.6:1. Solution B was internal standard reagent, which was made using the following method: 54.25 mg of cyclohexanol was accurately weighed and then fixed with 5 mL solution A. Solution C, as a relaxation agent, was a 5 mg/mL chromium acetylpyruvate solution.

Pyrolysis Analysis

The fast pyrolysis of lignin samples was performed using a high temperature Tandem u-Reactor RX-3050TR pyrolyzer, and the pyrolysis products were characterized by gas chromatography-mass spectrometry (GC-MS, Agilent 7890B/5977A, USA). The 0.50-mg lignin sample was pyrolyzed at 500°C. The initial temperature was set at 50°C and maintained at this temperature for 1 min. The temperature then rose to 280°C at 6°C/min and was maintained at this temperature for 5 min. The pyrolyzed gas was put into gas chromatography for detection under helium purging. The carrier gas flow was 50 mL/min, and the split ratio was set as 30:1. After pyrolysis, the mass spectrum peaks were compared with the results in the National Institute of Standards and Technology (NIST), and the identified chemicals were analyzed quantitatively according to the literature.

Oxidation Resistance Test

According to Lu et al. (2012), DPPH (1,1-diphenyl-2-trinitrophenylhydrazine) was used to determine the antioxidant capacity of lignin. Different amounts of lignin were dissolved in a 0.1-mL water/dioxane (1/9, V/V) mixture to prepare 0.05–5 mg/mL of lignin solution. 3.9 mL DPPH ethanol solution (25 mg/L) was then added to the above solution. The absorption of the sample at 517 nm was determined by ultraviolet visible spectrophotometer (UV-1800, Shimadzu, Japan). The inhibition rate of lignin on DPPH was calculated according to the following formula (4):

$$\text{DPPH inhibition rate}\ (\%) = \frac{A_0 - A_1}{A_0} \quad (4)$$

A_0 was the absorbance of the control sample, A_1 was the absorbance after reaction with lignin.

Characterization of Solid Residues

Component Analysis

The solid residues obtained by different alkali treatment conditions were defined as R1, R2, R3, and R4, respectively. The procedure for determining the lignin composition were the same as those for the above extracted lignin samples. The yield of solid residues was calculated according to the following formula (5):

$$\text{Yield}_{\text{SR}}\ (\%) = \frac{W_{\text{SR}}}{W_{\text{FR}}} \times 100\% \quad (5)$$

Yield_{SR}, W_{SR} and W_{FR} represent the yield of solid residue, the mass of solid residue, the mass of furfural residue.

Functional Group Analysis

The infrared spectrum of corncob, furfural residue, and the solid residue were determined by attenuated total reflection fourier transform infrared spectroscopy (ATR-FTIR). The infrared spectrum of the sample was determined by vertex 70 (Bruker company, Germany). A certain amount of the sample was mixed and ground with KBr according to the mass ratio of 1:100. Thirty-two scans were performed at a resolution of 2 cm^{-1} with a scanning range of 4,000–400 cm^{-1}.

Solid State NMR Spectra Analysis

The solid-state NMR spectra (CP/MAS ^{13}C NMR) of the samples were determined by the 400 M Bruker NMR (AVANCE III HD 400). The 4-mm rotary tube was used, and the speed was 5 kHz. The contact time and pulse delay time were 1.5 ms and 3.16, respectively (Dong et al., 2013).

RESULTS AND DISCUSSION

Composition Analysis

The element content, empirical formula, and C_9 form structural formula of corncob furfural residue and NaOH extracted lignin samples were studied (**Table 1**). The C_9 form structural formula indicated that the sample was a hydroxyphenyl structure, which was calculated from six carbon benzene rings and three carbon propane side chains. The components content of corncob, furfural residue and extracted lignin samples were also measured (**Table 2**). As shown in **Table 1**, compared with corncob, the content of hydrogen (H) and oxygen (O) in furfural residue were significantly reduced, because corncob was composed of three major components: cellulose ($C_6H_{12}O_6$), hemicellulose ($C_5H_{10}O_5$), and lignin ($C_{10}H_{14}O$). In view of the structural formula of the three components, the proportion of hydrogen and oxygen in cellulose and hemicellulose were relatively high, and the proportion of carbon in lignin was relatively high. Combined with the thermal stability of these three components and the proportion of the content in biomass, the decrease of H and O content in furfural residue was attributed to the conversion of hemicellulose into furfural (Gallo et al., 2013), which was in accordance with the fact that no xylan was detected in furfural residue (**Table 2**). Compared with furfural residue, the content of carbon (C) and hydrogen (H) in the alkali extracted lignin sample were increased, while the content of oxygen (O) was decreased. According to the proportion of C, H, and O elements in the three components, the alkali treated lignin samples didn't contain or contained a small amount of xylan and glucan (T1 and soda lignin contained a small amount xylan and glucan, **Table 2**), which showed that cellulose and hemicellulose were completely removed from lignin. The content of hydrogen in the lignin samples was higher than that in the furfural residue, meaning that the lignin samples may contain relatively high hydroxyl content.

The yield and component content of lignin samples obtained by alkali cooking technology were shown in **Table 2**, T1 and soda lignin contained 6.7 and 0.5% cellulose, while no cellulose was detected in other lignin samples (T2 and T3), which may be related to the more lignin-carbohydrate complex (LCC) in alkali extract liquor of corncob and furfural residue. LCC and lignin with a higher molecular weight were easily extracted by a stronger alkali solution (Zhu, 2008). The content of acid insoluble lignin in soda lignin was higher than that in other samples. The cell wall of corncob was easily damaged by strong alkaline treatment, and more lignin with a high molecular weight was dissolved to form soda lignin (Phongpreecha et al., 2017). Moreover, another reason was that H_2SO_4 was industrially used to remove the most hemicellulose and a part of lignin from corncob, so furfural residue was lower for acid insoluble lignin. The lignin content of furfural residue after alkaline cooking treatment also confirmed this phenomenon. The yields of lignins obtained from T1, T2, and T3 were in the order of T1 > T2 > T3. The high yield of lignin was obtained by severe alkali treatment of furfural residue.

TABLE 1 | Elemental analysis and formula of corncob, furfural residue, and extracted lignin samples.

Samples	N%	C%	H%	O%	Empirical formal	C_9 formula
Corncob	0.26	41.42	7.26	51.05	$C_{3.45}H_{7.26}O_{3.19}N_{0.019}$	$C_9H_{18.94}O_{8.32}N_{0.05}$
FR	0.36	54.65	6.39	38.59	$C_{4.55}H_{6.39}O_{2.41}N_{0.026}$	$C_9H_{12.64}O_{4.77}N_{0.05}$
T1	0.79	54.67	6.74	38.28	$C_{4.55}H_{6.74}O_{2.39}N_{0.056}$	$C_9H_{13.31}O_{4.72}N_{0.11}$
T2	0.82	54.72	7.04	37.96	$C_{4.56}H_{7.04}O_{2.37}N_{0.058}$	$C_9H_{13.89}O_{4.68}N_{0.11}$
T3	0.78	55.87	7.13	36.22	$C_{4.65}H_{7.13}O_{2.26}N_{0.056}$	$C_9H_{13.78}O_{4.37}N_{0.11}$
Soda lignin	0.26	59.64	7.44	32.66	$C_{4.97}H_{7.44}O_{2.04}N_{0.019}$	$C_9H_{13.48}O_{3.70}N_{0.03}$

FR, furfural residue.

TABLE 2 | Yield and chemical composition of corncob, furfural residue and extracted lignin samples.

Samples	Yield (%)	Component (%)				
		Cellulose	Hemi.	AIL	ASL	Ash
Corncob	–	34.10 ± 0.99	31.92 ± 0.15	10.85 ± 0.25	5.95 ± 0.08	1.46 ± 0.04
FR	–	29.56 ± 0.80	–	62.97 ± 0.45	1.50 ± 0.03	2.86 ± 0.06
T1	27.73 ± 0.08	6.71 ± 0.12	–	80.92 ± 0.32	3.12 ± 0.11	0.11 ± 0.02
T2	26.62 ± 0.45	–	–	79.43 ± 0.37	3.34 ± 0.06	–
T3	22.94 ± 0.17	–	–	78.31 ± 0.09	3.72 ± 0.11	–
Soda lignin	14.34 ± 0.07	0.52 ± 0.05	1.21 ± 0.06	91.82 ± 0.09	4.01 ± 0.07	0.72 ± 0.07

"–", not detected; Hemi., hemicellulose; AIL, acid insoluble lignin; ASL, acid soluble lignin; FR, furfural residue.

It could be explained that the higher molecular weight lignin was dissolved with harsh alkali treatment conditions, further accumulated and precipitated in the acid precipitation method, thus more acid insoluble lignin was obtained. The order of the molecular weight of lignin samples was T1 > T2 > T3, which also showed that lignin with a larger molecular weight could be dissolved in a strong alkaline environment (**Table 3**) (Thring, 1994; Phongpreecha et al., 2017). The precipitation of the above alkali extracted lignin was related to the molecular weight of lignin. A large amount of alkali soluble lignin could not be precipitated due to its small molecular weight. Only a small amount of high molecular weight lignin extracted by strong alkaline conditions could be precipitated (Zhu, 2008). Therefore, a higher lignin yield could be achieved under stronger alkali treatment conditions.

Functional Group Analysis

In order to better understand the structure changes of samples during the preparation of furfural, the attenuated total reflection (ATR) of corncob and furfural residue are shown in **Figure 1A**. The vibration peak at 896 cm^{-1} is the characteristic peak of the β- glucoside bond (Sun et al., 2012), which was obviously weakened after acid treatment, indicating that cellulose was destroyed or degraded during the preparation of furfural from corncob catalyzed by strong acid (H_2SO_4). Hemicellulose is a kind of polymer composed of many monosaccharides, its infrared characteristics come from the C=O stretching vibration in acetyl and carboxyl groups. The vibration peak of corncob at 1,725 cm^{-1} assigns to the C=O stretching vibration in hemicellulose, the vibration peaks at 1,371 and 1,248 cm^{-1} assign to the C–O stretching vibration in polysaccharide, and the C–O stretching vibration in hemicellulose acetyl, and the vibration peak at 996 cm^{-1} is the typical absorption peak of the arabinose based xylan structure, which disappeared or weakened after acid treatment. The C–O stretching vibration appeared at 1,025 cm^{-1} and decreased sharply to 1,158 cm^{-1}. The changes of the above vibration peaks indicated that hemicellulose was degraded to a large extent (Rahimi et al., 2016). After acid treatment, the vibration peak of furfural residue at 1,057 cm^{-1} belongs to C=O and OH vibration. Lignin is a kind of aromatic polymer with many complex functional groups. In **Figure 1A**, the vibration peak at 1,513 cm^{-1} belongs to the aromatic skeleton vibration of lignin, and the vibration peak at 1,602 cm^{-1} assigns to the stretching vibration of the aromatic skeleton and C=O. After acid treatment, the two vibration peaks increased significantly, which was attributed to the increase of lignin relative content in corncob after the conversion of hemicellulose to furfural (Liu L. et al., 2009; Xu et al., 2015), indicating that the residual solid residue of corncob, after the preparation of furfural by acid catalysis, contained lignin and retained the basic structure of lignin.

TABLE 3 | Molecular weight distribution of the extracted lignin samples.

Sample	M_w	M_n	M_w/M_n
T1	2,273	950	2.39
T2	1,894	895	2.12
T3	1,600	864	1.85
Soda lignin	1,952	846	2.31

The infrared spectra of alkali extracted lignin samples are shown in **Figure 1B**. The infrared spectra of lignin samples under different alkali treatment conditions were very similar. The three main characteristic peaks of the lignin structure, such as 1,601, 1,509 and 1,424 cm^{-1}, were obviously present in the infrared spectra of lignin samples, indicating that the basic lignin structure existed in the samples. The vibration peak at 1,695 cm^{-1} belongs to the C=O stretching vibration in the non-conjugated ketone or carbonyl compounds (Yang et al., 2013). The vibration peak intensity of the lignin samples was similar,

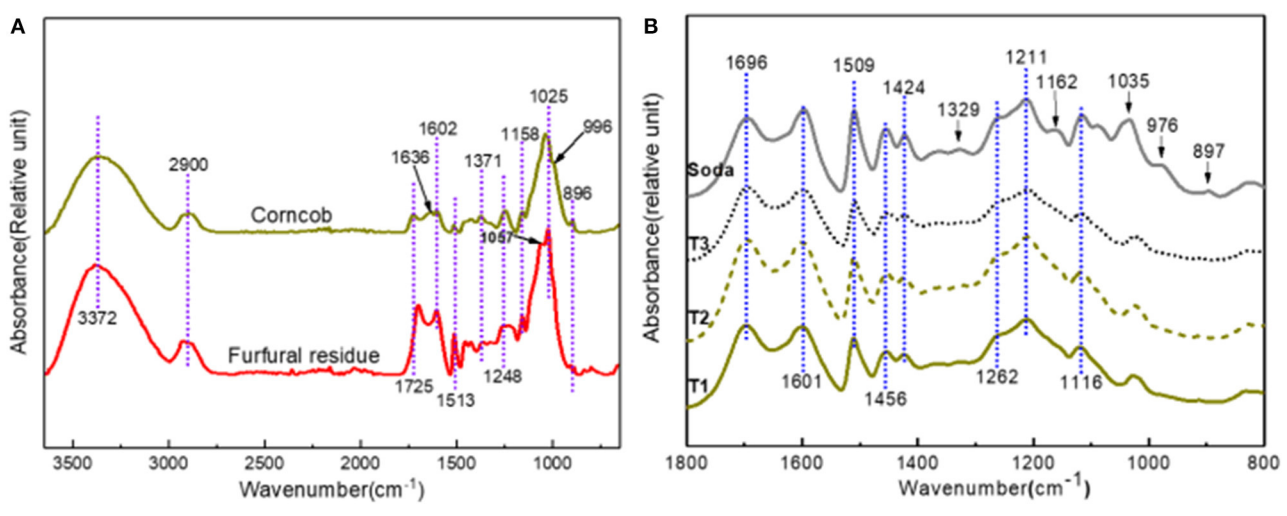

FIGURE 1 | ATR spectra of corncob, furfural residue **(A)** and extracted lignin samples **(B)**.

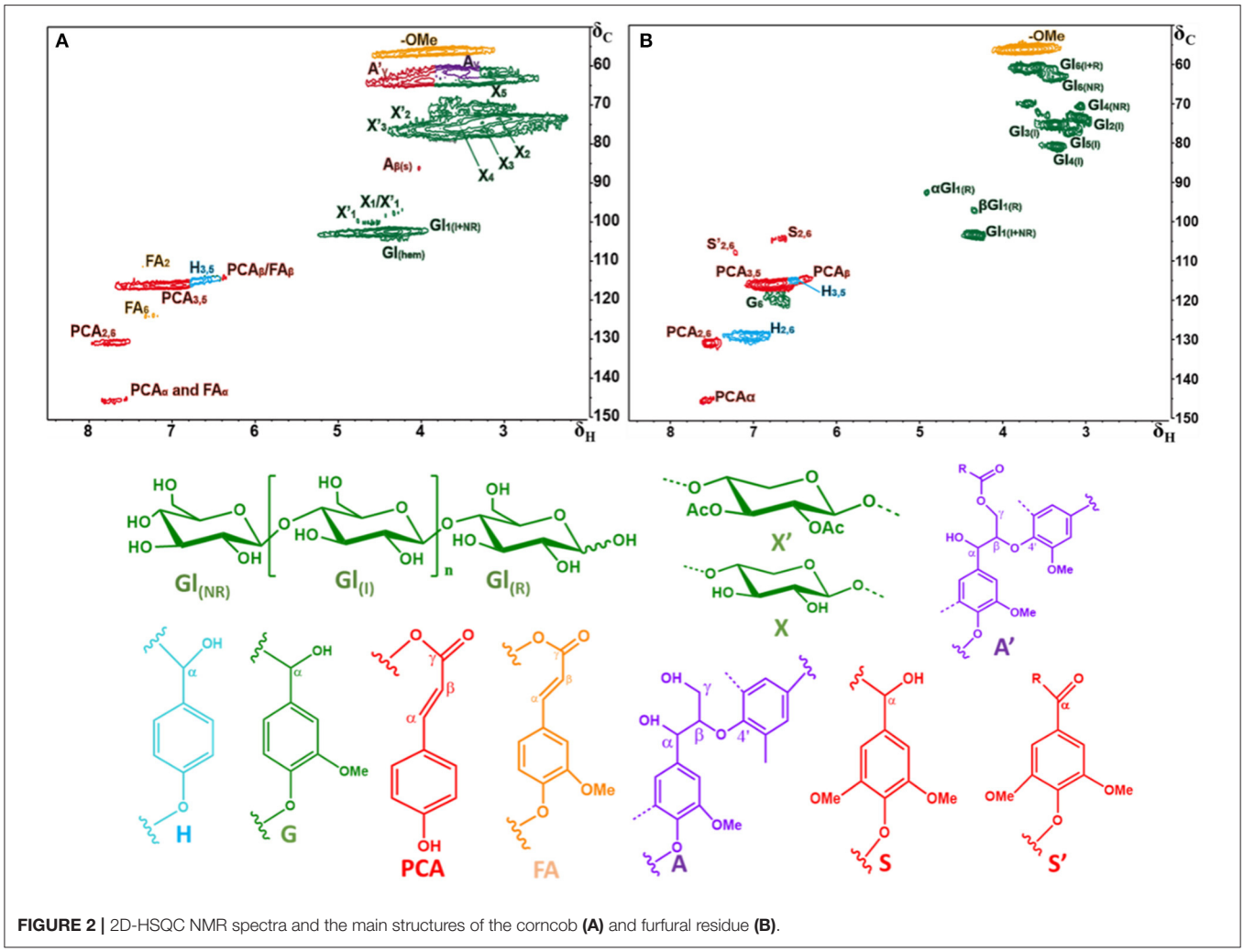

FIGURE 2 | 2D-HSQC NMR spectra and the main structures of the corncob **(A)** and furfural residue **(B)**.

indicating that the lignin obtained from corncob and furfural residue were oxidized, and a similar degree was observed (Yang et al., 2013). The vibrations at 1,601, 1,509, 1,456, and 1,424 cm^{-1} are attributed to the vibration of lignin aromatic skeleton and C–H deformation vibration (Xu et al., 2013; Rodríguez-Gutiérrez et al., 2014). Compared with the vibration peak of the lignin sample in furfural residue, the signal peak of the soda lignin sample was stronger, which indicated that the soda lignin sample contained a greater benzene ring structure. The signal peaks at 1,329 and 1,116 cm^{-1} are derived from the C–H vibration in syringyl based structural units (Villaverde et al., 2009). These characteristic peaks disappeared or weakened in lignin samples, indicating that there was a relatively rich syringyl in soda lignin. In addition, the signal peaks at 832 and 1,035 cm^{-1} belong to the C–H vibration in the *p*-hydroxyphenyl structural unit. The signal peak at 1,162 cm^{-1} is the characteristic peak of *p*-hydroxycinnamic acid. The vibration at 1,262 cm^{-1} is related to the C=O stretching vibration in the guaiacyl structural unit. The peak at 1,211 cm^{-1} belongs to the vibration of C–C, C–O, and C=O in the condensed guaiacyl structural unit (Barsbay and Güner, 2007; Miao et al., 2014).

2D HSQC NMR Spectra Analysis

The 2D HSQC NMR spectra and the main structure of corncob and furfural residue are displayed in **Figure 2**, and the assignment of signal peaks of lignin and carbohydrate in 2D HSQC NMR spectra are summarized in **Table 4**. The 2D HSQC NMR spectra of **Figure 2A** shows that the carbohydrate found in corncob was mainly xylan, and the signal peak of cellulose was weak or even disappeared, which was due to the decrease of the fluidity of crystalline cellulose in the corncob and the overlap of some signal peaks (Kim et al., 2008b). The signal peaks of X2, X3, X4, and X5 in corncob are attributed to C2/H2, C3/H3, C4/H4, and C5/H5 in β-D-xylopyranoside of corncob xylan. The signal peaks at X2'and X3' are derived from the partial acetylation of C2 and C3 in xylan (Rencoret et al., 2009). The signal peaks of other carbohydrates including X1, X1', and $GL_{1(hem)}$ belong to β-D-xylopyranoside, 2-*O*-acetyl-β-D-xylopyranoside, and C1/H1 in (1→3)+(1→6)-β-D-glucopyranoside (Van Erven et al., 2017). The 2D HSQC NMR spectrum of furfural residue was obviously different from that of corncob, and the results are illustrated in **Figure 2B**. The signal peaks of xylose (X1, X2, X3, X4, X5) or acetylated xylose (X1', X2', X3') disappeared completely

TABLE 4 | Assignment of $^{13}C/^{1}H$ correlation of signals in the 2D HSQC NMR spectra.

Label	δ_C/δ_H	Assignment
LIGNIN SIGNALS		
$-OCH_3$	55.6/3.73	C/H in methoxyls
$A_{\beta(s)}$	85.9/4.12	C_β/H_β in β-*O*-4' substructures linked to a S unit (A)
$S_{2,6}$	103.8/6.69	C_2/H_2 and C_6/H_6 in etherified syringyl units (S)
$S'_{2,6}$	106.4/7.19	C_2/H_2 and C_6/H_6 in α-oxidized syringyl units (S')
FA_2	111.4/7.32	C_2/H_2 in ferulates (FA)
PCA_β/FA_β	113.5/6.27	C_β/H_β in *p*-coumarates (PCA) and ferulates (FA)
$H_{3,5}$	114.5/6.62	C_3/H_3 and C_5/H_5 in *p*-hydroxyphenyl units (H)
G_6	118.7/6.77	C_6/H_6 in guaiacyl units (G)
$PCA_{3,5}$	115.5/6.77	C_3/H_3 and C_5/H_5 in *p*-coumarates (PCA)
FA_6	123.3/7.20	C_6/H_6 in ferulates (FA)
$H_{2,6}$	128.0/7.05	C_2/H_2 and C_6/H_6 in *p*-hydroxyphenyl units (H)
$PCA_{2,6}$	130.8/7.46	C_2/H_2 and C_6/H_6 in *p*-coumarates (PCA)
PCA_α/FA_α	144.4/7.45	C_α/H_α in *p*-coumarates (PCA) and ferulates (FA)
CARBOHYDRATE SIGNALS		
$Gl_{6(I+R)}$	60.6/3.60 and 3.80	C_6/H_6 in (1→ 4)-β-D-glucopyranoside (I+R)
$Gl_{6(NR)}$	62.7/3.35 and 3.47	C_6/H_6 in β-D-glucopyranoside (NR)
X_5	62.8/3.20 and 3.86	C_5/H_5 in β-D-xylopyranoside
$Gl_{4(NR)}$	70.1/3.02	C_4/H_4 in β-D-glucopyranoside (NR)
X_2	72.6/3.02	C_2/H_2 in β-D-xylopyranoside
$Gl_{2(I)}$	73.2/3.05	C_2/H_2 in (1→ 4)-β-D-glucopyranoside (I)
X_2'	73.1/4.25	C_2/H_2 in 2-*O*-acetyl-β-D-xylopyranoside
X_3	73.7/3.23	C_3/H_3 in β-D-xylopyranoside
$Gl_{3(I)}$	74.6/3.35	C_3/H_3 in (1→ 4)-β-D-glucopyranoside (I)
X_3'	74.7/4.41	C_3/H_3 in 3-*O*-acetyl-β-D-xylopyranoside
X_4	75.3/3.52	C_4/H_4 in β-D-xylopyranoside
$Gl_{5(I)}$	76.4/3.15	C_5/H_5 in (1→ 4)-β-D-glucopyranoside (I)
$Gl_{4(I)}$	80.5/3.32	C_4/H_4 in (1→ 4)-β-D-glucopyranoside (I)
$\alpha Gl_{1(R)}$	92.1/4.92	C_1/H_1 in α-D-glucopyranoside (R)
$\beta Gl_{1(R)}$	96.5/4.25	C_1/H_1 in β-D-glucopyranoside (R)
X'_1	99.3/4.50	C_1/H_1 in 2-*O*-acetyl-β-D-xylopyranoside
X_1/X'_1	101.6/4.29	C_1/H_1 in β-D-xylopyranoside + 3-*O*-acetyl-β-D-xylopyranoside
$Gl_{1(I+NR)}$	102.6/4.31	C_1/H_1 in (1→ 4)-β-D-glucopyranoside (I+NR)
$Gl_{1(hem)}$	103.0/4.25	C_1/H_1 in (1→ 3)+(1→ 6)-β-D-glucopyranoside (in hemicelluloses)

I, internal units; R, reducing end units; NR, non-reducing end units.

in furfural residue, because hemicellulose was hydrolyzed and dissolved during the preparation of furfural from corncob. There were some carbohydrate signal peaks in furfural residue, which came from cellulose or modified cellulose. Gl_I, $Gl_{(R)}$, and $Gl_{(NR)}$ belong to unchanged cellulose or cellulose containing reducing and non-reducing end groups in furfural residue, respectively (De Menezes et al., 2017). These changes indicated that the cellulose of corncob was modified or degraded in the production process of furfural.

Figure 3 presents the 2D HSQC NMR spectra of alkali extracted lignins and soda lignin. In **Figure 3**, the H, S, G, and PCA structural units were mainly distributed in the aromatic regions of these lignin samples. Although clear signals of lignin units were observed in the aromatic regions, no signals were detected in the lignin linkages regions. The reason is as follows: the signal of lignin linkages regions and side chain structure were lost due to the serious damage caused by alkali treatment, while the strong signals of lignin were observed because the benzene ring structure of lignin was not damaged. The signal peaks at δ_C/δ_H 106.4/7.19 were observed in all lignin samples, which belong to the oxidation structure (S') of the S structural unit at $C_{2,6}/H_{2,6}$, indicating that the structure of lignin samples was partially oxidized (Kaparaju and Felby, 2010). The signal peaks of the lignin samples at δ_C/δ_H 114.9/6.77 belong to the $C_{3,5}/H_{3,5}$ structure in the H structural unit, and were also related to C5/H5 in the G unit and $C_{3,5}/H_{3,5}$ in PCA. $C_{2,6}/H_{2,6}$ in H structural units were also observed at δ_C/δ_H 127.9/7.19. In addition, the signal peaks at 110.8/6.97, 114.5/6.70, and 119.0/6.78 of δ_C/δ_H belong to C_2/H_2, C_5/H_5, and C_6/H_6 structures in the G-type unit (Mousavioun and Doherty, 2010; Rönnols et al., 2015), indicating that G-type units existed in all lignin samples and the content was relatively rich, which was closely related to the types and characteristics of raw materials. The lignin samples extracted from furfural residue contain abundant G, H, S units, and the S-type unit was easy to oxidize.

Quantitative Phosphorus Spectra Analysis

The quantitative phosphorus spectra of alkali extracted lignins and soda lignin are illustrated in **Figure 4**. Based on the analysis of quantitative phosphorus spectra, the functional groups on the lignin samples of TMDP phosphating were quantified (**Table 5**). From **Table 5**, there was no significant difference between the hydroxyl content of the soda lignin sample and that of the alkali extracted furfural residue lignin, and the hydroxyl content of lignin from T3 was significantly higher than that of soda lignin. The order of hydroxyl content in lignin samples was T3 > T2 > T1, which was due to the different severities of the alkali treatment conditions. Compared with soda lignin, the hydroxyl content of guaiacyl (non-condensed) in the alkali extracted lignin samples decreased while that of *p*-hydroxyphenyl increased. Moreover, with the harsh conditions of alkali extraction, the hydroxyl content of guaiacyl (non-condensable) in the obtained lignin samples decreased more and more seriously, which was related to the loss of methoxyl in the guaiacyl structural units during alkali extraction (Rönnols et al., 2015). However, compared with the soda lignin sample, the content of carboxyl and hydroxyl groups in the alkali extracted lignin samples increased significantly, which may be related to the oxidation of lignin in the production process of furfural or the impurities of fatty acids in lignin (Constant et al., 2016). Thus, the highest content of hydroxyl in the lignin samples was 4.02 mM/g under T3, which was higher than that in the soda lignin samples (3.41 mM/g). Therefore, lignin samples with rich

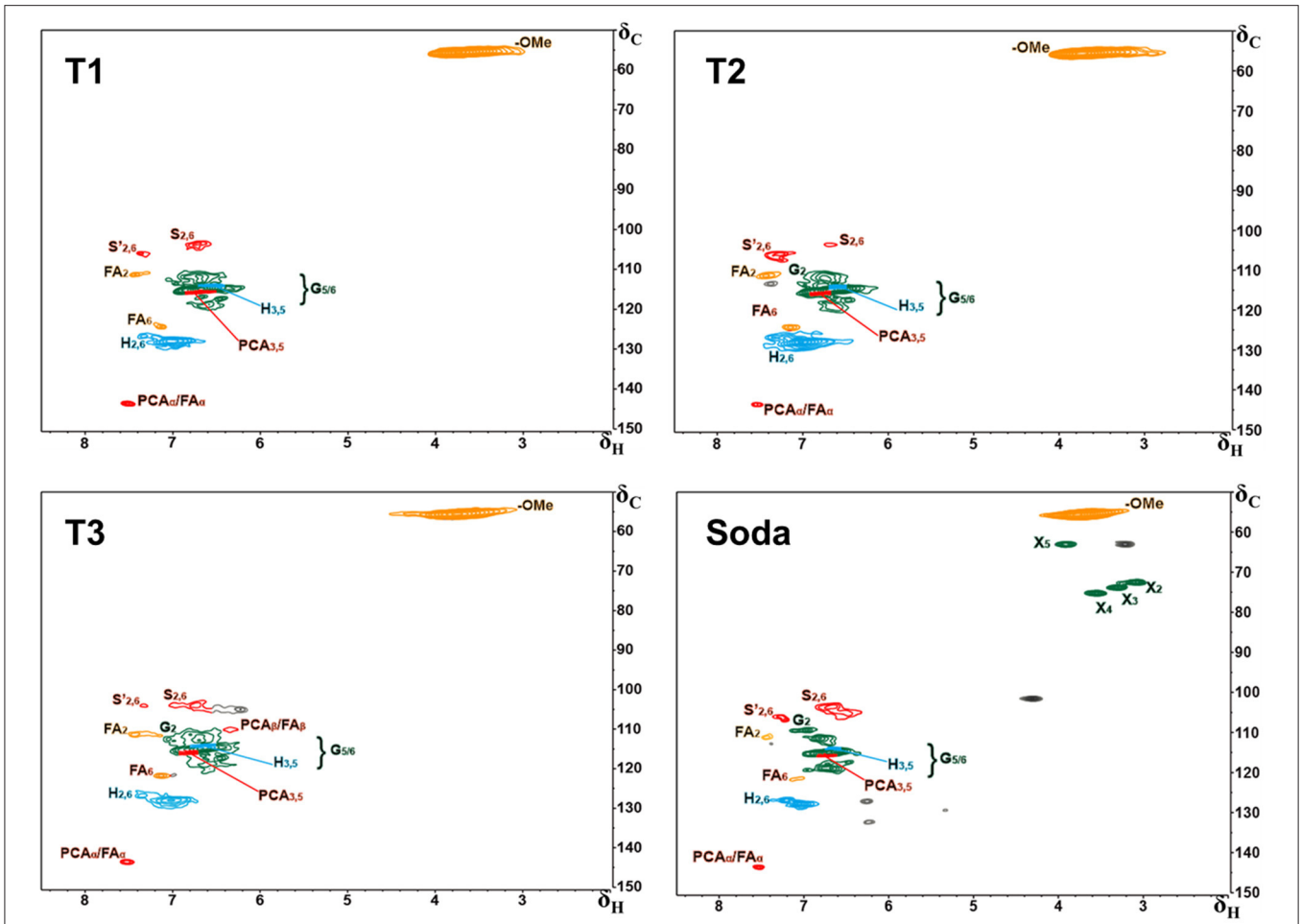

FIGURE 3 | 2D-HSQC-NMR spectra of the extracted lignin samples.

hydroxyl content could be obtained from furfural residue in the appropriate alkaline extraction condition. The lignin could be used as additives of some antioxidants (Mousavioun and Doherty, 2010), which is of great significance for the efficient utilization of lignin in furfural residue.

Pyrolysis Analysis

The samples of corncob, furfural residue, and extracted lignin were analyzed by pyrolysis gas chromatography-mass spectrometry (PyGC-MS). The degradation products and relative abundance of lignin samples are listed in **Table S1**. It is obvious that the main small molecules produced in the pyrolysis of lignin samples were *p*-hydroxyphenyl (H), syringyl (S), and guaiacyl (G). The relative contents of phenols derived from lignin and the contents of H, G, S, and S/G are listed in **Table S1**. The high content of 4-vinylguaicol was produced in the pyrolysis of corncob, furfural residue, and lignin samples, which had a significant impact on the content of the G unit in the pyrolysis products. However, it should be noted that 4-vinylguaicol was mainly derived from the decarboxylation of ferulic acid in gramineous materials (Del Río et al., 2012; Río et al., 2015). In other words, this part of the guaiacyl structural unit was from ferulic acid. Therefore, this part of guaiacyl could not be used as a part of the G-type structural unit to calculate the ratio of H, G, S. After the removal of 4-vinylguaicol, the ratio of H, G, S and the ratio of H, G, S containing 4-vinylguaicol are also listed in **Table S1**. Obviously, there were significant differences in the composition of lignin in different samples. Taking 4-vinylguaicol into account, corncob and furfural residue contained abundant G-type unit (46.5 and 49.3%). After 4-vinylguaicol was not considered, the G-type structural unit in corncob decreased to 30.5%, which confirmed that 4-vinylguaicol was released from the G-type structural unit and ferulic acid. However, the change of the G-type structural unit in furfural residue was not significant at 41.5%, implying that there was an abundant G-type structural unit in furfural residue, which could also be seen from 2D HSQC NMR spectra. Many small phenolic molecules were released from lignin samples, according to the degree of treatment, and the contents of H, G, and S were obviously different. As the treatment conditions become more and more severe, the content of the H-type unit increased gradually, and the proportion of the G-type unit and S-type unit decreased,

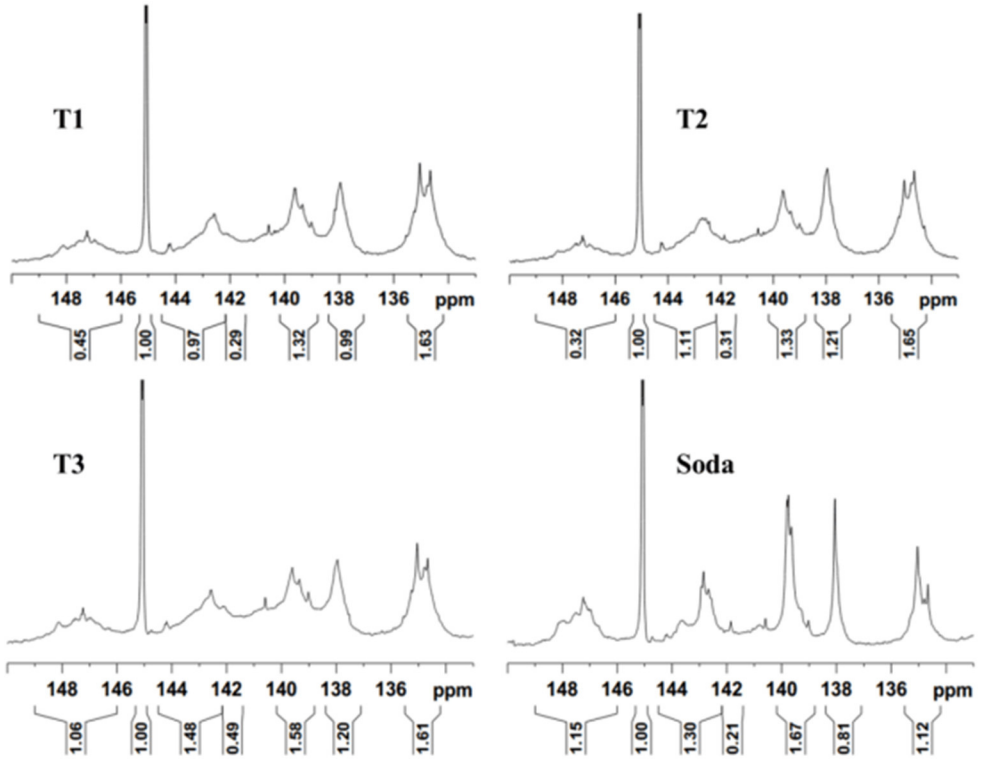

FIGURE 4 | ^{31}P-NMR spectra of the extracted lignin samples.

which may be related to the removal of methoxyl in the G-type and S-type units under severe conditions (Harman-Ware et al., 2013). The content of the G-type unit of lignin samples under T1, T2, and T3 was 29.9, 36.9, and 42.3%, respectively. The results of Py-GC/MS showed that similar S/G (1.0–1.1) values and a high proportion of the G-type unit were present in the three lignin samples. Therefore, the extracted lignin could be applied in many chemical fields based on the chemical properties. Lignin, which contains a lot of hydroxyl, could be used to scavenge free radicals, develop antioxidant products, and to provide reactivity for the synthesis of phenolic resin. Lignin with a large number of G-type units could activate the benzene ring, which has potential in the synthesis of benzene ring structures containing methoxy groups.

TABLE 5 | ^{31}P-NMR results of the extracted lignin samples (mM/g).

Assignment	δ P-NMR	Soda	Furfural residue treatment		
			T1	T2	T3
Aliphatic OH	149.0–146.0	0.62	0.24	0.17	0.57
Syringyl OH	144.7–142.1	0.70	0.53	0.60	0.80
Condensed guaiacyl OH	142.1–141.5	0.14	0.16	0.17	0.27
Non condensed guaiacyl OH	140.2–138.8	0.90	0.71	0.72	0.86
p-hydroxyphenyl OH	138.4–137.1	0.44	0.54	0.66	0.65
Carboxylic acid OH	135.5–134.0	0.61	0.88	0.89	0.87
Total OH		3.41	3.06	3.21	4.02

Soda, soda lignin.

Antioxidant Analysis

Figure 5 displays the inhibition of different lignin samples on DPPH. The clearance rate of lignin samples to DPPH was significantly related to its concentration. The inhibition rate of DPPH increased with the increase of lignin concentration. Among them, the antioxidant activity of the lignin sample extracted under T3 was the best one, and the scavenging rate of the DPPH radical was 91.5%. The order of the antioxidant strength of samples was as follows: T3 > soda lignin > T2 > T1 > BHT > furfural residue > corncob, shown in **Figure 5**. Obviously, the antioxidant activity of lignin samples obtained by alkali extraction was higher than that of commercial antioxidant BHT, which was related to the hydroxyl content in lignin samples by alkali extraction, and the conclusion was consistent with the results of the phosphorus spectrum test. However, the oxidation resistance of corncob and furfural residue was weak, which may be related to the characteristics of the sample itself and the undissolved lignin. Therefore, lignin samples extracted under different alkali conditions have a promising application as potential antioxidants in food and cosmetics.

Solid Residue Analysis

Component Analysis

The components of corncob, furfural residue, and the alkali treated solid residue were analyzed, and the results are shown in **Table 6**. Obviously, 77.25% glucan was observed in the alkali treated corncob solid residue, and the yield of the solid residue was 28.11%. The glucan content was significantly higher than that of the corncob and furfural residue because lignin in the raw material was removed by alkali extraction. However, after alkali treatment of furfural residue, the content of glucan in solid residues were 7.89, 10.55, and 12.70%, and the corresponding yields were 63.4, 64.7, and 75.4 under T1, T2, T3. This result showed that the content of glucan in alkali treated furfural residue was significantly reduced, and with the severity of alkali treatment, the content of glucan in furfural residue decreased. This results were contrary to the increase of glucan content in alkali treated corncob, which was attributed to the removal of hemicellulose in the process of preparing furfural by acid catalysis. The removal of hemicellulose further resulted in the exposure of cellulose to the alkali solution, so partial cellulose was degraded into small molecules in the reaction solution (Yang and Pei, 2001). In addition, the increase of acid insoluble lignin content in solid residue was mainly due to the carbonization of partial cellulose into lignin-like substances under the condition of high-temperature alkali treatment. Furthermore, the harsh alkali treatment conditions lead to the aggravation of cellulose carbonization (Hoekman et al., 2011). As shown in **Table 2**, the dissolution rate of lignin also increased when increasing the severity of reaction conditions. The dissolution rates of lignins were 27.7, 26.6, and 22.9% under T1, T2, and T3, while the content of acid insoluble lignin in solid residues were 82.41, 74.78, and 70.43%, respectively (**Table 6**), which also indicated that some lignin-like black carbon may be produced under the condition of a high-temperature alkali treatment. These results showed that the removal of lignin by alkaline cooking technology was not suitable for cellulose utilization from industrial furfural residue.

The total mass balance of extracted lignin samples and alkali treated solid residues in the separation and recovery process is shown in **Table 7**. The reduction of total mass after separation was mainly due to the hydrolysis of cellulose in the reaction solution and the carbonization of cellulose to form lignin-like substances. The components of solid residue were mainly cellulose and lignin-like substances generated by cellulose.

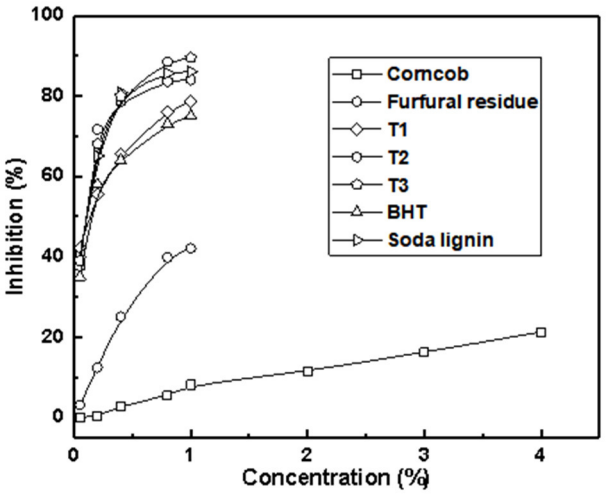

FIGURE 5 | Scavenging activity of lignin samples compared with commercial antioxidants for DPPH radical.

Functional Group Analysis

The infrared spectra of solid residues extracted from furfural residue under different alkali treatment conditions are shown in **Figure 6**. There was a similar structure in solid residues under

TABLE 7 | The total mass balance of extracted lignin samples and alkali treated solid residues in the separation and recovery process.

Sample	Yield[a] (%)		Total (%)
	Lignin	Solid residues	
T1	27.73 ± 0.08	63.42 ± 0.07	91.15
T2	26.62 ± 0.45	64.73 ± 0.09	91.35
T3	22.94 ± 0.17	75.41 ± 0.10	98.35
Soda lignin	14.34 ± 0.07	28.12 ± 0.1	42.46

[a] *The yield of lignin and solid residues were based on the mass of furfural residue.*

TABLE 6 | Chemical composition of the corncob, original and alkali treated furfural residues.

Sample	Yield (%)	Component (%)				
		Cellulose	Hemicellulose	AIL	ASL	Ash
Corncob	–	34.10 ± 0.99	31.92 ± 0.15	10.85 ± 0.25	5.95 ± 0.08	1.46 ± 0.04
FR	–	29.56 ± 0.80	–	62.97 ± 0.45	1.50 ± 0.03	2.86 ± 0.06
R1	63.42 ± 0.07	7.89 ± 0.08	–	82.41 ± 0.80	0.14 ± 0.01	3.36 ± 0.11
R2	64.73 ± 0.09	10.55 ± 0.11	–	74.78 ± 0.10	0.18 ± 0.01	3.44 ± 0.70
R3	75.41 ± 0.10	12.70 ± 0.11	–	70.43 ± 0.10	0.21 ± 0.02	0.32 ± 0.01
R4	28.12 ± 0.1	77.25 ± 0.12	10.35 ± 0.1	0.63 ± 0.02	0.31 ± 0.01	–

"–", not detected; AIL, acid insoluble lignin; ASL, acid soluble lignin; FR, furfural residue.

different alkali treatments. The absorption peaks at 1,587 and 1,510 cm^{-1} are attributed to C=C stretching vibration on the skeleton of the lignin benzene ring, which indicated that there were lignin-like structure substances in solid residues. Vibrations at 2,899, 1,425, 1,371, 1,159, 1,106, 1,027, and 896 cm^{-1} are related to the cellulose in solid residues. Among them, the vibration at 1,425 cm^{-1} is attributed to the asymmetric bending vibration of C–H in methyl $–CH_3$ and methylene $–CH_2$. The absorption peak at 1,371 cm^{-1} is –CH bending vibration and C–O stretching vibration in cellulose (Ma et al., 2015). The strength of characteristic peaks (1,425, 1,159, 1,027, and 896 cm^{-1}) of cellulose in furfural residue solid residue was significantly lower than that of cellulose in corncob solid residue, indicating that partial cellulose in furfural residue was degraded, dissolved, or carbonized into lignin-like structure substances, which was consistent with the results of the component analysis in **Table 6**. Moreover, the characteristic peak intensity of lignin (1,587 and 1,510 cm^{-1}) in the furfural solid residue was significantly higher than that in corncob solid residue, implying that the lignin of corncob was effectively dissolved in the alkali solution, but the lignin dissolution of furfural residue was poor, and could even not be dissolved.

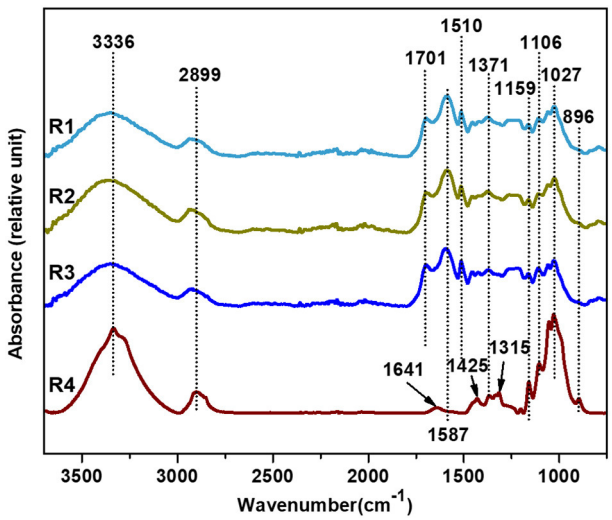

FIGURE 6 | FT-IR spectra of the alkali treated furfural residue.

Solid State NMR Spectra Analysis

The structure of corncob, furfural residue, and solid residue was analyzed by solid-state NMR spectra, and the results are shown in **Figure 7**. Compared with untreated corncob and furfural residue, the relative strength of the cellulose signal peak in alkali treated solid residue was weakened, and the lignin signal peak was enhanced, which was consistent with the results of the component and functional group analysis. The intensity of signal peaks at 89.1 or 88.9 ppm was weakened, indicating that the crystalline cellulose in furfural residue was destroyed and the relative content of cellulose was reduced under alkali treatment. The decrease of signal peak at 83.4 or 84.2 ppm showed the decrease of amorphous cellulose, which was due to the destruction of the cellulose structure by alkali treatment, indicating that partial cellulose had undergone a peeling reaction and gradually dissolved into small molecules (Liu et al., 2006a). The signal peaks at the chemical shifts of 126.9 or 128.9 ppm and 148.3 or 147.5 ppm are attributed to the carbon in the benzene ring structure of lignin and the carbon in the β-O-4 structure of the syringyl group, respectively (Liu et al., 2006b). The signal peak at 56.4 ppm is attributed to the carbon of the methoxy group in the lignin aromatic structure (Dong et al., 2013). Compared with the untreated corncob and furfural residue, the signal relative intensity of lignin or lignin-like substances in the solid residue

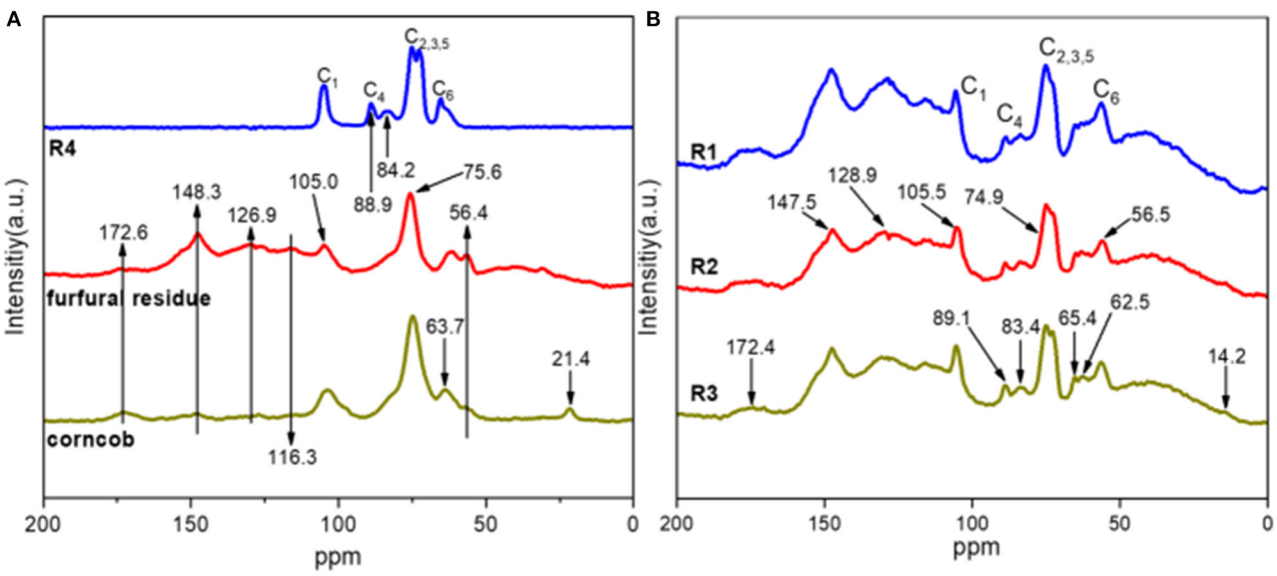

FIGURE 7 | *13C* CP/MAS NMR spectra of corncob, alkali treated corncob, original **(A)**, and alkali treated furfural residue **(B)**.

was enhanced, indicating that the relative content of lignin-like substances increased after alkali treatment, which was related to the carbonization of partial cellulose.

CONCLUSION

This study has provided insightful information on the composition and structural characteristics of alkali extracted lignin from furfural residue and its solid residue. The basic structural units (G, S, and H) were present in extracted lignin, in which the G-type unit accounted for the main proportion. The hydroxyl content was rich in lignin, and the highest hydroxyl content was 4.02 mM/g by T3. Moreover, the alkaline cooking treatment had little influence on the structure of the obtained lignin, and the extracted lignin had a great inhibition effect on DPPH free radicals, which give them special properties for different applications, particularly as potential antioxidants in food and cosmetic industry.

DATA AVAILABILITY STATEMENT

All datasets generated for this study are included in the article/**Supplementary Material**.

AUTHOR CONTRIBUTIONS

RL, XiaohW, and QL designed and finished the preparation and characterization analysis of lignin. FY, CL, XiaoyW, and JR supervised the project, helped design the experiments, and evaluated the data. The results of the manuscript were discussed by all authors.

FUNDING

This work was supported by the Program for National Natural Science Foundation of China (Nos. 21978104 and 21576103), the Nature Science Foundation of Guangdong Province (No. 2019A1515011654), The Guangdong Program for Support of Top-notch Young Professionals (No. 2016TQ03Z585), and the Fundamental Research Funds for the Central Universities of SCUT, China (Nos. 2019PY17, 2019PY13).

SUPPLEMENTARY MATERIAL

The Supplementary Material for this article can be found online at: https://www.frontiersin.org/articles/10.3389/fenrg.2020.00083/full#supplementary-material

REFERENCES

Akim, L. G., Argyropoulos, D. S., Jouanin, L., Leplé, J.-C., Pilate, G., Pollet, B., et al. (2001). Quantitative ^{31}P NMR spectroscopy of lignins from transgenic poplars. *Holzforschung* 55, 386–390. doi: 10.1515/HF.2001.064

Barsbay, M., and Güner, A. (2007). Miscibility of dextran and poly(ethylene glycol) in solid state: effect of the solvent choice. *Carbohydr. Polym.* 69, 214–223. doi: 10.1016/j.carbpol.2006.09.028

Cequier, E., Aguilera, J., Balcells, M., and Canela-Garayoa, R. (2019). Extraction and characterization of lignin from olive pomace: a comparison study among ionic liquid, sulfuric acid, and alkaline treatments. *Biomass Convers. Biorefin.* 9, 241–252. doi: 10.1007/s13399-019-00400-w

Constant, S., Wienk, H. L. J., Frissen, A. E., Peinder, P. D., Boelens, R., and Van Es, D. S., et al. (2016). New insights into the structure and composition of technical lignins: a comparative characterisation study. *Green Chem.* 18, 2651–2665. doi: 10.1039/C5GC03043A

De Menezes, F. F., Rencoret, J., Nakanishi, S. C., Nascimento, V. M., Silva, V. F. N., and Gutierrez, A., et al. (2017). Alkaline pretreatment severity leads to different lignin applications in sugarcane biorefineries. *ACS Sustain. Chem. Eng.* 5, 5702–5712. doi: 10.1021/acssuschemeng.7b00265

Del Río, J. C., Prinsen, P., Rencoret, J., Nieto, L., and Gutiérrez, A. (2012). Structural characterization of the lignin in the cortex and pith of elephant grass (Pennisetum purpureum) stems. *J. Agric. Food Chem.* 60, 3619–3634. doi: 10.1021/jf300099g

Dong, X. Q., Yang, J. S., Zhu, N., Wang, E. T., and Yuan, H. L. (2013). Sugarcane bagasse degradation and characterization of three white-rot fungi. *Bioresour. Technol.* 131, 443–451. doi: 10.1016/j.biortech.2012.12.182

Gallo, J. M. R., Alonso, D. M., Mellmer, M. A., and Yeap, J. H. (2013). Production of furfural from lignocellulosic biomass using beta zeolite and biomass-derived solvent. *Top. Catal.* 56, 1775–1781. doi: 10.1007/s11244-013-0113-3

Granata, A., and Argropouls, D. S. (1995). 2-chloro-4,4,5,5-tetramethyl-1,3,2-dioxaphospholane, a reagent for the accurate determination of the uncondensed and condensed phenolic moieties in lignins. *J. Agric. Food Chem.* 43, 1538–1544. doi: 10.1021/jf00054a023

Harman-Ware, A. E., Crocker, M., Kaur, A. P., Meier, M. S., Kato, D., and Lynn, B. (2013). Pyrolysis–GC/MS of sinapyl and coniferyl alcohol. *J. Anal. Appl. Pyrol.* 99, 161–169. doi: 10.1016/j.jaap.2012.10.001

Hoekman, S. K., Broch, A., and Robbins, C. (2011). Hydrothermal carbonization (HTC) of lignocellulosic biomass. *Energy Fuels* 25, 1802–1810. doi: 10.1021/ef101745n

Kaparaju, P., and Felby, C. (2010). Characterization of lignin during oxidative and hydrothermal pre-treatment processes of wheat straw and corn stover. *Bioresour. Technol.* 101, 3175–3181. doi: 10.1016/j.biortech.2009.12.008

Karp, E. M., Donohoe, B. S., O'Brien, M. H., Ciesielski, P. N., Mittal, A., and Biddy, M. J., et al. (2014). Alkaline pretreatment of corn stover: bench-scale fractionation and stream characterization. *ACS Sustain. Chem. Eng.* 2, 1481–1491. doi: 10.1021/sc500126u

Katahira, R., Mittal, A., Mckinney, K., Chen, X., Tucker, M., Johnson, D., et al. (2016). Base-catalyzed depolymerization of biorefinery lignins. *ACS Sustain. Chem. Eng.* 4, 1474–1486. doi: 10.1021/acssuschemeng.5b01451

Kim, H., Ralph, J., and Akiyama, T. (2008a). Solution-state 2D NMR of ball-milled plant cell wall gels in DMSO-d_6/pyridine-d_5. *Bioenergy Res.* 8, 576–591. doi: 10.1039/B916070A

Kim, H., Ralph, J., and Akiyama, T. (2008b). Solution-state 2D NMR of ball-milled plant cell wall gels in DMSO-d_6. *Bioenergy Res.* 1, 56–66. doi: 10.1007/s12155-008-9004-z

Liu, C. F., Ren, J. L., Xu, F., Liu, J. J., Sun, J. X., and Sun, R. C. (2006a). Isolation and characterization of cellulose obtained from ultrasonic irradiated sugarcane bagasse. *J. Agric. Food Chem.* 54, 5742–5748. doi: 10.1021/jf060929o

Liu, C. F., Sun, R., and Ye, J. (2006b). Structural and thermal characterization of sugarcane bagasse phthalates prepared with ultrasound irradiation. *Polym. Degrad. Stab.* 91, 280–288. doi: 10.1016/j.polymdegradstab.2005.05.005

Liu, L., Sun, J., Li, M., Wang, S., Pei, H., and Zhang, J. (2009). Enhanced enzymatic hydrolysis and structural features of corn stover by $FeCl_3$ pretreatment. *Bioresour. Technol.* 100, 5853–5858. doi: 10.1016/j.biortech.2009.06.040

Liu, Z., Luo, X. G., Li, Y., Li, L., and Huang, Y. (2009). Extraction of lignin from pulping black liquor by organic acid. *Mater. Sci. Forum* 620–622, 571–574. doi: 10.4028/www.scientific.net/MSF.620-622.571

Lu, Q., Liu, W., Yang, L., Zu, Y., Zu, B., and Zhu, M., et al. (2012). Investigation of the effects of different organosolv pulping methods on

antioxidant capacity and extraction efficiency of lignin. *Food Chem.* 131, 313–317. doi: 10.1016/j.foodchem.2011.07.116

Ma, L., Cui, Y., Cai, R., Liu, X., Zhang, C., and Xiao, D. (2015). Optimization and evaluation of alkaline potassium permanganate pretreatment of corncob. *Bioresour. Technol.* 180, 1–6. doi: 10.1016/j.biortech.2014.12.078

Miao, W., Jinhui, P., Xueming, Z., and Runcang, S. (2014). Enhancement of lignin biopolymer isolation from hybrid poplar by organosolv pretreatments. *Int. J. Polym. Sci.* 2014, 1–10. doi: 10.1155/2014/194726

Miller, J., Evans, L., Mudd, J. E., and Brown, K. (2002). Batch microreactor studies of lignin depolymerization by bases. 2. aqueous solvents. *Off. Sci. Tech. Inform. Tech. Rep.* 30, 61–78. doi: 10.2172/800964

Miller, J. E., Evans, L., Littlewolf, A., and Trudell, D. E. (1999). Batch microreactor studies of lignin and lignin model compound depolymerization by bases in alcohol solvents. *Fuel* 78, 1363–1366. doi: 10.1016/S0016-2361(99)00072-1

Moghaddam, L., Rencoret, J., Maliger, V. R., Rackemann, D. W., Harrison, M. D., and Gutiérrez, A., et al. (2017). Structural characteristics of bagasse furfural residue and its lignin component. an NMR, Py-GC/MS, and FTIR study. *ACS Sustain. Chem. Eng.* 5, 4846–4855. doi: 10.1021/acssuschemeng.7b00274

Mousavioun, P., and Doherty, W. O. S. (2010). Chemical and thermal properties of fractionated bagasse soda lignin. *Ind. Crops Prod.* 31, 52–58. doi: 10.1016/j.indcrop.2009.09.001

Moxley, G., Gaspar, A. R., Higgins, D., and Xu, H. (2012). Structural changes of corn stover lignin during acid pretreatment. *J. Indust. Microbiol. Biotechnol.* 39, 1289–1299. doi: 10.1007/s10295-012-1131-z

Nitsos, C., Stoklosa, R., Karnaouri, A., Dimitrij, V., Lange, H., Hodge,D., et al. (2016). Isolation and characterization of organosolv and alkaline lignins from hardwood and softwood biomass. *ACS Sustain. Chem. Eng.* 4, 5181–5193. doi: 10.1021/acssuschemeng.6b01205

Phongpreecha, T., Hool, N. C., Stoklosa, R. J., Klett, A. S., Foster, C. E., Bhalla, A., et al. (2017). Predicting lignin depolymerization yields from quantifiable properties using fractionated biorefinery lignins. *Green Chem.* 19, 5131–5143. doi: 10.1039/C7GC02023F

Rahimi, K. S. M., Brown, R. J., Tsuzuki, T., and Rainey, T. J. (2016). A comparison of cellulose nanocrystals and cellulose nanofibres extracted from bagasse using acid and ball milling methods. *Adv. Nat. Sci. Nanosci. Nanotechnol.* 7:035004. doi: 10.1088/2043-6262/7/3/035004

Ren, G. J., Zhang, C. L., Zhao, J. X., and Gao, X. R. (2009). Adsorption performance of furfural residue for Cr(VI). *Plat. Finish.* 31, 9–11.

Rencoret, J., Marques, G., Gutierrez, A., Nieto, L., Santos, J. I., Jiménez-Barbero, J., et al. (2009). HSQC-NMR analysis of lignin in woody (Eucalyptus globulus and Picea abies) and non-woody (Agave sisalana) ball-milled plant materials at the gel state. *Holzforschung* 63, 691–698. doi: 10.1515/HF.2009.070

Río, J. C. D., Lino, A. G., Colodette, J. L., Lima, C. F., Gutiérrez, A., Martínez, A. T., et al. (2015). Differences in the chemical structure of the lignins from sugarcane bagasse and straw. *Biomass Bioenergy* 81, 322–338. doi: 10.1016/j.biombioe.2015.07.006

Rodríguez-Gutiérrez, G., Rubio-Senent, F., Lama-Muñoz, A., García, A., and Fernández-Bolaños, J. (2014). Properties of lignin, cellulose, and hemicelluloses isolated from olive cake and olive stones: binding of water, oil, bile acids, and glucose. *J. Agric. Food Chem.* 62, 8973–8981. doi: 10.1021/jf502062b

Rönnols, J., Schweinebarth, H., Jacobs, A., Stevanic, J. S., Olsson, A. M., Reimann, A., et al. (2015). Structural changes in softwood kraft lignin during non-oxidative thermal treatment. *Nordic Pulp Paper Res. J.* 30, 550–561. doi: 10.3183/npprj-2015-30-04-p550-561

Sun, S. N., Li, M. F., Yuan, T. Q., Xu, F., and Sun, R. C. (2012). Effect of ionic liquid pretreatment on the structure of hemicelluloses from corncob. *J. Agric. Food Chem.* 60, 11120–11127. doi: 10.1021/jf3021464

Sun, Y. D., Sun, R., Jiang, J. X., and Zhu, L. W. (2008). Study on conversion process for furfural residue manufacture to ethanol by simultaneous saccharification and fermentation. *Modern Chem. Industry* 85, 93–101. doi: 10.1212/WNL.0000000000001984

Tao, L., Chen, X., Aden, A., Kuhn, E., Himmel, M. E., and Tucker, M., et al. (2012). Improved ethanol yield and reduced minimum ethanol selling price (mesp) by modifying low severity dilute acid pretreatment with deacetylation and mechanical refining: 2) techno-economic analysis. *Biotechnol. Biofuels* 5:69. doi: 10.1186/1754-6834-5-69

Thring, R. W. (1994). Alkaline degradation of ALCELL® lignin. *Biomass Bioenergy* 7, 125–130. doi: 10.1016/0961-9534(94)00051-T

Tiappi, D. M. F., Nicolas, V., Mario, A., Nicolas, J., Happi, G. T., Patrick, G., et al. (2019). Chemical composition analysis and structural features of banana rachis lignin extracted by two organosolv methods. *Ind. Crops Prod.* 132, 269–274. doi: 10.1016/j.indcrop.2019.02.022

Van Erven, G., De Visser, R., Merkx, D. W. H., Strolenberg, W., De Gijsel, P., and Gruppen, H., et al. (2017). Quantification of lignin and its structural features in plant biomass using ^{13}C lignin as internal standard for pyrolysis-GC-SIM-MS. *Anal. Chem.* 89, 10907–10916. doi: 10.1021/acs.analchem.7b02632

Vigneault, A., Johnson, D. K., and Chornet, E. (2007). Base-catalyzed depolymerization of lignin: separation of monomers. *Can. J. Chem. Eng.* 85, 906–916. doi: 10.1002/cjce.5450850612

Villaverde, J. J., Li, J., Ek, M., Ligero, P., and Vega, A. D. (2009). Native lignin structure of miscanthus x giganteus and its changes during acetic and formic acid fractionation. *J. Agric. Food Chem.* 57, 6262–6270. doi: 10.1021/jf900483t

Wang, Q., Liu, Y., Liu, S., Wang, W., Yu, Q., Fu, J., et al. (2019). Comprehensive thermochemical utilization of biomass residues from furfural plants and ELW technology. *Fuel* 252, 116–124. doi: 10.1016/j.fuel.2019.04.089

Wang, Y., Xu, Z. Y., Song, X., Yang, B., and Zhang, D. (2017). The preparation of low-cost adsorbent for heavy metal based on furfural residue. *Mater. Manufact. Proc.* 32, 87–92. doi: 10.1080/10426914.2016.1198017

Xu, G., Wang, L., Liu, J., and Wu, J. (2013). FTIR and XPS analysis of the changes in bamboo chemical structure decayed by white-rot and brown-rot fungi. *Appl. Surf. Sci.* 280, 799–805. doi: 10.1016/j.apsusc.2013.05.065

Xu, J. K., Sun, Y. C., and Sun, R. C. (2015). Synergistic effects of ionic liquid plus alkaline pretreatments on eucalyptus: lignin structure and cellulose hydrolysis. *Proc. Biochem.* 50, 955–965. doi: 10.1016/j.procbio.2015.03.014

Yang, D., Zhong, L. X., Yuan, T. Q., Peng, X. W., and Sun, R. C. (2013). Studies on the structural characterization of lignin, hemicelluloses and cellulose fractionated by ionic liquid followed by alkaline extraction from bamboo. *Ind. Crops Prod.* 43, 141–149. doi: 10.1016/j.indcrop.2012.07.024

Yang, S., and Pei, J. (2001). *Plant Fiber Chemistry*. Beijing: China Light Industry Press.

Zhang, H., Zheng, R., Cheng, J., and Huang, H. (2010). Determination of components of lignocellulose by NREL. *Anal. Lab.* 29, 15–18.

Zhu, C. (2008). *Study on the Fractionation and Structural Characteristics of LCC in Wheat Straw Alkali Extraction*. Nanjing Forestry University.

Conflict of Interest: The authors declare that the research was conducted in the absence of any commercial or financial relationships that could be construed as a potential conflict of interest.

frontiers in Energy Research

ORIGINAL RESEARCH
published: 11 June 2020
doi: 10.3389/fenrg.2020.00114

An Investigation Into the Upgrading Process of Lignin Model Dimer—Phenethyl Phenyl Ether by *in situ* ^{2}H NMR and GC-MS

Yunyi Yang[1,2], *Zhihong Wu*[1,2], *Ying Luo*[1,2], *Guangting Han*[3,4], *Wei Jiang*[3,4], *Maorong Wang*[3,4] *and Haoxi Ben*[1,2]*

[1] School of Energy and Environment, Southeast University, Nanjing, China, [2] Key Laboratory of Energy Thermal Conversion and Control of Ministry of Education, Nanjing, China, [3] School of Textile and Clothing, Qingdao University, Qingdao, China, [4] Laboratory of New Fiber Materials and Modern Textile, Qingdao, China

A key challenge in studying the upgrading process for the thermochemical conversion of biomass, such as lignin, is to understand the underlying mechanisms of catalytic conversion at the atomic scale. In this study, a method combined with *in situ* ^{2}H NMR and GC-MS was proposed for investigating the conversion of phenethyl phenyl ether (PPE) in the hydrotreating process, as catalyzed by Pd, Ru, and Pt loaded onto C or γ-Al_2O_3. The results indicated that Pd/γ-Al_2O_3 prefers to produce more ether bond-cleaved products, while Pt prefers to produce more hydrogenation products from PPE. Furthermore, based on this new strategy, a possible reaction mechanism of PPE with Pd/γ-Al_2O_3 was presented from the atomic point of view, showing the potential of this *in situ* detection method for reaction mechanism studies. Besides, mechanistic investigations by GC-MS were accomplished for the hydrothermal treatment of PPE for comparison with the new method. The results showed that the *in situ* ^{2}H NMR combined with GC-MS provided a deeper understanding of the catalytic mechanism compared to GC-MS alone.

Keywords: lignin, *in situ* ^{2}H NMR, GC-MS, mechanism, upgrading process

OPEN ACCESS

Edited by:
Fengxia Yue, South China University of Technology, China

Reviewed by:
Selhan Karagoz, Karabük University, Turkey
Halil Durak, Yüzüncü Yil University, Turkey
Yanding Li, Massachusetts Institute of Technology, United States

***Correspondence:**
Haoxi Ben
benhaoxi@gmail.com

Specialty section:
This article was submitted to Bioenergy and Biofuels, a section of the journal Frontiers in Energy Research

Received: *17 March 2020*
Accepted: *13 May 2020*
Published: *11 June 2020*

Citation:
Yang Y, Wu Z, Luo Y, Han G, Jiang W, Wang M and Ben H (2020) An Investigation Into the Upgrading Process of Lignin Model Dimer—Phenethyl Phenyl Ether by in situ ^{2}H NMR and GC-MS. Front. Energy Res. 8:114. doi: 10.3389/fenrg.2020.00114

INTRODUCTION

Lignin is a waste material from the paper industry and a by-product from second-generation bio-ethanol production processes. Lignin is also abundant in waste biomass from agriculture, as well as yard and forestry wastes (Barton et al., 2018). Furthermore, lignin is the only renewable aromatic resources in nature (Konnerth et al., 2015). However, as low-heat fuels or additives of concrete, the commercial utilization rate of lignin is still <10%, which is far lower than that of cellulose and hemicellulose (Li et al., 2015; Wang et al., 2019). Under this circumstance, by converting lignin into fuel or valuable chemicals through appropriate methods, reducing use of fossil fuel and lower emissions of carbon dioxide could be achieved (David and Ragauskas, 2010). Thus, how to make more reasonable use of lignin has attracted the attention of researchers around the world.

At present, common conversion methods of lignin include pyrolysis, acid or alkali catalysis, hydrocracking, gasification, and reductive transformation (Katahira et al., 2016; Shuai et al., 2016; Fan et al., 2018; Santana et al., 2018; Sirousrezaei et al., 2018). Among these, the premise of the efficient utilization of lignin is the depolymerization of lignin (Chio et al., 2019; Zhang and Wang, 2020). In terms of structure, lignin is a three-dimensional polymer which is mainly composed of

basic phenylpropane units, such as p-hydroxyphenyl, guaiacyl and syringyl (Zakzeski et al., 2010). These basic units are connected by C-C or C-O bonds. From **Table 1**, the reported abundance of C-O bonds is more than that for C-C bonds in softwood and hardwood (Chakar and Ragauskas, 2004; Zakzeski et al., 2010). Besides, the theoretical calculation of a C-O bond's dissociation energy is usually smaller than that of a C-C bond in lignin model compounds, which indicates that the dissociation of lignin usually starts with a C-O bond. Therefore, the cleavage of C-O bonds is of great significance for the depolymerization of lignin (Elder and Beste, 2014).

Hydrogenolysis, where H_2 is used at high temperature and high pressure with metal catalysts, is regarded as an effective way to cleave the bond of C-O for the purpose of converting lignin into high-value liquid precursors (Yan and Dyson, 2013). Thus, it is crucial to find a suitable catalyst for breaking C-O bonds effectively. However, lignin has a relatively complex structure albeit without a defined one. Thus, model compounds have been employed to represent some typical structures of lignin. Phenethyl phenyl ether (PPE) has been commonly used to represent the β-O-4 linkage, which is one of the major linkages in the lignin structure. Recently, Mauriello et al. (2018) applied the co-precipitation technique to synthesize Pd/Ni to catalyze the conversion of PPE. In 2013, Song et al. (2013) employed Pd/C, Ru/C, and Ni/C for hydrogenation and cracking reactions of PPE. Most of the research focuses on the catalytic effect of different catalysts on PPE but less on the catalytic mechanism. However, the study of catalytic mechanism is also of considerable importance in the synthesis of catalysts and the design of production processes (Shuang et al., 2019).

To study inner mechanisms, choosing appropriate techniques to monitor the reaction is important. GC-MS has been most widely used in various chemical reactions in order to speculate the reaction process. However, some specific reaction process and intermediate products cannot be effectively recorded and studied with GC-MS. Recently, *in situ* monitoring using NMR has attractive attention. Richter et al. (2019) used *in situ* ^{13}C NMR spectra to identify final products, intermediates, and by-products during the whole reaction, which in turn helped to reveal the inner mechanism of electrocatalytic oxidation of alcohol. An *in situ* ^{1}H NMR technique was also employed by Wang et al. in order to follow the reaction of inulin biomass (Wang et al., 2015). The above-mentioned studies showed that *in situ* detection is an effective way to understand the reaction mechanism. Isotope labeling combined with ^{2}H NMR is another effective means for investigating the reaction mechanism. Wang et al. (2018) employed CD_4 to trace the hydrogen atoms of methane in the co-pyrolysis of methane and cellulose, providing evidence of methane incorporation into aromatic compounds by ^{2}H NMR characterization. In our previous research, the ring-opening mechanism of lignin model compounds was investigated by ^{2}H NMR as well (Ben et al., 2016).

In this study, we proposed a strategy of isotopic (deuterium) labeling combined with *in situ* ^{2}H NMR monitoring and GC-MS to detect and analyze the catalytic upgrading process of PPE. Pt, Pd, and Ru on two commonly used supporting materials (carbon and Al_2O_3) served as catalysts. For comparison, our strategy and GC-MS alone were separately applied in the hydrotreating process and hydrothermal treatment of PPE. Furthermore, based on the data from the whole reaction, a possible transformation mechanism at the atomic scale was proposed and discussed. This research showed the potential of a high-pressure *in situ* ^{2}H NMR monitoring method using isotopic labeling for studying the upgrading process of biomass model compounds.

TABLE 1 | Reported abundance of major linkages in softwood and hardwood lignin (Chakar and Ragauskas, 2004; Zakzeski et al., 2010).

C-O linkage Abundance Per 100 C_9-units	**β-O-4**	**4-O-5**	**Dibenzodioxocin**	
Softwood	45–50	4–7	5–7	
Hardwood	60–62	7–9	0–2	
C-C linkage Abundance Per 100 C_9-units	**β-β**	**5–5**	**β-1**	**β-5**
Softwood	2–4	19–22	7–9	9–12
Hardwood	3–12	3–9	1–7	3–11

MATERIALS AND METHODS

Materials

PPE, tetramethylsilane-d12(TMS-d12), chloroform, phenol, ethyl benzene, phenylethyl alcohol, cyclohexanone, cyclohexanol and cyclohexane ethanol were purchased from Sigma-Aldrich (St. Louis, MO) and used as received. Pt/Al_2O_3(5%), Pt/C(5%), Pd/Al_2O_3(5%), Pd/C(5%), Ru/Al_2O_3(5%), and Ru/C(5%) were purchased from Sigma-Aldrich and dried to remove moisture before use. Deuterium gas was purchased from Airgas.

Experiment and Experimental Procedure

Hydrotreating Process

A reaction mixture was prepared in a 5 mm NMR tube (Wilmad), with 100 μL of PPE, 0.5 μL of TMS-d12 and 2 mg of catalyst. The NMR tube was purged five times with D_2 to remove the air. The initial pressure in the NMR tube was set to 700 kPa, after which it was inserted into the preheated NMR spectrometer where the temperature was 100°C. The spectra were recorded every hour for 16 h. Finally, the samples which reacted in the NMR tube were dissolved in chloroform for subsequent GC-MS analysis.

Hydrothermal Treatment

5 mg of PPE, 0.3 mg of catalyst and 5 ml of water were added to the reaction tube. The reactor was purged with H_2 three times to exclude air and then pressurized to 700 kPa with H_2. The reactor was kept at 100°C for 12 h. The products were filtered and extracted with 1 mL of chloroform for GC-MS analysis. The external label method was used for the quantitative analysis of products.

Characterization of Products

The products from hydrotreating process were analyzed by ^{2}H NMR and GC-MS, while the products from hydrothermal treatment were analyzed by GC-MS.

All ^{2}H NMR data were recorded with a Bruker Avance/DMX 600 MHz NMR spectrometer. ^{2}H NMR spectra were detected with 1.5 s of acquisition time, 2 s of relaxation delay and 1,024 scans by Bruker's pulse program "zg2h" with the lock channel in a Bruker's BBO probe. Then, data were processed by MestReNova 11.0 with automatic phase correction and six-order Bernstein polynomial. The chemical shift for ^{2}H NMR was referenced to 0.00 ppm of TMS-d12.

The analysis of GC-MS was accomplished by an Agilent G1530A gas chromatograph (GC) interfaced with a HP 5973 mass spectrometer. The GC injector was operated at 280°C. 61.3 mL/min of constant He flow was applied to the capillary column (Agilent 190915-433). The GC oven was programmed as follows: hold at 50°C for 1 min, heated up to 280°C with a ramp of 10.0°C/min and hold at 280°C for 1 min.

Theoretical Chemical Calculation Method

All theoretical chemical calculations were conducted by Gaussian09. For the calculation of chemical shifts, model compounds were optimized with B3LYP/6-31g+(d, p) while frequency calculations were performed on the optimized model to ensure that there was no virtual frequency. Gauge-independent atomic orbital (GIAO) methodology combined with B3LYP/6-311g+(2d, p) was used to acquire the NMR isotropic shielding tensors. In order to reduce the error, linear regression was employed to convert the calculation results to chemical shifts. The relevant formula is as follows where the intercept is 31.8884 and the slope is −1.0481 (Jain et al., 2009; Pierens, 2014).

$$\delta = \frac{intercept - \sigma}{-slope}$$

The M06-2X method and the 6-31G+(d, p) basis set were employed to calculate the C-H bond dissociation energy (BDE) of PPE at 100°C and 700 kPa (Wang and Liu, 2016).

RESULTS AND DISCUSSION

The hydrotreating process and hydrothermal treatment were conducted as the two common approaches to the lignin upgrading process. For insights into the catalytic mechanism of PEE, a milder condition (100°C and 700 kPa) was used in this study, which allowed for the preservation of potential intermediates.

Hydrotreating Process

Figures 1, **2** and **Figures S1–S4** show the results of the deuterium-traced reaction of PPE as catalyzed by Pd, Ru, and Pt which were loaded onto C or γ-Al_2O_3.

The Analysis of the Chemical Shift of Products

In ^{2}H NMR analysis, the chemical shifts in the functional groups refer to **Table S1** (Mullen et al., 2009; Naik et al., 2010; Bordoloi et al., 2015; Ardiyanti et al., 2016; Tessarolo et al., 2016). Accordingly, the peaks from 0.4 to 1.8 ppm belong to aliphatic deuterium. Besides, the possible reaction pathway of PPE in the hydrotreating process is shown in **Figure S5**, according to the products of GC-MS. Therefore, aliphatic deuterium should derive from deuterium labeled ethylbenzene, cyclohexanol, ethyl cyclohexane, and the hydrogenation products of PPE. Based on the GC-MS data (**Figures S6–S8**), deuterium labeled ethyl cyclohexane cannot be detected. Furthermore, the content of deuterium labeled cyclohexanol was limited. Thus, the detected aliphatic deuterium mainly belonged to deuterium labeled ethylbenzene and hydrogenation products of PPE. The existence of deuterium labeled ethylbenzene represents a break in the β-O-4 bond while the other products containing aliphatic deuterium point to the hydrogenation of PPE (**Figure S5**). By comparing the products catalyzed by Pd/γ-Al_2O_3 and Pt/γ-Al_2O_3 (**Figures S6–S8**), we see that Pd/γ-Al_2O_3 can promote the cleavage of ether bond better, while more hydrogenation products could be produced under the catalysis of Pt/γ-Al_2O_3.

The difference in the conversion products of PPE under different catalysts was also reflected in ^{2}H NMR. The areas of the two peaks around 1.43 ppm and 2.01 ppm in **Figure 1** (Pd/γ-Al_2O_3) were much larger than in the case of **Figure 2** (Pt/γ-Al_2O_3). Besides, these two peaks had similar areas and appeared simultaneously 3 h after the start of reaction (**Figure 1**). From **Table S1**, the peak at 2.01 ppm did not belong to deuterium labeled ethylbenzene nor to the hydrogenation products of PPE. The peak at 1.43 ppm belonged to the range of β-CH_3 attached to the aromatic ring, which may have been produced by deuterium labeled ethylbenzene. Meanwhile, according to the data from the Gaussian simulation (**Table S2**), the terminal aliphatic deuterium of ethylbenzene was assigned to the peak around 1.33 ppm, which is close to the chemical shift of 1.43 ppm. Combined with GC-MS data, the peak at 1.43 ppm should belong to deuterium labeled ethylbenzene and the peak at 2.01 ppm should belong to deuterium labeled phenol. Thus, the remaining peaks in the range from 0.4 ppm to 1.8 ppm were mainly assigned to the products from the hydrogenation of PPE. From **Figure S9**, the relative aliphatic deuterium content under Pt/γ-Al_2O_3 was greater than that under Pd/γ-Al_2O_3. This means that the Pt/γ-Al_2O_3 can better promote the hydrogenation of PPE. The result was also consistent with the GC-MS data (**Figure S8**).

Pd

The data above have shown that Pd/γ-Al_2O_3 can effectively catalyze the cleavage of the β-O-4 bond. Further study of the data reveals the mechanism. In **Figure 1**, there are two special peaks around 6.89 and 2.89 ppm which do not belong to the conversion products of PPE. First, the peak at 6.89 ppm belongs to aromatic deuterium (**Table S1**), which should come from the exchange of H/D. Consistently, the products from the H/D exchange of PPE molecules were detected in GC-MS as well (**Figure S10**). It can be inferred from **Figure S10** that the hydrogen which was

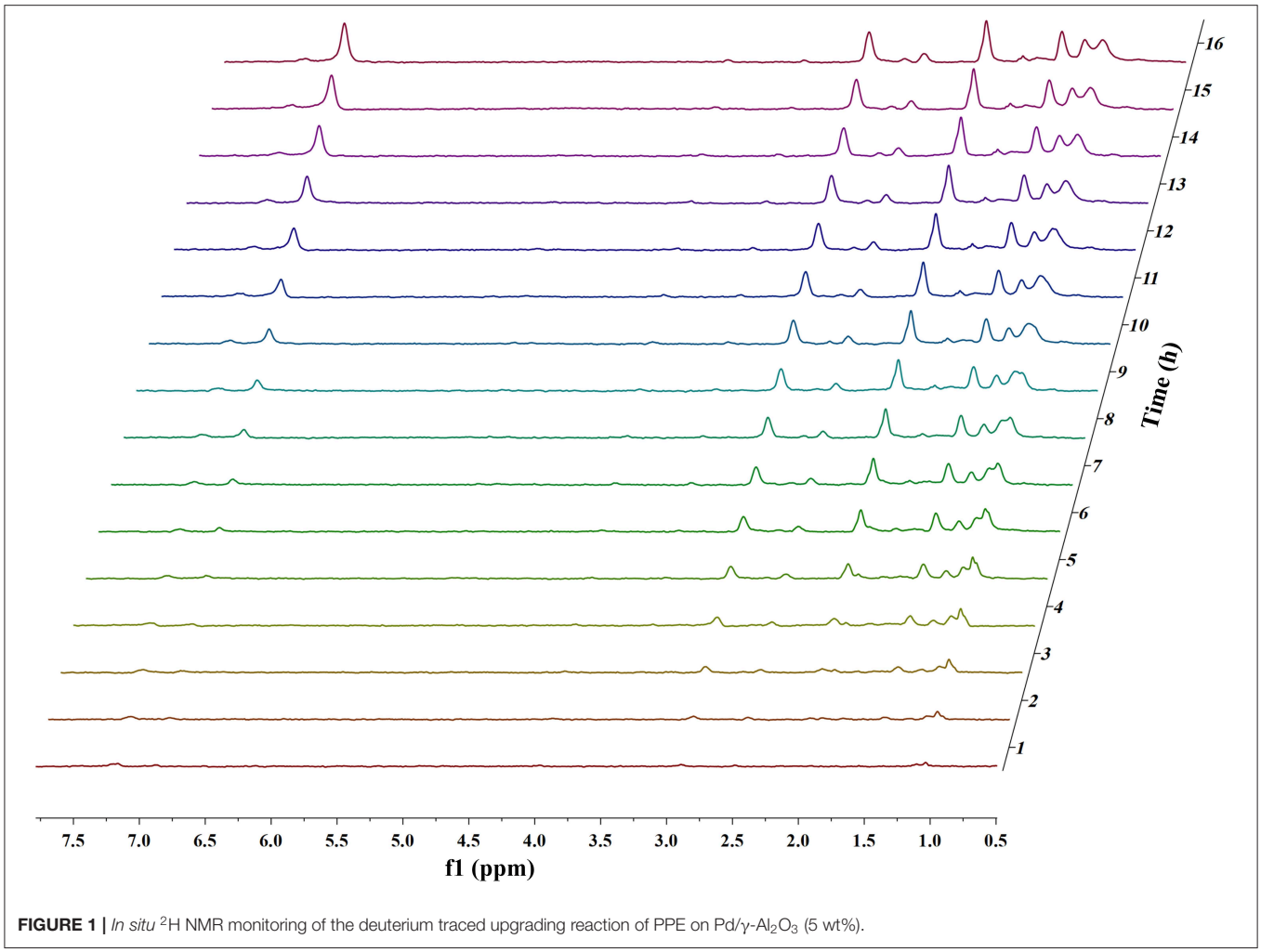

FIGURE 1 | *In situ* ^{2}H NMR monitoring of the deuterium traced upgrading reaction of PPE on Pd/γ-Al_2O_3 (5 wt%).

exchanged with deuterium was the hydrogen 13(14) (the number of atoms can be found in to the **Figure 3**) and the hydrogen of benzene.

To further determine the location of H/D exchanges in PPE, Gaussian simulations of chemical shifts and BDE calculations were introduced to this study. The predicted chemical shift in hydrogen 13(14) was about 3.10 ppm, while that for hydrogen 16(17) was around 3.79 ppm (**Table S3**). Besides, Barton's research showed that the chemical shift in hydrogen 13(14) was 3.00 ppm, while that for hydrogen 16(17) was 4.05 ppm in ^{1}H NMR (Barton et al., 1987). This means that hydrogen 13(14) might be exchanged with the deuterium. In addition, as the BDE of C-H13 is far lower than that of C-H16 according to Gaussian simulation, the bond of C-H13 can more easily perform an H/D exchange (**Table S4**). Therefore, the chemical shift of 2.89 ppm should be assigned to the deuterium exchanged with H13(14). Furthermore, based on the predicted value of the chemical shift (**Table S3**) and Barton's research, the peak at 6.89 ppm should belong to the deuterium exchanged with the hydrogen atom on the benzene ring attached to the oxygen atom (Barton et al., 1987). However, the exact hydrogen atom has not thus far been determined. The result of Gaussian optimization illustrated that the PPE molecules were usually configured as shown in **Figure 4**. Considering H13(14) exchanged with deuterium at the surface of Pd/γ-Al_2O_3, it can be inferred that the Pd/γ-Al_2O_3 could hold PPE molecules in this special position (**Figure 4**) to perform H/D exchanges. Hence, H23 was more likely exchanged with deuterium at the surface of Pd/γ-Al_2O_3 than the other hydrogen atom on the benzene ring. Besides, through semi-quantitative analysis, it was found that using Pd/γ-Al_2O_3 led to more H/D exchanges compared with other catalysts (**Figure S11**).

Additionally, it is noteworthy that this special position in **Figure 4** allows the β-O-4 bond to be fully exposed to the surface of Pd/γ-Al_2O_3, facilitating the cleavage of the ether bond. It is the possible mechanism that Pd/γ-Al_2O_3 can more effectively catalyze the cracking of the ether bond (**Figure 4**). This help us understand the catalytic mechanism from the aspect of atomic scale.

The *in situ* ^{2}H NMR results from the deuterium traced upgrading reaction of PPE on Pd/C showed that the peaks were concentrated on the products from the hydrogenation of PPE

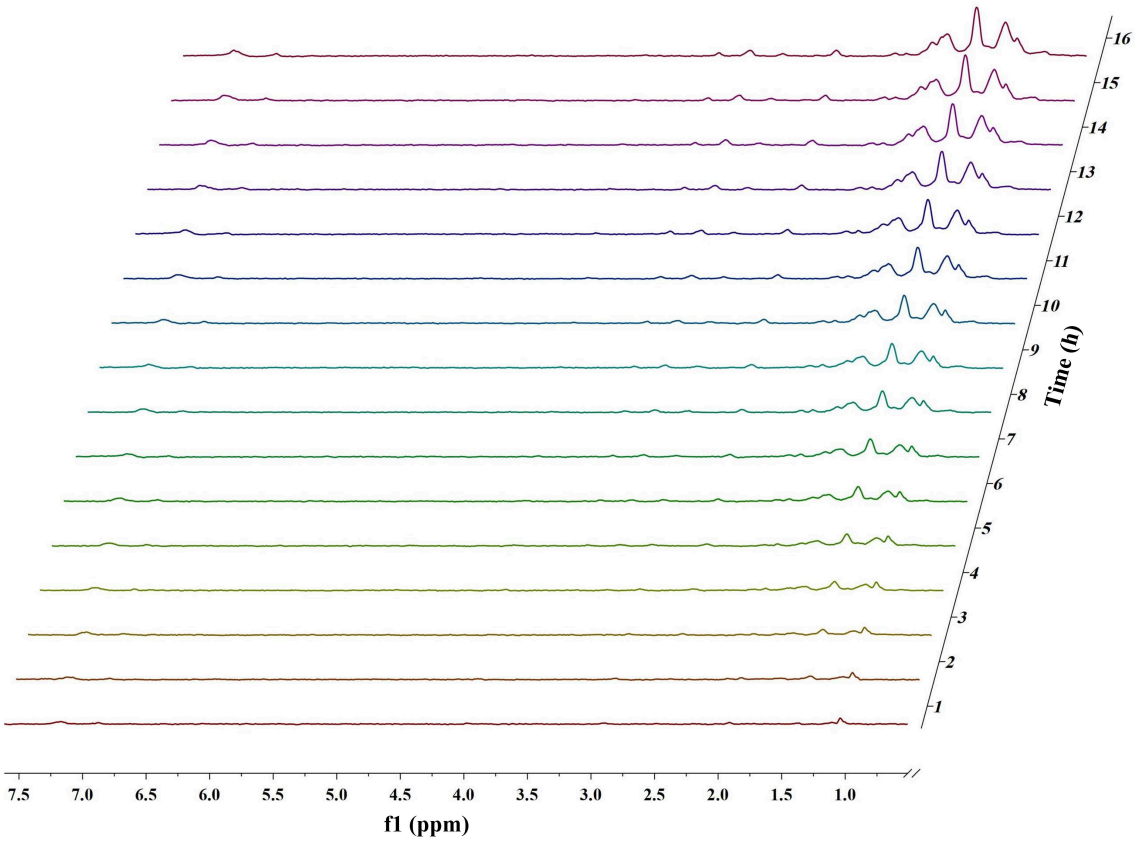

FIGURE 2 | *In situ* ^{2}H NMR monitoring of the deuterium traced upgrading reaction of PPE on Pt/γ-Al_2O_3 (5 wt%).

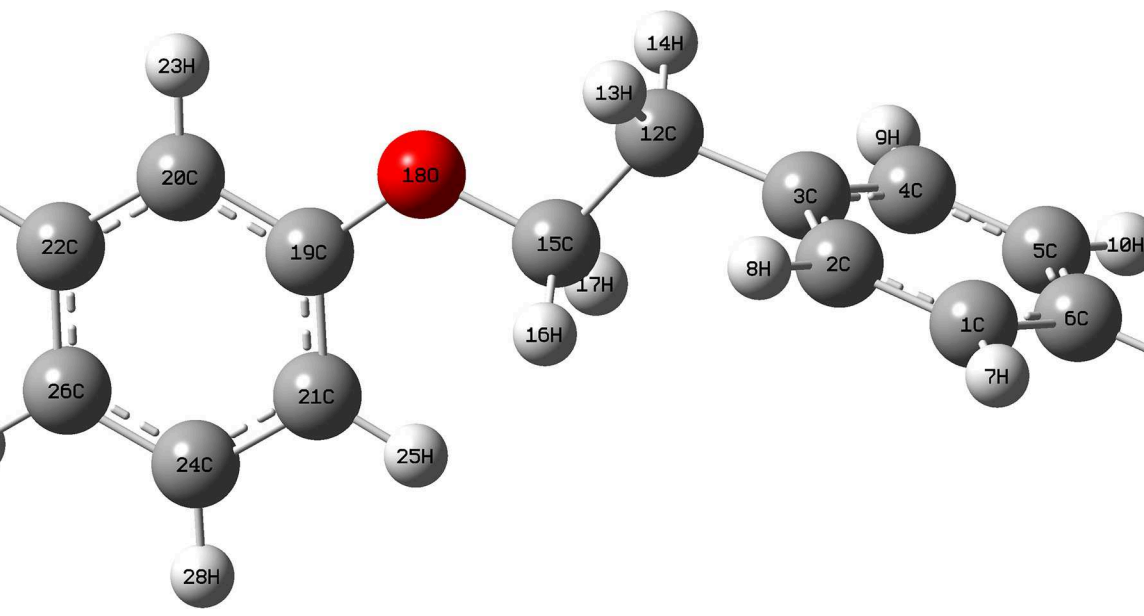

FIGURE 3 | Model structure of PPE.

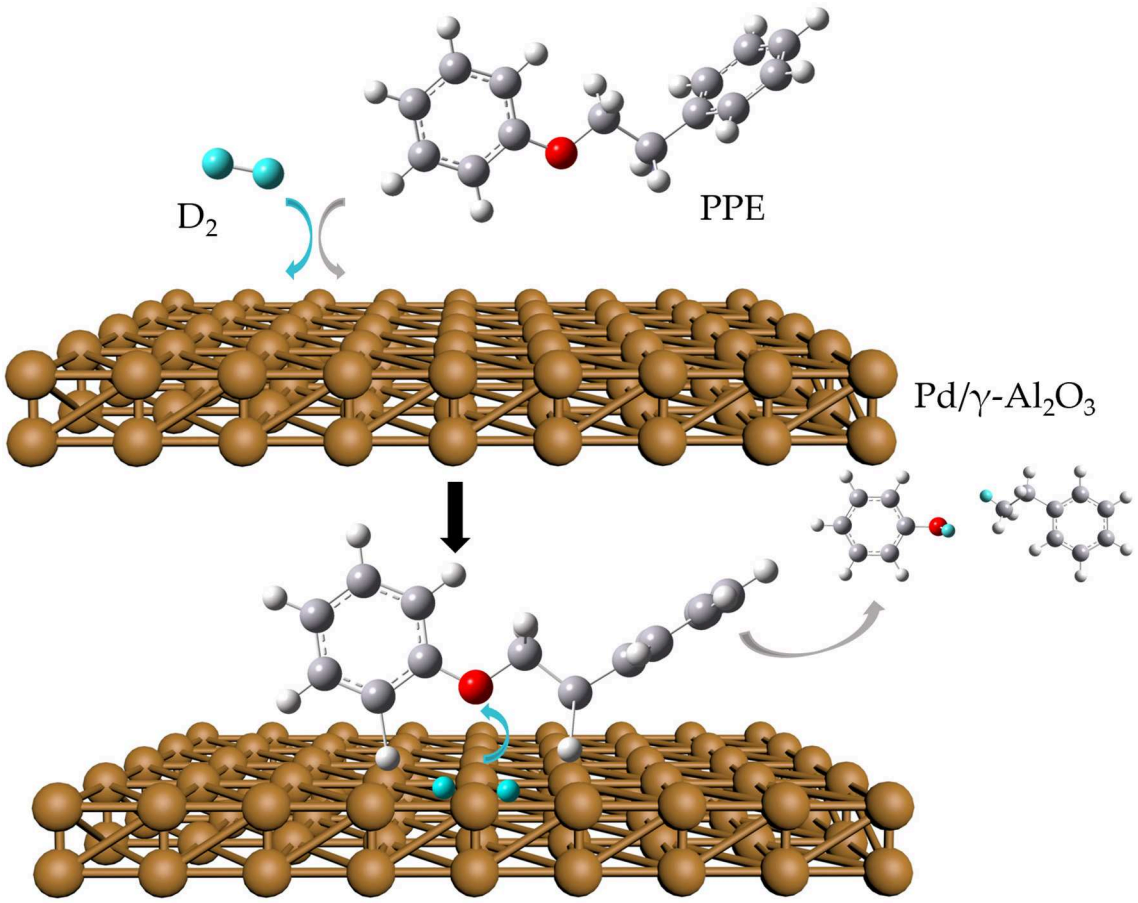

FIGURE 4 | Possible cleavage mechanism of PPE Pd/γ-Al_2O_3.

(**Figure S1**). Compared with Pd/γ-Al_2O_3, which can catalyze the cleavage of ether bonds, Pd/C tended to exhibit catalytic hydrogenation. It is reported that the noble metals mainly show the function of hydrogenation while the acidic support could exhibit the function of cracking the C-O bond (Robinson et al., 2016; Funkenbusch et al., 2019; Kim et al., 2019). Therefore, Pd/γ-Al_2O_3 which has a noble metal on an acidic support should exhibit better cleavage function than Pd/C which has a noble metal on an inactive support. This may be the reason why Pd/γ-Al_2O_3 can catalyze the cleavage of ether bonds more effectively than Pd/C. Besides, the results show that the substrate of Pd had a certain influence on the upgrading process in this condition.

Ru

From **Figures S3, S4**, the chemical shift in the products catalyzed by Ru was mainly around 1.0 ppm, thus belonging to the hydrogenation products of PPE. By comparing the relative aliphatic deuterium content, the efficiency of Ru supported by carbon and γ-Al_2O_3 was both lower than for the two other noble metals in the upgrading of PPE (**Figure S9**). Meanwhile, the products from the H/D exchange by Ru were also limited (**Figure S11**). Thus, the catalytic activity of Ru was not satisfied under this reaction conditions.

Pt

For Pt/γ-Al_2O_3 and Pt/C, the detected results indicated that Pt can promote the hydrogenation of the benzene ring in PPE. Due to overlaps in the chemical shift between the hydrogenation products in ^{2}H NMR, further detailed characterizations for the hydrogenation products were accomplished by GC-MS. The GC-MS results (**Figure S8**) indicated that, compared with Pd/γ-Al_2O_3, Pt/γ-Al_2O_3 performed a better hydrogenation process in realizing more partial and full hydrogenation products, while the conversion ratio of PPE was similar under Pd/γ-Al_2O_3 and Pt/γ-Al_2O_3 (**Figure S12**). Another interesting phenomenon was that Pd/γ-Al_2O_3 preferred to promote hydrogenation on the aliphatic attached aromatic ring (the left benzene ring in the PPE structure in **Figure 5**), while Pt/γ-Al_2O_3 preferred to promote hydrogenation on the oxygen-attached aromatic ring (the right benzene ring in the PPE structure in **Figure 5**) or on both rings.

Obviously, the products of Pd/γ-Al_2O_3 and Pd/C were different based on the data. However, the products upgraded

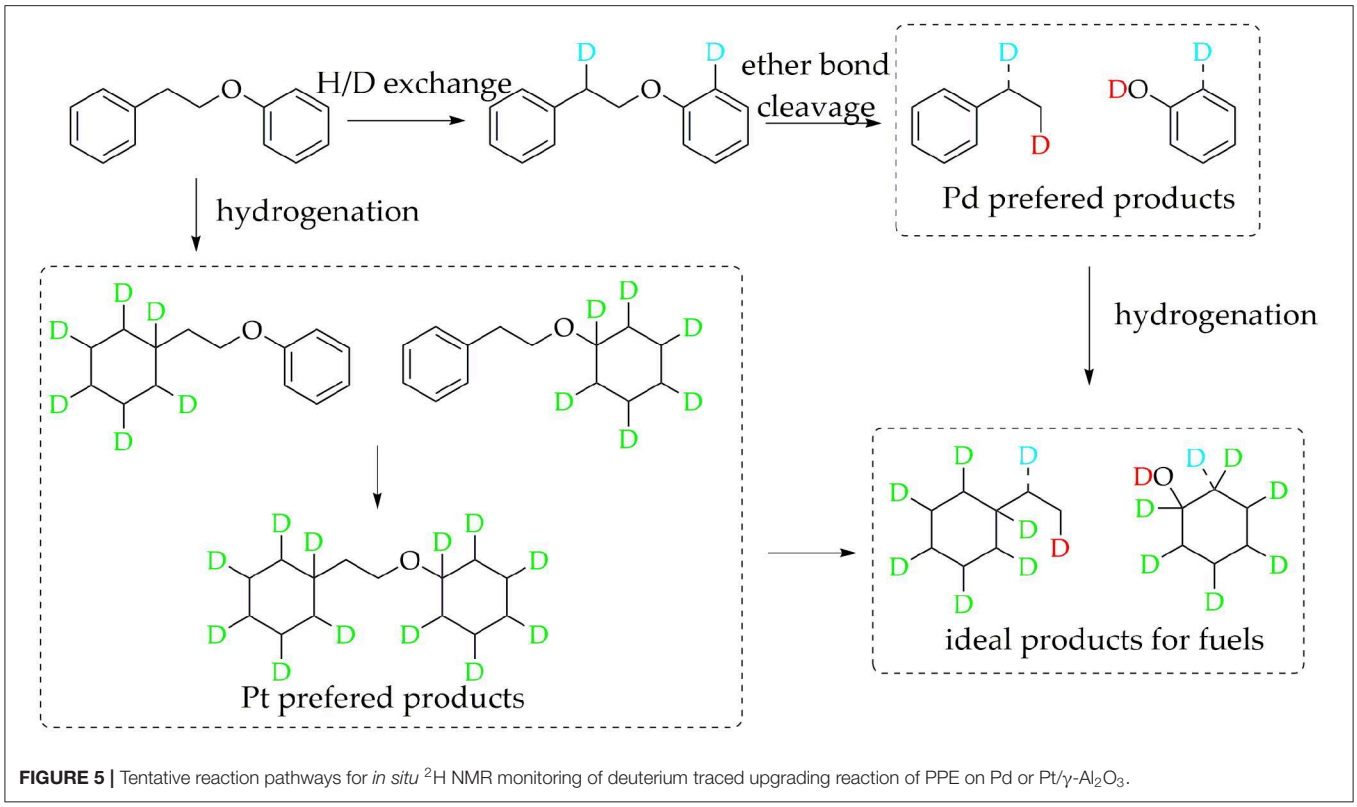

FIGURE 5 | Tentative reaction pathways for *in situ* ^{2}H NMR monitoring of deuterium traced upgrading reaction of PPE on Pd or Pt/γ-Al_2O_3.

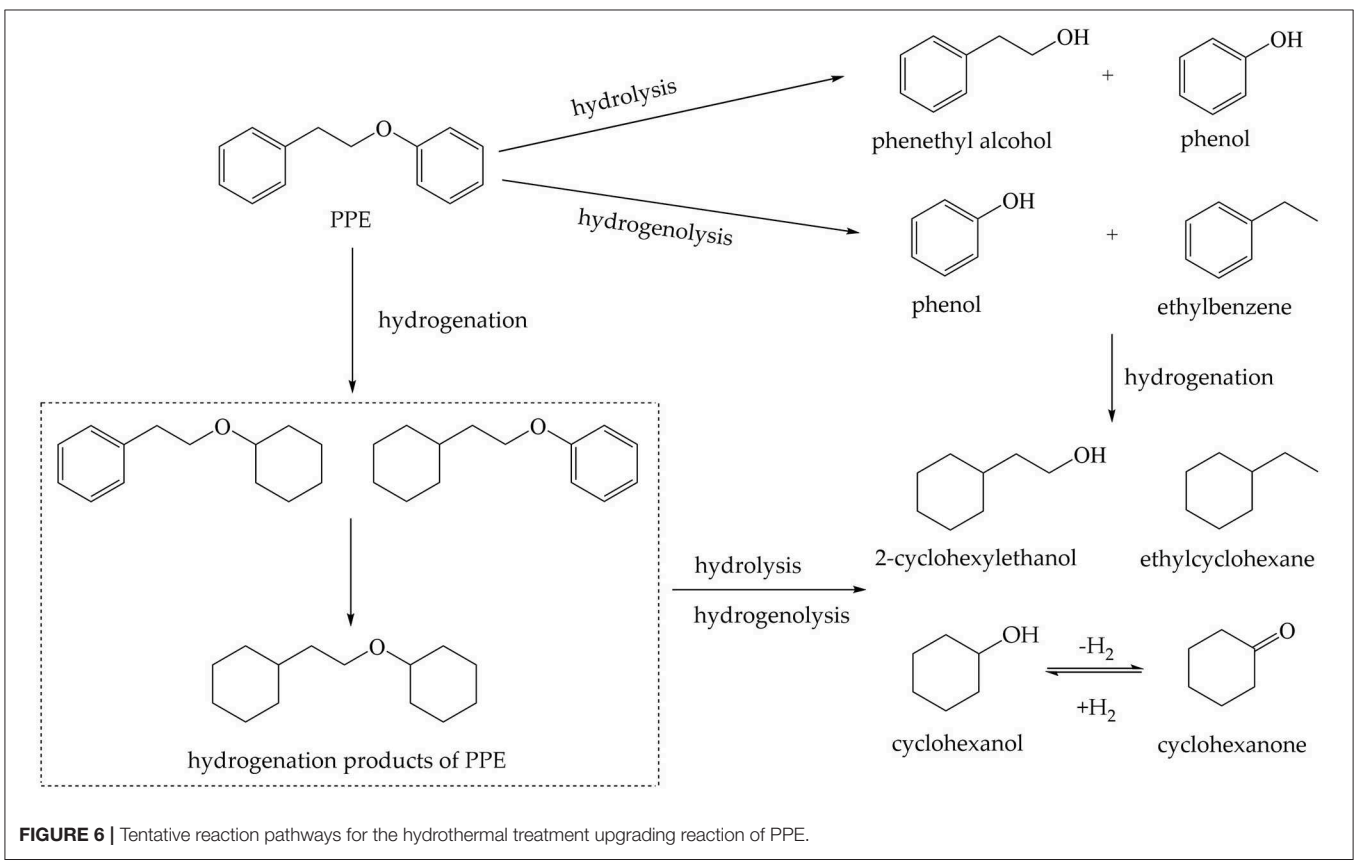

FIGURE 6 | Tentative reaction pathways for the hydrothermal treatment upgrading reaction of PPE.

by Pt/γ-Al_2O_3 (**Figure 2**) and Pt/C (**Figure S2**) did share similar peaks. Analogously, the products upgraded by Ru/γ-Al_2O_3 (**Figure S3**) and Ru/C (**Figure S4**) were nearly the same. This means that the supporting materials affect the reaction pathways differently for diverse catalysts. Besides, the carbon supported catalysts appeared to have lower activity to upgrade PPE in this condition compared with γ-Al_2O_3 supported catalysts (**Figure S9**).

Based on the discussion above, the tentative reaction pathways were proposed as **Figure 5**. In general, Pd/γ-Al_2O_3 promoted the cleavage of the ether bond, while Pt/γ-Al_2O_3 was beneficial for hydrogenation. Our detection strategy captured valuable information in the upgrading reaction of PPE, which is meaningful for understanding the catalytic mechanism and the design of new catalyst. For example, in order to achieve better hydrogenolysis of the ether bond, Pd/γ-Al_2O_3 can be used as a catalyst. Further, a bimetallic catalyst of Pd/γ-Al_2O_3 combined Pt/γ-Al_2O_3 may be able to realize an ideal upgrading for PPE or even real lignin, in turn promoting the production of cycloparaffin.

Hydrothermal Treatment

Although the effects of catalysts were different, the composition of the products was similar in the hydrothermal treatment of PPE catalyzed on Pd, Ru and Pt loaded onto C or γ-Al_2O_3 (**Table S5**). It was reported that the dissociation energy of C19-O was higher than that of C15-O (101.1 vs. 69.9 kJ/mol), which indicated that C15-O was more susceptible to be cleaved, producing phenol and ethylbenzene by hydrogenolysis (Gomez-Monedero et al., 2017). But, in this study, the yield of phenol was far more than for ethylbenzene. Meanwhile, phenethyl alcohol was detected. The research conducted by Gomez-Monedero et al. (2017) showed that the C19-O bond of PPE can be cleaved in methanol solution by hydrogenolysis generating benzene and phenethyl alcohol. However, benzene was not found in this reaction system, indicating that the hydrogenolysis of C19-O did not occur. Thus, phenylethyl alcohol in the product component was primarily derived from the hydrolysis of the ether bond. Therefore, both hydrogenolysis and hydrolysis reactions were involved in the hydrothermal process.

Among reaction products, there were also some products from hydrogenation. The hydrogenation ratio under hydrothermal conditions (**Figure S13**) shows the order of hydrogenation ability: Pd/C>Pt/γ-Al_2O_3>Pd/γ-Al_2O_3>Pt/C>Ru/C>Ru/γ-Al_2O_3. Although Pd/C had the highest conversion ratio for PPE, the hydrogenation ratio was more than 50%, which suggests that the reaction process was not selective. For Ru/γ-Al_2O_3, the hydrogenation ratio for PPE was the lowest and the cleavage ratio of ether bond was around 70%. This indicated that Ru/γ-Al_2O_3 had the best capacity for the cleavage of the ether bond under this condition. Besides, Pt/γ-Al_2O_3, Pd/γ-Al_2O_3, Ru/C and Pt/C had similar catalytic effects. For these catalysts, the ability to catalyze the cleavage of C-O bonds was better than the ability to promote hydrogenation. 4-(2-(cyclohexyloxy)ethyl)cyclohex-1-ene and 5-(2-(cyclohex-2-en-1-1-yl)ethoxy)cyclohexa-1,3-diene were detected in the reaction system, which indicated that the hydrogenation of the reactants was not sufficient. The yields of cyclohexanol, ethyl cyclohexane and 2-cyclohexylethanol were also limited. These may be explained by the low pressure of H_2.

The possible reaction paths for PPE in the hydrothermal treatment upgrading reaction are shown in **Figure 6**. However, if merely based on the results of GC-MS, the initial reaction cannot be identified, neither can the microscopic mechanism. Compared with using GC-MS alone, *in situ* ^{2}H NMR monitoring combined with GC-MS acquired much more information. For the hydrotreating process, we first proposed the mechanism for the catalytic cracking of PPE by Pd/γ-Al_2O_3 at the atomic scale, which underlines the superiority of this method in micro-mechanism analysis. Compared with the use of GC-MS alone, *in situ* ^{2}H NMR monitoring combined with isotope labeling and GC-MS can predict the reaction process and the mechanism for the catalyst more effectively.

CONCLUSIONS

This study proposed a novel reaction monitoring strategy which is high-pressure *in situ* ^{2}H NMR and GC-MS for the upgrading process. This strategy exhibited powerful capabilities for identifying reaction products and provided deeper insights into the mechanisms. By employing this method, investigations into catalytic mechanisms for the hydrotreating process of PPE using Pd, Ru and Pt loaded onto C or γ-Al_2O_3 were accomplished. The results indicated that Pd/γ-Al_2O_3 was found to have better capacity for catalyzing the break in ether bonds, while Pt tented to produce more hydrogenation products. In addition, two special positions in PPE have been found to have a significantly higher H/D exchange ratio when using Pd/γ-Al_2O_3, which indicated that Pd/γ-Al_2O_3 may be able to hold PPE molecules in this special conformation in order to better perform ether bond cleavage. The possible catalytic mechanism of PPE by Pd/γ-Al_2O_3 was given from an atomic point of view. By comparing with GC-MS used alone, the superiority of this method in predicting the reaction process and catalyst mechanism was further shown. We believe that this method could open up a new direction in exploring the mechanism behind many kinds of reactions.

DATA AVAILABILITY STATEMENT

The datasets generated for this study are available on request to the corresponding author.

AUTHOR CONTRIBUTIONS

HB proposed the conception of the study and directed the project. HB and YY conducted the experiment. ZW and YL

performed the statistical analysis. YY and HB wrote the original draft. GH, WJ, and MW reviewed the manuscript.

FUNDING

This research was funded by from the National Natural Science Foundation of China under Grand No. 51706044, the Natural Science Foundation of the Jiangsu of China under Grand No. BK20170666, and the Recruitment Program for Young Professionals in China.

SUPPLEMENTARY MATERIAL

The Supplementary Material for this article can be found online at: https://www.frontiersin.org/articles/10.3389/fenrg.2020.00114/full#supplementary-material

REFERENCES

Ardiyanti, A. R., Bykova, M. V., Khromova, S. A., Yin, W., Venderbosch, R. H., Yakovlev, V. A., et al. (2016). Ni-based catalysts for the hydrotreatment of fast pyrolysis oil. *Energy Fuels* 30, 1544–1554. doi: 10.1021/acs.energyfuels.5b02223

Barton, D. H. R., Finet, J. P., Motherwell, W. B., and Pichon, C. (1987). The chemistry of pentavalent organobismuth reagents. part 8. phenylation and oxidation of alcohols by tetraphenylbismuth esters. *J. Chem. Soc. Perkin Trans.* 1, 251–259. doi: 10.1039/P19870000251

Barton, R. R., Carrier, M., Segura, C., Fierro, J. L. G., Park, S., Lamb, H. H., et al. (2018). Ni/HZSM-5 catalyst preparation by deposition-precipitation. part 2. catalytic hydrodeoxygenation reactions of lignin model compounds in organic and aqueous systems. *Appl. Cataly. A General* 562, 294–309. doi: 10.1016/j.apcata.2018.06.012

Ben, H., Jarvis, M. W., Nimlos, M. R., Gjersing, E. L., Sturgeon, M. R., Foust, T. D., et al. (2016). Application of a pyroprobe–deuterium NMR system: deuterium tracing and mechanistic study of upgrading process for lignin model compounds. *Energy Fuels* 30, 2968–2974. doi: 10.1021/acs.energyfuels.5b02729

Bordoloi, N., Narzari, R., Chutia, R. S., Bhaskar, T., and Kataki, R. (2015). Pyrolysis of mesua ferrea and pongamia glabra seed cover: characterization of bio-oil and its sub-fractions. *Bioresour. Technol.* 178, 83–89. doi: 10.1016/j.biortech.2014.10.079

Chakar, F. S., and Ragauskas, A. J. (2004). Review of current and future softwood kraft lignin process chemistry. *Ind. Crops Prod.* 20, 131–141. doi: 10.1016/j.indcrop.2004.04.016

Chio, C., Sain, M., and Qin, W. (2019). Lignin utilization: a review of lignin depolymerization from various aspects. *Renew. Sust. Energ. Rev.* 107, 232–249. doi: 10.1016/j.rser.2019.03.008

David, K., and Ragauskas, A. J. (2010). Switchgrass as an energy crop for biofuel production: a review of its ligno-cellulosic chemical properties. *Energy Environ. Sci.* 3, 1182–1190. doi: 10.1039/B926617H

Elder, T., and Beste, A. (2014). Density functional theory study of the concerted pyrolysis mechanism for lignin models. *Energy Fuels* 28, 5229–5235. doi: 10.1021/ef5013648

Fan, L., Chen, P., Zhou, N., Liu, S., Zhang, Y., Liu, Y., et al. (2018). *In-situ* and *ex-situ* catalytic upgrading of vapors from microwave-assisted pyrolysis of lignin. *Bioresour. Technol.* 247, 851–858. doi: 10.1016/j.biortech.2017.09.200

Funkenbusch, L. T., Mullins, M. E., Salam, M. A., Creaser, D., and Olsson, L. (2019). Catalytic hydrotreatment of pyrolysis oil phenolic compounds over Pt/Al2O3 and Pd/C. *Fuel* 243, 441–448. doi: 10.1016/j.fuel.2019.01.139

Gomez-Monedero, B., Faria, J., Bimbela, F., and Ruiz, M. P. (2017). Catalytic hydroprocessing of lignin β-O-4 ether bond model compound phenethyl phenyl ether over ruthenium catalysts. *Biomass Convers. Biorefin.* 7, 385–398. doi: 10.1007/s13399-017-0275-5

Jain, R., Bally, T., and Rablen, P. R. (2009). Calculating accurate proton chemical shifts of organic molecules with density functional methods and modest basis sets. *J. Org. Chem.* 74, 4017–4023. doi: 10.1021/jo900482q

Katahira, R., Mittal, A., Mckinney, K., Chen, X., Tucker, M. P., Johnson, D. K., et al. (2016). Base-catalyzed depolymerization of biorefinery lignins. *ACS Sustain. Chem. Eng.* 4, 1474–1486. doi: 10.1021/acssuschemeng.5b01451

Kim, S., Kwon, E. E., Kim, Y. T., Jung, S., and Lee, J. (2019). Recent advances in hydrodeoxygenation of biomass-derived oxygenates over heterogeneous catalysts. *Green Chem.* 21, 3715–3743. doi: 10.1039/C9GC01210A

Konnerth, H., Zhang, J., Ma, D., Prechtl, M. H. G., and Yan, N. (2015). Base promoted hydrogenolysis of lignin model compounds and organosolv lignin over metal catalysts in water. *Chem. Eng. Sci.* 123, 155–163. doi: 10.1016/j.ces.2014.10.045

Li, C., Zhao, X., Wang, A., Huber, G. W., and Zhang, T. (2015). Catalytic transformation of lignin for the production of chemicals and fuels. *Chem. Rev.* 115, 11559–11624. doi: 10.1021/acs.chemrev.5b00155

Mauriello, F., Paone, E., Pietropaolo, R., Balu, A. M., and Luque, R. (2018). Catalytic transfer hydrogenolysis of lignin-derived aromatic ethers promoted by bimetallic Pd/Ni systems. *ACS Sust. Chem. Eng.* 6, 9269–9276. doi: 10.1021/acssuschemeng.8b01593

Mullen, C. A., Strahan, G. D., and Boateng, A. A. (2009). Characterization of various fast-pyrolysis bio-oils by NMR spectroscopy. *Energy Fuels* 23, 2707–2718. doi: 10.1021/ef801048b

Naik, S., Goud, V. V., Rout, P. K., and Dalai, A. K. (2010). Supercritical CO2 fractionation of bio-oil produced from wheat–hemlock biomass. *Bioresour. Technol.* 101, 7605–7613. doi: 10.1016/j.biortech.2010.04.024

Pierens, G. K. (2014). 1H and 13C NMR scaling factors for the calculation of chemical shifts in commonly used solvents using density functional theory. *J. Comput. Chem.* 35, 1388–1394. doi: 10.1002/jcc.23638

Richter, J. B., Eßbach, C., Senkovska, I., Kaskel, S., and Brunner, E. (2019). Quantitative *in situ*13C NMR studies of the electro-catalytic oxidation of ethanol. *Chem. Commun.* 55, 6042–6045. doi: 10.1039/C9CC02660F

Robinson, A. M., Hensley, J. E., and Medlin, J. W. (2016). Bifunctional catalysts for upgrading of biomass-derived oxygenates: a review. *Acs Catal.* 8, 5026–5043. doi: 10.1021/acscatal.6b00923

Santana, J. A., Carvalho, W. S., and Ataide, C. H. (2018). Catalytic effect of ZSM-5 zeolite and HY-340 niobic acid on the pyrolysis of industrial kraft lignins. *Ind. Crops Prod.* 111, 126–132. doi: 10.1016/j.indcrop.2017.10.023

Shuai, L., Amiri, M. T., Questellsantiago, Y. M., Heroguel, F., Li, Y., Kim, H., et al. (2016). Formaldehyde stabilization facilitates lignin monomer production during biomass depolymerization. *Science* 354, 329–333. doi: 10.1126/science.aaf7810

Shuang, C., Guilin, Z., and Caixia, M. (2019). Green and renewable bio-diesel produce from oil hydrodeoxygenation: strategies for catalyst development and mechanism. *Renew. Sust. Energy Rev.* 101, 568–589. doi: 10.1016/j.rser.2018.11.027

Sirousrezaei, P., Jae, J., Ha, J., Ko, C. H., Kim, J. M., Jeon, J., et al. (2018). Mild hydrodeoxygenation of phenolic lignin model compounds over a FeReOx/ZrO2 catalyst: zirconia and rhenium oxide as efficient dehydration promoters. *Green Chem.* 20, 1472–1483. doi: 10.1039/C7GC03823B

Song, Q., Cai, J., Zhang, J., Weiqiang, Y. U., Wang, F., and Jie, X. (2013). Hydrogenation and cleavage of the C-O bonds in the lignin model compound phenethyl phenyl ether over a nickel-based catalyst. *Chinese J. Catal.* 34, 651–658. doi: 10.1016/S1872-2067(12)60535-X

Tessarolo, N. S., Silva, R. V. S., Vanini, G., Casilli, A., Ximenes, V. L., Mendes, F. L., et al. (2016). Characterization of thermal and catalytic pyrolysis bio-oils by high-resolution techniques: 1H NMR, GC×GC-TOFMS and FT-ICR MS. *J. Anal. Appl. Pyrolysis* 117, 257–267. doi: 10.1016/j.jaap.2015.11.007

Wang, A., Austin, D., He, P., Mao, X., Zeng, H., and Song, H. (2018). Direct catalytic co-conversion of cellulose and methane to renewable petrochemicals. *Catal. Sci. Technol.* 8, 5632–5645. doi: 10.1039/C8CY01749B

Wang, H., Pu, Y., Ragauskas, A., and Yang, B. (2019). From lignin to valuable products–strategies, challenges, and prospects. *Bioresour. Technol.* 271, 449–461. doi: 10.1016/j.biortech.2018.09.072

Wang, M., and Liu, C. (2016). Theoretic studies on decomposition mechanism of o -methoxy phenethyl phenyl ether: primary and secondary reactions. *J. Anal. Appl. Pyrolysis* 117, 325–333. doi: 10.1016/j.jaap.2015.10.016

Wang, Y., Pedersen, C. M., Qiao, Y., Deng, T., Shi, J., and Hou, X. (2015). *In situ* NMR spectroscopy: Inulin biomass conversion in ZnCl2 molten salt hydrate medium—SnCl4 addition controls product distribution. *Carbohydr. Polym.* 115, 439–443. doi: 10.1016/j.carbpol.2014.09.011

Yan, N., and Dyson, P. J. (2013). Transformation of biomass via the selective hydrogenolysis of CO bonds by nanoscale metal catalysts. *Curr. Opin. Chem. Eng.* 2, 178–183. doi: 10.1016/j.coche.2012.12.004

Zakzeski, J., Bruijnincx, P. C. A., Jongerius, A. L., and Weckhuysen, B. M. (2010). The catalytic valorization of lignin for the production of renewable chemicals. *Chem. Rev.* 110, 3552–3599. doi: 10.1021/cr900354u

Zhang, C., and Wang, F. (2020). Catalytic lignin depolymerization to aromatic chemicals. *Acc. Chem. Res.* 53, 470–484. doi: 10.1021/acs.accounts.9b00573

Conflict of Interest: The authors declare that the research was conducted in the absence of any commercial or financial relationships that could be construed as a potential conflict of interest.

frontiers in Energy Research

ORIGINAL RESEARCH
published: 08 July 2020
doi: 10.3389/fenrg.2020.00149

Effects of CELF Pretreatment Severity on Lignin Structure and the Lignin-Based Polyurethane Properties

Yun-Yan Wang[1†], Priya Sengupta[2,3], Brent Scheidemantle[2,3], Yunqiao Pu[4,5†], Charles E. Wyman[2,3,5], Charles M. Cai[2,3,5†] and Arthur J. Ragauskas[4,5,6†]*

[1] Department of Forestry, Wildlife, and Fisheries, Center for Renewable Carbon, The University of Tennessee Institute of Agriculture, Knoxville, TN, United States, [2] Department of Chemical and Environmental Engineering, Bourns College of Engineering, University of California, Riverside, Riverside, CA, United States, [3] Center for Environmental Research and Technology (CE-CERT), Bourns College of Engineering, University of California, Riverside, Riverside, CA, United States, [4] Joint Institute for Biological Science, Biosciences Division, Oak Ridge National Laboratory, Oak Ridge, TN, United States, [5] The Center for Bioenergy Innovation (CBI), Oak Ridge National Laboratory, Oak Ridge, TN, United States, [6] Department of Chemical and Biomolecular Engineering, The University of Tennessee, Knoxville, Knoxville, TN, United States

OPEN ACCESS

Edited by:
Junyong Zhu,
United States Forest Service (USDA),
United States

Reviewed by:
Peter Deuss,
University of Groningen, Netherlands
Somnath D. Shinde,
Sandia National Laboratories (SNL),
United States

***Correspondence:**
Arthur J. Ragauskas
aragausk@utk.edu

†ORCID:
Yun-Yan Wang
orcid.org/0000-0002-0866-4640
Yunqiao Pu
orcid.org/0000-0003-2554-1447
Charles M. Cai
orcid.org/0000-0002-5047-0815
Arthur J. Ragauskas
orcid.org/0000-0002-3536-554

Specialty section:
This article was submitted to Bioenergy and Biofuels, a section of the journal Frontiers in Energy Research

Received: 11 March 2020
Accepted: 16 June 2020
Published: 08 July 2020

Citation:
Wang Y-Y, Sengupta P, Scheidemantle B, Pu Y, Wyman CE, Cai CM and Ragauskas AJ (2020) Effects of CELF Pretreatment Severity on Lignin Structure and the Lignin-Based Polyurethane Properties. Front. Energy Res. 8:149. doi: 10.3389/fenrg.2020.00149

Conversion of technical lignin into performance biopolymers such as polyurethane offers environmental and economic advantages when combined with production of biofuels from biomass sugars, presenting significant interest toward studying the role of pretreatment on lignin structure and functionality. Co-solvent enhanced lignocellulosic fractionation (CELF) pretreatment, employing acidic aqueous tetrahydrofuran (THF) mixtures, was developed to effectively break down the lignin-carbohydrate matrix and promote extraction of lignin from lignocellulosic biomass with desirable purity and yield. In this study, we report the effects of CELF pretreatment reaction severity on the molecular structure of CELF-extracted lignin and its impact toward the mechanical properties of the resulting lignin-based polyurethanes. Reaction temperature was found to play the most significant role, compared to reaction time and acidity, in manipulating structural features such as molecular weight, functionality and intra-polymer structure. At the severe reaction conditions at 180°C, the order of reactivity for primary lignin interlinkages characterized by semiquantitative HSQC NMR analysis were found to be β-ether > phenylcoumaran (β−5′) > resinol (β−β′) facilitating a high degree of depolymerization and yielding a high frequency of free phenolics and reduced aliphatic hydroxyl groups. All side-chain interlinkages were depleted converting guaiacyl subunits into condensed forms, while still retaining uncondensed syringyl subunits. Under the mild 150°C temperature reaction, CELF lignin had higher molecular weight and retained more β-ether interlinkages. The results from CELF lignin-based polyurethane synthesis indicated that the tensile properties depended on the miscibility of CELF lignin with other components and low molecular weight cuts improved the dispersion of lignin in the polyurethane network. Pre-mixing of CELF with poly(ethylene glycol) (PEG) reduced the brittleness and improved the ductility of the CELF lignin-PEG polyurethanes.

Keywords: poplar lignin, NMR, lignin-based polyurethanes, pretreatment conditions, mechanical properties

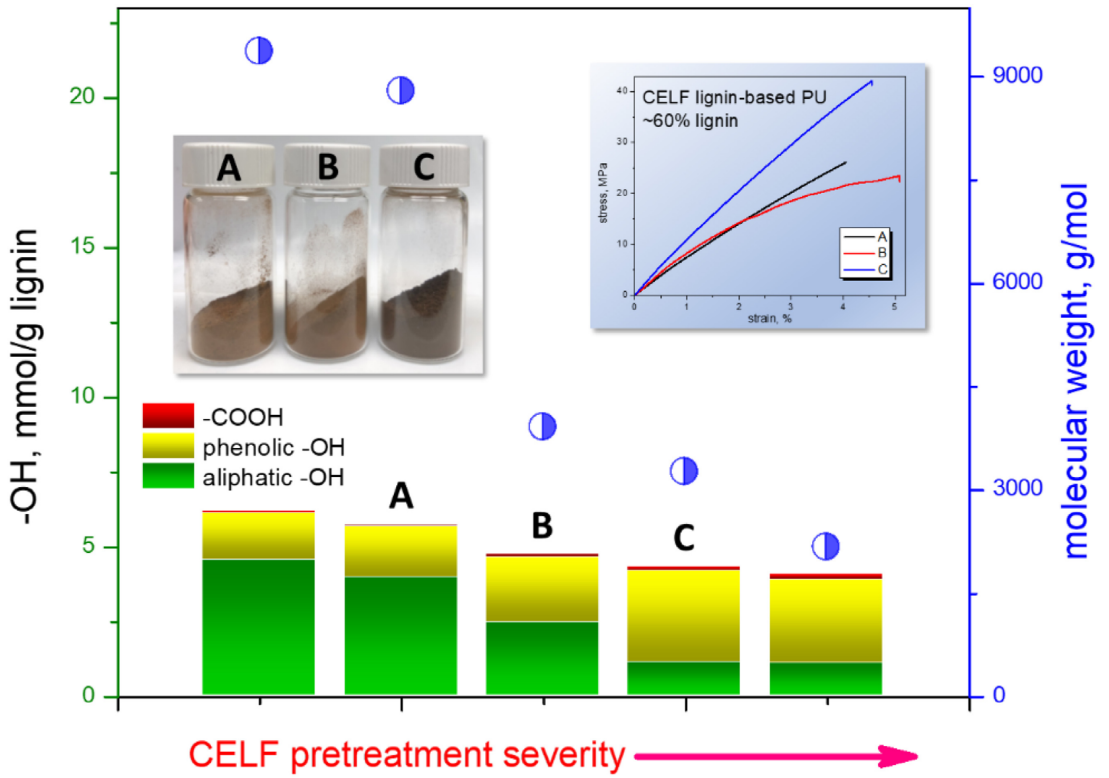

GRAPHICAL ABSTRACT | The impact of pretreatment severity on the structure of CELF lignin and tensile properties of CELF lignin-based PU.

INTRODUCTION

Lignin found in lignocellulosic biomass is a class of heterogeneous biopolymers typically derived from three types of phenylpropanoid subunits: guaiacyl (G), syringyl (S), and *p*−hydroxylphenyl (H) (Higuchi, 2003). Angiosperm poplar lignin is composed of S, G with a varying S/G ratio depending on the species and a small amount of H subunits which are connected by six predominant interlinkages: β−*O*−4′, β−β′, β−5′, 5−5′, β−1′ and 4–*O*–5′ (Sannigrahi et al., 2010). In the plant cell wall, about 3% of the lignin subunits are covalently bonded with hemicelluloses to form lignin-hemicellulose matrix and lignin provides drought-resistance and a protective barrier against pathogen invasion (Balakshin et al., 2007; Giummarella et al., 2019). The recalcitrance of plant cell wall is designed by nature to be resistant to biological and chemical degradation. Therefore, in order to reduce the costs associated with processing lignocellulosic biomass to biofuels and biochemicals, pretreatment is often employed to modify the plant cell wall to improve accessibility of cellulolytic enzymes to the crystalline cellulose domains from which fermentable glucose can be released (Mostofian et al., 2016).

In order to improve upon conventional aqueous biomass pretreatment methods, the addition of miscible co-solvents greatly improves the dissolution of lignin that is critical in maximizing utilization of all major biomass fractions by subsequent catalytic and biological conversion methods. Co-solvent-based pretreatment technologies employing tetrahydrofuran (THF), γ-valerolactone (GVL), and Cyrene in aqueous solutions have been shown to provide significant functional advantages in improving microbial and enzymatic accessibility of cellulose while also achieving clean extraction of lignin and high total sugar recovery, merits that are important toward improving the competitiveness of liquid fuels from biomass (Shuai et al., 2016; Smith et al., 2017; Liu et al., 2018; Petridis and Smith, 2018; Meng et al., 2020). The pretreatment method that employs THF as a co-solvent is known as Co-solvent enhanced lignocellulosic fractionation (CELF). THF has uniquely lower boiling point so that it can be simply boiled out of the solution after pretreatment in order to induce lignin precipitating out of solution and to recover THF. This avoids potentially more complicated and energy-intensive solvent recovery methods, such as CO_2-induced phase modification or anti-solvent extraction, that have been proposed for the recovery of high boiling co-solvents (Wyman et al., 2016). In previous studies, CELF has demonstrated wide operating flexibility in terms of reaction conditions such as temperature, solvent ratio, duration, and acid loading to finely control the extent of cellulose and lignin dissolution independently to support sugar hydrolysis at lower severities and to support tandem sugar hydrolysis and dehydration to furfurals at higher severities (Cai et al., 2013; Nguyen et al., 2016; Seemala et al., 2018). THF is non-pernicious and is considered a toxicologically safer alternative to dioxane and can be classified as a green

chemical if produced from furfural by catalytic decarbonylation followed by hydrogenation (Cai et al., 2013; Fowles et al., 2013; Meng et al., 2018). Recently, all-atom molecular-dynamics (MD) simulation studies have probed the functionality of THF-water mixtures to "relax" native lignin globules into non-aggregated random-coils under the CELF pretreatment reaction environment to facilitate both lignin solvation and depolymerization, offering a wider operating range to alter the structure and degree of polymerization of lignin during pretreatment (Mostofian et al., 2016; Smith et al., 2016). This high degree of lignin tunability opens a broad range of potential pathways for upgrading lignin such as biopolymers, carbon substrates, antioxidants, resins, and hydrocarbon fuels (Ragauskas et al., 2006, 2014). While structural characterization of CELF lignin resulting from reaction conditions identified for achieving optimal total sugar recovery or high furfural yields have been reported previously (Meng et al., 2018, 2019b; Wang et al., 2018), a systematic study focused on elucidating the impact of pretreatment temperature, reaction time, and acid loading on lignin structure is needed to understand the potential spectrum of chemical moieties and inter-unit components that would be available to serve future lignin valorization efforts. Herein, the correlation between CELF pretreatment severity and resultant CELF lignin characteristics from hardwood poplar was established quantitatively by using ^{31}P nuclear magnetic resonance (NMR), heteronuclear Single Quantum Coherence (HSQC) NMR, gel permeation chromatography (GPC), thermal gravimetric analysis (TGA) and differential scanning calorimetry (DSC). To improve our understanding of lignin fragmentation by acidolysis under CELF conditions, we tracked potential side-reactions such as lignin condensation and loss of monosaccharides as well as the primary acidolysis reaction on the lignin β–*O*–4′ interlinkages. Lignin has been considered as a sustainable and low-cost replacement for petrochemical polyols in the production of commercial polyurethanes products (Wang et al., 2017a). In the study of Kraft lignin-based polyurethanes, it was found that the mechanical strength of the polyurethane network was dependent on the molecular weight of Kraft lignin cuts prepared by sequential precipitation, and the presence of long-chain polyethylene glycol was able to improve the ductility of the materials (Wang et al., 2019). The understanding of CELF lignin molecular features, in return, facilitated the screening of lignin species for producing CELF lignin-based polyurethane (CL-PU) products such as adhesives.

MATERIALS AND METHODS

Materials

The poplar wood chips used for this study is known as BESC standard poplar. It was determined through compositional analysis (NREL protocol TP-510-42618) to contain 21.2% acid-insoluble lignin (Sluiter et al., 2012). Before pretreatment, the poplar chips were knife-milled and passed through a 1 mm particle screen. Chemicals reagents such as THF, sulfuric acid, poly[(phenyl isocyanate)-co-formaldehyde] (PMDI, M_n∼340) and dibutyltin dilaurate were purchased from Sigma-Aldrich and Fisher Scientific.

CELF Pretreatment

Poplar wood chips were loaded into a 1 L Hastelloy Parr autoclave reactor (236HC Series, Parr Instruments Co., Moline, IL, United States) equipped with twin pitched-blade Rushton impellers at a solid to liquid loading of 7.5 wt%. The chips were soaked overnight at 4°C in a 1:1 (w/w) THF-water solution containing dilute mixtures of sulfuric acid (0.025 M to 0.1 M or 0.25–1% in liquid). The pretreatment reactions were carried out at temperatures of 150, 160, and 180°C for durations of 15 and 30 min. All reactions were maintained at target temperature (±1°C) by convective heating by using a 4 kW fluidized sand bath (Model SBL-2D, Techne, Princeton, NJ, United States), and the reactor temperature was measured directly by using an internally fixed thermocouple (Omega, K-type). To arrest the reaction after the allotted duration, the reactor was submerged in a large room-temperature water bath. The pretreated solids were then vacuum filtered and separated from the pretreatment liquor at room temperature through a paper filter. Finally, the dry mass of the solids and the mass of the liquor was recorded.

CELF Lignin Recovery and Purification

The liquid fraction collected from post filtration was poured in a beaker and titrated to pH ∼7 using ammonium hydroxide. THF was then boiled out of solution at 80°C under a hot plate with continuous stirring at 130 rpm for about 4 h. The beaker and contents were then allowed to cool to room temperature overnight and the liquor was then poured out. Lignin that had precipitated onto the beaker after the removal of THF and liquor was rinsed with water and then placed in a dark oven at 65°C to dry overnight. The resulting lignin was collected and placed onto a glass fiber filter paper. The lignin was then washed with diethyl ether followed by a water wash to remove soluble impurities and placed in an oven at 65°C to dry overnight to a moisture content of <3% (determined by gravimetric analysis at 105°C). The lignin was then ground to a fine powder by a mortar and pestle.

Structural Characterization of CELF Lignin

Quantitative ^{31}P NMR and the heteronuclear single quantum coherence (HSQC) NMR spectra were acquired on a Bruker Avance III HD 500-MHz spectrometer according to a previously published literature (Wang et al., 2018; Meng et al., 2019a). In the quantitative ^{31}P NMR experiments, a 90° pulse width, 1.2 s acquisition time, 25 s pulse delay were used in collecting 64 scans. 20∼30 mg (accurately weighed) CELF lignin sample was dissolved in 700 μL pyridine/$CDCl_3$ (1.6:1, v/v) with 1 mg/mL chromium(III) acetylacetonate and 2.5 mg/mL *N*-hydroxy-5-norbornene-2,3-dicarboximide (internal standard). The lignin sample was subjected to NMR analysis promptly after phosphitylating with 60 μL 2-chloro-4,4,5,5 tetramethyl-1,3,2-dixoaphospholane (TMDP). The obtained ^{31}P NMR spectra were calibrated by using the

TMDP-water phosphitylation product (δ132.2 ppm) as the internal reference. The HSQC NMR spectra were processed and analyzed by using TopSpin software (version 3.5pl7, Bruker).

Gel Permeation Chromatography

Dried CELF lignin sample (∼2 mg) was acetylated and processed according to a previous literature (Wang et al., 2018). The acetylated CELF lignin was dissolved and then incubated in tetrahydrofuran for 24 h. The molecular weight analysis was performed on an Agilent GPC SECurity 1200 system equipped with several Waters Styragel columns (Water Corporation, Milford, MA, United States), an Agilent UV detector (λ = 280 nm) at a flow rate of 1.0 mL/min at 30°C.

Thermal Analyses

The thermal gravimetric analysis (TGA) of lignin was operated on a TA Q50 thermogravimetric analyzer (TA Instruments) heating in a nitrogen atmosphere. The sample (∼10 mg) was initially incubated at 105°C for 15 min to remove the last trace of moisture and THF. Then, the temperature was raised from 105 to 900°C at 10°C/min. The differential scanning calorimetry (DSC) measurements were performed in heat-cool-heat mode on a TA Q2000 DSC (TA Instruments) with a heating/cooling rate of 20°C/min.

CL-PU Synthesis and Characterization

The CL-PUs were synthesized by polycondensation as described in a previous literature, and they were denoted according to the corresponding CELF lignin samples (Wang et al., 2019). In this work, the selected CELF lignin samples, CELF2, CELF3 and CELF4, were disolved in THF with or without poly(ethylene glycol) (PEG, M_w = 4,000, Alfa Aesar) (1:1, w/w). The polyol/THF mixture was incubated in a thermal shaker (Alkali Scientific Inc.) at 140 rpm, 60°C for 1 h, and then it was combined with a THF solution containing PMDI with NCO/OH ratio at 1:1 and 1.5% dibutyltin dilaurate. After 3-day curing at room temperature, the CL-PU samples were kept at 150°C for 3 h. The tensile testing was carried out on a dual column Instron 5567 universal testing system equipped with a 500 N static load cell. For each CL-PU sample, three dog-bone specimens were tested according to ASTM D638 standard (Type V) at a strain rate of 0.1 mm/min.

RESULTS AND DISCUSSION

Delignification in Acidic CELF Pretreatment

Poplar wood meal was pretreated under five CELF pretreatment conditions varying in catalyst dosage, temperature and duration time as summarized in **Table 1**. The THF-water content was fixed at 1:1 (w/w) which has been determined to be the minimum THF needed to achieve high delignification (Cai et al., 2013). The resultant CELF lignin samples were denoted "CELF1 – CELF5" referring to the degree of pretreatment severity. During the CELF pretreatment, the macromolecular lignin was degraded into fragments and dissolved in the THF-water mixture. Below 180°C, the removal of lignin increased steadily when the poplar biomass was pretreated at elevated temperature or with higher catalyst dosage. However, total CELF lignin yield after 180°C reaction was significantly higher for CELF5 (142.1% of total lignin in poplar biomass) as compared to CELF4 (94.4% of total lignin in poplar biomass). The mass in excess of 100% for the CELF5 sample was likely due to cross-polymerization reactions between soluble sugars and lignin during pretreatment and the formation of pseudo-lignin, a polyphenolic compounds derived from carbohydrates subjected to dilute acid reaction (Sannigrahi et al., 2011; Hu et al., 2012; Shinde et al., 2018). For example, Hu et al. found that up to 87% of the holocellulose was converted into acid insoluble pseudo-lignin including approximately 30% aqueous-dioxane-soluble pseudo-lignin after a severe two-step dilute acid pretreatment at 180°C (Hu et al., 2012). Pseudo-lignin preferentially forms *via* polymerization or polycondensation of carbohydrate degradation products at high temperature in the presence of oxygen during acid pretreatment (Hu and Ragauskas, 2014). It consumes valuable fuel precursors such as furfural, 5-hydroxylmethylfurfural, and levulinic acid; moreover, similar to lignin, pseudo-lignin absorbs on the surface of biomass and creates a recalcitrant barrier against cellulosic enzymatic hydrolysis (Hu et al., 2012). Therefore, the generation of pseudo-lignin should be suppressed during CELF pretreatment to provide higher yields of reactive intermediates from both the sugars and lignin in biomass.

TABLE 1 | CELF pretreatment conditions and mass yield (%) of CELF lignin in total poplar lignin.

Lignin sample	H_2SO_4 (wt%)	Temperature (°C)	Duration (min)	Lignin yield (%)
CELF1	0.25	150	15	65.2
CELF2	0.5	150	15	69
CELF3	0.5	160	15	75.5
CELF4	0.5	180	15	94.4
CELF5	1	180	30	142.1

Another index to evaluate the efficiency of CELF pretreatment is the molecular weight of the CELF lignin. The GPC profiles presented in **Figure 1** showed the typical bimodal molecular weight distribution pattern for all five CELF lignin samples, and the impact of pretreatment severity on lignin depolymerization can be visualized by the intensity changes of high- and low-molecular weight peaks. At low pretreatment temperature (150°C), the high molecular-weight peaks were found to be predominant for CELF1 and CELF2, and mild degradation of lignin occurred as its M_w was reduced by 20∼25% compared with the reported value of poplar cellulolytic enzyme lignin (CEL) (M_w ∼ 12,000) (Meng et al., 2018). The most dramatic changes in molecular weights and polydispersity (PDI) were observed between CELF2 and CELF3: more than 50% reduction of M_w was achieved by increasing the pretreatment temperature from 150 to 160°C while other variables remained the same. However, M_w of CELF4 obtained at 180°C was decreased by an additional 17% compared with CELF3 (160°C). At 180°C, the reduction in molecular

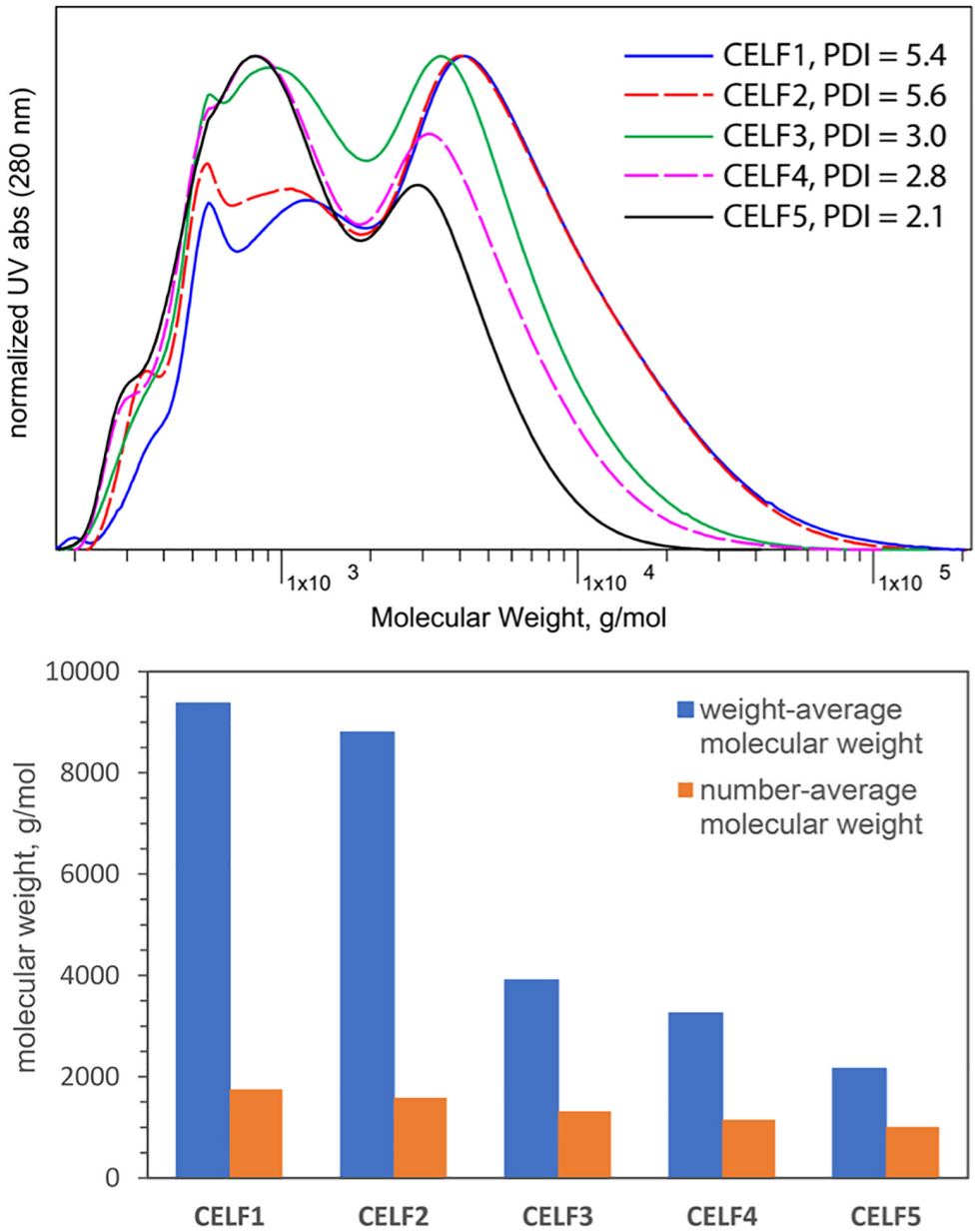

FIGURE 1 | GPC profiles, weight-average and number average molecular weights of CELF lignin obtained under different pretreatment conditions.

weight was caused by β–*O*–4′ acidolysis which was, however, partially compensated by the repolymerization of degraded lignin fragments via condensation.

Impacts of Pretreatment Severity on the Structural Features of CELF Lignin

Acid-catalyzed delignification preferentially starts from β–*O*–4′ linked alkyl aryl ethers with a free phenolic end, and the cleavage reaction proceeds along the polymer chain until reaching more recalcitrant bonds (Sturgeon et al., 2014). Under the acidic condition, the C_α position of beta ether loses a water molecule and forms a benzylic carbocation. The beta ether cleavage involves two pathways giving two end products: phenylacetaldehyde and Hibbert ketone (**Scheme 1A**), when sulfuric acid is used as the catalyst, forming Hibbert ketone is thermodynamically favored (Lundquist and Lundquist, 1972; Imai et al., 2011; Sturgeon et al., 2014). In addition to lignin depolymerization at low pH, C–C crosslinking between lignin components occurs via condensation reactions such

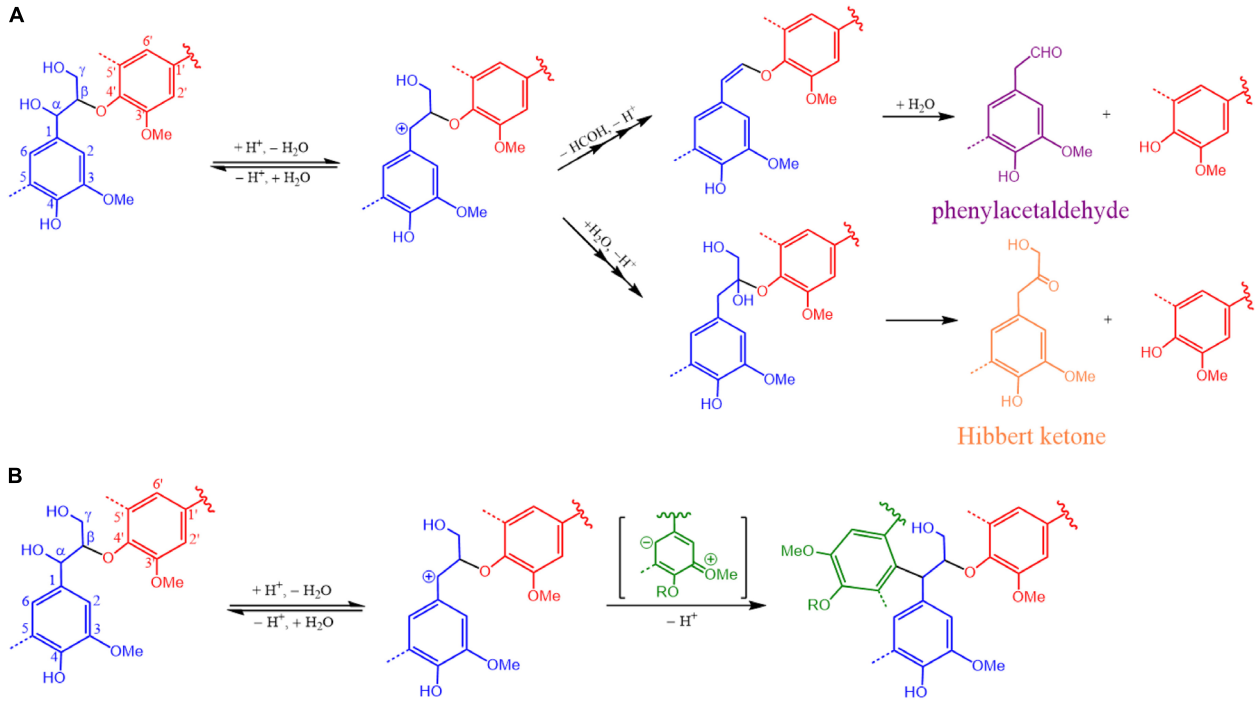

SCHEME 1 | Mechanisms of acid-catalyzed β–*O*–4′ cleavage **(A)** and C_α condensation **(B)**.

as the one occurring on C_α as depicted in **Scheme 1B** (Li et al., 2018).

The multifunctionality of lignin macromolecules includes aliphatic, phenolic and carboxylic –OH groups. The phenolic -OH group can be classified into guaiacyl, C_5-substituted and *p*-hydroxyphenyl. The hydroxyl contents of CELF1∼5 determined by ^{31}P NMR analysis and the corresponding spectra are shown in **Table 2** and **Figure 2A**, respectively. As the CELF pretreatment adopts more severe conditions, more free phenolic hydroxyl groups were released as a result of acid-catalyzed β–*O*–4′ cleavage, and they became the major functional groups (∼70%) found in CELF lignin when the pretreatment temperature was raised to 180°C (**Figure 2B**). Meanwhile, the relative content of aliphatic hydroxyl groups decreased from 74 to 26%. In the predominant lignin substructure, β–*O*–4′ alkyl aryl ether, the loss of aliphatic -OH groups arises from several factors including the cleavage of the monomeric components, oxidation of hydroxyl groups, and dehydration of side chain C_α and C_γ leading to C_α condensation or formation of stilbene structures (Hallac et al., 2010; Meng et al., 2018). The contents of syringyl and guaiacyl phenolic -OH groups increased comparably with the release of free phenolic ones (**Table 2** and **Figure 2C**). However, unlike the former two, the *p*-hydroxyphenyl end units mainly derived from *p*-hydroxybenzoate were found to be more vulnerable to cleavage as its corresponding hydroxyl content decreased from ∼20 to ∼5% of the phenolic hydroxyl content.

Detailed structural evolution of CELF lignin in relation to the pretreatment severity can be mapped by semiquantitative HSQC NMR analysis. As shown in **Figure 3**, the 2D HSQC spectra of CELF1, 3 and 5 prepared under mild, medium and harsh pretreatment conditions, were distinguishably different based upon the appearance and disappearance of

TABLE 2 | CELF lignin hydroxyl contents determined by quantitative ^{31}P NMR analysis.

OH content, mmol/g lignin	CELF1	CELF2	CELF3	CELF4	CELF5
Aliphatic	4.55 ± 0.04	3.94 ± 0.01	2.45 ± 0.05	1.11 ± 0.02	1.07 ± 0.02
Phenolic	1.56 ± 0.05	1.71 ± 0.05	2.18 ± 0.03	3.05 ± 0.01	2.81 ± 0.05
Carboxylic	0.08 ± 0.01	0.07 ± 0.01	0.10 ± 0.01	0.15 ± 0.00	0.17 ± 0.02
Total	6.19 ± 0.08	5.72 ± 0.05	4.72 ± 0.08	4.31 ± 0.03	4.04 ± 0.09
C_5-substituted	0.76 ± 0.03	0.9 ± 0.02	1.30 ± 0.01	1.71 ± 0.01	1.71 ± 0.02
Guaiacyl	0.50 ± 0.02	0.54 ± 0.03	0.67 ± 0.02	1.02 ± 0.00	0.97 ± 0.00
p-Hydroxyphenyl	0.30 ± 0.01	0.28 ± 0.01	0.21 ± 0.00	0.22 ± 0.00	0.13 ± 0.01

The error values were obtained from standard deviation of duplicate results.

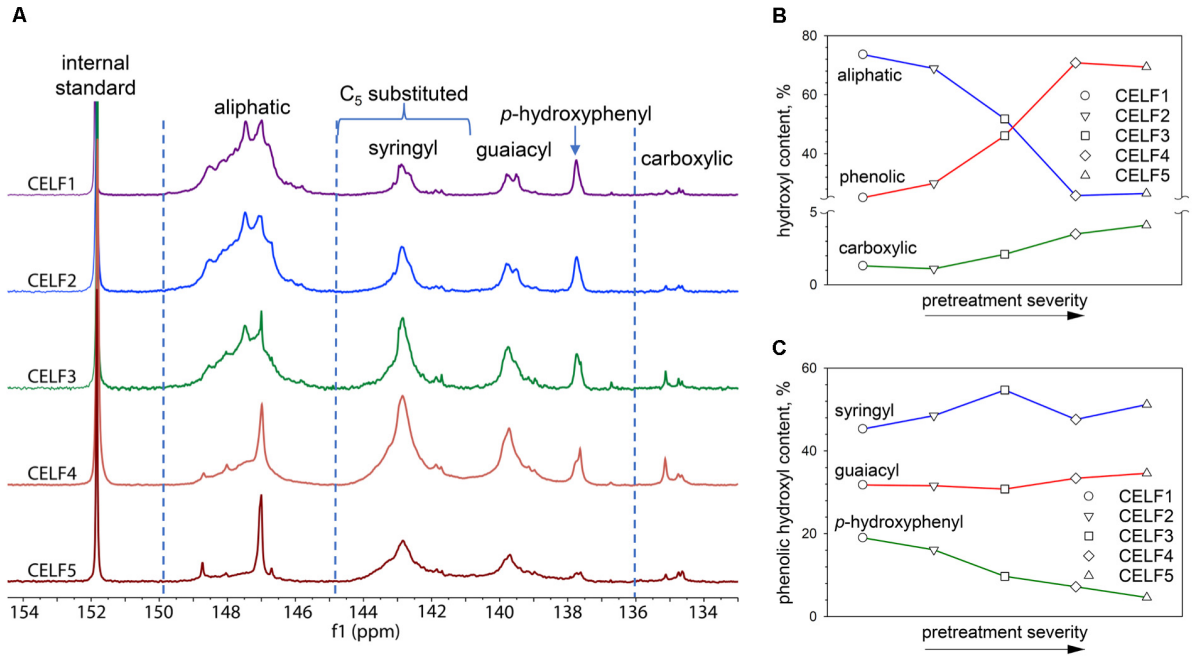

FIGURE 2 | (A) Quantitative ^{31}P NMR spectra of TMDP phosphitylated CELF lignin samples. **(B)** The relative quantities (%) of aliphatic, phenolic and carboxylic hydroxyl groups in total lignin hydroxyl groups. **(C)** The relative contents (%) of syringyl, guaiacyl and *p*-hydroxyphenyl hydroxyl groups in total lignin phenolic hydroxyl groups.

some specific structural features. In the aliphatic region, CELF1 possessed clear and intensive characteristic cross-peaks such as β–*O*–4′ alkyl aryl ether (A), β–β′ resinol (B) and β–5′ phenylcoumaran (C) substructures, but it showed much fewer traces of carbohydrate signals compared with the poplar CEL (Meng et al., 2018). In the aromatic region, in addition to those well-defined cross-peaks of S and G subunits, and *p*-hydroxybenzoate substructure (PB), new cross-peaks of $S_{condensed}$ and $G_{2,condensed}$ representing condensed S and G subunits, can be found around δ105.7∼106.9/δ6.46∼6.53 ppm and δ112.8/δ6.78 ppm, respectively. In the G subunits, condensation reactions can occur on open aromatic C_5 or C_6 and cause chemical shift migration of C_2–H_2 in the HSQC spectrum. In the spectrum of CELF3, the peak areas of $S_{condensed}$ and $G_{2,condensed}$ expanded, and a weak cross-peak of C_γ–H_γ in lignin-bound Hibbert ketone (HK) end group can be observed. Under extreme pretreatment condition (1 wt% H_2SO_4, 180°C and 30 min duration time), CELF5 lost all side-chain interlinkages. The missing G_2 and G_6, remaining G_5 cross-peaks indicated that all G subunits were in a condensed form and substitution on C_6 was preferred at 180°C. Moreover, 5-hydroxymethylfurfural, a dehydration product of glucose, was found in CELF lignin, given that the cross-peaks of its C_3–H_3 (δ122.8∼124.2/δ7.50∼7.55 ppm), C_4–H_4 (δ109.6∼110.1/δ6.43∼6.62 ppm) and C_6–H_6 (δ55.8/δ4.55 ppm) can be clearly observed in the spectra of CELF4 and CELF5 (Constant et al., 2016).

The quantified impacts of pretreatment severity on lignin structure is summarized in **Figure 4**. Compared with other CELF lignin samples, CELF1 underwent minimal structural modification and preserved most of the native lignin structural features such as high frequency of β–*O*–4′ interlinkages [41 per 100 (S + G) units] and high molecular weight (**Figure 4A**). The content of β–*O*–4′ decreased rapidly from CELF1 to CELF5; on the other hand, β–β′ and β–5′ interlinkages were more resistant to acidolysis, but they were eventually cleaved or transformed at 180°C, and β–5′ that can only be formed from G subunits was removed more rapidly. Due to the presence of C_5-methoxyl group, S subunits are favorably linked through β–*O*–4′. It was found that the transgenic poplar lignin composed of ∼98% S subunits possessed similar β–*O*–4′, but higher β–β′ content compares with wild poplar species (Stewart et al., 2009). Interestingly, in this work, the change of S/G with increasing pretreatment severity indicated that only at 180°C the loss of S subunits started to surpass the G ones accompanying with the removal of β–β′ (**Figure 4B**). Below 180°C, $S_{2,6condensed}$/S was higher than $G_{2condensed}$/G, but under harsh pretreatment conditions (180°C), the trend was reversed, and less than 80% of the S subunits were in condensed form. In the HSQC spectra of CELF lignin samples (**Figure 3**), the cross-peak at δ106.3/δ7.25 ppm is assigned to $C_{2,6}$ in the oxidized S subunits, and S_{ox}/S was hardly affected by pretreatment severity (**Figure 4B**). It has been reported that oxidation of C_α or C_γ–OH in β–*O*–4′ substructure can lower the C–*O*–aryl bond strength, and consequently facilitate lignin depolymerization (Guo et al., 2018). Therefore, the oxidized S subunits were presumably located at the end of the CELF lignin polymer chain.

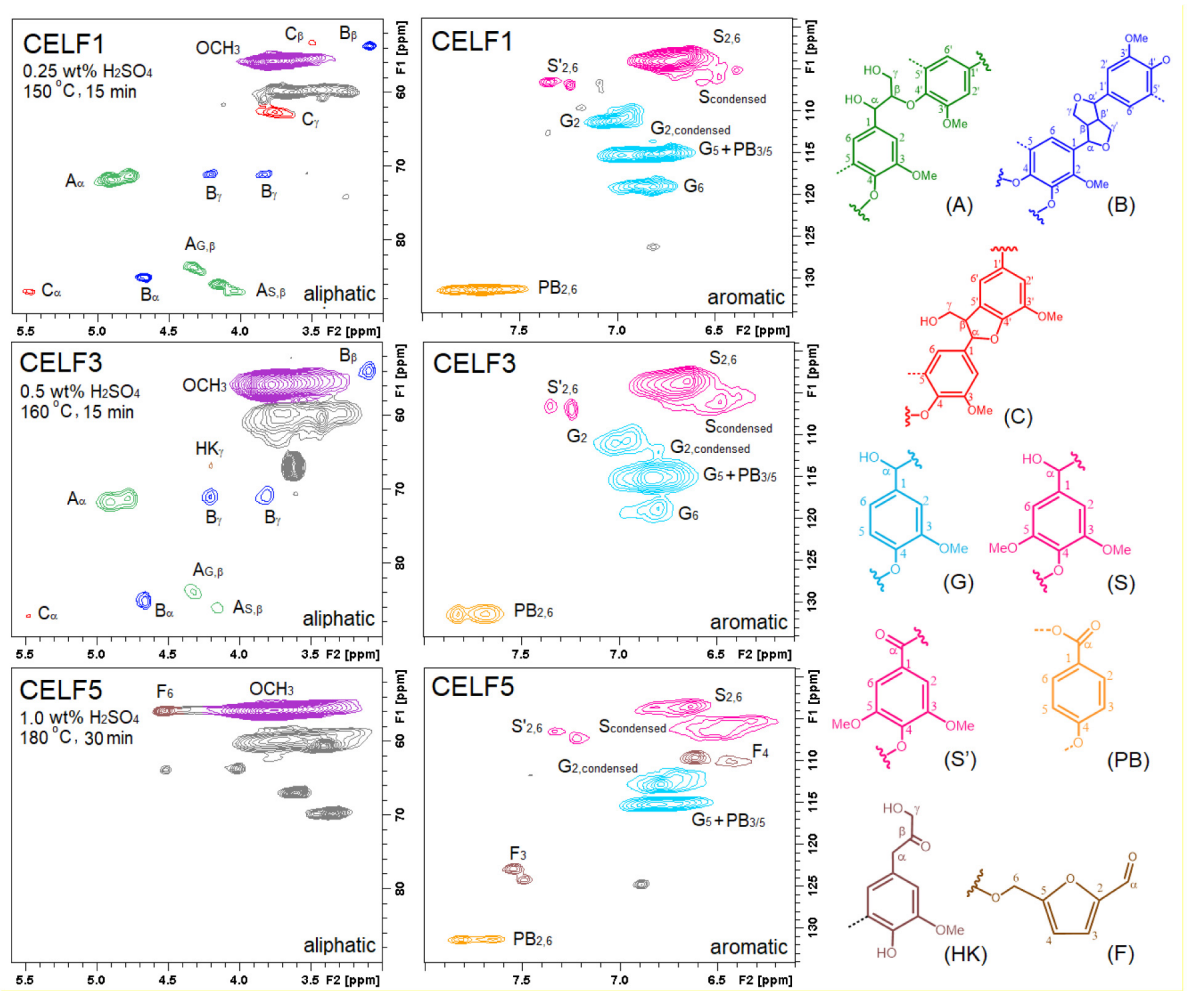

FIGURE 3 | HSQC spectra of CELF1, 3 and 5. Structure (A) β–*O*–4′ linked alkyl aryl ether substructure; (B) β–β′ linked resinol substructure; (C) β–5′ and α–*O*–4′ linked phenylcoumaran substructure; (G) guaiacyl unit; (S) syringyl unit; (S′) oxidized syringyl unit; (PB) *p*–hydroxybenzoate substructure; (HK) Hibbert ketone; (F) etherified 5-(hydroxylmethyl) furfural.

Correlation Between Thermal Behaviors and Molecular Structure of CELF Lignin

One of the pathways to the valorization of lignin isolated from CELF process is to incorporate them into polymeric materials; therefore, it is essential to have a deep fundamental understanding of their thermal behaviors. The DSC profiles in **Figure 5A** exhibited two distinct glass transition patterns for CELF lignin depending on the molecular structure that can be tuned by pretreatment severity. Below 180°C (CELE1∼3), glass transition temperature (T_g) of CELF lignin is positively correlated to molecular weight. The CELF lignin samples obtained at 180°C are highly condensed and crosslinked through rigid C–C bonds rather than C–O bonds. Although their molecular weights were significantly lower than CELF1∼3, no clear glass transition state can be observed for CELF4 and CELF5 within the experimental temperature range. In **Figure 5B**, the TGA thermograms indicated that the CELF lignin samples underwent three degradation steps. The most prominent peak arising from breaking C–C interlinkages and demethoxylation of aromatic rings at 350∼400°C can be observed for all CELF lignin samples (Wang et al., 2018). However, the peak was shrinking as the pretreatment becomes harsher, and such phenomenon is consistent with the decreasing S/G ratio caused by demethoxylation. The peak around 280°C is mainly caused by the bond rupture of ether interlinkages and aliphatic side chains, which release phenolic compounds, aldehydes, and carboxylic acids (Zhao et al., 2014). Its decay reflected lignin molecular structure evolving from flexible and native-like to a rigid and highly condensed under elevated pretreatment severity. The mass loss around 150°C is mainly attributed to dehydration of aliphatic hydroxyl groups (Hirose et al., 1998).

Screening CELF Lignin for CL-PUs

The CELF lignin samples, CELF2, CELF3 and CELF4 prepared under 150, 160, and 180°C pretreatment temperatures, were selected for producing CL-PUs. As shown in **Table 3**, the CL-PUs

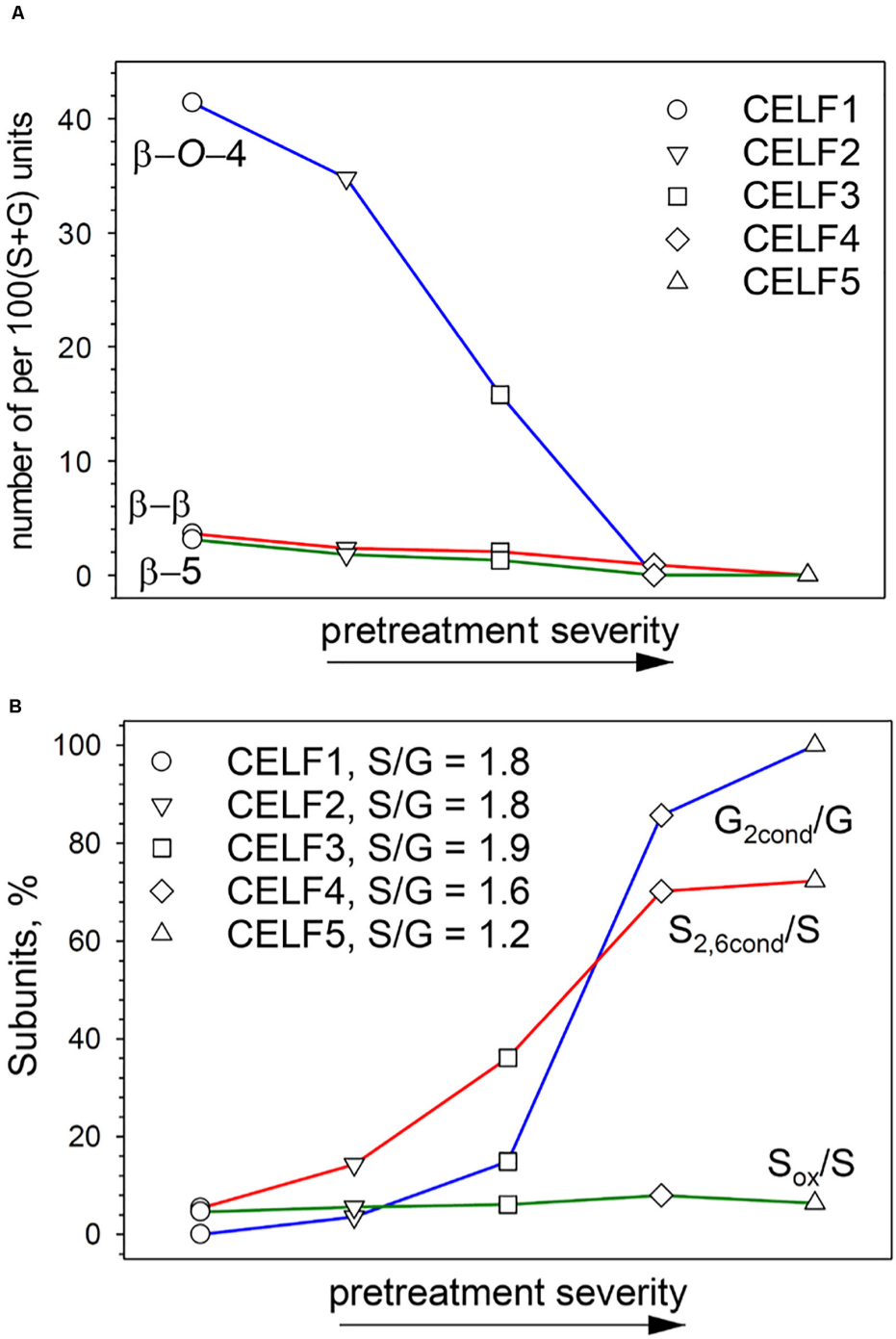

FIGURE 4 | Semiquantitative HSQC analyses of CELF lignin interunit linkages and subunits. **(A)** Changes of β–O–4′, β–β′ and β–5′ interunit linkage contents [per 100 (S + G) units] with increasing pretreatment severity; **(B)** Changes of condensed guaiacyl (G_{2cond}), condensed syringyl ($S_{2,6cond}$) and oxidized syringyl (S_{ox}) subunit contents with increasing pretreatment severity.

(CL2, CL3, and CL4) using lignin as the solo polyol were brittle materials with elongation at break (ϵ_b) hardly exceeded 5%, and their Young's modulus (E), ultimate stress (σ_{max}) increased as higher pretreatment temperature was employed. The aliphatic -OH groups in lignin are found more reactive in polyurethane synthesis, and urethane formation on the aromatic ring are less favorable due to steric hindrance effect and acidic character of phenolic -OH groups (Cateto et al., 2011). However, in this work, the mechanical properties of CL-PUs were determined by the miscibility between CELF lignin and PMDI in THF. In the

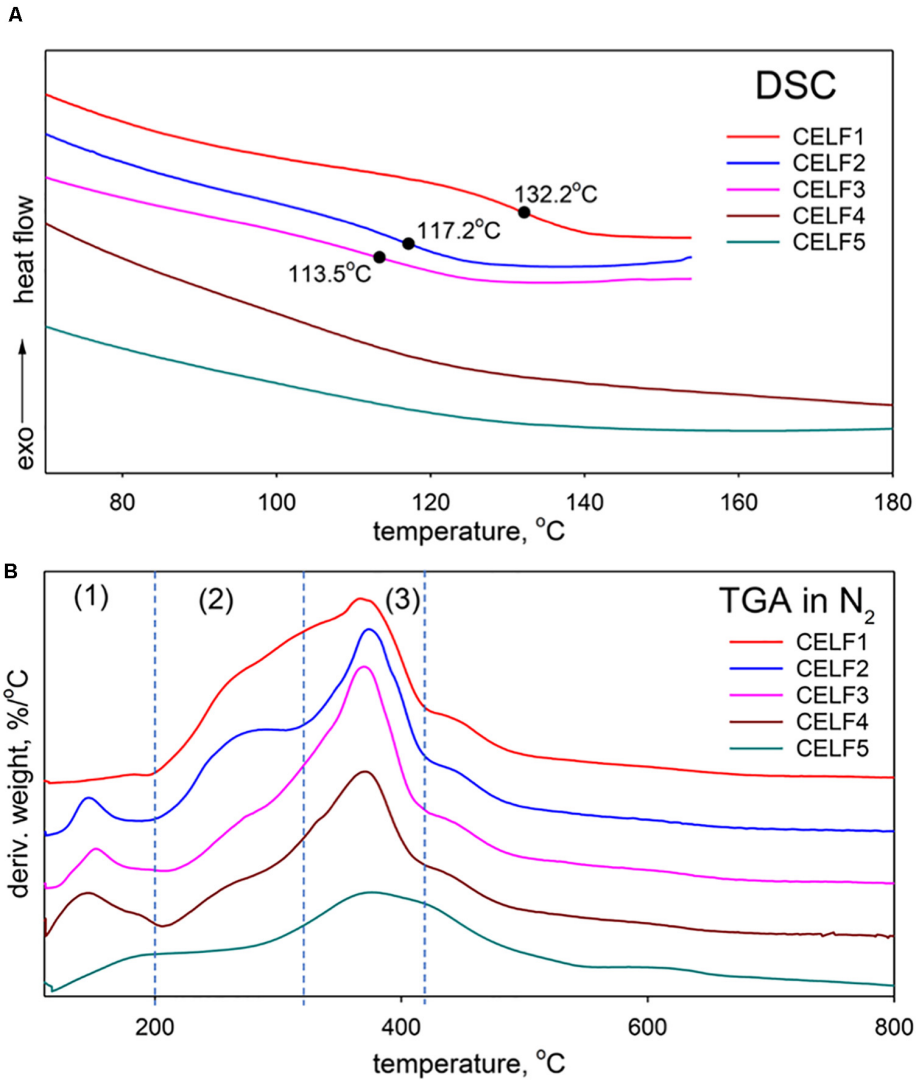

FIGURE 5 | (A) DSC and **(B)** TGA analyses of CELF lignin samples obtained under different pretreatment conditions.

TABLE 3 | The tensile properties of CL-PUs: Young's modulus (E), ultimate stress (σ_{max}) and elongation at break (ϵ_b).

CL-PU[a]	E (GPa)	σ_{max} (MPa)	ϵ_b (%)	Lignin (%)
CL2	0.80 ± 0.16	22.01 ± 6.35	3.46 ± 0.80	59.6
CL3	0.97 ± 0.09	27.85 ± 13.19	4.50 ± 0.46	61.7
CL4	1.04 ± 0.10	39.92 ± 8.92	4.47 ± 1.06	62.9
CL2-PEG[b]	0.21 ± 0.03	9.23 ± 2.04	7.13 ± 1.96	36.5
CL3-PEG[b]	0.21 ± 0.01	13.20 ± 1.18	24.23 ± 5.05	37.4
CL4-PEG[b]	0.07 ± 0.00	8.87 ± 1.90	89.77 ± 26.3	37.9

The error values were obtained from standard deviation of triplicate results. [a]NCO/OH = 1:1. [b]CELF lignin/PEG = 1:1 (w/w).

sequential precipitation study, it was found that CELF lignin cuts with higher molecular weight inclined to precipitate out from the THF-methanol co-solvent as the solvent polarity decreased (Wang et al., 2018). Similarly, in this work, the solvation behavior of CELF lignin was manipulated by its molecular weight. CELF2 (M_w = 8800 g/mol) and CELF3 (M_w = 3900 g/mol) were not completely soluble in THF at 60°C, and further precipitation occurred when they were mixing with PMDI in THF. Compared to CELF3, CELF 4 (M_w = 3250 g/mol) possessed higher proportion of lower-molecular-weight lignin species as shown in the GPC profiles (**Figure 1**). CELF4 was fully soluble in THF at room temperature, and as a result, CL4 exhibited better E and σ_{max} given the fact that CELF4 is structurally highly condensed and rigid. It was reported that PEG was able to form strong hydrogen bonds with lignin aliphatic and phenolic -OH groups, and thus disrupt the non-covalent intermolecular interaction between macromolecular lignin species (Kadla and Kubo, 2003; Wang et al., 2017b). Herein, 50% (w/w) PEG was pre-mixed with CELF lignin samples aiming to promote the solvation of the latter ones in THF. In general, the soft segments formed by PEG

reduced the brittleness and improved the ductility of the CL-PEG PUs (**Table 3**). Consistent with the control set, the variation of ϵ_b for CL-PEG PUs indicated that the efficacy of PEG depended on the solvation behavior of CELF lignin.

CONCLUSION

Poplar biomass was pretreated in the CELF process under different conditions, in which lignin was depolymerized and extracted with acidic aqueous THF. The pretreatment severity strongly influenced the molecular weight, multifunctionality and intra-polymer structure characteristics of the co-product lignin. Mild CELF pretreatment at low temperature was conducted to reduce the changes on lignin chemical structure and preserve high molecular weight, high β–*O*–4′, and aliphatic hydroxyl contents. When the pretreatment temperature was increased from 150 to 180°C, the content of aliphatic hydroxyl groups was reduced 4-fold, which had a negative impact on the multifunctionality of CELF lignin. The studies of CELF lignin thermal behaviors confirmed that CELF lignin isolated from high-severity pretreatment was composed of hetero-oligomers with rigid and highly condensed molecular structure. Considering the efficiency of CELF process, high temperature (180°C) should be avoided given that monosaccharides can be wasted on the massive side-reactions forming pseudo-lignin and etherification between lignin and 5-hydroxymethylfurfural during the pretreatment. On the other hand, the synthesis of CL-PU indicated that the tensile properties depended on the miscibility of CELF lignin with other components such as PMDI, and the presence of PEG would disrupt the strong hydrogen bonding between lignin macromolecules and improve the dispersion of CELF lignin in the PU network. Therefore, for CELF lignin prepared under mild pretreatment conditions such as at 150 and 160°C, fractionation to separate out high molecular weight cuts will be required to improve its dispersion in the CELF lignin-based polyurethanes.

AUTHOR'S NOTE

The views and opinions of the authors expressed herein do not necessarily state or reflect those of the United States Government or any agency thereof. Neither the United States Government nor any agency thereof, nor any of their employees, makes any warranty, expressed or implied, or assumes any legal liability or responsibility for the accuracy, completeness, or usefulness of any information, apparatus, product, or process disclosed, or represents that its use would not infringe privately owned rights. The publisher, by accepting the article for publication, acknowledges that the United States Government retains a non-exclusive, paid-up, irrevocable, worldwide license to publish or reproduce the published form of this manuscript, or allow others to do so, for United States Government purposes. The Department of Energy will provide public access to these results of federally sponsored research in accordance with the DOE Public Access Plan (http://energy.gov/downloads/doe-public-access-plan).

DATA AVAILABILITY STATEMENT

All datasets generated for this study are included in the article/**Supplementary Material**.

AUTHOR CONTRIBUTIONS

Y-YW experiment design, data analyses, wrote and revised the manuscript. PS and BS conducted the pretreatment experiments and prepared CELF lignin samples. YP conducted HSQC NMR and data interpretation, revised the manuscript. CW, CC, and AR initiated the project, responsible for getting the funds, revised the manuscript. All authors read and approved the final manuscript.

FUNDING

We acknowledge the support through the U.S.D.A. National Institute of Food and Agriculture Grant 9008-004957 titled "Integrated Biorefinery to Produce Ethanol, High-Value Polymers, and Chemicals from Lignocellulosic Biomass." Oak Ridge National Laboratory is managed by UT-Battelle, LLC under Contract DE-AC05-00OR22725 with the U.S. Department of Energy (DOE). This study was supported, in part, by the Center for Bioenergy Innovation (CBI), a U.S. Department of Energy Bioenergy Research Center supported by the Office of Biological and Environmental Research in the DOE Office of Science.

SUPPLEMENTARY MATERIAL

The Supplementary Material for this article can be found online at: https://www.frontiersin.org/articles/10.3389/fenrg.2020.00149/full#supplementary-material

REFERENCES

Balakshin, M. Y., Capanema, E. A., and Chang, H.-M. (2007). MWL fraction with a high concentration of lignin-carbohydrate linkages: isolation and 2D NMR spectroscopic analysis. *Holzforschung* 61, 1–7. doi: 10.1515/HF.2007.001

Cai, C. M., Zhang, T., Kumar, R., and Wyman, C. E. (2013). THF co-solvent enhances hydrocarbon fuel precursor yields from lignocellulosic biomass. *Green Chem.* 15, 3140–3145. doi: 10.1039/C3GC41214H

Cateto, C. A., Barreiro, M. F., Rodrigues, A. E., and Belgacem, M. N. (2011). Kinetic study of the formation of lignin-based polyurethanes in bulk. *React. Funct. Poly.* 71, 863–869. doi: 10.1016/j.reactfunctpolym.2011.05.007

Constant, S., Wienk, H. L. J., Frissen, A. E., Peinder, P. D., Boelens, R., and van Es, D. S. (2016). New insights into the structure and composition of technical lignins: a comparative characterisation study. *Green Chem.* 18, 2651–2665. doi: 10.1039/C5GC03043A

Fowles, J., Boatman, R., Bootman, J., Lewis, C., Morgott, D., Rushton, E., et al. (2013). A review of the toxicological and environmental hazards and risks of

tetrahydrofuran. *Crit. Rev. Toxicol.* 43, 811–828. doi: 10.3109/10408444.2013.836155

Giummarella, N., Pu, Y., Ragauskas, A. J., and Lawoko, M. (2019). A critical review on the analysis of lignin carbohydrate bonds. *Green Chem.* 21, 1573–1595. doi: 10.1039/C8GC03606C

Guo, H., Miles-Barrett, D. M., Neal, A. R., Zhang, T., Li, C., and Westwood, N. J. (2018). Unravelling the enigma of ligninOX: can the oxidation of lignin be controlled? *Chem. Sci.* 9, 702–711. doi: 10.1039/C7SC03520A

Hallac, B. B., Pu, Y., and Ragauskas, A. J. (2010). Chemical transformations of buddleja davidii lignin during ethanol organosolv pretreatment. *Energy Fuels* 24, 2723–2732. doi: 10.1021/ef901556u

Higuchi, T. (2003). Pathways for monolignol biosynthesis via metabolic grids: coniferyl aldehyde 5-hydroxylase, a possible key enzyme in angiosperm syringyl lignin biosynthesis. *Proc. Jpn. Acad. Ser. B* 79B, 227–236. doi: 10.2183/pjab.79B.227

Hirose, S., Kobashigawa, K., Izuta, Y., and Hatakeyama, H. (1998). Thermal degradation of polyurethanes containing lignin studied by TG-FTIR. *Polym. Int.* 47, 247–256.

Hu, F., Jung, S., and Ragauskas, A. (2012). Pseudo-lignin formation and its impact on enzymatic hydrolysis. *Bioresour. Technol.* 117, 7–12. doi: 10.1016/j.biortech.2012.04.037

Hu, F., and Ragauskas, A. (2014). Suppression of pseudo-lignin formation under dilute acid pretreatment conditions. *RSC Adv.* 4, 4317–4323. doi: 10.1039/C3RA42841A

Imai, T., Yokoyama, T., and Matsumoto, Y. (2011). Revisiting the mechanism of β-O-4 bond cleavage during acidolysis of lignin IV: dependence of acidolysis reaction on the type of acid. *J. Wood Sci.* 57, 219–225. doi: 10.1007/s10086-010-1166-6

Kadla, J. F., and Kubo, S. (2003). Miscibility and Hydrogen Bonding in Blends of Poly(ethylene oxide) and Kraft Lignin. *Macromology* 36, 7803–7811. doi: 10.1021/ma0348371

Li, Y., Shuai, L., Kim, H., Motagamwala, A. H., Mobley, J. K., Yue, F., et al. (2018). An "ideal lignin" facilitates full biomass utilization. *Sci. Adv.* 4:eaau2968. doi: 10.1126/sciadv.aau2968

Liu, E., Li, M., Das, L., Pu, Y., Frazier, T., Zhao, B., et al. (2018). Understanding lignin fractionation and characterization from engineered switchgrass treated by an aqueous ionic liquid. *ACS Sustain. Chem. Eng.* 6, 6612–6623. doi: 10.1021/acssuschemeng.8b00384

Lundquist, K., and Lundquist, R. (1972). Acid degradation of lignin part VII. The cleavage of ether bonds. *ACTA Chem. Scand.* 26, 2005–2023.

Meng, X., Crestini, C., Ben, H., Hao, N., Pu, Y., Ragauskas, A. J., et al. (2019a). Determination of hydroxyl groups in biorefinery resources via quantitative 3^1P NMR spectroscopy. *Nat. Protoc.* 14, 2627–2647. doi: 10.1038/s41596-019-0191-1

Meng, X., Parikh, A., Seemala, B., Kumar, R., Pu, Y., Christopher, P., et al. (2018). Chemical transformations of poplar lignin during cosolvent enhanced lignocellulosic fractionation process. *ACS Sustain. Chem. Eng.* 6, 8711–8718. doi: 10.1021/acssuschemeng.8b01028

Meng, X., Parikh, A., Seemala, B., Kumar, R., Pu, Y., Wyman, C. E., et al. (2019b). Characterization of fractional cuts of co-solvent enhanced lignocellulosic fractionation lignin isolated by sequential precipitation. *Bioresour. Technol.* 272, 202–208. doi: 10.1016/j.biortech.2018.09.130

Meng, X., Pu, Y., Li, M., and Ragauskas, A. J. (2020). A biomass pretreatment using cellulose-derived solvent Cyrene. *Green Chem.* 22, 2862–2872. doi: 10.1039/D0GC00661K

Mostofian, B., Cai, C. M., Smith, M. D., Petridis, L., Cheng, X., Wyman, C. E., et al. (2016). Local phase separation of co-solvents enhances pretreatment of biomass for bioenergy applications. *J. Am. Chem. Soc.* 138, 10869–10878. doi: 10.1021/jacs.6b03285

Nguyen, T. Y., Cai, C. M., Osman, O., Kumar, R., and Wyman, C. E. (2016). CELF pretreatment of corn stover boosts ethanol titers and yields from high solids SSF with low enzyme loadings. *Green Chem.* 18, 1581–1589. doi: 10.1039/C5GC01977J

Petridis, L., and Smith, J. C. (2018). Molecular-level driving forces in lignocellulosic biomass deconstruction for bioenergy. *Nat. Rev. Chem.* 2, 382–389. doi: 10.1038/s41570-018-0050-6

Ragauskas, A. J., Beckham, G. T., Biddy, M. J., Chandra, R., Chen, F., Davis, M. F., et al. (2014). Lignin valorization: improving lignin processing in the biorefinery. *Science* 344, 709–720.

Ragauskas, A. J., Williams, C. K., Davison, B. H., Britovsek, G., Cairney, J., Eckert, C. A., et al. (2006). The path forward for biofuels and biomaterials. *Science* 311:484. doi: 10.1126/science.1114736

Sannigrahi, P., Kim, D. H., Jung, S., and Ragauskas, A. (2011). Pseudo-lignin and pretreatment chemistry. *Energy Environ. Sci.* 4, 1306–1310. doi: 10.1039/C0EE00378F

Sannigrahi, P., Ragauskas, A. J., and Tuskan, G. A. (2010). Poplar as a feedstock for biofuels: a review of compositional characteristics. *Biofuels Bioprod. Biorefin.* 4, 209–226. doi: 10.1002/bbb.206

Seemala, B., Meng, X., Parikh, A., Nagane, N., Kumar, R., Wyman, C. E., et al. (2018). Hybrid catalytic biorefining of hardwood biomass to methylated furans and depolymerized technical lignin. *ACS Sustain. Chem. Eng.* 6, 10587–10594. doi: 10.1021/acssuschemeng.8b01930

Shinde, S. D., Meng, X., Kumar, R., and Ragauskas, A. J. (2018). Recent advances in understanding the pseudo-lignin formation in a lignocellulosic biorefinery. *Green Chem.* 20, 2192–2205. doi: 10.1039/C8GC00353J

Shuai, L., Questell-Santiago, Y. M., and Luterbacher, J. S. (2016). A mild biomass pretreatment using γ-valerolactone for concentrated sugar production. *Green Chem.* 18, 937–943. doi: 10.1039/C5GC02489G

Sluiter, A., Hames, B., Ruiz, R., Scarlata, C., Sluiter, J., Templeton, D., et al. (2012). "Determination of structural carbohydrates and lignin in biomass," in *Laboratory Analytical Procedure (LAP)*, (Golden, CO: National Renewable Energy Laboratory).

Smith, M. D., Cheng, X., Petridis, L., Mostofian, B., and Smith, J. C. (2017). Organosolv-Water Cosolvent phase separation on cellulose and its influence on the physical deconstruction of cellulose: a molecular dynamics analysis. *Sci. Rep.* 7:14494. doi: 10.1038/s41598-017-15048-7

Smith, M. D., Mostofian, B., Cheng, X., Petridis, L., Cai, C. M., Wyman, C. E., et al. (2016). Cosolvent pretreatment in cellulosic biofuel production: effect of tetrahydrofuran-water on lignin structure and dynamics. *Green Chem.* 18, 1268–1277. doi: 10.1039/C5GC01952D

Stewart, J. J., Akiyama, T., Chapple, C., Ralph, J., and Mansfield, S. D. (2009). The effects on lignin structure of overexpression of Ferulate 5-hydroxylase in hybrid poplar. *Plant Physiol.* 150, 621–635. doi: 10.1104/pp.109.137059

Sturgeon, M. R., Kim, S., Lawrence, K., Paton, R. S., Chmely, S. C., Nimlos, M., et al. (2014). A mechanistic investigation of acid-catalyzed cleavage of aryl-ether linkages: implications for lignin depolymerization in acidic environments. *ACS Sustain. Chem. Eng.* 2, 472–485. doi: 10.1021/sc400384w

Wang, Y.-Y., Cai, C. M., and Ragauskas, A. J. (2017a). Recent advances in lignin-based polyurethanes. *Tappi J.* 16, 203–207.

Wang, Y.-Y., Chen, Y.-R., and Sarkanen, S. (2017b). Blend configuration in functional polymeric materials with a high lignin content. *Faraday Discuss.* 202, 43–59. doi: 10.1039/C7FD00083A

Wang, Y.-Y., Li, M., Wyman, C. E., Cai, C. M., and Ragauskas, A. J. (2018). Fast fractionation of technical lignins by organic cosolvents. *ACS Sustain. Chem. Eng.* 6, 6064–6072. doi: 10.1021/acssuschemeng.7b04546

Wang, Y.-Y., Wyman, C. E., Cai, C. M., and Ragauskas, A. J. (2019). Lignin-based polyurethanes from unmodified kraft lignin fractionated by sequential precipitation. *ACS Appl. Poly. Mater.* 1, 1672–1679. doi: 10.1021/acsapm.9b00228

Wyman, C. E., Cai, C. M., and Kumar, R. (2016). "Bioethanol from lignocellulosic biomass," in *Encyclopedia of Sustainability Science and Technology*, ed. R. A. Meyers (New York, NY: Springer), 1–27.

Zhao, J., Xiuwen, W., Hu, J., Liu, Q., Shen, D., and Xiao, R. (2014). Thermal degradation of softwood lignin and hardwood lignin by TG-FTIR and Py-GC/MS. *Poly. Degrad. Stabil.* 108, 133–138. doi: 10.1016/j.polymdegradstab.2014.06.006

Conflict of Interest: The authors declare that the research was conducted in the absence of any commercial or financial relationships that could be construed as a potential conflict of interest.

frontiers in Energy Research

ORIGINAL RESEARCH
published: 02 September 2020
doi: 10.3389/fenrg.2020.00148

Preparation of Graphene-Like Porous Carbons With Enhanced Thermal Conductivities From Lignin Nano-particles by Combining Hydrothermal Carbonization and Pyrolysis

Huiling Dong[1], Min Li[2], Yongcan Jin[2], Yan Wu[1], Caoxing Huang[2] and Jinlai Yang[3]**

[1] College of Furnishings and Industrial Design, Nanjing Forestry University, Nanjing, China, [2] Jiangsu Co-Innovation Center for Efficient Processing and Utilization of Forest Resources, Nanjing Forestry University, Nanjing, China, [3] Key Laboratory of High Efficient Processing of Bamboo of Zhejiang Province, China National Bamboo Research Center, Hangzhou, China

OPEN ACCESS

Edited by:
Li Shuai,
Fujian Agriculture and Forestry University, China

Reviewed by:
Chuan-Ling Si,
Tianjin University of Science and Technology, China
Rangana Jayawickramage,
Tomson Technologies LLC, United States

***Correspondence:**
Caoxing Huang
hcx@njfu.edu.cn
Jinlai Yang
5491936@163.com

Specialty section:
This article was submitted to Bioenergy and Biofuels, a section of the journal Frontiers in Energy Research

Received: *11 May 2020*
Accepted: *15 June 2020*
Published: *02 September 2020*

Citation:
Dong H, Li M, Jin Y, Wu Y, Huang C and Yang J (2020) Preparation of Graphene-Like Porous Carbons With Enhanced Thermal Conductivities From Lignin Nano-particles by Combining Hydrothermal Carbonization and Pyrolysis. Front. Energy Res. 8:148. doi: 10.3389/fenrg.2020.00148

Lignin nano-particles (LNPs) exhibit properties that distinguish them from the production of other lignin-based materials. However, little research has been performed to investigate whether porous carbons produced from LNPs exhibit a performance superior to those derived from untreated lignin. In this study, lignin was fabricated into LNPs and used to prepare high-performance porous carbons with enhanced thermal conductivities compared to that of carbons from neat lignin. Two different preparation protocols were employed: direct pyrolysis and hydrothermal carbonization followed by pyrolysis. Carbons obtained from 100 to 300 nm LNPs possessed more graphene-like structures than carbons from unaltered lignin. In addition, carbons prepared using a combination of hydrothermal carbonization and pyrolysis exhibited higher specific surface areas (108.81–220.75 m^2/g) and total pore volumes (0.098–0.166 cm^3/g) than those prepared via direct pyrolysis. In addition, LNP-derived carbons exhibited superior thermal conductivities (0.45 W/mK) and thermal conductivity rates (0.51°C/s). This work provides the useful finding that superior graphene-like porous carbons can be produced by transforming lignin into LNP and then hydrothermally carbonizing the resulting material prior to pyrolysis.

Keywords: lignin nano-particles, porous carbon, thermal conductivity, hydrothermal carbonization, graphene

INTRODUCTION

Graphene is a type of two-dimensional material composed of sp^2-structured monolayer carbon. Graphene continues to garner significant attention and utilization due to its extraordinary properties, such as its high theoretical surface area, exceptional thermal conductivity, and elevated Young's modulus (Lee et al., 2008; Yu et al., 2011). Based on these remarkable properties, graphene has been used to prepare materials including solar cells, high-performance supercapacitors, sensors and biosensors, polymer composite reinforcement fillers, and hydrogen storage materials (Hou et al., 2011; Huang et al., 2011; Sun et al., 2019). Various methods can be used to prepare graphene,

including the redox of graphene oxide, chemical vapor deposition, and surface separation of graphite (Xu et al., 2011; Liu et al., 2017). Although high-quality graphene can be obtained via the aforementioned methods, urgent technical and biological issues remain. These issues include a lack of mass production capacity, as well as environmental and human health concerns due to a reliance on toxic or hazardous reagents (Vlassiouk et al., 2013). To avoid these issues while maintaining the desired graphene properties, researchers have developed several graphene-like materials such as carbon nitride sheets, activated porous carbon (Ojha et al., 2017), carbon nanotubes (Araujo et al., 2012), and MoS_2 nanoplates (Hwang et al., 2011). These materials offer performances that are comparable to that of graphene for various applications.

Activated or porous carbons stand out among the previously mentioned graphene-like materials. This promising carbon material has tunable porosity, a large surface area, and intriguing electrical conductivity properties (Vinu, 2008). Depending on the preparation conditions and catalysts used, a variety of carbons can be fabricated to exhibit high specific surface areas and porosities that make them applicable as either high-performance supercapacitors or photocatalytic additives (Lv et al., 2015; Zhu et al., 2017; Foong et al., 2020). These carbons are generally produced from fossil sources such as coal and petroleum, or biomass sources such as rice husks, corn stalks, and bamboo residues (Abioye and Ani, 2015; Chen et al., 2018, 2019; Han et al., 2020). The material is generated from a feedstock via carbonization or pyrolysis, which are considered to have high techno-economic feasibilities due to their relatively low costs and good environmental compatibilities.

Of the various precursors used to prepare porous carbons, lignin is attractive because of its high carbon content (∼55–65%) and abundant supply from the pulp and paper industries. Lignin is a byproduct of wood pulp delignification (Pang et al., 2020b; Yoo et al., 2020). Dissolved lignin (typically in a solution called black liquor) is commonly burned to recover pulping chemicals and provide steam for power production (Shuai et al., 2016; Pang et al., 2020a). However, some manufacturers have begun to develop lignin products of lignosulphonate, adhesive, and foam as additional revenue streams for pulp and paper mills (Li and Ragauskas, 2012; Pang et al., 2020b; Pei et al., 2020). Lignin is also chemically well-suited to transformation into graphene-like porous carbons, particularly because they contain functional groups and have an abundance of benzene rings (Liu et al., 2017; Dong et al., 2020; Wang et al., 2020). In addition, the plentiful aromatic carbon atoms in the guaiacyl and syringyl groups in lignin are sp^2 hybridized, which is the basic unit of graphene (Liu et al., 2017). Hence, lignin is speculated to have great potential as a feedstock for activated carbon production. However, investigation of this topic has been limited.

Several methods have been investigated as a means of producing porous carbons with high specific surface areas and pore volumes from various biomass sources. In general, methods include physical activation (steam, CO_2, and air), chemical activation (H_3PO_4, $ZnCl_2$, and KOH), and combined physicochemical methods (Kılıç et al., 2015; Salehin et al., 2015; Demiral et al., 2016). The chemicals used in these processes inevitably cause environmental pollution and equipment corrosion. Hence, physical treatments are the preferred facile, green approaches to producing porous carbon. High pressure homogeneous (HPH) technology is a conventional approach that offers high efficiency, reproducibility, and ease of industrial scale-up (Donsi et al., 2010). It has been reported that HPH technology can be regarded as nanotechnology because of its ability to prepare nano-scale products (e.g., nano-crystalline cellulose and nano-lignin particles) from biomass resources (Li et al., 2012). All of these nano-scale products exhibit interesting properties, such as high mechanical strengths, large specific surface areas, and low thermal properties. We hypothesize that the use of nano-lignin particles as a feedstock may generate porous carbons with better performance than those derived from untreated lignin. Importantly, no work has been done to investigate such materials as precursors for porous carbon preparation.

The high thermal conductivity of graphene suggests that it can be applied to microelectronics and thermal management. Since Balandin (2011) discovered that graphene exhibited remarkably better thermal conductivity than conventional carbon nanotubes, graphene has been applied to heat management of high-power electronics, including thermal dissipation systems for chips and batteries in smartphones, tablets, smart VR systems, and wearable devices (Wu et al., 2019; Zheng et al., 2019; Yang et al., 2020). Many studies have shown that polymer composite thermal conduction capabilities can be improved significantly via the blending or grafting of graphene (Yu et al., 2007; Ji et al., 2014). Hence, if graphene-like carbon prepared from lignin exhibits better thermal conductivity than lignin, it may be valuable as a thermally conductive filler for polymer composites.

In this study, porous carbons were produced from both kraft lignin and lignin nano-particles (LNPs) in an effort to investigate whether the differences between these raw materials could positively affect the properties of the resulting materials. Porous carbons were pyrolyzed via two protocols: one-step direct pyrolysis and a two-step procedure in which hydrothermal carbonization was performed prior to pyrolysis. The resulting carbon samples were characterized using various instruments. The thermal conductivities of the prepared carbons were analyzed using an infrared thermal imager. This work investigates processing variables that can be applied to lignin carbonization in order promote the valorization of lignin.

MATERIALS AND METHODS

Materials

The kraft lignin used in this study was obtained from bamboo black liquor via acid precipitation according to the method in our previous work (Huang et al., 2019a,b; Lin et al., 2020). The obtained lignin was purified by diethyl ether. After purification, a lignin suspension was prepared by adding the lignin powder to distilled water at a solids content of 0.5% (w/w). The suspension was then homogenized using a laboratory high-pressure homogenizer at 30°C and 500 bar to obtain LNP.

All chemicals were purchased from their manufacturers and were used without further purification.

Fabrication of Carbon From Lignin

Two protocols were used to fabricate porous carbon from LNP and precipitated lignin. The first procedure (protocol 1) was a one-step method in which powdered materials were placed in a ceramic ark. This ark was then loaded into a tube furnace and subjected to pyrolysis under nitrogen. The heating procedure was as follows: (1) heating from 30 to 180°C at 2°C/min, followed by 1 h at the final temperature; (2) heating from 180 to 450°C at 2°C/min, followed by 1 h at the final temperature; and (3) heating from 450 to 1100°C at 2°C/min, with the final temperature maintained for 3 h. The carbons produced from untreated lignin and LNP were termed GN-1-LIN and GN-1-LNP, respectively.

The second procedure (protocol 2) involved two steps. First, a lignin solution (20 g in 100 g of water) was hydrothermally carbonized at 250°C and 150 MPa for 3 h. The resulting hydrothermally carbonized solids were then subjected to pyrolysis using the same tube furnace and heating procedure as protocol 1. The pyrolyzed carbons produced from untreated lignin and LNP were termed GN-2-LIN and GN-2-LNP, respectively.

Characterization

Lignin and prepared carbon morphologies were characterized using scanning (SEM, S4800, Hitachi, Japan) and transmission electron microscopy (TEM, JEM 2100, JEOL Ltd., Japan) at accelerating voltages of 200 and 15 kV, respectively. Fourier transform infrared (FTIR) analysis was performed using a Nicolet 6700 spectrometer (Nicolet Instrument Company, United States). Signals were recorded over a scanning range of 4000–400 cm^{-1}. X-ray diffraction (XRD) patterns were obtained using a diffractometer (Rigaku Ultima IV, Japan) and Cu Ka radiation. The operating parameters were a 40 kV voltage, 40 mA of current, a 5°/min scan speed, and a 2 theta range of 5°–80°. Raman spectra were obtained using a confocal Raman microscope (T64000, Horiba Scientific, France) with an excitation wavelength of 532 nm, power of 22 mW, integration time of 30 s, and three accumulations. X-ray photoelectron spectroscopy (XPS) was carried out by a Thermo Escalab spectrometer with an Al-K*a* ($h\nu$ = 1486.6 eV). Nitrogen adsorption and desorption were performed and the Brunauer–Emmett–Teller (BET) method was used to analyze the specific surface area using a Micromeritics ASAP 2020 instrument. Pore size distributions were evaluated via the Barrett–Joyner–Halenda method.

Thermal Conductivity Analysis

Thermal conductivity analysis was performed using a hot disk thermal constant analyzer (TPS 2500, Hot Disk AB Company, Sweden) via the transient plane heat source method. Temperature distribution images were captured using an infrared thermal imager during heating.

RESULTS AND DISCUSSION

Morphologies of Lignin and Graphene-Like Porous Carbons

Industrial kraft lignin is typically a powder with a microscopic three-dimensional structure (Dallmeyer et al., 2014). Fabrication of LNPs has been reported as an attractive avenue for generating new, valuable applications for lignin (Ma et al., 2019). In this study, a solvent-free, high-pressure homogeneous technology was used to fabricate LNP from kraft lignin. The purpose of this effort was to explore whether LNP could be pyrolyzed into graphene-like porous carbons with better properties than those made from untreated lignin. Lignin and LNP morphologies were observed via SEM and TEM and are shown in **Figures 1a,b**, **2a,b**, respectively.

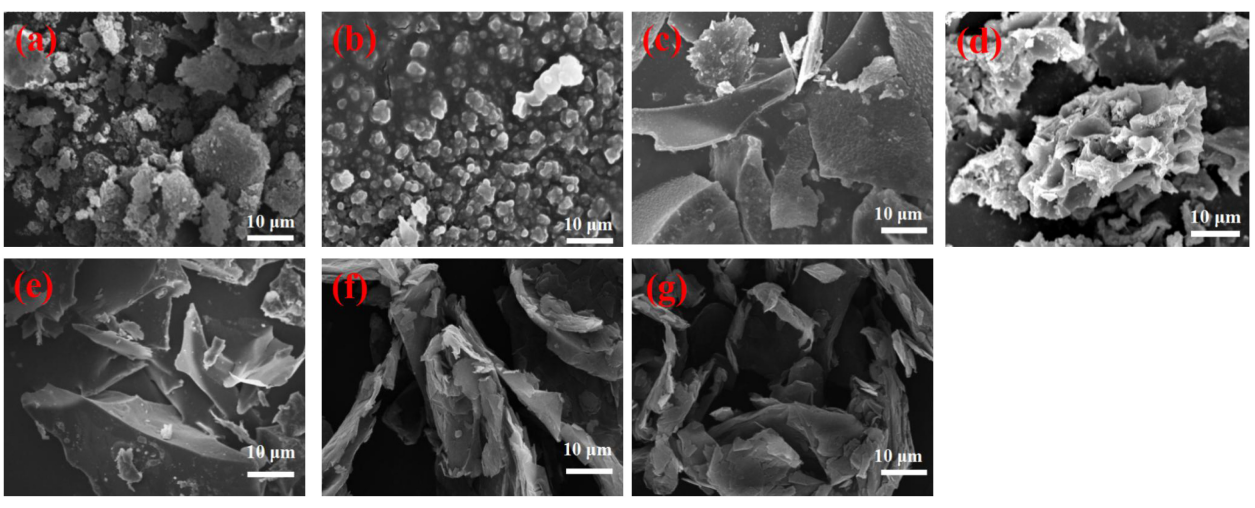

FIGURE 1 | SEM images of kraft lignin **(a)**, LNP **(b)**, and prepared carbons GN-1-LIN **(c)**, GN-2-LIN **(d)**, GN-1-LNP **(e)**, GN-2-LNP **(f)**, and commercial graphene **(g)**.

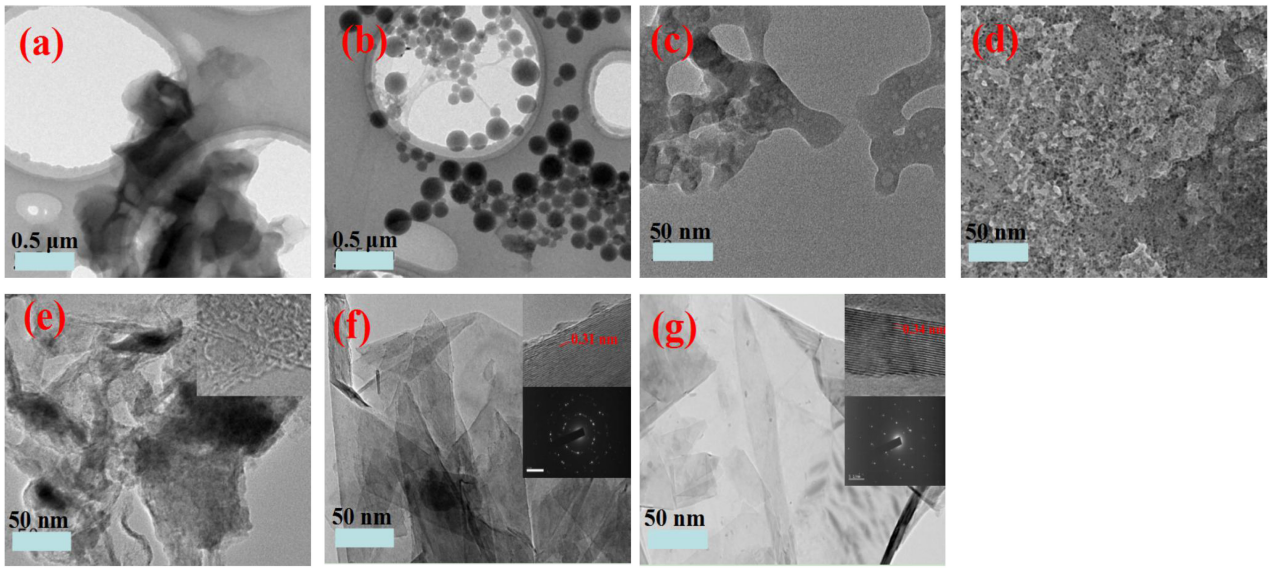

FIGURE 2 | TEM images of kraft lignin **(a)**, LNP **(b)**, and prepared carbons GN-1-LIN **(c)**, GN-2-LIN **(d)**, GN-1-LNP **(e)**, GN-2-LNP **(f)**, and commercial graphene **(g)**.

Figure 1a shows that neat lignin has a disordered micro-structure comprised of various shapes. **Figure 1b** shows that the LNPs produced are spherical particles with mostly uniform morphologies. Similar results are seen via TEM (**Figure 2b**). Nano-particle sizes are in the 100–300 nm range. Interestingly, this is similar to the sizes of LNPs derived from commercial lignin using solvent (tetrahydrofuran and dimethylsulfoxide) exchange and sonication (Ma et al., 2019; Sipponen et al., 2019).

Both lignin and LNP were used as precursors for preparation of four different activated carbons via two different production protocols. The morphologies of the prepared carbons were observed via SEM and TEM and are shown in **Figures 1c–f**, **2c–f**, respectively. In **Figures 1c,d**, agglomerated architectures of thick flakes and particles are observed from GN-1-LIN (first protocol) and GN-2-LIN (second protocol) carbons made from untreated lignin. This observation is in agreement with the work of Foong et al. (2020). It can also be seen that the formation of sheet-like surfaces is generally favored among LNP-derived carbons. Specifically, carbons made from LNPs via protocol 1 (GN-1-LNP) and protocol 2 (GN-2-LNP) exhibit prominent wrinkled surface textures with curling and sharp edges (**Figures 1e,f**). These properties are intrinsic graphene features of graphene, which can be more clearly observed in commercial graphene (**Figure 1g**). It is well known that corrugation and scrolling of the lamellae and edges are intrinsic graphene properties, which can clearly be observed in the TEM image of commercial graphene (**Figure 2g**; Barone et al., 2006; Tang et al., 2013). These properties were absent in the TEM images of carbons made from lignin (**Figures 2c,d**). **Figure 2e** showed that GN-1-LNP possessed some lamellae and edges similar to graphene, which can more clearly observed in the TEM image of GN-2-LNP (**Figure 2f**). The GN-2-LNP shows the in-plane lattice spacing of 0.31 nm corresponding to the (0 0 2) and (0 0 2) planes, and the spacing is closer to the 0.34 nm of graphene. Meanwhile, the GN-2-LNP shows a more similar diffraction pattern to the graphene, indicating the GN-2-LNP has a more similar polycrystalline structure with the graphene. According to the aforementioned results, it can be seen that the LNP-based carbons produced via protocol 2 contain more desirable features, such as smooth surfaces with creases and multi-layers with thin lamels (**Figure 2f**), than those produced via protocol 1. These results indicate that the combination of hydrothermal carbonization and pyrolysis generates porous carbons with greater morphological similarity to graphene-like structures than pyrolysis alone.

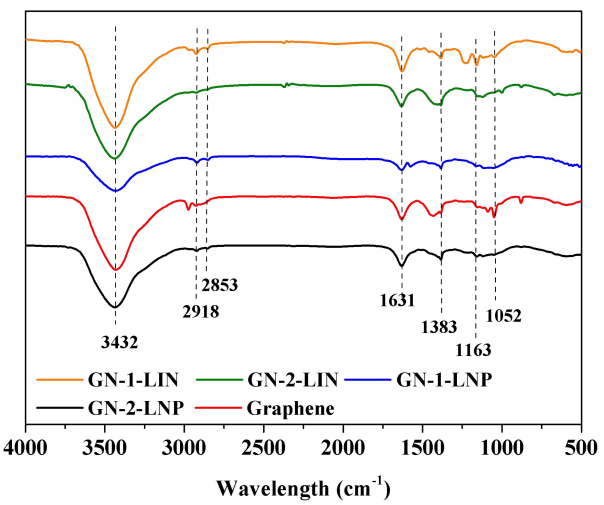

FIGURE 3 | FTIR spectra of the prepared carbons and commercial graphene.

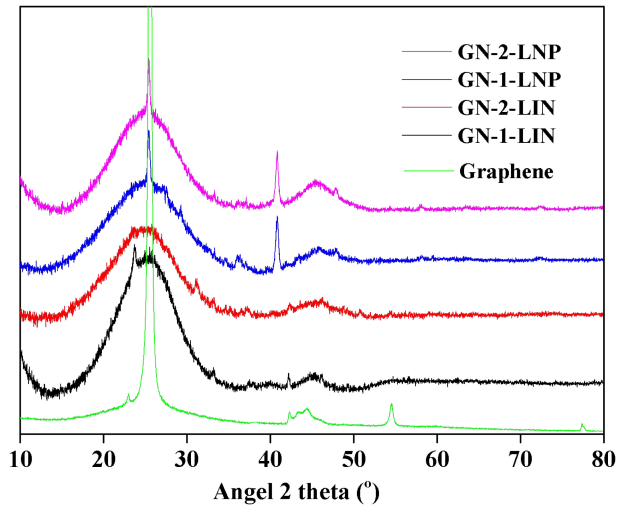

FIGURE 4 | XRD patterns of the prepared carbons and commercial graphene.

FTIR Spectra of Prepared Graphene-Like Porous Carbons

Fourier transform infrared was used to investigate the differences between the chemical structures of the porous carbons that we prepared and commercial graphene. The FTIR spectra are shown in **Figure 3**. The obvious peak at 1631 cm^{-1} is attributed to the graphene sheet C=C skeletal vibration (Song et al., 2012). The broad intense bands around 3432 and 1163 cm^{-1} correspond to the stretching vibrations of O–H and C–O functional groups, respectively, at the edges of graphene (Fernandes et al., 2018). The vibration peaks at 2918 and 2853 cm^{-1} correspond to the symmetric and antisymmetric stretching vibrations of CH_2 groups in graphene (Spitalsky et al., 2011). Importantly, the main graphene peaks are also visible without shifts in the FTIR spectra of our porous carbons. This indicates that graphene-like structures may be formed in lignin-based carbons manufactured using our protocols.

XRD Patterns of Prepared Graphene-Like Porous Carbons

X-ray diffraction patterns are an effective way to study the crystalline structures and layers comprising graphene (Morgan and Gilman, 2003; Vinodhkumar et al., 2018). The XRD spectra of the prepared carbons were obtained and compared to that of commercial graphene (**Figure 4**). It is well known that the (0 0 2) plane of graphene can exhibit a sharp reflection at $2\theta = 25.5°$ (Vinodhkumar et al., 2018). In **Figure 4**, both peaks at 25.6° are found in the patterns of commercial graphene, GN-1-LNP, and GN-2-LNP samples. This indicates that these carbons contain stacked graphene layers. However, GN-1-LIN and GN-2-LIN exhibit broad (0 0 2) graphitic plane diffraction peaks that are slightly shifted to a lower angle of 24.5°. In addition, GN-1-LNP and GN-2-LNP exhibit sharper (0 0 2) plane intensities than GN-1-LIN and GN-2-LIN. The work of Yan et al. (2018) also found that the degree of lignin graphitization can be improved via application of a treatment that forms nanoparticles. However, it should be pointed out that the XRD spectra of lignin derived

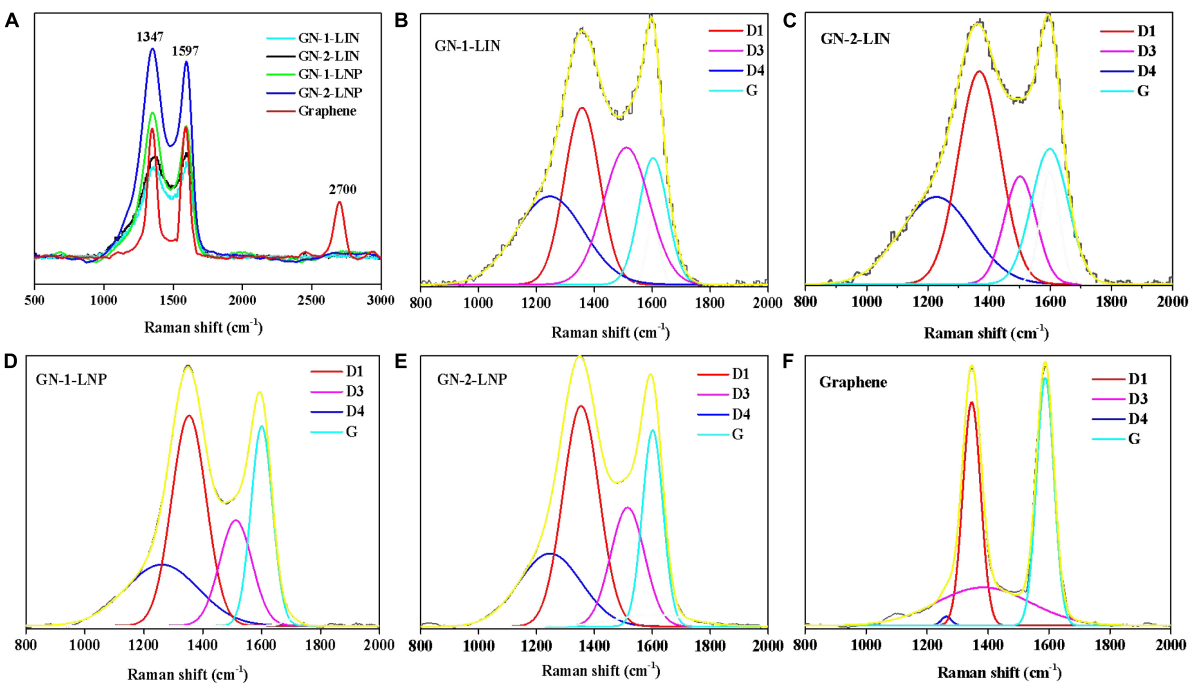

FIGURE 5 | Raman spectra of the prepared carbons and commercial graphene **(A)**, deconvoluted Raman spectra of GN-1-LIN **(B)**, GN-2-LIN **(C)**, GN-1-LNP **(D)**, GN-2-LNP **(E)**, and commercial graphene **(F)**.

carbons shows broader peaks than that of commercial graphene at around 25°. This can be explained as the lignin-derived carbons show small sheets and relatively low crystal structure, which are the inherent characteristics of biomass-based carbon materials that can show the broader (0 0 2) peaks around 25° (Han et al., 2017; Liu et al., 2017). Overall, from the aforementioned results, it can be seen that LNP appears to be the ideal starting material for the preparation of porous carbon based on the similarity of the resulting graphene-like structures to those in commercial graphene.

Raman Spectroscopy of Graphene-Like Porous Carbons

The aforementioned FTIR and XRD analyses reveal that the prepared carbons possess graphene-like structures. However, these results do not help one to understand specific differences between carbons that correlate with performance. Hence, Raman spectroscopy, a technology used to investigate edge strain and defects in graphene and graphitic materials (Vinu, 2008), was used to analyze the prepared porous carbons and commercial graphene.

Figure 5A shows that graphene exhibits two strong peaks at 1347 and 1597 cm^{-1}, which are attributed to the characteristic graphene D- and G-bands, respectively (Vinodhkumar et al., 2018; Sun et al., 2019). The G band is typically an in-plane stretching vibration of sp^2 hybrid carbon atoms in graphene. The D band is derived from disorder or defect vibration peaks in graphene (Dresselhaus et al., 2010; Sun et al., 2019). It can also represent a ring adjacent to a graphene edge or defect. **Figure 5** shows that the prepared carbons also exhibit G- and D-band vibrations. These edge strain and defect commonalties indicate that the prepared carbons exhibit structural properties analogous to those of graphene.

TABLE 1 | The I_D/I_G ratios, pore structures, and thermal conductivities of lignin, LNP, and the prepared carbons.

	I_{D1}/I_G	Specific surface area (m^2/g)	Total pore volume (cm^3/g)	Thermal conductivity (W/mK)	Amount of C–C in the C 1s (%)
GN-1-LIN	1.62	62.26	0.061	0.21	31.8
GN-2-LIN	1.77	108.81	0.098	0.22	31.8
GN-1-LNP	1.66	67.95	0.063	0.25	41.9
GN-2-LNP	1.36	220.75	0.166	0.45	49.5
graphene	0.93	/	/	/	49.6
lignin	/	18.78	0.027	0.11	/
LNP	/	30.35	0.045	0.18	/

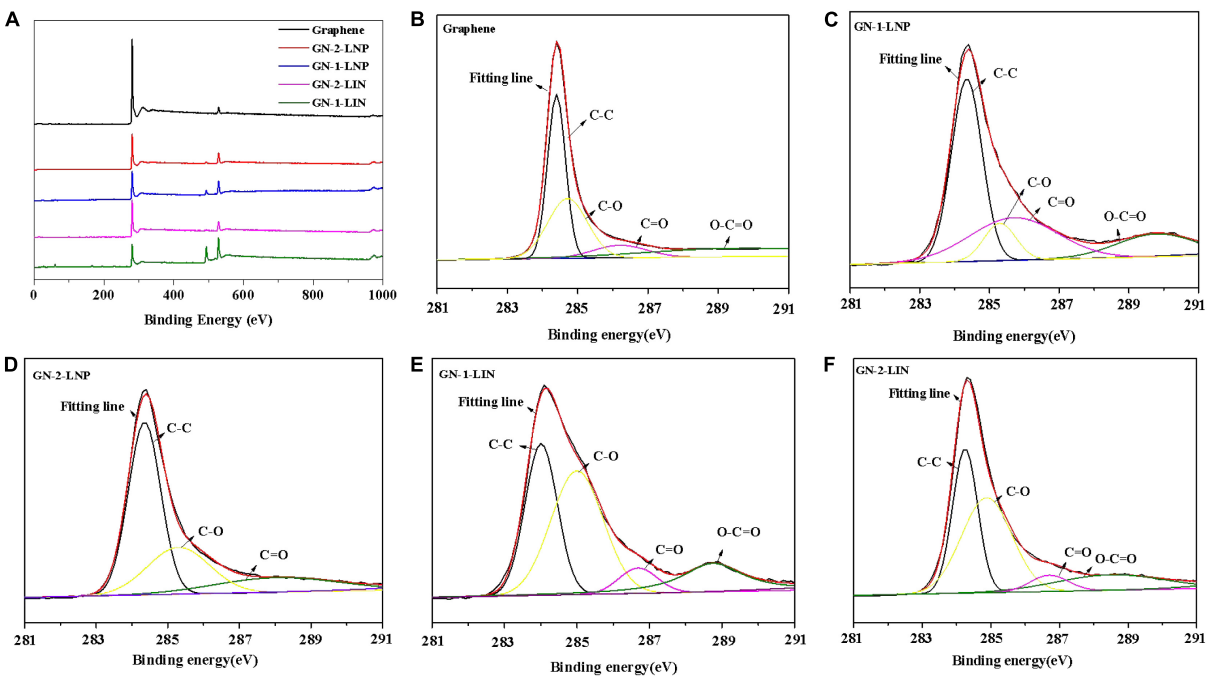

FIGURE 6 | XPS spectra of the prepared carbons and commercial graphene **(A)**, deconvoluted C 1s spectra of commercial graphene **(B)**, GN-1-LNP **(C)**, GN-2-LNP **(D)**, GN-1-LIN **(E)**, and GN-2-LIN **(F)**.

In Raman spectroscopy, the intensity of the G band can be used to determine the graphene thickness (Foong et al., 2020). **Figure 5A** shows that GN-1-LNP exhibits the same intensity as commercial graphene, which is lower than that of GN-2-LNP. These intensities indicate that the carbon derived from LNP via a combination of hydrothermal carbonization and pyrolysis possesses more graphene layers. The deconvolutions of Raman spectra are applied for all samples, and four Lorentzian functions are used to fit the D1, G, D3, and D4 bands (Lu et al., 2020), as shown in **Figures 5B–F**. In the fitted curves, D1-band and G-band are representative of the sp^2 hybridized carbon with structural defects or at plane edges and sp^2 hybridized carbon bond stretching in an ideal graphitic lattice (Hoekstra et al., 2016). Hence, the intensities ratio between the D1-band and G-band (I_{D1}/I_G) is indicative of the degree of graphitization (Dresselhaus et al., 2010; Liu et al., 2017; Lu et al., 2020). As shown in **Table 1**, the I_{D1}/I_G ratio of graphene is 0.93, which is lower than those of GN-1-LIN (1.62), GN-2-LIN (1.77), GN-1-LNP (1.66), and GN-2-LNP (1.36). These results indicate that using nano-particular lignin as a starting material can decrease the extent of disorder and defects in the prepared carbons, compared to that from the untreated lignin. Hence, it is hypothesized that the nano-lignin subjected to a combination of hydrothermal carbonization and pyrolysis possesses showed the potential ability to prepare the carbons with an enhanced degree of graphitization.

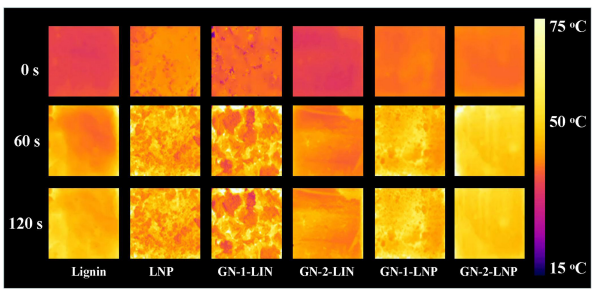

FIGURE 7 | Temperature distributions in the samples during heating.

XPS Spectroscopy of Graphene-Like Porous Carbons

To further understand the elemental composition of samples, the XPS spectra were obtained and shown in **Figure 6**. The survey XPS spectrum of the prepared porous carbons and commercial graphene (**Figure 6A**) shows strong peaks of C 1s at 284.4 eV and O 1s at 530.1 eV. The high resolution C 1s spectra (**Figures 6C–F**) showed the prepared carbons have two types of carbon, graphitic carbon (C–C) and oxygenated carbon (C–O, C=O, and O–C=O), which are also found in the C 1s curves of commercial graphene at the same binding energy (**Figure 6B**). The deconvolution of the C 1s can provide the relative amount of C–C (sp^2) in the sample (Kang et al., 2017). As shown in **Table 1**, the amount of C–C in commercial graphene was 49.6%, which was higher than those of GN-1-LIN (31.8%), GN-2-LIN (31.8%), GN-1-LNP (41.9%), and GN-2-LNP (49.5%). Among the prepared carbons, GN-2-LNP possessed the highest value of the relative amount of C–C, indicating it had the better graphitization (Mendes et al., 2020). These results are in accordance with the results from Raman analysis, which again indicate that using the combination of hydrothermal carbonization and pyrolysis show more potential to prepare the carbon with an enhanced degree of graphitization from nano-lignin than that from untreated lignin.

Pore Structure Analysis of Prepared Graphene-Like Porous Carbons

In this study, we sought to prepare porous carbons from LNP that are more similar to graphene than those prepared from untreated lignin. To further investigate the pore structures of the prepared carbons, N_2 sorption and desorption isotherms were measured. The BET model is used to calculate the specific surface areas shown in **Table 1**.

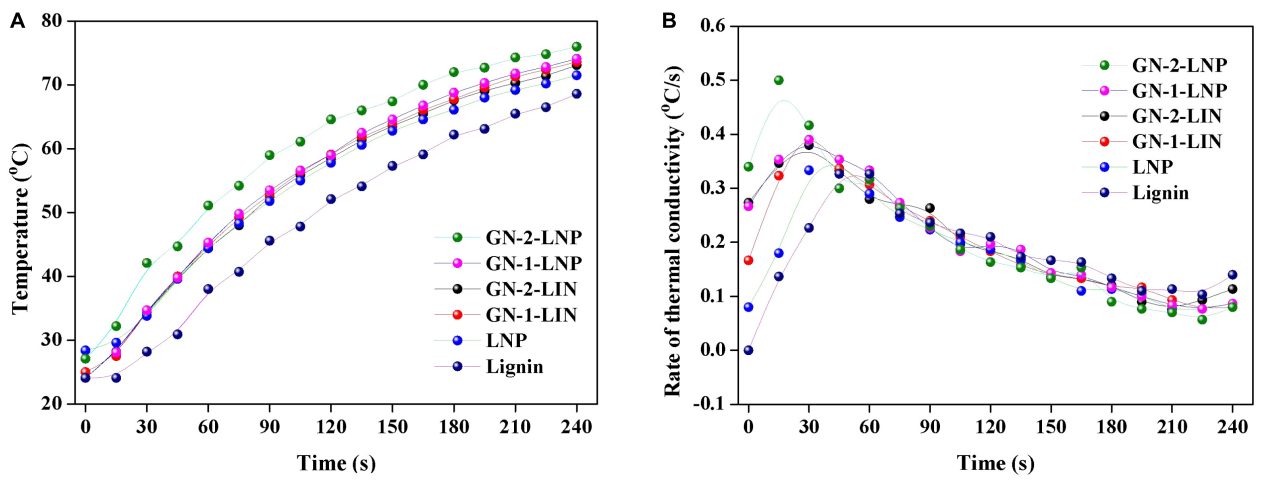

FIGURE 8 | (A) Real-time temperature and **(B)** rate of thermal conductivity curves.

Table 1 shows that the BET specific surface area and pore volume of lignin are 18.75 and 0.027 cm^3/g, respectively. These values increase to 30.35 and 0.045 cm^3/g once a sample is homogenized to form LNP. The carbons obtained via protocol 1, GN-1-LIN and GN-1-LNP, both exhibit similar BET specific surface areas (62.26 and 67.95 m^2/g, respectively) and pore volumes (0.061 and 0.063 cm^3/g, respectively). In contrast, protocol 2 (hydrothermal carbonization followed by pyrolysis) clearly produces porous carbons with larger surface areas and pore volumes. The BET specific surface area and pore volume of GN-2-LIN are 108.81 and 0.098 cm^3/g, respectively. Those of GN-2-LNP are 220.75 and 0.166 cm^3/g, respectively. These results indicate that the application of hydrothermal carbonization prior to pyrolysis produces better pore structures than pyrolysis alone. In addition, GN-2-LNP exhibits better pore structure properties than GN-2-LIN, which indicates that LNP has more potential than lignin for porous carbon production. This phenomenon may be explained by pore structure enlargement by flake- and sheet-like structures in GN-2-LNP. A similar finding was reported by Ojha et al. (2017). Although the BET specific surface area of GN-2-LNP are lower than those reported for carbons (1100 and 3775 m^2/g) in the aforementioned work (Zhang et al., 2015; Hu and Hsieh, 2017), our results are valuable because they reveal that nano-scale lignin and the combination of hydrothermal carbonization and pyrolysis show more potential for porous carbon preparation.

Analysis of the Thermal Conduction Capabilities of Prepared Graphene-Like Porous Carbons

It is well known that graphene exhibits better thermal conductivity than other thermally conductive materials (Yu et al., 2011). This has supported its use in modern electronics and other daily necessities. As the prepared carbons derived from the nano-lignin possessed the graphene like structures, it is important to also evaluate the thermal conductivity of lignin-derived carbons if they are intended to prepare the conductivity-based materials. The thermal conductivities of all samples are shown in **Table 1**. In addition, thermal images of samples taken during heating are shown in **Figure 7**. Finally, real-time temperature curves and thermal conductivity rate curves derived during heating are shown in **Figures 8A,B**, respectively.

Table 1 shows that GN-1-LIN and GN-2-LIN exhibit similar thermal conductivities (0.21 W/mK). This value is slightly improved to 0.28 W/mK in a carbon prepared from LNP using protocol 1. However, the thermal conductivity increases significantly from 0.22 W/mK to 0.45 W/mK when the carbon is prepared from LNP using protocol 2. This increase is also observed via the infrared thermal images in **Figure 7**, which show the temperature responses that occur during heating of GN-2-LIN and GN-2-LNP. The temperature of GN-2-LNP increases much more rapidly than that of GN-2-LIN, which indicates that the former material has a higher thermal conductivity. Overall, it can be concluded that the LNP treated by protocol 2 showed a higher ability to prepare the carbons with enhanced thermal conductivity.

Thermal conductivity rate curves, which are derived from the real-time temperature curves in **Figure 8A**, are shown in **Figure 8B**. GN-2-LNP exhibits the highest rate of thermal conductivity (0.51°C/s at 15 s). This is higher than those of the other three samples at double the time (0.38°C/s at 30 s). This means that GN-2-LNP has the best thermal diffusion capabilities of the prepared carbons. This superior performance might be due to its higher proportion of graphene-like structures (Yu et al., 2011). Overall, the thermal conduction ability analysis reveals that the graphene-like carbon made from nano-scale lignin has better thermal conduction capabilities than the carbon made from un-treated lignin. This is in line with our initial expectations. The higher thermal conduction rate of GN-2-LNP indicates that it has potential thermal management applications.

CONCLUSION

Lignin nano-particles with a size range of 100–300 nm were prepared from lignin using a high-pressure homogenizer with the intention of fabricating them into graphene-like carbon. LNP treated by a combination of hydrothermal carbonization and pyrolysis showed more potential for porous carbon based on its high proportion of graphene-like structures and degree of graphitization. Application of hydrothermal carbonization prior to pyrolysis made a strong contribution to the resultant carbon's higher specific surface areas and total pore volume. In addition, the LNP showed a better capacity to prepare the carbon with higher thermal conductivity (0.45 W/mK) and rate of thermal conductivity (0.51°C/s) compared to un-treated lignin.

DATA AVAILABILITY STATEMENT

The raw data supporting the conclusions of this article will be made available by the authors, without undue reservation.

AUTHOR CONTRIBUTIONS

HD carried out all the experiments and wrote the manuscript. ML and YW performed the data analysis. YJ, CH, and JY designed the work and revised the manuscript. All authors discussed the results.

FUNDING

This work was supported by the National Natural Science Foundation of China (31730106) and Natural Science Foundation of Jiangsu Province (BK20180772).

REFERENCES

Abioye, A. M., and Ani, F. N. (2015). Recent development in the production of activated carbon electrodes from agricultural waste biomass for supercapacitors: a review. *Renew. Sust. Energ. Rev.* 52, 1282–1293. doi: 10.1016/j.rser.2015.07.129

Araujo, P. T., Terrones, M., and Dresselhaus, M. S. (2012). Defects and impurities in graphene-like materials. *Mater. Today* 15, 98–109. doi: 10.1016/S1369-7021(12)70045-7

Balandin, A. A. (2011). Thermal properties of graphene and nanostructured carbon materials. *Nat. Mater.* 10, 569–581. doi: 10.1038/nmat3064

Barone, V., Hod, O., and Scuseria, G. E. (2006). Electronic structure and stability of semiconducting graphene nanoribbons. *Nano Lett.* 6, 2748–2754. doi: 10.1021/nl0617033

Chen, D., Gao, A., Ma, Z., Fei, D., Chang, Y., and Shen, C. (2018). In-depth study of rice husk torrefaction: characterization of solid liquid and gaseous products oxygen migration and energy yield. *Bioresource Technol.* 253, 148–153. doi: 10.1016/j.biortech.2018.01.009

Chen, D., Wang, Y., Liu, Y., Cen, K., Cao, X., Ma, Z., et al. (2019). Comparative study on the pyrolysis behaviors of rice straw under different washing pretreatments of water acid solution and aqueous phase bio-oil by using TG-FTIR and Py-GC/MS. *Fuel* 252, 1–9. doi: 10.1016/j.fuel.2019.04.086

Dallmeyer, I., Lin, L. T., Li, Y., Ko, F., and Kadla, J. F. (2014). Preparation and characterization of interconnected kraft lignin-based carbon fibrous materials by electrospinning. *Macromol. Mater. Eng.* 299, 540–551. doi: 10.1002/mame.201300148

Demiral, I., Aydın Şamdan, C., and Demiral, H. (2016). Production and characterization of activated carbons from pumpkin seed shell by chemical activation with ZnCl2. *Water Treat.* 57, 2446–2454. doi: 10.1080/19443994.2015.1027276

Dong, H., Zheng, L., Yu, P., Jiang, Q., Wu, Y., Huang, C., et al. (2020). Characterization and application of lignin-carbohydrate complexes from lignocellulosic materials as antioxidants for scavenging in vitro and in vivo reactive oxygen species. *ACS Sustain. Chem. Eng.* 8, 256–266. doi: 10.1021/acssuschemeng.9b05290

Donsi, F., Wang, Y., Li, J. I, and Huang, Q. (2010). Preparation of curcumin submicrometer dispersions by high-pressure homogenization. *J. Agr. Food Chem.* 58, 2848–2853. doi: 10.1021/jf903968x

Dresselhaus, M. S., Jorio, A., Hofmann, M., Dresselhaus, G., and Saito, R. (2010). Perspectives on carbon nanotubes and graphene Raman spectroscopy. *Nano Lett.* 10, 751–758. doi: 10.1021/nl904286r

Fernandes, D. M., Araújo, M. P., Haider, A., Mougharbel, A. S., Fernandes, A. J., Kortz, U., et al. (2018). Polyoxometalate-graphene electrocatalysts for the hydrogen evolution reaction. *ChemElectroChem* 5, 273–283. doi: 10.1002/celc.201701210

Foong, L. K., Khojasteh, H., Amiri, M., Heydaryan, K., Salavati-Niasari, M., Almasi-Kashi, M., et al. (2020). Environmental friendly approach for facile synthesis of graphene-like nanosheets for photocatalytic activity. *J. Alloy Compd.* 823:153696. doi: 10.1016/j.jallcom.2020.153696

Han, H., Chao, S., Yang, X., Wang, X., Wang, K., Bai, Z., et al. (2017). Ni nanoparticles embedded in N doped carbon nanotubes derived from a metal organic framework with improved performance for oxygen evolution reaction. *Int. J. Hydrogen Energ.* 42, 16149–16156. doi: 10.1016/j.ijhydene.2017.05.043

Han, H., Lou, Z., Wang, P., Wang, Q., Li, R., Zhang, Y., et al. (2020). Synthesis of Ultralight and Porous Magnetic g-C3N4/g-Carbon Foams with Excellent Electromagnetic Wave (EMW) Absorption Performance and Their Application as a Reinforcing Agent for 3D Printing EMW Absorbers. *Ind. Eng. Chem. Res.* 59, 7633–7645. doi: 10.1021/acs.iecr.0c00665

Hoekstra, J., Beale, A. M., Soulimani, F., Versluijs-Helder, M., Van De Kleut, D., Koelewijn, J. M., et al. (2016). The effect of iron catalyzed graphitization on the textural properties of carbonized cellulose: magnetically separable graphitic carbon bodies for catalysis and remediation. *Carbon* 107, 248–260. doi: 10.1016/j.carbon.2016.05.065

Hou, J., Shao, Y., Ellis, M. W., Moore, R. B., and Yi, B. (2011). Graphene-based electrochemical energy conversion and storage: fuel cells supercapacitors and lithium ion batteries. *Phys. Chem. Chem. Phys.* 13, 15384–15402. doi: 10.1039/C1CP21915D

Hu, S., and Hsieh, Y. L. (2017). Lignin derived activated carbon particulates as an electric supercapacitor: carbonization and activation on porous structures and microstructures. *RSC Adv.* 7, 30459–30468. doi: 10.1039/C7RA00103G

Huang, C., Lin, W., Lai, C., Li, X., Jin, Y., and Yong, Q. (2019a). Coupling the post-extraction process to remove residual lignin and alter the recalcitrant structures for improving the enzymatic digestibility of acid-pretreated bamboo residues. *Bioresource Technol.* 285:121355. doi: 10.1016/j.biortech.2019.121355

Huang, C., Wang, X., Liang, C., Jiang, X., Yang, G., Xu, J., et al. (2019b). A sustainable process for procuring biologically active fractions of high-purity xylooligosaccharides and water-soluble lignin from Moso bamboo prehydrolyzate. *Biotechnol. Biofuels* 12:189. doi: 10.1186/s13068-019-1527-3

Huang, X., Yin, Z., Wu, S., Qi, X., He, Q., Zhang, Q., et al. (2011). Graphene-based materials: synthesis characterization properties and applications. *Small* 7, 1876–1902. doi: 10.1002/smll.201002009

Hwang, H., Kim, H., and Cho, J. (2011). MoS2 nanoplates consisting of disordered graphene-like layers for high rate lithium battery anode materials. *Nano Lett.* 11, 4826–4830. doi: 10.1021/nl202675f

Ji, H., Sellan, D. P., Pettes, M. T., Kong, X., Ji, J., Shi, L., et al. (2014). Enhanced thermal conductivity of phase change materials with ultrathin-graphite foams for thermal energy storage. *Energ. Environ. Sci.* 7, 1185–1192. doi: 10.1039/C3EE42573H

Kang, M. H., Qiu, G., Chen, B., Jouvray, A., Teo, K. B., Cepek, C., et al. (2017). Transport in polymer-supported chemically-doped CVD graphene. *J. Mater. Chem. C* 5, 9886–9897. doi: 10.1039/C7TC02263H

Kılıç, M., Apaydın-Varol, E., and Pütün, A. E. (2015). Preparation and surface characterization of activated carbons from Euphorbia rigida by chemical activation with ZnCl2 K2CO3 NaOH and H3PO4. *Appl. Surf. Sci.* 261, 247–254. doi: 10.1016/j.apsusc.2012.07.155

Lee, C., Wei, X., Kysar, J. W., and Hone, J. (2008). Measurement of the elastic properties and intrinsic strength of monolayer graphene. *Science* 321, 385–388. doi: 10.1126/science.1157996

Li, J., Wei, X., Wang, Q., Chen, J., Chang, G., Kong, L., et al. (2012). Homogeneous isolation of nanocellulose from sugarcane bagasse by high pressure homogenization. *Carbohyd. Polym.* 90, 1609–1613. doi: 10.1016/j.carbpol.2012.07.038

Li, Y., and Ragauskas, A. J. (2012). Kraft lignin-based rigid polyurethane foam. *J. Wood Chem. Technol.* 32, 210–224. doi: 10.1080/02773813.2011.652795

Lin, W., Xing, S., Jin, Y., Lu, X., Huang, C., and Yong, Q. (2020). Insight into understanding the performance of deep eutectic solvent pretreatment on improving enzymatic digestibility of bamboo residues. *Bioresource Technol.* 306:123163. doi: 10.1016/j.biortech.2020.123163

Liu, F., Chen, Y., and Gao, J. (2017). Preparation and characterization of biobased graphene from Kraft lignin. *Bioresources* 12, 6545–6557.

Lu, Y., Liu, Z., You, S. W., McLoughlin, L., Bridgers, B., Hayes, S., et al. (2020). Electrospun carbon/iron nanofibers: the catalytic effects of iron and application in Cr (VI) removal. *Carbon* 166, 227–244. doi: 10.1016/j.carbon.2020.05.031

Lv, B., Zheng, C., Xu, L., Zhou, X., Cao, H., and Liu, Z. (2015). Porous graphene-like materials prepared from hollow carbonaceous microspheres for supercapacitors. *ChemNanoMat* 1, 422–429. doi: 10.1002/cnma.201500081

Ma, M., Dai, L., Si, C., Hui, L., Liu, Z., and Ni, Y. (2019). Facile preparation of super long-term stable lignin nanoparticles from black liquor. *ChemSusChem* 12, 5239–5245. doi: 10.1002/cssc.201902287

Mendes, L. F., de Siervo, A., de Araujo, W. R., and Paixão, T. R. L. C. (2020). Reagentless fabrication of a porous graphene-like electrochemical device from phenolic paper using laser-scribing. *Carbon* 159, 110–118. doi: 10.1016/j.carbon.2019.12.016

Morgan, A. B., and Gilman, J. W. (2003). Characterization of polymer-layered silicate (clay) nanocomposites by transmission electron microscopy and X-ray diffraction: a comparative study. *J. Appl. Polym. Sci.* 87, 1329–1338. doi: 10.1002/app.11884

Ojha, K., Kumar, B., and Ganguli, A. K. (2017). Biomass derived graphene-like activated and non-activated porous carbon for advanced supercapacitors. *J. Chem. Sci.* 129, 397–404. doi: 10.1007/s12039-017-1248-8

Pang, B., Cao, X. F., Sun, S. N., Wang, X. L., Wen, J. L., Lam, S. S., et al. (2020a). The direct transformation of bioethanol fermentation residues for production of high-quality resins. *Green Chem.* 22, 439–447. doi: 10.1002/cssc.202000299

Pang, B., Lam, S. S., Shen, X. J., Cao, X. F., Liu, S. J., Yuan, T. Q., et al. (2020b). Valorization of technical lignin for production of desirable resins with high substitution rate and controllable viscosity. *ChemSusChem* 13, 1–10.

Pei, W., Shang, W., Liang, C. Jiang, X, Huang, C., and Yong, Q. (2020). Using lignin as the precursor to synthesize Fe_3O_4@lignin composite for preparing electromagnetic wave absorbing lignin-phenol-formaldehyde adhesive. *Ind. Crop. Prod.* 154:112638. doi: 10.1016/j.indcrop.2020.112638

Salehin, S., Aburizaiza, A. S., and Barakat, M. A. (2015). Recycling of residual oil fly ash: synthesis and characterization of activated carbon by physical activation methods for heavy metals adsorption. *Int. J. Environ. Res.* 9, 1201–1210. doi: 10.22059/IJER.2015.1010

Shuai, L., Amiri, M. T., Questell-Santiago, Y. M., Héroguel, F., Li, Y., Kim, H., et al. (2016). Formaldehyde stabilization facilitates lignin monomer production during biomass depolymerization. *Science* 354, 329–333. doi: 10.1126/science.aaf7810

Sipponen, M. H., Lange, H., Crestini, C., Henn, A., and Österberg, M. (2019). Lignin for nano- and microscaled carrier systems: applications trends and challenges. *ChemSusChem* 12, 2039–2054. doi: 10.1002/cssc.201900480

Song, C., Wu, D., Zhang, F., Liu, P., Lu, Q., and Feng, X. (2012). Gemini surfactant assisted synthesis of two-dimensional metal nanoparticles/graphene composites. *Chem. Commun.* 48, 2119–2121. doi: 10.1039/C2CC16890A

Spitalsky, Z., Danko, M., and Mosnacek, J. (2011). Preparation of functionalized graphene sheets. *Curr. Org. Chem.* 15, 1133–1150. doi: 10.2174/138527211795202988

Sun, S., Zhang, M., Umemura, K., and Zhao, Z. (2019). Investigation and characterization of synthesis conditions on sucrose-ammonium dihydrogen phosphate (SADP) adhesive: bond performance and chemical transformation. *Materials* 12:4078. doi: 10.3390/ma12244078

Tang, L. C., Wan, Y. J., Yan, D., Pei, Y. B., Zhao, L., Li, Y. B., et al. (2013). The effect of graphene dispersion on the mechanical properties of graphene/epoxy composites. *Carbon* 60, 16–27. doi: 10.1016/j.carbon.2013.03.050

Vinodhkumar, G., Ramya, R., Vimalan, M., Potheher, I., and Cyrac Peter, A. (2018). Reduced graphene oxide based on simultaneous detection of neurotransmitters. *Prog. Chem. Biochem. Res.* 1, 40–49.

Vinu, A. (2008). Two-dimensional hexagonally-ordered mesoporous carbon nitrides with tunable pore diameter surface area and nitrogen content. *Adv. Funct. Mater.* 18, 816–827. doi: 10.1002/adfm.200700783

Vlassiouk, I., Fulvio, P., Meyer, H., Lavrik, N., Dai, S., Datskos, P., et al. (2013). Large scale atmospheric pressure chemical vapor deposition of graphene. *Carbon* 54, 58–67. doi: 10.1016/j.carbon.2012.11.003

Wang, S., Li, H., Xiao, L. P., and Song, G. (2020). Unraveling the structural transformation of wood lignin during deep eutectic solvent treatment. *Front. Energy Res.* 8:48. doi: 10.3389/fenrg.2020.00048

Wu, Y., Wu, X., Yang, F., Xu, L., and Sun, M. (2019). Study on the preparation and adsorption property of polyvinyl alcohol/cellulose nanocrystal/graphene composite aerogels (PCGAs). *J. Renew. Mater.* 7, 1181–1195. doi: 10.32604/jrm.2019.07493

Xu, M., Fujita, D., Sagisaka, K., Watanabe, E., and Hanagata, N. (2011). Production of extended single-layer graphene. *ACS Nano* 5, 1522–1528. doi: 10.1021/nn103428k

Yan, Q., Zhang, X., Li, J., Wang, C., Zhang, J., and Cai, Z. (2018). Catalytic conversion of Kraft lignin to bio-multilayer graphene materials under different atmospheres. *J. Mater. Sci.* 53, 8020–8029. doi: 10.1007/s10853-018-2172-0

Yang, J. W., Yu, Z. Y., Cheng, S. J., Chung, J. H., Liu, X., Wu, C. Y., et al. (2020). Graphene oxide-based nanomaterials: an insight into retinal prosthesis. *Int. J. Mol. Sci.* 21:2957. doi: 10.3390/ijms21082957

Yoo, C. G., Meng, X., Pu, Y., and Ragauskas, A. J. (2020). The critical role of lignin in lignocellulosic biomass conversion and recent pretreatment strategies: a comprehensive review. *Bioresource Technol.* 2020:122784. doi: 10.1016/j.biortech.2020.122784

Yu, A., Ramesh, P., Itkis, M. E., Bekyarova, E., and Haddon, R. C. (2007). Graphite nanoplatelet-epoxy composite thermal interface materials. *J. Phys. Chem. C* 111, 7565–7569. doi: 10.1021/jp071761s

Yu, W., Xie, H., Wang, X., and Wang, X. (2011). Significant thermal conductivity enhancement for nanofluids containing graphene nanosheets. *Phys. Lett. A* 375, 1323–1328. doi: 10.1016/j.physleta.2011.01.040

Zhang, W., Zhao, M., Liu, R., Wang, X., and Lin, H. (2015). Hierarchical porous carbon derived from lignin for high performance supercapacitor. *Colloid Surface A* 484, 518–527. doi: 10.1016/j.colsurfa.2015.08.030

Zheng, C., Yue, Y., Gan, L., Xu, X., Mei, C., and Han, J. (2019). Highly stretchable and self-healing strain sensors based on nanocellulose-supported graphene dispersed in electro-conductive hydrogels. *Nanomaterials* 9:937. doi: 10.3390/nano9070937

Zhu, L., Shen, F., Smith, R. L. Jr., Yan, L., Li, L., and Qi, X. (2017). Black liquor-derived porous carbons from rice straw for high-performance supercapacitors. *Chem. Eng. J.* 316, 770–777. doi: 10.1016/j.cej.2017.02.034

Conflict of Interest: The authors declare that the research was conducted in the absence of any commercial or financial relationships that could be construed as a potential conflict of interest.

frontiers in Energy Research

ORIGINAL RESEARCH
published: 18 September 2020
doi: 10.3389/fenrg.2020.00181

Understanding the Structural Changes of Lignin Macromolecules From Balsa Wood at Different Growth Stages

*Chen Zhang[1], Ling-Hua Xu[1], Cheng-Ye Ma[1], Han-Min Wang[1], Yuan-Yuan Zhao[2], Yu-Ying Wu[1] and Jia-Long Wen[1,2]**

[1] Beijing Key Laboratory of Lignocellulosic Chemistry, Beijing Forestry University, Beijing, China, [2] Beijing Advanced Innovation Center for Tree Breeding by Molecular Design, Beijing Forestry University, Beijing, China

Lignin is the most abundant aromatic biomacromolecule on the earth, which is an attractive raw material for producing bio-based chemicals, materials, and fuels. However, the complexity, heterogeneity, and variability of the lignin structure always hinders the value-added application of different sources of raw materials. In this study, double enzymatic lignin (DEL) was isolated from balsa grown for different lengths of time to understand the structural variations of lignin macromolecules during the growth of balsa for the first time. Confocal Raman microscopy and component analysis were used to monitor the lignin accumulation in balsa. Meanwhile, the structural characteristics and chemical reactivity of DELs were synthetically characterized by advanced 2D-HSQC and ^{31}P-NMR techniques. It was found that the balsa lignin is a typical hardwood lignin and it is overwhelmingly composed of C–O bonds (i.e., β-*O*-4 linkages), whose content is elevated with increasing tree-age. Interestingly, carbon–carbon linkages (e.g., β-β and β-5) in these DELs isolated from 3-and 5-year-old balsa are gradually disappearing. Considering the increasing molecular weight of DELs with tree-age, it was concluded that lignin macromolecules in balsa wood were gradually polymerized within the growth period. Furthermore, abundant C–O linkages with less C–C linkages in the DELs from 3 and 5-year-old balsa wood suggested that these feedstocks are promising in current lignin-first biorefinery and will facilitate the conversion of aromatic chemicals from the lignin macromolecule. In short, a comprehensive understanding of native lignin during the growth of balsa wood will not only advance the understanding of biosynthetic pathways of lignin biopolymer, but also facilitate the deconstruction and value-added applications of this kind of feedstock.

Keywords: balsa wood, lignin macromolecules, structural characterization, native lignin, 2D-HSQC NMR

OPEN ACCESS

Edited by:
Li Shuai,
Fujian Agriculture and Forestry University, China

Reviewed by:
Yanding Li,
Massachusetts Institute of Technology, United States
Somnath D. Shinde,
Sandia National Laboratories (SNL), United States

***Correspondence:**
Jia-Long Wen
wenjialonghello@126.com;
wenjialong@bjfu.edu.cn

Specialty section:
This article was submitted to Bioenergy and Biofuels, a section of the journal Frontiers in Energy Research

Received: *10 May 2020*
Accepted: *09 July 2020*
Published: *18 September 2020*

Citation:
Zhang C, Xu L-H, Ma C-Y, Wang H-M, Zhao Y-Y, Wu Y-Y and Wen J-L (2020) Understanding the Structural Changes of Lignin Macromolecules From Balsa Wood at Different Growth Stages. Front. Energy Res. 8:181. doi: 10.3389/fenrg.2020.00181

INTRODUCTION

Lignin is the most abundant natural biopolymer in the plant cell wall of the lignocellulosic biomass. Structurally, it is a heterogeneous and aromatic macromolecule polymer, which is mainly comprised of three kinds of component units, syringyl (S) units, guaiacyl (G) units, and *p*-hydroxyphenyl (H) units by biosynthesizing under the regulation of different kinds of enzymes

(Ralph et al., 2004; Rinaldi et al., 2016; Baruah et al., 2018). These units are linked by ether (e.g., β-*O*-4) and carbon–carbon (β-5, β-β, etc.) bonds via free radical coupling reactions (Ralph and Landucci, 2010). Besides these lignin substructures, lignin and hemicelluloses are also linked by ether and ester bonds, forming the common lignin-carbohydrate complexes (LCC), such as phenyl glycoside, benzyl ether, and γ-ester (Balakshin et al., 2011; Yuan et al., 2011; Huang et al., 2018). However, the native structure of lignin varies with tree species (Wang et al., 2017), growth stages (Wang et al., 2020), different cell wall tissues (Wen et al., 2013a), leading to challenges in the utilization of lignocellulosic feedstocks. Therefore, detailed investigation of microscopic distribution of lignin in cell wall and molecular structures of lignin in the lignocellulosic biomass will facilitate deconstruction and value-added applications of the plant cell walls in the current biorefinery (Ragauskas and Yoo, 2018).

Balsa wood (*Ochroma pyramidale*) grows in tropical forests of the Americas, and is the lightest and fastest-growing tree in the world (O'Dowd, 1979). The diameter of the balsa wood trunk changes quite dramatically as it grows (**Supplementary Figure S1**). Balsa wood was introduced into southern China in the 1950s and 1960s (Shu, 1998), and it has also been planted on a large scale in Fujian, Yunnan, Guangdong, and southern districts in China. Balsa wood is currently used in the production of aero models, adsorption materials, and heat insulation materials (Fu et al., 2017; Guan et al., 2018). Lignin plays an important role in plant growth. Due to its fast growth rate and high wood yield during the balsa growing process, understanding the lignin accumulation and structural variations of lignin macromolecules in the balsa plant cell wall is of great importance. From the perspective of the utilization of lignocellulose, the presence of lignin in the plant cell wall is deemed to be a major biomass recalcitrance (Yuan et al., 2013; Huang et al., 2019). Thus, lignin is generally removed in the preliminary steps of biorefinery (Ding et al., 2012; Zeng et al., 2014). Moreover, during the different processing methods for balsa wood, a lot of processing leftovers were produced. Therefore, understanding the chemical composition and structural features of native lignin in balsa wood will facilitate the deconstruction of the compact cell wall and value-added applications of the fractionated components (lignin, hemicelluloses, and cellulose) in the current biorefinery.

Based on the above considerations, it is necessary to illustrate the structural features of native lignin. The basic knowledge available for isolation methods (MWL, CEL, EMAL, and their improved form) of native lignin were reported by some pioneers (Björkman, 1954; Chang et al., 1975; Wu and Argyropoulos, 2003; Zhang et al., 2010). Recently, a native lignin named double enzymatic lignin (DEL) was developed for isolating native lignin from different biomasses due to the ideal yields and unaltered structures (Chen et al., 2017; Wang et al., 2017, 2020). In the present study, balsa wood with different growth years (1, 3, and 5 years) were used to reveal structural changes of lignin macromolecules. Herein, DEL samples were isolated from the different growth stages of wood for the first time, NMR and GPC techniques were performed to investigate the structural changes of lignin during the different growth stages. Furthermore, Raman microscopy was performed to investigate the lignin distribution in the cell walls of balsa wood.

MATERIALS AND METHODS

Materials

The balsa wood was prepared from 1-, 3-, and 5-year-old trees, harvested from one Forestry Center in Fujian Province, China. The raw materials were harvested in summer and then underwent air-drying. The air-dried wood was smashed into powder (20–60 mesh), dried in an oven at 60°C for 24 h, then extracted in a Soxhlet extractor for 6 h with ethanol/benzene (1:2, v/v). The chemical compositions of the different balsa woods were analyzed according to the method from the National Renewable Energy Laboratory (NREL; Sluiter et al., 2008). To isolate the native lignin DEL, the pre-extracted balsa woods were air-dried and then milled in the planetary ball mill (450 rpm, 5 h) to obtain the ball-milled powder (Wang et al., 2020). The chemicals were purchased from Sigma-Aldrich (Shanghai), and the commercial cellulase (Cellic CTec2, 100 FPU/mL) was provided by Novozymes (Beijing, China).

Preparation of DELs From Different Growth Stages of Balsa Wood

The isolation of DEL was performed according to our previous publications (Chen et al., 2017; Wang et al., 2020). In detail, ball-milled balsa wood (1, 3, and 5 years) powders were subjected to enzymatic hydrolysis in the acetate buffer (0.05 mol/L, 200 mL, pH 4.8), then cellulase (50 FPU/g) was added. The reaction mixtures were incubated in a rotary shaker (50°C, 150 rpm) for 48 h. The enzymatic residues were washed repeatedly with hot water to remove the hydrolyzed carbohydrates, centrifuged, and freeze-dried. The obtained solids underwent ball-milling for 2 h and then underwent the same enzymatic hydrolysis. After the purification and freeze-drying process, the DEL samples were achieved, labeled as DEL-1, DEL-3, and DEL-5.

Characterizations of Lignin

The characterizations of the lignin were described in detail in the **Supplementary Material** section.

RESULTS AND DISCUSSION

Chemical Composition of Balsa Wood During Different Growth Stages

Biomass characterization of balsa wood is crucial to understand the component changes of balsa wood during growth stages. The characterization of lignin not only enhance the understanding of structural changes during the growth process of balsa wood, but also facilitate the subsequent dissociation, utilization, and conversion of balsa components into chemicals, energy, and biomaterials in the current biorefinery scenario. The chemical compositions of balsa wood with different growth stages (1, 3, and 5 year) are displayed in **Table 1**. As shown, the content of cellulose

TABLE 1 | Chemical composition of different growth years of balsa wood (w/w, %).

Materials	Cellulose	Hemicelluloses[a]	KL[b]	ASL[c]	TL[d]	Total
1	45.04 ± 0.9	16.93 ± 0.3	18.03 ± 0.5	4.04 ± 0.1	22.07	84.04
3	44.57 ± 1.2	17.15 ± 0.2	19.67 ± 0.4	5.25 ± 0.1	24.92	86.64
5	42.03 ± 1.0	18.02 ± 0.2	18.60 ± 0.5	5.45 ± 0.1	24.05	84.10

[a]*Hemicelluloses are composed of xylose, mannose and uronic acid.* [b]*Klason lignin.* [c]*Acid soluble lignin.* [d]*Total lignin.*

in balsa wood decreased from 45.0 to 42.0% as the growth years increased. This is in disagreement with other hardwood species, such as poplar wood, at early growth stages (3–18 months) (Wang et al., 2020). However, the relatively high contents of cellulose in balsa woods at different growth stages suggested that balsa woods are more likely to release more cellulose for cellulose-based materials and fermentable glucose production. By contrast, the content of hemicelluloses in balsa wood was slightly elevated with increased tree-age. Correspondingly, the lignin content was first increased from 22.1% for 1-year-old to 25.0% for 3-year-old balsa wood, then the lignin content in 5-year-old balsa wood was slightly decreased to 24.1%. This revealed that the accumulation of lignin increased with the growth of balsa wood and eventually stabilized in the mature period. In short, investigating the chemical composition of balsa wood and the detailed structural features of lignin macromolecules from balsa wood will facilitate the subsequent fractionation and conversion of the main components.

Confocal Raman Microscopy Characterization of Lignin and Carbohydrate Distribution

Confocal Raman Microscopy (CRM) is a useful tool that can provide an intuitionistic observation of lignin and carbohydrates in cell walls with a high resolution (Chen et al., 2017). The spatial dynamic distribution of lignin and carbohydrates in the cell walls from different growth stages of balsa woods can be monitored by CRM. Different concentrations of lignin in corner middle lamella (CCML), compound middle lamella (CML), and secondary (S) can be reflected by different intensities in CRM (Agarwal, 2006; Li et al., 2015). Raman images of lignin and carbohydrate distribution in the plant cell wall from balsa wood (different tree-age) are shown in **Figure 1**. Obviously, it was found that distributing concentrations of lignin and carbohydrates in different regions were quite different. The richest lignin was observed in CCML, followed by CML, and the lowest concentration of lignin was found in SW. This distribution patterns are verified in the different growth stages of balsa wood. In addition, it was observed that the relative concentration of lignin in the CCML, CML, and SW regions become higher from 1 to 3 years and slightly reduced in 5-year-old balsa wood, which was in line with the content of lignin in different growth stages of balsa wood (**Table 1**). In fact, the increased concentration of lignin in the CCML and CML regions of cell walls implied that lignin macromolecules can serve as a natural adhesive to further support plant cell walls during balsa growth. Contrary to the distribution of lignin in the cell wall, carbohydrate distribution was abundant in the SW layer, while carbohydrate concentration was lowest in CCML regions. Furthermore, it was observed from CRM images that the cell wall thickness obviously increases with the growth stages of balsa wood.

Yields and Associated Carbohydrates of Lignin Fractions

Prior to structural characterization of native lignin in plant cell walls, it is hoped that the yield of isolated native lignin would be high enough so that the characterization of lignin could truly reveal the lignin composition and structural features in the cell wall. In the current study, the structural variations of lignin from different growth years of balsa wood can be achieved via isolation and characterization of DEL. From **Table 2**, it was found that the crude yields of the three DEL samples are more than 100% (from 102.6 to 105.4%). It should be noted that the content of associated carbohydrates in these DELs is from 5.84 to 8.02% (based on the total weight of lignin). Among the associated carbohydrates, xylose and glucose are the dominant sugars. The phenomenon is easy to explain because DEL is a residual lignin after removing xylans and cellulose by the enzymatic hydrolysis process. However, as the main components in a plant cell wall, hemicelluloses (xylans) and cellulose could not be totally removed. Meanwhile, a small amount of galactose also contributed to the total associated carbohydrates in these DEL samples. After eliminating the effect of carbohydrates on yield, the yield of lignin without carbohydrates is from 96.7 to 98.0%. In short, DEL with a high yield is a better representation of the entire lignin in the plant cell walls and can reveal the structural changes of native lignin from balsa wood with different tree-age.

Molecular Weights Analysis of DELs

In order to improve the solubility of DEL in tetrahydrofuran for GPC determination, acetylation of DEL was performed as previously reported (Wang et al., 2017). The molecular weights (M_w and M_n) and polydispersity index (PDI, M_w/M_n) of acetylated DEL samples are shown in **Table 3**, which were calculated from the GPC curves (relative values related to polystyrene). GPC results showed that *Mw* of DEL gradually elevated from 8460 g/mol (1-year-old balsa) to 8800 g/mol (3-year-old balsa) and then further climbed to 10,050 g/mol (5-year-old balsa). These results suggested that polymerization degrees of lignin macromolecules increase gradually as balsa wood grows. The increased trend has also been observed in our recent study (Wang et al., 2020). Meanwhile, the PDI (about 1.5) is less than those (1.8–2.0) of DELs from poplar wood (Wang et al., 2020). This implied that the lignin macromolecules from balsa are more homogeneous, which is beneficial to the utilization of this kind of lignin. In fact, the homogeneous lignin is mostly related to

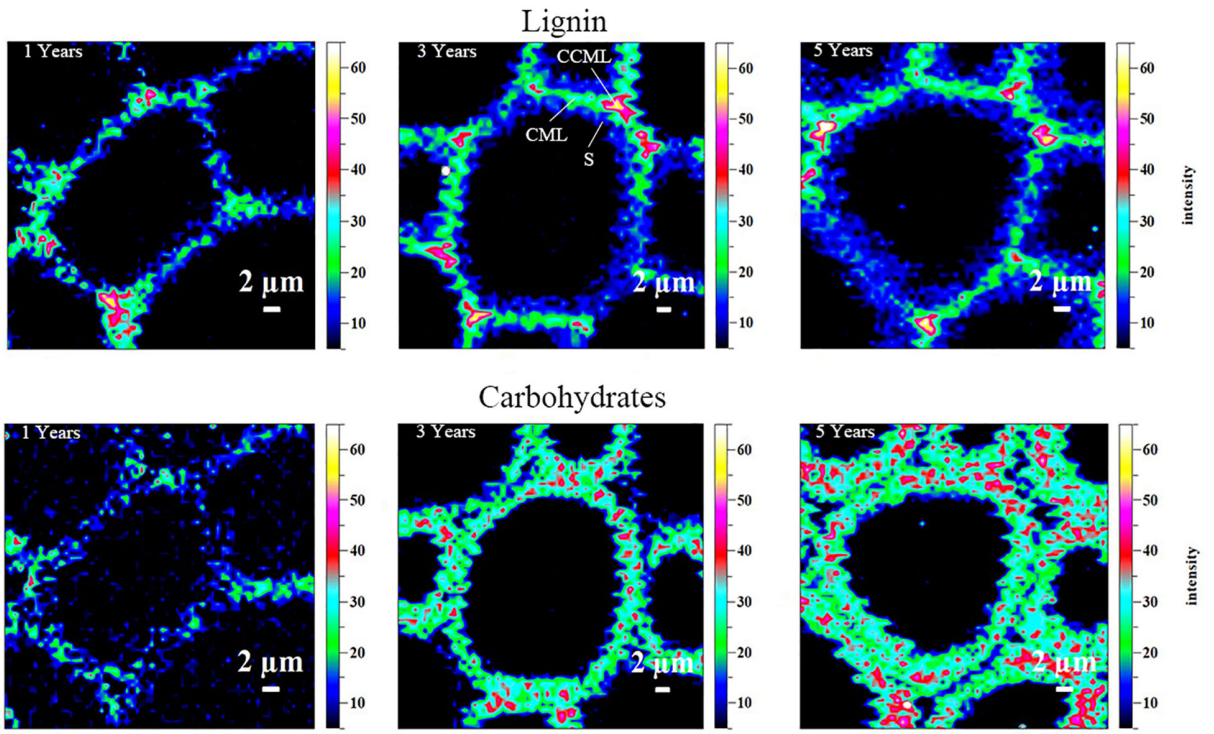

FIGURE 1 | Raman images of the lignin (by integrating from 1547 to 1707 cm^{-1}) and carbohydrates (by integrating the band at 2889 cm^{-1}) distributions in the different growth years of balsa wood cell walls.

TABLE 2 | Yields and carbohydrate content of lignin fractions.

Samples	Yield (%)[a]	Total carbohydrates (%)	Yield (%)[b]	Carbohydrates content (%)		
				Gal[c]	Glu[c]	Xly[c]
DEL-1	103.7	5.84	98.0	0.56	2.84	2.44
DEL-3	102.6	6.10	96.7	0.52	3.22	2.36
DEL-5	105.4	8.02	97.6	0.60	3.67	3.75

[a]The yield of lignin was calculated based on the Klason lignin of different balsa wood (with carbohydrates). [b]The yield of lignin was calculated based on the Klason lignin of different balsa wood (without carbohydrates). [c]Gal, galactose; Glu, glucose; Xyl, xylose.

TABLE 3 | Weight-average molecular weights (M_w) and number-average molecular weights (M_n), and polydispersity (M_w/M_n) of the lignin fractions.

Samples	M_w	M_n	M_w/M_n
DEL-1	8460 ± 40	5740 ± 60	1.47
DEL-3	8800 ± 60	5790 ± 70	1.52
DEL-5	10050 ± 90	6710 ± 50	1.50

the inherent structure of lignin, which will be verified in the subsequent NMR section.

2D-HSQC Spectra of DELs

To obtain the chemical composition and detailed structural characteristics of native lignin from balsa wood, the DEL samples were characterized by the 2D-HSQC NMR and the spectra were analyzed according to previous publications regarding the 2D-HSQC characterizations of different lignin sources (Kim and Ralph, 2010; del Río et al., 2012; Wen et al., 2013b). In addition, the recent advances in characterization of lignin polymer by solution-state NMR (especially 2D-HSQC spectra) have been reviewed in detail in our previous publication (Wen et al., 2013b). The side-chain and aromatic regions in 2D-HSQC NMR spectra of the DELs as well as the main identified substructures are depicted in **Figure 2**. It was found that the 2D-HSQC NMR spectra of lignin from balsa wood are analogical to those from other hardwood species, such as eucalyptus wood (Wang et al., 2017). However, the DELs from different growth stages of balsa wood presented impressive spectral characteristics. Based on these NMR spectra, it was found that the native lignin samples from balsa wood under different tree-ages exhibited gradually changing structural features, which is also the important basis for subsequent utilizations of balsa wood.

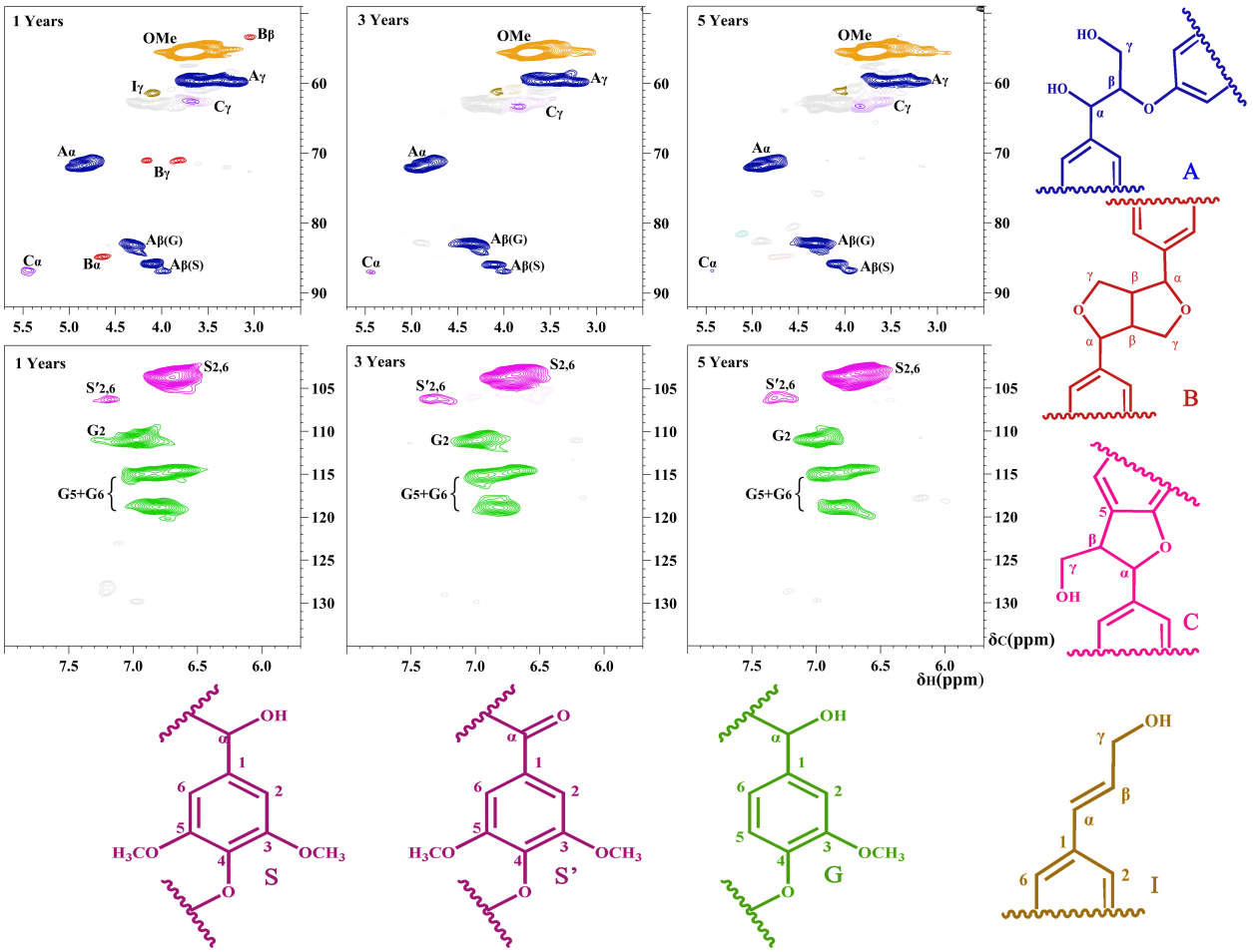

FIGURE 2 | Side-chain and aromatic regions in the 2D-HSQC NMR spectra of the DELs isolated from balsa wood.

In general, the side-chain regions in the 2D-HSQC spectra provided useful information on the substructures in the lignin macromolecules. In this study, it was found that the structural characteristics of different DEL samples exhibited distinct spectra, suggesting that native lignin in different growth years of balsa wood are fundamentally different. These different lignin structures also laid a foundation for the oriented pretreatment and processing of balsa wood. Regarding to the spectral assignments, it should be noted that all the spectra presented the prominent signal corresponding to β-*O*-4 aryl ethers (A). However, the carbon–carbon (C–C) substructures (e.g., β-β and β-5), which are very common in most wood species, only partly appeared in native lignin from the 1-year-old balsa wood. By contrast, the DEL samples from 3-year and 5-year-old balsa wood are predominantly composed of β-*O*-4 aryl ethers (A), only a minor amount of β-5 linkages and *p*-hydroxycinnamyl alcohol end group (I) substructures were detected in these DEL samples. In fact, the native lignin with abundant C-O bonds (β-*O*-4 linkages) and less carbon–carbon (C–C) bonds (β-β, β-5, and β-1) is a promising feedstock for the current biorefinery process. As we known, some transgenic poplar wood (up-regulation of F5H in poplar wood) also achieves this purpose and obtains the native lignin with high C–O and less C–C bonds (Rinaldi et al., 2016; Shuai et al., 2016), however, the transgenic technology is high-cost and there is still instability in the cultivation of forest resources at present. Thus, the utilization cost of large amounts of naturally occurring biomass resources would be significantly reduced and availability would be much higher. Additionally, protective lignin extraction strategies were successfully proposed to protect the C–O linkages and simultaneously suppress the formation of C–C linkages, which is beneficial to subsequent production of lignin monomers with high-yield via catalytic hydrogenolysis (Luterbacher et al., 2015; Shuai et al., 2016; Lan et al., 2018). Therefore, it can be concluded that 3- and 5-year-old balsa wood has great potential for the subsequent lignin-first biorefinery scenario.

In the aromatic region, syringyl (S) and guaiacyl (G) were clearly presented. In more detail, the S units showed a visible signal for the $S_{2,6}$ correlations, and the minor signal for the Cα-oxidized S-units (S') also appeared. Besides, there are three distinct cross-signals of G units: C2–H2, C5–H5, and C6–H6. For the aromatic region of the spectra, there seems to be no obvious

TABLE 4 | Quantification of lignin fractions by quantitative 2D-HSQC NMR method.

Samples	β-*O*-4	β-β	β-5	S/G[a]
DEL-1	66.33[b] (84.92%)[c]	5.31 (6.80%)	6.47(8.28%)	1.25
DEL-3	66.76(98.19%)	Tr[d]	1.23(1.81%)	2.49
DEL-5	68.81(99.29%)	Tr	0.49(0.71%)	2.95

[a]S/G ratio obtained by this equation: S/G ratio = 0.5I($S_{2,6}$)/I (G_2). [b]Results expressed per 100 Ar based on quantitative 2D-HSQC spectra. [c]Relative abundance of linkages (% of total side chains involved). [d]Tr, trace.

difference between these DEL samples. However, quantification of characteristic correlated signals in different DELs can provide detailed information regarding the chemical composition and relative content of different linkages (Wen et al., 2013b). As we all known, understanding the S/G ratio of DEL will not only help to reveal the rule of lignin accumulation and deposition in plant cell walls, but will also facilitate the subsequent delignification and deconstruction of this kind of feedstock (Rinaldi et al., 2016; Akinosho et al., 2017).

In the present study, it was observed that the S/G ratio of DEL from different growth stages (1, 3, and 5-year-old) of balsa wood is 1.25, 2.49, and 2.95, respectively. These continuously increasing S/G ratios suggested that S-type lignin is naturally synthesized in the late stage of the plant cell wall formation of balsa wood. In addition, the existence of S units preferentially promoted the formation of β-*O*-4 linkage in a hardwood biomass (Ralph and Landucci, 2010). This prediction was also demonstrated in the present study since the abundance of β-*O*-4 linkages is positively related to the S/G ratios of these lignin macromolecules (**Table 4**). For example, the abundance of β-*O*-4 linkages based on 100Ar in DEL-1, DEL-3, and DEL-5 was 66.33, 66.76, and 68.81/100Ar, respectively. Meanwhile, relative abundance of linkages based on total side chains also exhibited a similar trend, the relative abundance of β-*O*-4 linkages in DEL-1, DEL-3, and DEL-5 was 84.92, 98.19, and 99.29%, respectively. Additionally, the gradually decreasing β-5 linkage is also related to the increased S/G ratio because β-5 linkage is mainly synthesized by the G units during the biosynthesis of the lignin macromolecule (Ralph and Landucci, 2010). Similarly, researchers have developed a toolkit for simulating lignin biosynthesis *in silico* and they found that increasing S-content drastically increases β-*O*-4 content under slow monomer addition conditions (Orella et al., 2019). This phenomenon also appears to be similar to what has been observed with F5H up-regulated lignin, in which the content of β-*O*-4 content is positively related to the ratio of S units in lignin (Stewart et al., 2009). In general, the structural characteristics of lignin components obtained from a feedstock biomass and biorefinery processes have a direct effect on the outcomes in future conversion processes. According to previous studies (Rinaldi et al., 2016; Schutyser et al., 2018), the abundant β-*O*-4 linkages in these DEL samples are conducive to the downstream conversion of lignin into aromatic molecules. However, apart from S/G ratios and β-*O*-4 abundance in lignin, the chemical reactivity (i.e., different functional groups) of the different lignin fractions is also the most important molecular feature that determines its availability in the conversion process of these lignin feedstocks (Wang et al., 2020).

^{31}P-NMR Analysis of DELs

The ^{31}P NMR technique can accurately quantify the content of functional groups (such as OH and COOH groups) of lignin with the aid of the internal standard (Argyropoulos, 1995). The functional groups in these lignin fractions can be determined by the ^{31}P NMR technique (**Supplementary Figure S2**) and the results are shown in **Table 5**. Based on the obtained data, it was found that the detected amount of phenolic OH is less and the content of S-type phenolic OH is similar to that of G-type phenolic OH. This fact suggested that β-*O*-4 linkage in these lignin macromolecules were mainly composed of S-type and G-type lignin units, thus only less phenolic OH was determined by the ^{31}P NMR spectra. Additionally, the continuously decreasing contents of phenolic OH groups (S-type phenolic OH, condensed G-type phenolic OH, and non-condensed G-type phenolic OH) from these lignin macromolecules were observed with the increasing age of the trees. This fact suggested that phenolic OH groups in DELs from 3 and 5-year-old balsa wood are occupied in the form of β-*O*-4 linkage and possible LCC bonds, such as phenyl glycoside bonds, which can be revealed by the high content of β-*O*-4 linkage and carbohydrates in DEL-3 and DEL-5. Therefore, deducting the possible effects of carbohydrates in lignin, the content of the phenolic OH group is inversely related to the amount of β-*O*-4 linkage in the lignin extracted from same feedstock using the same method. In general, if a native lignin contains less content of S-type and G-type phenolic OH groups, the content of β-*O*-4 linkage is abundant. With regard to the COOH groups, it was found that the COOH in DEL-1 was higher than those from DEL-3 and DEL-5. Considering the difference of aliphatic OH and COOH groups in these lignin fractions, it should be realized that the amounts of aliphatic OH and COOH groups is not only

TABLE 5 | Quantification of lignin fractions by quantitative ^{31}P-NMR method (mmol/g).

Samples	Aliphatic OH	S-type phenolic OH	G-type phenolic OH		Carboxylic Group
			C[a]	NC[b]	
DEL-1	4.21	0.42	0.08	0.43	0.12
DEL-3	3.60	0.33	0.05	0.29	0.07
DEL-5	2.85	0.27	0.05	0.23	0.08

[a]C, condensed. [b]NC, non-condensed.

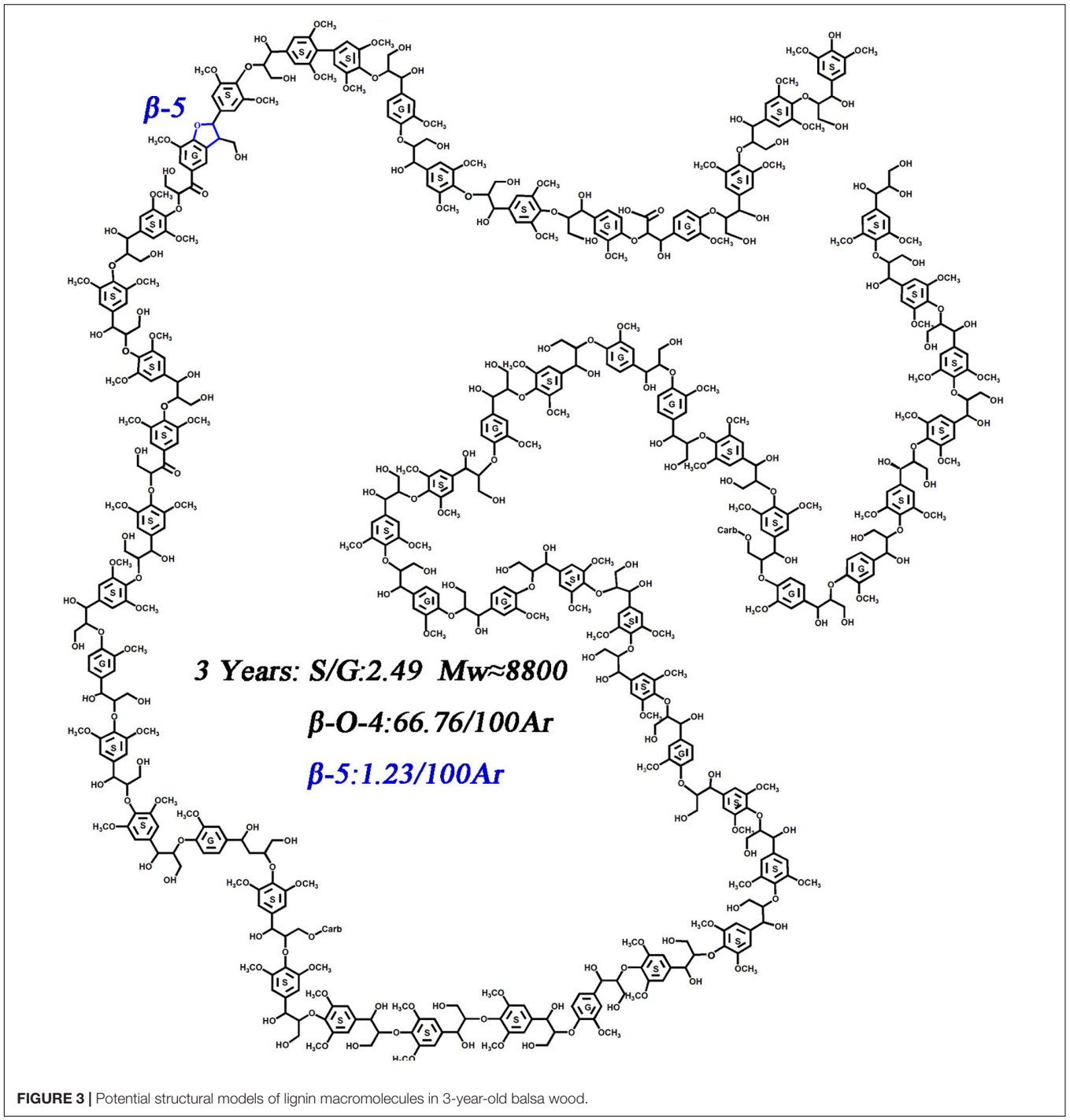

FIGURE 3 | Potential structural models of lignin macromolecules in 3-year-old balsa wood.

related to the different lignin substructures, but also affected by molecular weights of lignin.

Possible Structural Models and Its Implications

Lignin is generally separated and collected through different pretreatments and can be further developed into the renewable biomaterials or value-added chemicals, which depend on the structural characteristics of the raw material lignin (Schutyser et al., 2018). In the present study, the potential structural models (**Figure 3** and **Supplementary Figure S3**) of native lignin macromolecules from different growing years of balsa feedstocks were proposed based on the structural characteristics of balsa lignin macromolecules such as molecular weights, C9 units, S/G ratios, and the relative contents of different interunit linkage. Although the structural models are not the authentic structures of native lignin, it can intuitively reflect the structural characteristics

of the native lignin from balsa trees. In short, this kind of native lignin has abundant β-*O*-4 linkages and such linear structure, which is conducive to the current reductive catalytic fractionation (RCF) process (Renders et al., 2017, 2019). Alternatively, to better utilize this kind of feedstock and achieve biomass valorization, a pretreatment is needed to effectively isolate high-quality lignin from this kind of feedstock prior to carbohydrate conversion, which is beneficial to the subsequent lignin-oriented biorefinery. Based on the obtained lignin, the structural characteristics and chemical reactivity of the obtained lignin should be further analyzed prior to final conversion of the isolated lignin into value-added chemicals (lignin monomers) and materials (lignin-based polymers). If the ultimate purpose of this lignin is to produce aromatic chemicals (lignin monomers), the isolation/fractionation method therefore should meet the following requirements, (1) maximally retaining the native β-*O*-4 bonds in lignin; (2) decreasing the formation of carbon–carbon bonds; and (3) identifying the structural features of lignin during the pretreatment method. The chemical composition and structural features of the isolated lignin can be investigated by reliable and powerful 2D-HSQC methodology, which can provide qualitative and quantitative information on lignin structure (Wen et al., 2013b). If the final application of lignin focuses on the development of lignin-based polymers, isolated lignin fractions with abundant OH groups are desired because most chemical modifications rely on the amount of OH groups (Laurichesse and Avérous, 2014). The ^{31}P-NMR technique is a powerful technique to quantify the amount of different hydroxyl groups in lignin, which will be beneficial to the chemical modification of isolated lignin in developing lignin-based materials. These advances in lignin structural analysis contribute to the subsequent value-added utilizations of lignin. In short, the above-mentioned structural information of native lignin from balsa wood will also bring new opportunities for current "lignin-first" biorefinery.

CONCLUSION

In the present study, the representative native residual DELs from different growth years of balsa wood were first used to characterize the structural variations and evolution of balsa lignin during the growth process. At the micro level, the accumulation of lignin in the plant cell wall is reinforced in the 3- and 5-year-old balsa wood. NMR results showed that the DELs from different growth years of balsa trees have abundant β-*O*-4 linkages (66.33–68.81/100Ar) and increasing S/G ratios (1.25–2.95). Remarkably, it was found that the lignin from 3- to 5-year-old balsa wood is overwhelmingly composed of β-*O*-4 linkages with fewer C–C linkages, which is beneficial for the production of aromatic chemicals from lignin. Thus, the linear lignin having a high content of β-*O*-4 linkages in the lignin is essential to achieve a high-yield of aromatic monomers in the lignin catalytic hydrogenolysis process. Alternatively, this kind of feedstock with abundant β-*O*-4 linkages is promising for the current RCF process. In short, investigating the balsa lignin not only broadens the current understanding of structural changes of lignin during the growth process of the balsa tree, but also facilitates the downstream utilization of balsa lignin in the current "lignin-first" biorefinery process.

DATA AVAILABILITY STATEMENT

The original contributions presented in the study are included in the article/**Supplementary Material**, further inquiries can be directed to the corresponding author.

AUTHOR CONTRIBUTIONS

CZ and L-HX carried out the experiments and wrote the draft manuscript. C-YM and H-MW performed the data process and visualization. Y-YZ provided the balsa wood raw materials and conducted CRM analysis. Y-YW performed the composition analysis of the balsa wood. J-LW designed the experiment, checked the data, and revised and improved the manuscript. All authors discussed the results and read the manuscript.

FUNDING

This work was supported by the Beijing Forestry University Outstanding Young Talent Cultivation Project (2019JQ03006), National Natural Science Foundation of China (31872698), and National Key Research and Development Program of China (2019YFB1503801).

SUPPLEMENTARY MATERIAL

The Supplementary Material for this article can be found online at: https://www.frontiersin.org/articles/10.3389/fenrg.2020.00181/full#supplementary-material

REFERENCES

Agarwal, U. P. (2006). Raman imaging to investigate ultrastructure and composition of plant cell walls: distribution of lignin and cellulose in black spruce wood (*Picea mariana*). *Planta* 224, 1141–1153. doi: 10.1007/s00425-006-0295-z

Akinosho, H. O., Yoo, C. G., Dumitrache, A., Natzke, J., Muchero, W., Brown, S. D., et al. (2017). Elucidating the structural changes to populus lignin during consolidated bioprocessing with *Clostridium thermocellum*. *ACS Sustain. Chem. Eng.* 5, 7486–7491. doi: 10.1021/acssuschemeng.7b01203

Argyropoulos, D. (1995). 31 P NMR in wood chemistry: a review of recent progress. *Res. Chem. Intermed.* 21:373. doi: 10.1007/bf03052265

Balakshin, M., Capanema, E., Gracz, H., Chang, H.-M., and Jameel, H. (2011). Quantification of lignin–carbohydrate linkages with high-resolution NMR spectroscopy. *Planta* 233, 1097–1110. doi: 10.1007/s00425-011-1359-2

Baruah, J., Nath, B. K., Sharma, R., Kumar, S., Deka, R. C., Baruah, D. C., et al. (2018). Recent trends in the pretreatment of lignocellulosic biomass for value-added products. *Front. Energy Res.* 6:141. doi: 10.3389/fenrg.2018.00141

Björkman, A. (1954). Isolation of lignin from finely divided wood with neutral solvents. *Nature* 174, 1057–1058. doi: 10.1038/1741057a0

Chang, H.-M., Cowling, E. B., and Brown, W. (1975). Comparative studies on cellulolytic enzyme lignin and milled wood lignin of sweetgum and spruce. *Holzforschung* 29, 153–159. doi: 10.1515/hfsg.1975.29.5.153

Chen, T.-Y., Wang, B., Wu, Y.-Y., Wen, J.-L., Liu, C.-F., Yuan, T.-Q., et al. (2017). Structural variations of lignin macromolecule from different growth years of Triploid of Populus tomentosa Carr. *Int. J. Biol. Macromol.* 101, 747–757. doi: 10.1016/j.ijbiomac.2017.03.146

del Río, J. C., Rencoret, J., Prinsen, P., Martínez, ÁT., Ralph, J., and Gutiérrez, A. (2012). Structural Characterization of Wheat Straw Lignin as Revealed by Analytical Pyrolysis, 2D-NMR, and Reductive Cleavage Methods. *J. Agricult. Food Chem.* 60, 5922–5935. doi: 10.1021/jf301002n

Ding, S.-Y., Liu, Y.-S., Zeng, Y., Himmel, M. E., Baker, J. O., and Bayer, E. A. (2012). How does plant cell wall nanoscale architecture correlate with enzymatic digestibility? *Science* 338, 1055–1060. doi: 10.1126/science.1227491

Fu, Q., Medina, L., Li, Y., Carosio, F., Hajian, A., and Berglund, L. A. (2017). Nanostructured wood hybrids for fire-retardancy prepared by clay impregnation into the cell wall. *ACS Appl. Mater. Interfaces* 9, 36154–36163. doi: 10.1021/acsami.7b10008

Guan, H., Cheng, Z., and Wang, X. (2018). Highly compressible wood sponges with a spring-like lamellar structure as effective and reusable oil absorbents. *ACS Nano* 12, 10365–10373. doi: 10.1021/acsnano.8b05763

Huang, C.-X., Lin, W.-Q., Lai, C.-H., Li, X., Jin, Y.-C., and Yong, Q. (2019). Coupling the post-extraction process to remove residual lignin and alter the recalcitrant structures for improving the enzymatic digestibility of acid-pretreated bamboo residues. *Bioresour. Technol.* 285:121355. doi: 10.1016/j.biortech.2019.121355

Huang, C.-X., Tang, S., Zhang, W.-Y., Tao, Y.-H., Lai, C.-H., Li, X., et al. (2018). Unveiling the structural properties of lignin–carbohydrate complexes in bamboo residues and its functionality as antioxidants and immunostimulants. *ACS Sustain. Chem. Eng.* 6, 12522–12531. doi: 10.1021/acssuschemeng.8b03262

Kim, H., and Ralph, J. (2010). Solution-state 2D NMR of ball-milled plant cell wall gels in DMSO-d(6)/pyridine-d(5). *Org. Biomol. Chem.* 8, 576–591. doi: 10.1039/b916070a

Lan, W., Amiri, M. T., Hunston, C. M., and Luterbacher, J. S. (2018). Protection Group Effects during α, γ-Diol Lignin Stabilization Promote High-Selectivity Monomer Production. *Angew. Chem.* 57, 1356–1360. doi: 10.1002/anie.201710838

Laurichesse, S., and Avérous, L. (2014). Chemical modification of lignins: towards biobased polymers. *Progr. Polym. Sci.* 39, 1266–1290. doi: 10.1016/j.progpolymsci.2013.11.004

Li, H.-Y., Sun, S.-N., Wang, C.-Z., and Sun, R.-C. (2015). Structural and dynamic changes of lignin in Eucalyptus cell walls during successive alkaline ethanol treatments. *Indus. Crops Products* 74, 200–208. doi: 10.1016/j.indcrop.2015.04.048

Luterbacher, J. S., Azarpira, A., Motagamwala, A. H., Lu, F., Ralph, J., and Dumesic, J. A. (2015). Lignin monomer production integrated into the γ-valerolactone sugar platform. *Energy Environ. Sci.* 8, 2657–2663. doi: 10.1039.C5EE01322D

O'Dowd, D. J. (1979). Foliar nectar production and ant activity on a neotropical tree. *Ochroma pyramidale*. *Oecologia* 43, 233–248. doi: 10.1007/BF00344773

Orella, M. J., Gani, T. Z. H., Vermaas, J. V., Stone, M. L., Anderson, E. M., Beckham, G. T., et al. (2019). Lignin-KMC: a toolkit for simulating lignin biosynthesis. *ACS Sustain. Chem. Eng.* 7, 18313–18322. doi: 10.1021/acssuschemeng.9b03534

Ragauskas, A. J., and Yoo, C. G. (2018). Editorial: advancements in biomass recalcitrance: the use of lignin for the production of fuels and chemicals. *Front. Energy Res.* 6:118. doi: 10.3389/fenrg.2018.00118

Ralph, J., and Landucci, L. L. (2010). "NMR of lignins," in *Lignin and Lignans: Advances in Chemistry*, eds J. Schmidt, D. Dimmel, and C. Heitner (Boca Raton, FL: CRC Press), 137–234. doi: 10.1201/EBK1574444865-c5

Ralph, J., Lundquist, K., Brunow, G., Lu, F., Kim, H., Schatz, P. F., et al. (2004). Lignins: natural polymers from oxidative coupling of 4-hydroxyphenyl-propanoids. *Phytochem. Rev.* 3, 29–60. doi: 10.1023/b:phyt.0000047809.65444.a4

Renders, T., Van den Bosch, S., Koelewijn, S., Schutyser, W., and Sels, B. (2017). Lignin-first biomass fractionation: the advent of active stabilisation strategies. *Energy Environ. Sci. Ees* 10, 1551–1557. doi: 10.1039/C7EE01298E

Renders, T., Van den Bossche, G., Vangeel, T., Van Aelst, K., and Sels, B. (2019). Reductive catalytic fractionation: state of the art of the lignin-first biorefinery. *Curr. Opin. Biotechnol.* 56, 193–201. doi: 10.1016/j.copbio.2018.12.005

Rinaldi, R., Jastrzebski, R., Clough, M. T., Ralph, J., Kennema, M., Bruijnincx, P. C., et al. (2016). Paving the way for lignin valorisation: recent advances in bioengineering. Biorefining and Catalysis. *Angew. Chem. Int. Ed. Engl.* 55, 8164–8215. doi: 10.1002/anie.201510351

Schutyser, W., Renders, T., Van den Bosch, S., Koelewijn, S. F., Beckham, G. T., and Sels, B. F. (2018). Chemicals from lignin: an interplay of lignocellulose fractionation, depolymerisation, and upgrading. *Chem. Soc. Rev.* 47, 852–908. doi: 10.1039/c7cs00566k

Shu, Z.-F. (1998). *The Lightest Tree-Balsa (in chinese)*. Yunnan: Yunnan Forestry.

Shuai, L., Amiri, M. T., Questell-Santiago, Y. M., Héroguel, F., Li, Y., Kim, H., et al. (2016). Formaldehyde stabilization facilitates lignin monomer production during biomass depolymerization. *Science* 354, 329–333. doi: 10.1126/science.aaf7810

Sluiter, A., Hames, B., Ruiz, R., Scarlata, C., Sluiter, J., Templeton, D., et al. (2008). Determination of structural carbohydrates and lignin in biomass. *Lab. Anal. Procedure* 1617, 1–16.

Stewart, J. J., Akiyama, T., Chapple, C., Ralph, J., and Mansfield, S. D. (2009). The effects on lignin structure of overexpression of ferulate 5-hydroxylase in hybrid poplar. *Plant Physiol.* 150, 621–635. doi: 10.1104/pp.109.137059

Wang, H.-M., Ma, C.-Y., Li, H.-Y., Chen, T.-Y., Wen, J.-L., Cao, X.-F., et al. (2020). Structural variations of lignin macromolecules from early growth stages of poplar cell walls. *ACS Sustain. Chem. Eng.* 8, 1813–1822. doi: 10.1021/acssuschemeng.9b05845

Wang, H.-M., Wang, B., Wen, J.-L., Yuan, T.-Q., and Sun, R.-C. (2017). Structural characteristics of lignin macromolecules from different eucalyptus species. *ACS Sustain. Chem. Eng.* 5, 11618–11627. doi: 10.1021/acssuschemeng.7b02970

Wen, J.-L., Sun, S.-L., Xue, B.-L., and Sun, R.-C. (2013a). Quantitative structural characterization of the lignins from the stem and pith of bamboo (*Phyllostachys pubescens*). *Holzforschung* 67, 613–627. doi: 10.1515/hf-2012-0162

Wen, J.-L., Sun, S.-L., Xue, B.-L., and Sun, R.-C. (2013b). Recent advances in characterization of lignin polymer by solution-state nuclear magnetic resonance (NMR) methodology. *Materials* 6, 359–391. doi: 10.3390/ma6010359

Wu, S.-B., and Argyropoulos, D. (2003). An improved method for lsolating lignin in high yield and purity. *J. Pulp Paper Sci.* 29, 235–240. doi: 10.1023/A:1025117327970

Yuan, T.-Q., Sun, S.-N., Xu, F., and Sun, R.-C. (2011). Characterization of lignin structures and lignin-carbohydrate complex (LCC) linkages by quantitative 13C and 2D HSQC NMR spectroscopy. *J. Agricult. Food Chem.* 59, 10604–10614. doi: 10.1021/jf2031549

Yuan, T.-Q., Xu, F., He, J., and Sun, R.-C. (2013). Role of lignin in a biorefinery: separation characterization and valorization. *J. Chem. Technol. Biotechnol.* 88, 346–352. doi: 10.1002/jctb.3996

Zeng, Y.-N., Zhao, S., Yang, S.-H., and Ding, S.-Y. (2014). Lignin plays a negative role in the biochemical process for producing lignocellulosic biofuels. *Curr. Opin. Biotechnol.* 27, 38–45. doi: 10.1016/j.copbio.2013.09.008

Zhang, A.-P., Lu, F.-C., Sun, R.-C., and Ralph, J. (2010). Isolation of cellulolytic enzyme lignin from wood preswollen/dissolved in dimethyl sulfoxide/N-methylimidazole. *J. Agric. Food Chem.* 58, 3446–3450. doi: 10.1021/jf903998d

Conflict of Interest: The authors declare that the research was conducted in the absence of any commercial or financial relationships that could be construed as a potential conflict of interest.

frontiers in Energy Research

ORIGINAL RESEARCH
published: 30 October 2020
doi: 10.3389/fenrg.2020.573198

Insights into Structural Transformations of Lignin Toward High Reactivity During Choline Chloride/Formic Acid Deep Eutectic Solvents Pretreatment

Si Hong[1†], *Xiao-Jun Shen*[2†], *Zhuohua Sun*[1] *and Tong-Qi Yuan*[1*]

[1]*Beijing Advanced Innovation Center for Tree Breeding by Molecular Design, Beijing Key Laboratory of Lignocellulosic Chemistry, Beijing Forestry University, Beijing, China,* [2]*Beijing National Laboratory for Molecular Sciences, CAS Key Laboratory of Colloid and Interface and Thermodynamics, CAS Research/Education Center for Excellence in Molecular Sciences, Institute of Chemistry, Chinese Academy of Sciences, Beijing, China*

OPEN ACCESS

Edited by:
Li Shuai,
Fujian Agriculture and Forestry University, China

Reviewed by:
Yanding Li,
Massachusetts Institute of Technology, United States
Somnath D. Shinde,
Sandia National Laboratories (SNL), United States

***Correspondence:**
Tong-Qi Yuan
ytq581234@bjfu.edu.cn

[†]*These authors have contributed equally to this work.*

Specialty section:
This article was submitted to Bioenergy and Biofuels, a section of the journal Frontiers in Energy Research

Received: *16 June 2020*
Accepted: *21 August 2020*
Published: *30 October 2020*

Citation:
Hong S, Shen X-J, Sun Z, Yuan T-Q (2020) Insights into Structural Transformations of Lignin Toward High Reactivity During Choline Chloride/Formic Acid Deep Eutectic Solvents Pretreatment. Front. Energy Res. 8:573198. doi: 10.3389/fenrg.2020.573198

Understanding lignin structural transformations during DES pretreatment would facilitate to produce lignin with tailor-made properties based on intended applications. To unravel the structural variant of lignin in the DES, the alkali lignin (AL) was pretreated in choline chloride/formic acid (ChCl/FA) (the ratio of 1:2) at 80–120 °C. Characterization of the AL and regenerated lignin samples were determined to understand lignin structure, such as linkage in lignin, phenolic OH content, molecular weight, and aromatic products. ChCl/FA DES pretreatment resulted in large amounts of the dissociation of β-*O*-4′ bonds, partial cleavage of carbon-carbon bonds (i.e., β-β′, β-5′), dehydration of hydroxyl radicals in lignin's side-chain, and demethoxylation reaction. Furthermore, various monomeric phenols derived from AL were also determined in spite of low combined yields, which facilitate the production of fine chemicals in the future. Detailed unmasking of lignin structural transformation during the DES process is conducive to the optimizing preparation of homogeneous lignin with low molecular weight.

Keywords: lignin, deep eutectic solvents, pretreatment, nuclear magnetic resonance, structural transformation

INTRODUCTION

Lignocellulose, mainly consisting of carbohydrates (cellulose and hemicellulose) and aryl-biopolymers (lignin), is the richest, green and renewable bioresource, which can be used to produce various fuels, materials, and fine chemicals (Zhang et al., 2017; Liu et al., 2019b; Dong et al., 2020). The transition from fossil fuels to biomass-based products using renewable lignocellulose has recently been gained considerable interest in biorefinery industries. However, biomass recalcitrance, especially the presence of lignin, would always hinder the successful conversion of lignocellulose to a variety of valuable co-products (Himmel et al., 2007; Ragauskas et al., 2014). Biomass pretreatment, which aims to destroy the inner recalcitrance, is an important step (Rastogi and Shrivastava, 2017; Huang et al., 2019; Soltaniana et al., 2020). Among pretreatment processing, lignin fractionation from lignocellulose remains the key step.

Recently, deep eutectic solvents (DES) have drawn increasing interest, which can be used as promising green solvents for lignocellulosic biomass process and delignification (Chen et al., 2018b;

Lin et al., 2019; Lin et al., 2020). DES are considered to be a eutectic mixture made up of hydrogen bond acceptor and hydrogen bond donor through hydrogen bond interactions, and its melting point is much lower than the individual components (Smith et al., 2014). As compared to conventional solvents and ionic liquids, DES owns some superiourities, such as ease of synthesis, availability, cost effectiveness in raw materials, good recyclability, and biocompatibility (Satlewal et al., 2018). Francisco et al. first showed high lignin solubility and low cellulose solubility in a range of DESs (Francisco et al., 2012). After that, various types of DES, such as ChCl/FA, ChCl/lactic acid, and ChCl/glycerol, have been prepared and applied to improve the saccharification efficiency of cellulose and delignification (Zhang et al., 2016; Hou et al., 2018; Tan et al., 2019). Yu and co-workers designed a microwave-assisted DES pretreatment method to achieve ultrafast fractionation of lignocellulose in 3 min (Liu et al., 2017a; Liu et al., 2017b). Wan and co-workers further revealed that ChCl/lactic acid pretreatment can extract 65–72% lignin from lignocellulose for only 45 s with microwave irradiation (Chen and Wan, 2018). Meanwhile, Song group systematically investigated the structural transformation of lignin during ChCl/lactic acid process via the experiments of isolated lignin and a series of β-O-4′ lignin model compounds and unraveled multiple pathways simultaneously occur during ChCl/lactic acid process, such as cleavage of β-O-4′, the repolymerization of active species, the production and derivation of mono products (Wang et al., 2020). Numerous DESs, especially carboxylic acid DES, have achieved the extraction of high-yield lignin among mild conditions. However, a significant amount of DES extracted lignin is still underutilized.

As the only renewable aromatic biopolymer in nature, lignin (ca.15–40 wt%) consists of three phenylpropanoid units linked through various ether bonds and carbon-carbon bonds (Sun et al., 2018). To achieve the upgrading of lignin extracted in the DES, it is necessary to unmask lignin structural transformation during DES pretreatment. Zhang and co-workers reported that ChCl/lactic acid pretreatment fractionated a large amount of lignin fragments with high purity from woody biomass, due to the breakage of β-O-4′ bonds in lignin and the suppression of lignin recondensation (Alvarez-Vasco et al., 2016). After that, Shen et al. illustrated that acidic DES pretreatment resulted in not only the depolymerization but also the condensation of the lignin fraction (Shen et al., 2019a; Shen et al., 2019b). However, Wan group found that acidified DES was able to remove more than 76% lignin under mild conditions, and the resulting lignin preserved β-O-4′ bonds and the structure was similar to the native lignin (Chen et al., 2018a, Chen et al., 2018b). As stated above, lignin suffered different chemical and structural changes via diverse DES pretreatment.

To investigate the lignin structural transformation during DES pretreatment, ChCl/FA was applied to pretreat AL at different temperatures (80, 100, and 120°C) for 6 h. The structure of the regenerated lignin was comprehensive analysis by nuclear magnetic resonance (NMR), gel permeation chromatography (GPC), and Fourier Transform Infrared (FT-IR) to verify the structural transformation of lignin in the selected DES. The depolymerized products of lignin were systematically determined via gas chromatography-mass spectrometry (GC-MS).

METHODS AND MATERIALS

Materials

Triploid of *Populus tomentosa* Carr (6 years old) were obtained from the Shandong province, China. The poplar was ground, then extracted in a Soxhlet extractor with toluene-ethanol (2:1 v/v) for 6 h, finally milled for 1 h in ZrO_2 bowl. Ball-milled wood (100 g) was treated with 1,500 ml of sodium hydroxide (1%) at 75°C for 3 h. The alkali lignin (AL) was separated based on the previous literature (Wen et al., 2014). The chemical composition of AL was analyzed according to NREL standard analytical procedure (Sluiter et al., 2008). The AL is composed of lignin (97.3%), total carbohydrates (1.1%), and others (1.6%). Choline chloride (ChCl) and formic acid (FA), purchased from Sigma-Aldrich, were used to synthesize DES at molar ratios of 1:2.

The Dissolution of Alkali Lignin

0.3 g AL and 6.0 g DESs were loaded in a pressure tube, which was treated at different temperatures (80, 100, and 120°C) for 6 h with 500 rpm. After finishing, samples were cooled down to room temperature. Then, the mixture was slowly added to acidic water (pH = 2) (40 ml) with 800 rpm for 20 min. Finally, the solid was collected via centrifugation at 10,000 rpm for 20 min, and then washed with acidic water for triplicate. The solid sample was lyophilized for 24 h to gain the regenerated lignin sample that was labeled as FA-X (e.g., FA-80). Meanwhile, the 50 ml supernatant was extracted with 400 ml ethyl acetate at room temperature. The mixture was stratified to take the organic phase. Subsequently, after removing the ethyl acetate at 35°C by rotary evaporation, lignin oil was obtained and label as F-X (e.g., F-80). FA and F referred to DESs type. X referred to the DES reaction temperature. All experiments were conducted two times.

RESULT AND DISCUSSION

The alkali lignin (AL) under the mild alkaline treatment was used as lignin model compounds due to the relatively low carbohydrates, no significant structural changes to the polymer backbone, nor condensation, which was close to the structure of protolignin in lignocellulose (Sun et al., 2000). Meanwhile, NMR analysis showed that AL remained various chemical linkages (e.g., 62.0% of β-*O*-4′ linkages) and no condensation occurred in the mild alkaline condition (**Figures 1 and 2**), which was similar with Liu group's AL in mild alkaline treatment (Liu et al., 2019a). ChCl/FA was selected to treat AL, due to its high delignification ability (Muley et al., 2019; Kohli et al., 2020). Herein, AL was pretreated with ChCl/FA DES at different temperatures, and then precipitated as the regenerated lignin. Results suggested that 58% of the regenerated lignin was obtained at 80°C after DES pretreatment (**Table 1**). The relatively low recovery yield

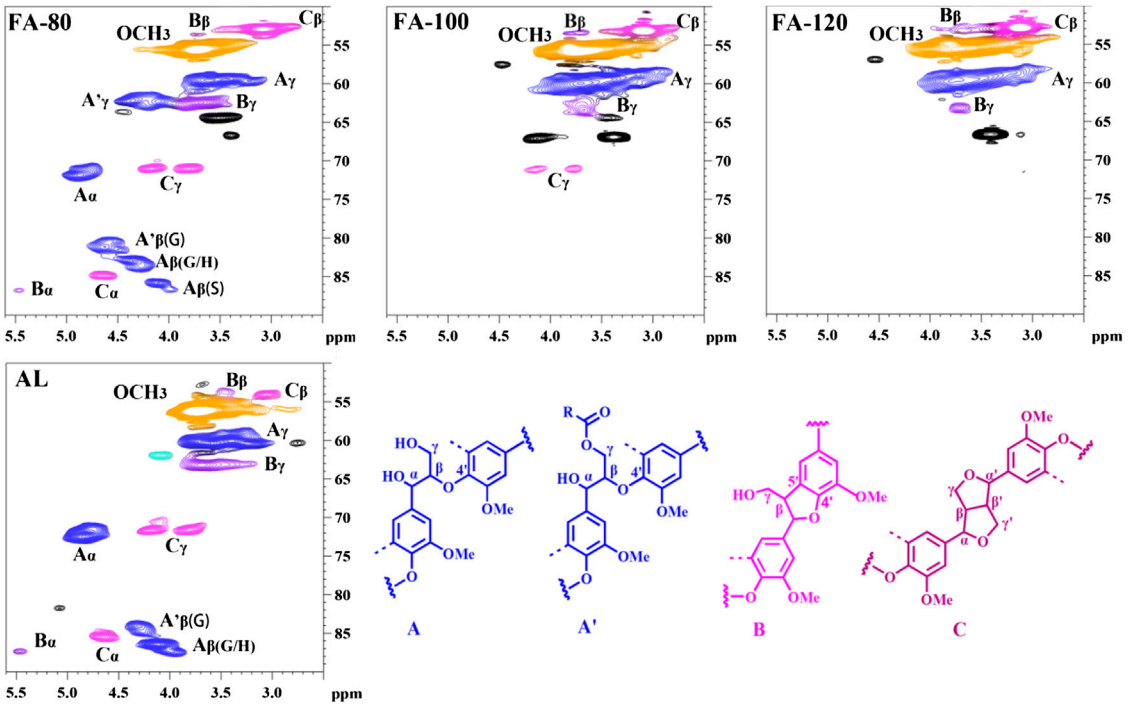

FIGURE 1 | Side-chain regions in the 2D-HSQC spectra of lignin samples.

indicated that some lignin fragments were degraded to small and soluble lignin fragment during DES pretreatment. Moreover, with the rise of pretreatment temperature, the recovery yield of lignin after DES pretreatment slightly decreased. The detailed structural transformation of the regenerated lignin was characterized by NMR, GPC, and FT-IR. The depolymerized products acquired after ChCl/FA DES processing were analyzed by GC-MS technology.

Structural Analysis of the Regenerated Lignin

Fourier Transform Infrared Analysis

FT-IR spectra were used to assess the lignin structural changes during DES pretreatment (**Supplementary Figure S1**). The peaks were assigned according to previous literatures (Faix, 1991). All of the regenerated lignin presented a similar peak pattern, while the intensity of these peaks was diminished as compared to that of AL. The wide FT-IR band at 3,448 cm^{-1} (hydroxyl groups) did not change strikingly, thus needing further analysis by ^{31}P spectra. **Supplementary Figure S1** showed that the peak intensity at 2,938 cm^{-1} (C-H stretch in methyl and methylene group) started to decrease slightly after pretreatment, implying that the DES pretreatment could result in demethoxylation reaction. The intensity of bond at 1,657 cm^{-1} (conjugated carbonyl absorption) became weak, whereas the newly appeared absorption peak around 1739 cm^{-1} (unconjugated ketone carbonyl and carboxyl carbonyl groups) was observed in the regenerated lignin. The possibility is that the acidic DES pretreatment resulted in the breakage of β-*O*-4′ bonds, thus appearing the unconjugated carbonyl groups, which is agreement with the subsequent GC-MS result of forming of Hibbert's ketone (unconjugated carbonyl chemicals). Recently, Song group proposed reaction pathway of β-*O*-4′ bonds breakage in lignin using acidic DES, and also found the monoketone compound with the unconjugated carbonyl groups (Wang et al., 2020). Another reason was that esterification may also occur between COOH group in FA and OH groups of γ position in lignin. The typical characteristic peaks at 1,600, 1,502, and 1,459 cm^{-1} represent aromatic skeletal vibrations, and 1,416 cm^{-1} corresponds to the C-H deformation combined with aromatic ring vibration. Particularly, the intensity of bonds at 1,330, 1,120, and 835 cm^{-1} decreased greatly, suggesting that S-type units could be degraded after the DES pretreatment. In addition, the signal at 1,024 cm^{-1} (aromatic C-H in-plane deformation) gradually got weak after the pretreatment, suggesting that condensation reactions prevented the in-plane deformation of aromatic C-H. The results indicated that DES pretreatment can destroy the lignin structure. However, the detailed transformations of the lignin structure need further confirmation by NMR spectra.

2D-HSQC Analysis

The interunit linkage changes of lignin samples before and after DES pretreatment can be characterized by 2D-HSQC. This technology is able to measure the specific carbon-hydrogen functionalities, which cannot be determined in ^{13}C NMR. According to the previous literatures, the detailed signals of lignin were assigned in **Supplementary Table S2** (Marita et al., 2001; Hallac et al., 2010; Sette et al., 2011; Meng et al., 2019).

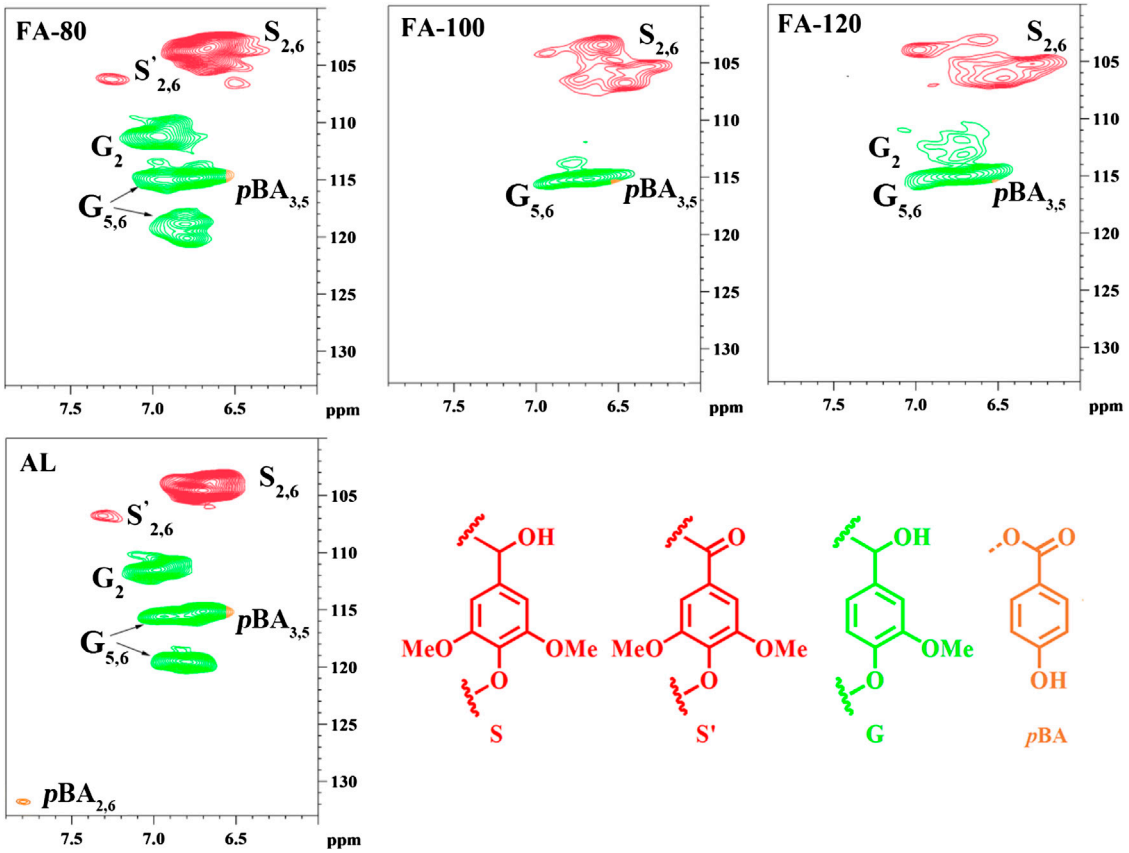

FIGURE 2 | Aromatic regions in the 2D-HSQC spectra of lignin samples.

TABLE 1 | Recovery yield of regenerated lignin samples and molecular weight of the lignin.

Samples	AL	FA-80	FA-100	FA-120
Yield (%)[a]	100	58	54	44
M_w (g mol^{-1})	5,080	2,230	1,640	1,650
M_n (g mol^{-1})	3,190	1900	1,360	1,360
PDI[b]	1.59	1.17	1.20	1.21

[a]*The yield was the mass ratio of lignin before and after the DES pretreatment.*
[b]*PDI = M_w/M_n, polydispersity index.*

In the side-chain regions (**Figure 1**), the peaks of β-*O*-4′ substructures and methoxyl groups were dominant in the regenerated lignin. After ChCl/FA DES process, the interunit linkages of lignin fragments changed. When comparing the spectra of AL and FA-80, the novel signals (marked with black) were observed, which was attributed to DES components. The signals of C_α-H_α in A substructures got weak at 80°C, and then completely disappeared at the high temperature, indicating that C_α in AL during DES pretreatment was modified. Moreover, the signals of C_β-H_β in the A substructures declined with the elevated temperature under DES pretreatment, indicating dissociation of β-*O*-4′ bonds. Note that the signal of C_γ-H_γ in A′ substructures was observed at 80 °C, suggesting that acylation could occur between γ-OH groups of lignin and COOH groups of FA. Nevertheless, the signal of A'_γ substructures entirely disappeared at the harsh condition, possibly due to the deacylation reaction. Besides, the signals of the B and C substructures became weak with the increased temperature, which implied that partial C-C bonds (e.g., β-β′ and β-5′) were degraded. Some studies also reported that C-C bonds could break down during DES pretreatment (Shen et al., 2019a; Hong et al., 2020; Wang et al., 2020). The quantitative analysis of the interunit linkages revealed that amounts of ether bonds and C-C bonds decreased when the pretreatment temperature increased (**Figure 2**).

In aromatic regions (**Figure 2**), signals of syringyl (S) and guaiacyl (G) substructures were detected. After DES pretreatment, the chemical shift of S units were altered, which implied that condensation could occur. Meanwhile, the signal of C_2-H_2 in G units gradually diminished as the increased temperature, indicating the possible formation of the condensed G units. Furthermore, S/G ratio of lignin was also a reliable method to evaluate the structural variant of the regenerated lignin samples. **Supplementary Table S1** clearly showed that S/G ratio in the regenerated lignin was relatively

TABLE 2 | Quantification of the functional groups in the lignin samples by quantitative ^{31}P-NMR method.

Samples	Carboxylic group	Aliphatic OH	Syringyl OH	Guaiacyl OH		*p*-hydroxylphenyl OH	Total phenolic OH
				C[a]	NC[b]		
AL	0.18	3.81	0.18	0.04	0.38	0.02	4.43
FA-80	0.22	3.72	0.76	0.15	0.79	0.13	5.55
FA-100	0.25	2.95	1.24	0.22	0.59	0.11	6.12
FA-120	0.29	1.52	2.41	0.48	1.06	0.28	5.75

[a]*C, condensed.*
[b]*NC, non-condensed.*

higher as compared to that in AL, and sharply raise when the temperature elevated. The possible reason for this result was that G-type units in lignin were prone to degraded or removed during DES pretreatment. Besides, it probably indicated that G-type units in lignin degraded more quickly than the S-type units. However, under the acidic lithium bromide trihydrate system at 110 °C, native lignin was depolymerized in the solid state with minimal condensation (Li et al., 2018). To effectively separate depolymerized lignin with a less condensed form from biomass, it is necessary to optimize DES pretreatment conditions.

^{31}P-NMR Analysis

The depolymerization and condensation reaction in lignin significantly influence the content of hydroxyl groups (OH) that have a significant effect on lignin valorization. The variations of OH content in lignin before and after pretreatment can be probed by ^{31}P NMR (**Table 2**; **Supplementary Figure S2**). It was found that the COOH amount in the regenerated lignin samples slightly increased after ChCl/FA DES pretreatment, suggesting that aliphatic OH may be oxidized into COOH. On the contrary, the content of aliphatic OH declined as the temperature increased, because of the dehydration and acylation reaction. For AL, the amount of guaiacyl OH was more than that of syringyl OH, which indicated that S-type substructures were inclined to form ether bonds. In addition, the significant increase of condensed guaiacyl OH was clearly observed. The result indicated that lignin experienced repolymerization, being in line with 2D-HSQC result. Furthermore, the amounts of phenolic OH in the regenerated lignin were more than that of AL. This was mainly because of the dissociation of β-*O*-4′ bonds, which was consistent with the result of 2D-HSQC analysis. However, the temperature did not significantly influence on the content of phenolic OH. This implied that significant amount of ether bonds was cleaved at the low temperature. In short, depolymerization and repolymerization of lignin could simultaneously occur during ChCl/FA DES processing, likewise observed in 2D-HSQC analysis.

^{13}C-NMR Analysis

To deeply explore the structural change of lignin in DES system, ^{13}C NMR was used for the determination of AL and the regenerated lignin. The distinct peaks were identified as follows, such as 119.4 ppm (G_6), 115.1 ppm (G_5), 111.3 ppm (G_2) and 104.4 ppm ($S_{2,6}$), confirming that the lignin from poplar is S-G type lignin (**Supplementary Figure S3**. The C_α, C_β, and C_γ of β-*O*-4′ bonds in lignin were located in 86.2, 72.4, and 59.8 ppm. These signal intensity of β-*O*-4′ bonds, etherified S_4 (138.4 ppm) and $S_{3,5}$ (152.7–152.3 ppm) units declined after DES pretreatment, while the increased intensity of non-etherified $S_{3,5}$ and G_3 units (147.2–147.4 ppm) were observed as compared to that of AL. The results proved that the ether linkages were dissociated during DES pretreatment. It was speculated that the signal located at 162.7 ppm was assigned to FA according to 2D-HSQC analysis. Quantification analysis of ^{13}C NMR showed that the content of aromatic C-C in AL was relatively lower (1.66/Ar) than that in FA-120 (1.98/Ar), while the content of aromatic C-H was also observed to reduce from 2.40/Ar in AL to 2.13/Ar in FA-120 (**Table 3**). This result proved that ChCl/FA DES pretreatment also can result in repolymerization reaction, which was according to 2D-HSQC and ^{31}P NMR analysis. Besides, the content of -OCH_3 in FA-120 was relatively lower (1.40/Ar) than that in AL (1.65/Ar). The reduced content of -OCH_3 indicated that demethoxylation reaction occurred during DES pretreatment.

TABLE 3 | The assignment and quantification of the signals of the 13C-NMR spectra (results expressed per Ar).

δ (ppm)	Assignment	AL	FA-120
155.0–140.0	Aromatic C-O	1.93	1.88
140.0–124.0	Aromatic C-C	1.66	1.98
124.0–102.0	Aromatic C-H	2.40	2.13
58.0–54.0	-OCH_3	1.65	1.40

Molecular Weights Analysis

The changes of molecular weights in lignin have the great effect on the structure of lignin. The depolymerization reactions are conducive to decreasing molecular weights of lignin, while the formation of heterogeneous lignin structure with the increasing molecular weight is mainly attributed to the condensation reaction. In the present study, the weight average molecular weights (M_w), number average molecular weight (M_n), and the polydispersity index (PDI) in lignin were showed in **Table 1**. Herein, M_w of AL was 5,080 g mol^{-1}and PDI was 1.59. However, the M_w of the lignin samples after ChCl/FA DES pretreatment sharply declined (2,230–1,640 g mol^{-1}) with respect to that of AL, implying that depolymerization of lignin during DES pretreatment was the dominating reaction. Furthermore, PDI of lignin fragments after pretreatment was lower (1.17–1.20) with

relation to that of AL, which showed the formation of more homogeneous lignin structure. In brief, ChCl/FA DES pretreatment can obtain the homogeneous lignin with the relatively low molecular weight.

Analysis of Lignin Oil

To improve the understanding of lignin structural transformation during DES pretreatment, the depolymerized compounds generated at the different temperature were identified by GC-MS analysis. After separating the regenerated lignin, the leftover liquid was extracted by ethyl acetate. After removing ethyl acetate, lignin oil containing degradation products of lignin was obtained (**Supplementary Figure S4**). The results were summarized in **Supplementary Table S3**. The depolymerized products were determined based on the previous literatures (Xiao et al., 2017; Lan et al., 2019; Li et al., 2019). These lignin oil included guaiacylacetone, guaiacyldiketone, syringaldehyde, syringylacetone, syringyldiketone and methylparaben, which were mainly composed of syringyl and guaiacyl derived phenolic compounds. Further, guaiacyldiketone and syringyldiketone were generated, indicating that the cleavage of ether bonds and oxidation reaction occurred after DES process. As depicted in Fig S5, the identified compounds enormously contained guaiacyl units with few syringyl units. This result indicated that G-type lignin could be prone to depolymerize than S-type lignin. However, the yield of depolymerized compounds was still low overall, due to the weak depolymerization of lignin in DES pretreatment. In addition, it was found that the reaction temperature notably impacted on the degraded products. The results showed that few degraded products were formed at a mild reaction pretreatment (i.e., 80°C), while the amount and kinds of degraded products increased when the temperature rose. This result implied that the higher temperature favored the depolymerization of lignin.

CONCLUSIONS

The present study deeply investigated the impact of the temperatures of ChCl/FA DES pretreatment on the structure and depolymerized products of lignin. The recovery yield of the regenerated lignin samples was around 44–75%, indicating a portion of lignin fraction was decomposed after pretreatment. Large amounts of β-*O*-4′ bonds with a fraction of carbon-carbon bonds (i.e., β-β′, β-5′) were cleaved when the reaction temperature increased, thereby leading to the increased phenolic OH groups and the decreased molecular weights. Besides, the decrease in aliphatic OH and OCH_3 groups was attributed to dehydration and demethoxylation, respectively. Furthermore, the γ-OH in regenerated lignin can be reacted with formic acid into γ-acetylated groups in the mild condition; however, high temperature led to further deacylation reaction. Various monomeric phenols derived from AL were also determined in spite of low combined yields, which facilitate the production of fine chemicals in future. The homogeneous lignin with the high phenolic OH and low molecular weight was obtained after DES pretreatment, which is readily transformed into high value-added materials and chemicals. This study provided a systematic and comprehensive knowledge on lignin transformation during DES pretreatment, which would be conducive to lignin extraction and valorization.

DATA AVAILABILITY STATEMENT

All datasets generated for this study are included in the article/ **Supplementary Material**.

AUTHOR CONTRIBUTIONS

SH carried out all experiments. SH, X-JS, ZS wrote and revised the manuscript. T-QY designed the work and revised the manuscript. All authors discussed the results.

FUNDING

This work was supported by the National Natural Science Foundation of China (31971613 and 31670587), the Fundamental Research Funds for the Central Universities (2015ZCQ-CL-02), and the Beijing Forestry University Outstanding Young Talent Cultivation Project (2019JQ03005).

SUPPLEMENTARY MATERIAL

The Supplementary Material for this article can be found online at: https://www.frontiersin.org/articles/10.3389/fenrg.2020.573198/full#supplementary-material

REFERENCES

Alvarez-Vasco, C., Ma, R., Quintero, M., Guo, M., Geleynse, S., and Ramasamy, K. K. (2016). Unique low-molecular-weight lignin with high purity extracted from wood by deep eutectic solvents (DES): a source of lignin for valorization. *Green Chem.* 18, 5133–5141. doi:10.1039/C6GC01007E.

Chen, Z., Bai, X. L., and Wan, C. X. (2018a). High-solid lignocellulose processing enabled by natural deep eutectic solvent for lignin extraction and industrially relevant production of renewable chemicals. *ACS Sustain. Chem. Eng.* 6, 12205–12216. doi:10.1021/acssuschemeng.8b02541.

Chen, Z., Reznicek, W. D., and Wan, C. (2018b). Deep eutectic solvent pretreatment enabling full utilization of switchgrass. *Bioresour. Technol.* 263, 40–48. doi:10.1016/j.biortech.2018.04.058.

Chen, Z., and Wan, C. (2018). Ultrafast fractionation of lignocellulosic biomass by microwave-assisted deep eutectic solvent pretreatment. *Bioresour. Technol.* 250, 532–537. doi:10.1016/j.biortech.2017.11.066.

Dong, H., Zheng, L., Yu, P., Jiang, Q., Wu, Y., Huang, C., et al. (2020). Characterization and application of lignin-carbohydrate complexes from lignocellulosic materials as antioxidants for scavenging in vitro and in vivo reactive oxygen species. *ACS Sustain. Chem. Eng.* 8, 256–266. doi:10.1021/acssuschemeng.9b05290.

Faix, O. (1991). Condensation indices of lignins determined by FTIR-spectroscopy. *Holz als Roh-und Werkstoff.* 49, 356. doi:10.1007/BF02662706.

Francisco, M., van den Bruinhorst, A., and Kroon, M. C. (2012). New natural and renewable low transition temperature mixtures (LTTMs): screening as solvents for lignocellulosic biomass processing. *Green Chem.* 14, 2153–2157. doi:10.1039/c2gc35660k.

Hallac, B. B., Pu, Y., and Ragauskas, A. J. (2010). Chemical transformations of Buddleja davidii lignin during ethanol Organosolv pretreatment. *Energy Fuels.* 24, 2723–2732. doi:10.1021/ef901556u.

Himmel, M. E., Ding, S.-Y., Johnson, D. K., Adney, W. S., Nimlos, M. R., and Brady, J. W. (2007). Biomass recalcitrance: engineering plants and enzymes for biofuels production. *Science* 315, 804–807. doi:10.1126/science.1137016.

Hong, S., Shen, X.-J., Pang, B., Xue, Z. M., Cao, X.-F., and Wen, J.-L. (2020). In-depth interpretation of the structural changes of lignin and formation of diketones during acidic deep eutectic solvent pretreatment. *Green Chem.* 22, 1851–1858. doi:10.1039/D0GC00006J.

Hou, X.-D., Li, A.-L., Lin, K.-P., Wang, Y.-Y., Kuang, Z.-Y., and Cao, S.-L. (2018). Insight into the structure-function relationships of deep eutectic solvents during rice straw pretreatment. *Bioresour. Technol.* 249, 261–267. doi:10.1016/j.biortech.2017.10.019.

Huang, C. X., Lin, W. Q., Lai, C. H., Li, X., Jin, Y. C., and Yong, Q. (2019). Coupling the post-extraction process to remove residual lignin and alter the recalcitrant structures for improving the enzymatic digestibility of acid-pretreated bamboo residues. *Bioresour. Technol.* 285, 121355. doi:10.1016/j.biortech.2019.121355.

Kohli, K., Katuwal, S., Biswas, A., and Sharma, B. K. (2020). Effective delignification of lignocellulosic biomass by microwave assisted deep eutectic solvents. *Bioresour. Technol.* 303, 122897. doi:10.1016/j.biortech.2020.122897.

Lan, W., de Bueren, J. B., and Luterbacher, J. S. (2019). Highly selective oxidation and depolymerization of α,γ-diol-protected lignin. *Angew. Chem. Int. Ed.* 58, 2649–2654. doi:10.1002/anie.201811630.

Li, H., Bunrit, A., Lu, J., Gao, Z., Luo, N., and Liu, H. (2019). Photocatalytic cleavage of aryl ether in modified lignin to non-phenolic aromatics. *ACS Catal.* 9, 8843–8851. doi:10.1021/acscatal.9b02719.

Li, N., Li, Y., Yoo, C. G., Yang, X., Lin, X., and Ralph, J. (2018). An uncondensed lignin depolymerized in the solid state and isolated from lignocellulosic biomass: a mechanistic study. *Green Chem.* 20, 4224–4235. doi:10.1039/C8GC00953H.

Lin, W. Q., Chen, D. F., Yong, Q., Huang, C. X., and Huang, S. L. (2019). Improving enzymatic hydrolysis of acid-pretreated bamboo residues using amphiphilic surfactant derived from dehydroabietic acid. *Bioresour. Technol.* 293, 122055. doi:10.1016/j.biortech.2019.122055.

Lin, W. Q., Xing, S., Jin, Y. C., Lu, X. M., Huang, C. X., and Yong, Q. (2020). Insight into understanding the performance of deep eutectic solvent pretreatment on improving enzymatic digestibility of bamboo residues. *Bioresour. Technol.* 306, 123163. doi:10.1016/j.biortech.2020.123163.

Liu, X. R., Li, Y. D., Ewulonu, C. M., Ralph, J., Xu, F., Zhang, Q., et al. (2019a). Mild alkaline pretreatment for isolation of native-like lignin and lignin-containing cellulose nanofibers (LCNF) from crop waste. *ACS Sustain. Chem. Eng.* 7, 14135–14142. doi:10.1021/acssuschemeng.9b02800.

Liu, Y. R., Nie, Y., Lu, X. M., Zhang, X. P., He, H. Y., Pan, F. J., et al. (2019b). Cascade utilization of lignocellulosic biomass to high-value products. *Green Chem.* 21, 3499–3535. doi:10.1039/C9GC00473D.

Liu, Y. Z., Chen, W. Z., Xia, Q. Q., Guo, B. T., Wang, Q. W., Liu, S. X., et al. (2017a). Efficient cleavage of lignin-carbohydrate complexes and ultrafast extraction of lignin oligomers from wood biomass by microwave-assisted treatment with deep eutectic solvent. *ChemSusChem* 10, 1692–1700. doi:10.1002/cssc.201601795.

Liu, Y. Z., Guo, B. T., Xia, Q. Q., Meng, J., Chen, W. S., Liu, S. X., et al. (2017b). Efficient cleavage of strong hydrogen bonds in cotton by deep eutectic solvents and facile fabrication of cellulose nanocrystals in high yields. *ACS Sustain. Chem. Eng.* 5, 7623–7631. doi:10.1021/acssuschemeng.7b00954.

Marita, J. M., Ralph, J., Lapierre, C., Jouanin, L., and Boerjan, W. (2001). NMR characterization of lignins from transgenic poplars with suppressed caffeic acid O-methyltransferase activity. *J. Chem. Soc., Perkin Trans.* 1, 2939–2945. doi:10.1039/b107219f.

Meng, X. Z., Crestini, C., Ben, H. X., Hao, N. J., Pu, Y. Q., Ragauskas, A. J., et al. (2019). Determination of hydroxyl groups in biorefinery resources via quantitative 31P NMR spectroscopy. *Nat. Protoc.* 14, 2627–2647. doi:10.1038/s41596-019-0191-1.

Muley, P. D., Mobley, J. K., Tong, X., Novak, B., Stevens, J., Moldovan, D., et al. (2019). Rapid microwave-assisted biomass delignification and lignin depolymerization in deep eutectic solvents. *Energy Convers. Manag.* 196, 1080–1088. doi:10.1016/j.enconman.2019.06.070.

Ragauskas, A. J., Beckham, G. T., Biddy, M. J., Chandra, R., Chen, F., Davis, M. F., et al. (2014). Lignin valorization: improving lignin processing in the biorefinery. *Science* 344, 1246843. doi:10.1126/science.1246843.

Rastogi, M., and Shrivastava, S. (2017). Recent advances in second generation bioethanol production: an insight to pretreatment, saccharification and fermentation processes. *Renew. Sustain. Energy Rev.* 80, 330–340. doi:10.1016/j.rser.2017.05.225.

Satlewal, A., Agrawal, R., Bhagia, S., Sangoro, J., and Ragauskas, A. J. (2018). Natural deep eutectic solvents for lignocellulosic biomass pretreatment: recent developments, challenges and novel opportunities. *Biotechnol. Adv.* 36, 2032–2050. doi:10.1016/j.biotechadv.2018.08.009.

Sette, M., Wechselberger, R., and Crestini, C. (2011). Elucidation of lignin structure by quantitative 2D NMR. *Chem. Eur J.* 17, 9529–9535. doi:10.1002/chem.201003045.

Shen, X.-J., Chen, T., Wang, H.-M., Mei, Q., Yue, F., Sun, S., et al. (2019a). Structural and morphological transformations of lignin macromolecules during bio-based deep eutectic solvent (DES) pretreatment. *ACS Sustain. Chem. Eng.* 8, 2130. doi:10.1021/acssuschemeng.9b05106.

Shen, X.-J., Wen, J.-L., Mei, Q.-Q., Chen, X., Sun, D., Yuan, T.-Q., et al. (2019b). Facile fractionation of lignocelluloses by biomass-derived deep eutectic solvent (DES) pretreatment for cellulose enzymatic hydrolysis and lignin valorization. *Green Chem.* 21, 275–283. doi:10.1039/C8GC03064B.

Sluiter, A., Hames, B., Ruiz, R., Scarlata, C., Sluiter, J., Templeton, D., et al. (2008). *Determination of structural carbohydrates and lignin in biomass*. Golden: CO: National Renewable Energy Laboratory (NREL).

Smith, E. L., Abbott, A. P., and Ryder, K. S. (2014). Deep eutectic solvents (DESs) and their applications. *Chem. Rev.* 114, 11060–11082. doi:10.1021/cr300162p.

Soltanian, S., Aghbashlo, M., Almasi, F., Hosseinzadeh-Bandbafha, H., Nizami, A.-S., Ok, Y. S., et al. (2020). A critical review of the effects of pretreatment methods on the exergetic aspects of lignocellulosic biofuels. *Energy Convers. Manag.* 212, 112792. doi:10.1016/j.enconman.2020.112792.

Sun, R., Tomkinson, J., Sun, X. F., and Wang, N. J. (2000). Fractional isolation and physico-chemical characterization of alkali-soluble lignins from fast-growing poplar wood. *Polymer* 41, 8409–8417. doi:10.1016/S0032-3861(00)00190-7.

Sun, Z., Fridrich, B., de Santi, A., Elangovan, S., and Barta, K. (2018). Bright side of lignin depolymerization: toward new platform chemicals. *Chem. Rev.* 118, 614–678. doi:10.1021/acs.chemrev.7b00588.

Tan, Y. T., Ngoh, G. C., and Chua, A. S. M. (2019). Effect of functional groups in acid constituent of deep eutectic solvent for extraction of reactive lignin. *Bioresour. Technol.* 281, 359–366. doi:10.1016/j.biortech.2019.02.010.

Wang, S., Li, H., Xiao, L.-P., and Song, G. (2020). Unraveling the structural transformation of wood lignin during deep eutectic solvent treatment. *Front. Energy Res.* 8, 48. doi:10.3389/fenrg.2020.00048.

Wen, J.-L., Yuan, T.-Q., Sun, S.-L., Xu, F., and Sun, R.-C. (2014). Understanding the chemical transformations of lignin during ionic liquid pretreatment. *Green Chem.* 16, 181–190. doi:10.1039/C3GC41752B.

Xiao, L.-P., Wang, S., Li, H., Li, Z., Shi, Z.-J., Xiao, L., et al. (2017). Catalytic hydrogenolysis of lignins into phenolic compounds over carbon nanotube supported molybdenum oxide. *ACS Catal.* 7, 7535–7542. doi:10.1021/acscatal.7b02563.

Zhang, C.-W., Xia, S.-Q., and Ma, P.-S. (2016). Facile pretreatment of lignocellulosic biomass using deep eutectic solvents. *Bioresour. Technol.* 219, 1–5. doi:10.1016/j.biortech.2016.07.026.

Zhang, Z., Song, J., and Han, B. (2017). Catalytic transformation of lignocellulose into chemicals and fuel products in ionic liquids. *Chem. Rev.* 117, 6834–6880. doi:10.1021/acs.chemrev.6b00457.

Conflict of Interest: The authors declare that the research was conducted in the absence of any commercial or financial relationships that could be construed as a potential conflict of interest.

frontiers in Energy Research

ORIGINAL RESEARCH
published: 30 March 2021
doi: 10.3389/fenrg.2021.640337

Efficient Synthesis of Pinoresinol, an Important Lignin Dimeric Model Compound

Fengxia Yue[1,2,3]*, *Wu Lan*[1], *Liming Zhang*[3], *Fachuang Lu*[1,2]*, *Runcang Sun*[4] and *John Ralph*[2]

[1] State Key Laboratory of Pulp and Paper Engineering, South China University of Technology, Guangzhou, China, [2] Department of Biochemistry and The DOE Great Lakes Bioenergy Research Center, The Wisconsin Energy Institute, University of Wisconsin, Madison, WI, United States, [3] Guangxi Key Laboratory of Clean Pulp and Papermaking and Pollution Control, College of Light Industry and Food Engineering, Guangxi University, Nanning, China, [4] Center for Lignocellulose Science and Engineering, School of Light Industry and Chemical Engineering, Dalian Polytechnic University, Dalian, China

Pinoresinol is a high-value monolignol-derived lignan used in plant defense and with human health-supporting effects. The synthetic yield and isolation efficiency of racemic pinoresinol from coniferyl alcohol by conventional radical coupling methods is sub-optimal. In this work, a facile and efficient synthetic approach was developed to synthesize pinoresinol with much higher yield. By using 5-bromoconiferyl alcohol, which was synthesized in high yield from 5-bromovanillin, to make 5,5′-bromopinoresinol via a peroxidase-mediated radical coupling reaction takes advantage of the smaller variety of radical coupling products from the 5-substituted monolignol, producing simpler product mixtures from which 5,5′-bromopinoresinol may be readily crystalized with good yield (total yield of 44.1% by NMR; isolated crystalline yield of 24.6%). Hydro-debromination of the crystalline 5,5′-bromopinoresinol to pinoresinol was essentially quantitative. Gram quantities of pinoresinol were conveniently synthesized by using this approach. This simple alternative pathway to make pinoresinol will impact pinoresinol-related research including structural characterization and modification of lignins, as well as clinical applications of pinoresinol and its derivatives.

Keywords: 5-bromoconiferyl alcohol, bromopinoresinol, coniferyl alcohol, radical coupling, lignin

OPEN ACCESS

Edited by:
Liandong Zhu,
Wuhan University, China

Reviewed by:
Anna Kärkönen,
Natural Resources Institute Finland (Luke), Finland
Yunqiao Pu,
Oak Ridge National Laboratory (DOE), United States
Toshiyuki Takano,
Kyoto University, Japan

***Correspondence:**
Fengxia Yue
yuefx@scut.edu.cn
Fachuang Lu
fachuanglu@wisc.edu

Specialty section:
This article was submitted to Bioenergy and Biofuels, a section of the journal Frontiers in Energy Research

Received: *11 December 2020*
Accepted: *05 March 2021*
Published: *30 March 2021*

Citation:
Yue F, Lan W, Zhang L, Lu F, Sun R and Ralph J (2021) Efficient Synthesis of Pinoresinol, an Important Lignin Dimeric Model Compound. Front. Energy Res. 9:640337. doi: 10.3389/fenrg.2021.640337

INTRODUCTION

Pinoresinol structures with a β-β′-linkage between two monolignols are important structures in the lignins from softwoods, dicots, and monocots, especially in some technical lignins from hardwood (Yue et al., 2012b; Li et al., 2020). Not only do they affect the lignification pathway, but also have implications for the biorefinery. Pinoresinol is also a vital lignan, a usually optically-active dimerization product of two coniferyl alcohol monolignols, that displays important physiological functions *in planta*, as well as in human nutrition and medicine (Lewis et al., 1995; Pellegrini et al., 2010). Lignans have drawn enormous attention because of their abundance in nature and their various biological activities including antibacterial, antifungal, antiviral, antioxidative, and/or cytotoxic properties (Paska et al., 2002; Min et al., 2003; Umezawa, 2003; Milder et al., 2005; Suzuki and Umezawa, 2007; Lin et al., 2016). Such lignans are commonly found as optically active β-β′-linked dimers (Davin et al., 1992; Pare et al., 1994), such as pinoresinol and syringaresinol as shown in **Figure 1**. Some lignans are structurally similar to dilignols, or units in oligolignols, that are

metabolites involved in lignification (Eberhardt et al., 1993; Pare et al., 1994; Morreel et al., 2004). Chiral (+)-pinoresinol and (−)-pinoresinol are formed through a dirigent-protein-mediated radical coupling of coniferyl alcohol (Halls et al., 2004). However, racemic pinoresinol and oligomers containing pinoresinol are often found in plant metabolites destined for lignin, a racemic polymer that contains significant amounts of pinoresinol substructures, especially for softwood lignins or plants that are down-regulated in syringyl-specific genes (Eberhardt et al., 1993; Ralph et al., 1999).

As one of the structurally simplest lignin dimers, pinoresinol is an important nucleation site formed by the self-coupling of coniferyl alcohol during lignification (Umezawa, 2003; Zhang et al., 2003; Ralph J. et al., 2004; Schroeder et al., 2006; Ralph et al., 2008; Yue et al., 2012a). The structure is frequently present in the lignin of woody and fibrous plants, but the amount varies significantly in different plants. Because of its wide range of bioactivities and its chemical structure related to lignin, pinoresinol and its lignan analog play very important roles in pharmaceutical research, lignin biosynthesis, and other related studies (Umezawa, 2003; Zhang et al., 2003; Ralph J. et al., 2004; Jung et al., 2006; Ralph et al., 2008; Yue et al., 2012a; Tamura et al., 2014). Moreover, substantial amounts of resinol (β-β′) structures, including pinoresinol and syringaresinol, remained and can be identified in several technical lignins, which is crucial to the phenolation of alkaline lignin, for example (Li et al., 2020; Zhao et al., 2020). Studies on the biosynthesis of pinoresinol structures in lignin, technical lignin modifications, pinoresinol-related lignans, and pinoresinol contributions to a healthy human diet or for disease prevention require easy access to pinoresinol. Normally, commercially available pinoresinol is isolated from natural sources, such as seeds of flax, sesame, whole-grain cereals, legumes, fruits, and some vegetables. Although pinoresinol is widely distributed in vascular plants, the content is at low level (Umezawa, 2003; Ralph et al., 2008; Li et al., 2019). The isolation processes, which involve a series of time-consuming and costly separation/purification steps, are not efficient and at very low yields (such as, 2.6 mg pinoresinol isolated from 8 kg of dried cinnamon) (Milder et al., 2005; Li et al., 2019). It is difficult to isolate sufficient pure pinoresinol and its derivatives from plant materials due to its low content and the complexity of plant extractives. Therefore, current commercial pinoresinol that is isolated from natural sources is expensive [$281 for 10 mg (>95%), Sigma-Aldrich]. Although many synthetic routes have been proposed to make optically active pinoresinol (Davin et al., 1992; Pare et al., 1994; Umezawa, 2003; Feng et al., 2006, 2007; Kim et al., 2010), racemic pinoresinol has been more often prepared from radical coupling of coniferyl alcohol catalyzed by various oxidants including silver oxide, ferric chloride, manganese acetate, or copper acetate, as well as oxidative enzymes (peroxidase or laccase) (Brezny and Alfoldi, 1982; Vermes et al., 1991; Quideau and Ralph, 1994; Zhang et al., 2003; Saliu et al., 2011; Yue et al., 2012a; Tamura et al., 2014). The yields of syringaresinol (analog of pinoresinol) from radical coupling reactions has always been much higher than those of pinoresinol because the occupied C5-position on sinapyl alcohol prevents the production of dimers from other coupling modes (Zhang et al., 2003). Therefore, the difficult access to pinoresinol limits its further exploration in research and clinical applications, and therefore a low-cost, environmentally friendly method is required to address this issue.

Herein we report an efficient synthetic strategy for pinoresinol. In this method, we used 5-bromoconiferyl alcohol for the radical coupling reaction to produce the β-β′-coupled compound as the main product. It is readily crystallized and subsequently hydrodebrominated to produce clean racemic pinoresinol.

EXPERIMENTAL

Materials and Methods

5-Bromovanillin (98%) was purchased from Acros Organics (New Jersey, USA). Horseradish peroxidase (HRP) (EC 1.11.1.7, 181 purpurogallin units per mg solid, type II) was purchased from Sigma Aldrich. All other chemicals and solvents used in this study were purchased from Aldrich (Milwaukee, WI, USA) and used as supplied.

Flash-chromatography was performed on a Biotage® Isolera One (Biotage, Charlottesville, VA) flash-chromatography instrument, using pre-packed (or re-packed) SNAP cartridges (50 or 100 g of silica-gel). Thin-layer chromatography separation was performed on 1 mm normal-phase silica-gel plates, Uniplate™ (UV 254, 20 × 20 cm). All synthesized compounds were characterized by the usual array of NMR. NMR spectra were acquired on a Bruker Biospin (Billerica, MA, USA) AVANCE 500 (500 MHz) spectrometer fitted with a cryogenically cooled 5 mm TCI gradient probe with inverse geometry (proton coils closest to the sample). Spectra were processed using Bruker's Topspin 3.5 (Mac) software. Standard Bruker implementations of one- and two-dimensional (gradient-selected COSY, HSQC and HMBC) NMR experiments were used for routine structural assignments of all synthesized compounds. Typically, 5–10 mg of sample was dissolved in about 0.5 mL deuterated solvent (acetone-d_6), and the central solvent peak (δ_H/δ_C 2.04/29.80) was used as the internal reference.

Synthesis of Pinoresinol

As shown in **Figures 2**, **3**, pinoresinol was synthesized via a simple multi-step route.

5-Bromovanillin acetate **2** was prepared by acetylation of 5-bromovanillin **1** with pyridine and acetic anhydride (1:1, v/v), which was accomplished in the traditional way using acetic anhydride in pyridine (∼100% yield). Compound **2**, NMR (acetone-d_6, **Supplementary Figure 1**) δ_H: 2.35 (3H, s, OAc), 3.95 (3H, s, OMe), 7.60 (1H, d, $J = 1.61$, A2), 7.80 (1H, d, $J = 1.61$, A6), 9.97 (1H, s, Hα); δ_C: 20.19 (OAc), 56.99 (A-OMe), 111.73 (A2), 118.45 (A5), 127.21 (A6), 136.71 (A1), 143.48 (A4), 154.33 (A3), 167.60 (OAc), 190.87 (α).

Compound **3** was synthesized via a Horner-Wadsworth-Emmons reaction (HWE reaction) from compound **2** (Ralph et al., 1992; Brandt et al., 1998; Touchard, 2004). Briefly, NaH (sodium hydride 60% dispersion in mineral oil, 3.62 g, 90.42 mmol) was washed with 50 mL cyclohexane by stirring more than

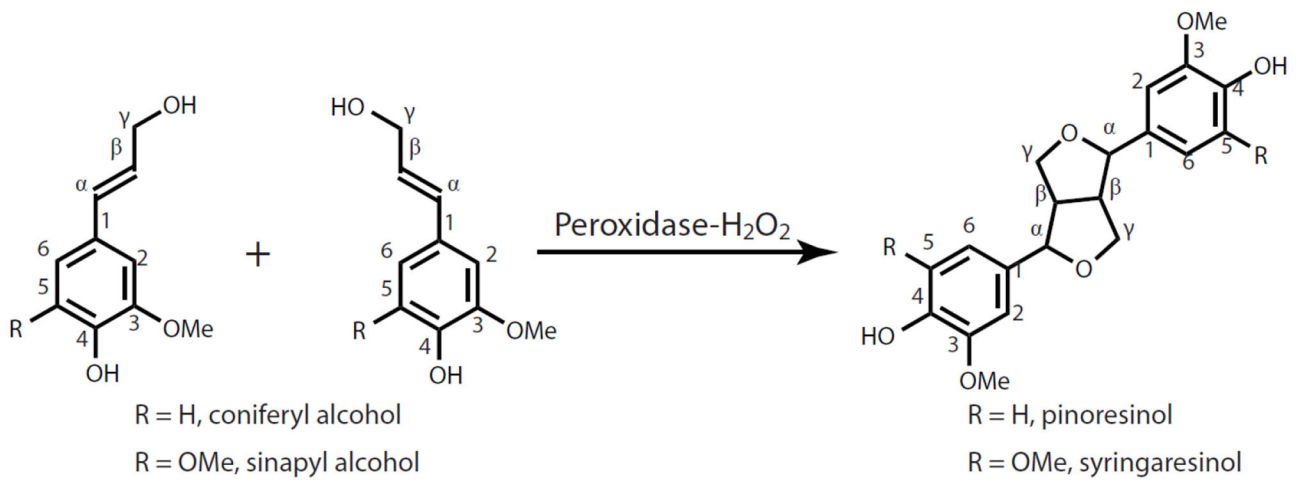

FIGURE 1 | Traditional pathways for synthesis of pinoresinol and syringaresinol.

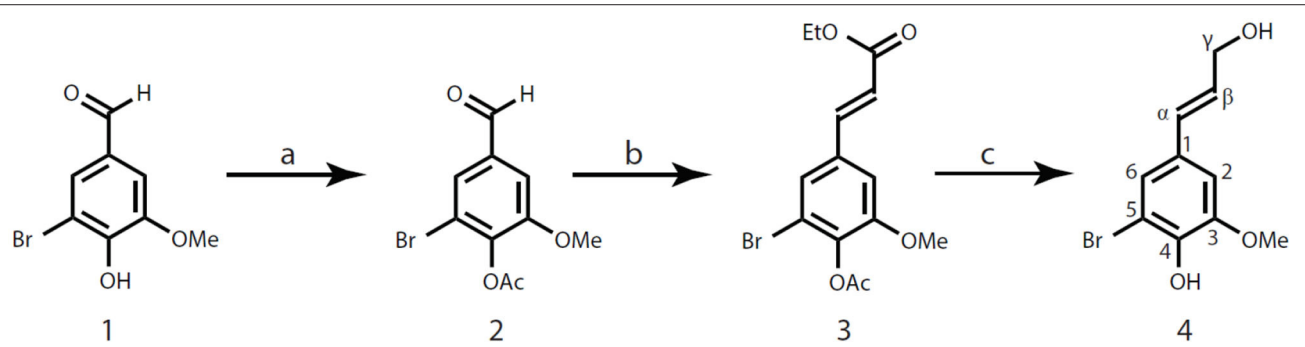

FIGURE 2 | Synthesis of 5-bromoconiferyl alcohol 4. (a) pyridine, acetic anhydride; (b) NaH, triethyl phosphonoacetate, THF; (c) diisobutylaluminum hydride (DIBAL-H), cyclohexane.

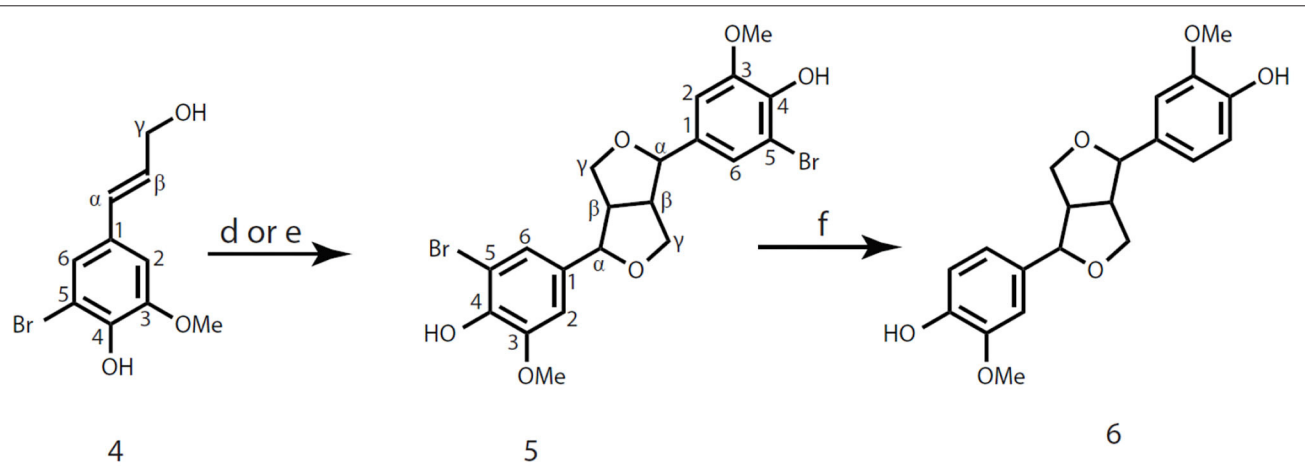

FIGURE 3 | Synthesis of pinoresinol from 5-bromoconiferyl alcohol 4. (d) H_2O_2, peroxidase; acetone-buffer; (e) $FeCl_3$, acetone-buffer; (f) Et_3N, Pd/C, H_2, methanol.

10 min in the reaction flask and the supernatant was carefully removed, to which 100 mL THF (tetrahydrofuran anhydrous, 99.9%) was added. The resultant slurry was continuously stirred for more than 5 min at 0°C (ice-water bath) before triethyl phosphonoacetate (10.14 g, 45.22 mmol) was added dropwise. After the addition of triethyl phosphonoacetate, the resulting solution was well-stirred at 0°C for 20 min until gas evolution ceased. 5-Bromovanillin acetate **2** (11.23 g, 41.11 mmol) dissolved in 10 mL THF was slowly added to the yellow solution in ice-water bath. The reaction mixture was kept stirring at 0°C for 1 h and monitored by TLC (*n*-hexanes/EtOAc, 5:1, v/v). After the reaction was completed, the excess agent was quenched by adding 1 M aqueous HCl solution to a pH value < 3. Then, the reaction mixture was evaporated to remove THF. The resultant product was re-dissolved in EtOAc and water, and extracted with EtOAc (300 mL × 2). The combined organic phase was washed with distilled water and saturated NH_4Cl solution, dried over anhydrous $MgSO_4$, filtered, and concentrated under reduced pressure at 40°C. The total recovery of crude product was 13.45 g (39.33 mmol, 95.7%). The crude product was dissolved and recrystallized in *n*-hexanes/EtOAc (5:1, v/v) to obtain crystalline compound **3** with a yield of 70.9%. Compound **3**, NMR (acetone-d_6, **Supplementary Figure 2**) δ_H: 1.27 (3H, t, $J = 7.09$, Aγ-OCH$_2$*Me*), 2.31 (3H, s, OAc), 3.92 (3H, s, OMe), 4.20 (2H, q, $J = 7.13$, Aγ-OC*H*$_2$Me), 6.62 (1H, d, $J = 15.96$, β), 7.49 (1H, d, $J = 1.81$, A2), 7.55 (1H, d, $J = 1.81$, A6), 7.60 (1H, d, $J = 15.96$, α); δ_C: 14.53 (Aγ-OCH$_2$*Me*), 20.21 (OAc), 56.87 (OMe), 60.90 (Aγ-OC*H*$_2$Me), 111.64 (A2), 118.02 (A5), 120.81 (β), 125.08 (A6), 135.21 (A1), 140.10 (A4), 143.08 (α), 153.84 (A3), 166.68 (Aγ), 167.87 (OAc). Melting point, 104.5–106.0°C.

Compound **4** was produced via DIBAL-H (di-iso-butyl-aluminum hydride) reduction of ethyl 5-bromoferulate **3** in n-hexanes as previously described (Quideau and Ralph, 1992). Ethyl 5-bromoferulate acetate **3** (6 g, 17.54 mmol) was added into a 500 mL reaction vessel and dissolved in 50 mL cyclohexane after which it was kept stirring for 5 min in an ice-water bath (to make sure reaction mixture at 0 °C). DIBAL-H (105 mL, 1.0 M solution in *n*-hexanes) was slowly added into the vigorously stirring solution via syringe, reaction vessel was sealed immediately with plastic cap after the addition. The reaction mixture turned clear in about 10 min, and was kept stirring at 0°C (ice-water bath) for 1 h. After the consumption of starting material **3** (monitored by TLC), the reaction was carefully quenched by with ethanol (5 mL) added dropwise at 0°C and released the gas generated at the same time. Subsequent addition of 1 M aqueous HCl solution until the mixture turned clear and colorless. The final pH value of the solution was < 3, and then extracted with EtOAc (200 mL × 2). Combined extracts were washed with saturated brine, dried over anhydrous $MgSO_4$, filtered, and evaporated under reduced pressure at 40°C to result in compound **4** as light yellow oil with the isolated yield over 90%. Compound **4**, NMR (acetone-d_6, **Supplementary Figure 3**) δ_H: 3.88 (3H, s, OMe), 4.20 (2H, dd, $J = 5.35, 1.68$, γ), 6.29 (1H, dt, $J = 15.90, 5.27$; β), 6.47 (1H, dt, $J = 15.90, 1.55$; α), 7.06 (1H, d, $J = 1.88$, A2), 7.11 (1H, d, $J = 1.88$, A6); δ_C: 56.56 (OMe), 63.07 (γ), 108.86 (A2), 109.27 (A5), 123.58 (A6), 128.77 (α), 129.80 (β), 130.96 (A1), 144.29 (A4), 149.04 (A3).

5,5′-Bromopinoresinol **5** was then prepared via two different coupling reactions catalyzed by peroxidase or $FeCl_3$ from 5-bromoconiferyl alcohol **4** (**Figure 3**).

Catalyzed by Peroxidase

5-Bromoconiferyl alcohol **4** (207 mg, 0.80 mmol) was dissolved in acetone (20 mL), to which phosphate buffer (200 mL, pH 5.0) was slowly added while kept stirring. (Note: We recognize that the buffering capacity is low for this system, but it is non-nucleophilic, so doesn't produce undesired quinone-methide-trapping products, and has been used reproducibly over many decades for radical coupling reactions, including for the preparation of synthetic lignins.) Then, H_2O_2-urea complex (38.2 mg, 1.02 eq. relative to the phenols) dissolved in buffer (∼2 mL) was added into the acetone-buffer system and followed by the addition of peroxidase (0.1 mg in 1 mL buffer). The solution turned light yellow and then became cloudy immediately after the addition of peroxidase. The reaction mixture was continuously stirring at room temperature for 45 min until the starting material **4** disappeared (monitored by TLC, *n*-hexanes/EtOAc, 1:1, v/v). The reaction was quenched by adding 1 M aqueous HCl solution (2 mL) to pH <3. 4,4′-Ethylenebisphenol (20.9 mg, 0.098 mmol) was then added as internal standard for quantification, and the resultant mixture was extracted with EtOAc (80 mL × 3). The combined organic phase was washed with saturated brine, dried over anhydrous $MgSO_4$, and concentrated under reduced pressure at 40°C. One part of the crude product mixture (20–30 mg dissolved in 0.6 mL acetone-d_6) was used for NMR directly. The calculated yield of product 5,5′-bromopinoresinol **5** was 44.1%, based on ^{1}H NMR integration. Another fraction of the products (about 55 mg) was loaded onto a 1 mm silica-gel plate and developed twice with EtOAc/*n*-hexanes (1:1). Each isolated product was characterized by NMR. Internal standard (5 mg) and 15 mg of 5,5′-bromopinoresinol **5** were isolated from the TLC plate. The yield of 5,5′-bromopinoresinol **5** was 30.4% after TLC purification.

Catalyzed by $FeCl_3$

5-Bromoconiferyl alcohol **4** (104 mg, 0.4 mmol) was dissolved in acetone (12.5 mL) to which phosphate buffer (125 mL, pH 5.02) was added. Then, iron (III) chloride ($FeCl_3$, 65 mg, 1.0 eq. relative to the phenols) dissolved in buffer (1–2 mL) was added into the acetone-buffer system. The reaction system was kept stirring at room temperature for 60 min until TLC (*n*-hexanes/EtOAc, 1:1, v/v) showed no starting material **4** remaining. Then, 4,4′-ethylenebisphenol (10.51 mg, 0.049 mmol) was added into the reaction mixture as an internal standard. Following the same workup procedure as for the peroxidase-catalyzed reaction, the crude product was used for NMR measurement and TLC purification. The calculated yield of product 5,5′-bromopinoresinol **5** was 30.1% (based on ^{1}H NMR integration) whereas the isolated yield was 20.4% (by TLC plate separation).

Scaled-Up Coupling Reaction of 5-Bromoconiferyl Alcohol 4

Scaled-up coupling of 5-bromoconiferyl alcohol **4** was carried out under the peroxidase-catalyzed condition as abovementioned. Briefly, 5-bromoconiferyl alcohol **4** (4.08 g, 15.75 mmol) was dissolved in acetone-phosphate buffer system (500 mL/2 L, v/v), followed by the addition of H_2O_2-urea complex (814 mg, 8.66 mmol) and peroxidase (10 mg) dissolved in the buffer, respectively. After the addition of peroxidase, the solution turned bright yellow immediately and then became a yellow slurry in 2 min. The reaction mixture was kept stirring at room temperature and monitored by TLC (*n*-hexanes/EtOAc, 1:1, v/v). The reaction was quenched when it was completed by adding 1 M aqueous HCl to pH <3 and then the acetone was evaporated. The resulting mixture was extracted with EtOAc (400 mL × 3). The combined organic phase was washed with brine, dried over anhydrous $MgSO_4$, and concentrated under reduced pressure. The crude product was purified by flash-chromatography (Biotage, 100 g silica gel column × 2) using *n*-hexanes/EtOAc (1:1, v/v) to obtain compound 5,5′-bromopinoresinol **5**. Compound **5** was then re-dissolved and crystallized from ethanol, with an isolated crystalline yield of 24.6%. Compound **5**, NMR (acetone-d_6, **Supplementary Figure 4**) δ_H: 3.10 (2H, m, β), 3.84 (2H, d, J = 3.68, γ1), 3.85 (6H, s, OMe), 4.22 (2H, m, γ2), 4.69 (2H, d, J = 4.10, α), 6.99 (2H, d, J = 1.86, A2), 7.11 (2H, dd, J = 1.88, 0.51; A6); δ_C: 55.03 (β), 56.60 (OMe), 72.29 (γ), 85.77 (α), 108.99 (A5), 109.38 (A2), 122.64 (A6), 134.99 (A1), 144.05 (A4), 148.91 (A3). Melting point, 210.2–211.5°C.

Pinoresinol **6** was produced via debromination of compound **5** under catalytic hydrogenation conditions at the presence of palladium on activated carbon (Pd/C, 10 wt% loading) and Et_3N in methanol (Sajiki et al., 2002). 5,5′-Bromopinoresinol **5** (810 mg, 1.57 mmol) was dissolved in 80 mL methanol (1% solution of compound **5**) with stirring, followed by the addition of Et_3N (381.3 mg, 3.77 mmol, 1.2 eq. vs. bromine) and Pd/C (24.3 mg, 10% Palladium on activated carbon, 3% of the weight of the aromatic bromide). The resulting mixture was kept stirring under a hydrogen-filled balloon for 2 h until TLC (CH_2Cl_2/MeOH, 20:1, v/v) showed that all compound **5** had been consumed. The solid catalyst was filtered off using a polyamide membrane (Whatman, 0.2 μm). The resulting filtrate was evaporated to remove methanol, then extracted with distilled water and EtOAc (100 mL × 2). The combined organic phase was washed with saturated NH_4Cl, dried over anhydrous $MgSO_4$, and concentrated under reduced pressure at 40°C to obtain pinoresinol **6** (560 mg, 1.57 mmol) as a light-yellow oil with the isolated yield of ∼100%. The obtained pinoresinol could be crystalized from the oily state (kept in refrigerator for a long time) or recrystallized in ethanol/n-hexanes and gave white crystals. Compound **6**, NMR (acetone-d_6, **Supplementary Figure 5**) δ_H: 3.07 (2H, m, β), 3.79 (2H, dd, J = 9.05, 3.80, γ1), 3.83 (6H, s, OMe), 4.19 (2H, m, γ2), 4.66 (2H, d, J = 4.32, α), 6.78 (2H, d, J = 8.01, A5), 6.83 (2H, dd, J = 8.15, 1.94; A6), 6.98 (2H, d, J = 1.93, A2), 7.53 (Ar-OH); δ_C: 55.16 (β), 56.14 (OMe), 72.12 (γ), 86.56 (α), 110.47 (A2), 115.46 (A5), 119.54 (A6), 134.08 (A1), 146.76 (A4), 148.21 (A3). The NMR data of compound **6** are consistent with the previously published data (Ralph S. et al., 2004). Melting point, 113.5–114.5°C.

RESULTS AND DISCUSSION

Synthesis of 5,5′-Bromopinoresinol 5

As described above, pinoresinol can be produced by dehydrodimerization of coniferyl alcohol in lignin biosynthesis. Many synthetic routes have been proposed to make optically active or racemic pinoresinol via chemical or enzymatic syntheses by radical coupling of coniferyl alcohol (Brezny and Alfoldi, 1982; Vermes et al., 1991; Davin et al., 1992; Pare et al., 1994; Umezawa, 2003; Zhang et al., 2003; Kim et al., 2006; Saliu et al., 2011; Yue et al., 2012a; Tamura et al., 2014; Ricklefs et al., 2015). Currently, the most commonly used approaches for the synthesis of pinoresinol are using oxidative enzymes (peroxidase or laccase) to catalyze coniferyl alcohol dimerization, though with poor selectivity and yield. The highest yield of pinoresinol that can be achieved by coupling of coniferyl alcohol is reported to be no more than 13% (Ricklefs et al., 2015). The low yield and selectivity resulted in difficult isolation and purification of pinoresinol from the crude mixtures (Sih et al., 1976; Vermes et al., 1991; Davin et al., 1992; Fukuhara et al., 2013). Another reason for the high cost of pinoresinol is that the starting material (coniferyl alcohol) of these reactions is also expensive. On the other hand, syringaresinol that results from homo-coupling of sinapyl alcohol was at much better selectivity and yield. The logical reason is that the substitution by the methoxyl group on the aromatic C-5 position prevents coupling reactions at this site and therefore reduces the number of possible coupling routes, leading to higher selectivity (Vermes et al., 1991; Zhang et al., 2003). This indicates that an ideal way to improve the synthesis of pinoresinol is to suppress the undesired side-reactions by substitution at the C-5 position. We therefore decided to use the 5-bromo analog as a starting substrate anticipating the subsequent efficient elimination of aryl bromine.

Accordingly, an efficient synthetic approach was designed to synthesize pinoresinol with higher yield than that of the conventional radical coupling pathway from coniferyl alcohol (**Figures 2**, **3**). 5-Bromoconiferyl alcohol **4** was used to make 5,5′-bromopinoresinol **5** via a peroxidase-mediated radical coupling reaction for the purpose of producing less complex product mixtures. In this study, we used 5-bromovanillin **1** as starting material as the bromine protects the aromatic C-5 position. Acetylation of 5-bromovanillin **1** using pyridine and acetic anhydride gave a quantitative conversation yield of bromovanillin acetate **2**. Next, an HWE reaction (using triethyl phosphonoacetate) was carried out to produce ethyl 5-bromoferulate **3** from compound **2**. The HWE reaction is a variation of the Wittig olefination reactions (Brandt et al., 1998). It is a chemical reaction of stabilized phosphonate carbanions with aldehydes (or ketones) to produce predominantly (*E*)-alkenes, and is most commonly applied to triesters of phosphono-acetic acid that leads to α,β-unsaturated esters. In

contrast to phosphonium ylides used in the Wittig reaction, phosphonate-stabilized carbanions are more nucleophilic and more basic. Likewise, phosphonate-stabilized carbanions can be alkylated, unlike phosphonium ylides the dialkylphosphate salt by-product is easily removed by aqueous extraction (Maryanoff and Reitz, 1989). In this approach, excess triethyl phosphonoacetate was added to the reaction solution to ensure the complete conversion of compound **2** as the phosphonate can be easily removed during a workup procedure. After the reaction, the obtained product was pure enough for the next step without requiring further purification. The total recovery yield of ethyl 5-bromoferulate **3** achieved 95.7%, and the yield for crystalline products was 70.9%. The following step was DIBAL-H reduction of ethyl 5-bromoferulate **3** to produce 5-bromoconiferyl alcohol **4** with a yield of over 90%. DIBAL-H, being a liquid and miscible in numerous solvents, is a unique and versatile organometallic hydride that has been widely used as reduction reagent for the preparation of fine organic chemicals and pharmaceuticals (Self et al., 1990; Quideau and Ralph, 1992; Yue et al., 2012a). For the reduction of compound **3**, DIBAL-H in *n*-hexanes (1.0 M solution in *n*-hexanes) solution was used instead of DIBAL-H in toluene. Although no significant difference on reaction activity between DIBAL-H hexane solution and toluene solution, using the n-hexanes solution simplifies the work-up procedure since it can easily form phase separation from water during extraction (Quideau and Ralph, 1992). It is important to note that the reaction should be slowly quenched with ethanol first, and then fully quenched with dilute HCl (1 M). Both ethanol and dilute HCl were added carefully and slowly while the reaction mixture was placed in ice-water bath and stirred vigorously. Ethanol was first added to degrade excess DIBAL-H and cleave the aluminum-oxygen bond. No precipitates can be observed during the ethanol quenching stage. Aqueous 1 M HCl was then slowly added and white precipitates quickly generated, and continued until the precipitates disappeared (normally when pH <3). In particular, the reaction during quenching process, to some extent, was delayed when adding ethanol and dilute HCl, Slow additions of ethanol and dilute HCl are therefore necessary to avoid the rapid generation of gas. Concentrated HCl is not recommended for the quenching process as it will destroy the product. This step provided a high yield and purity of 5-bromoconiferyl alcohol **4** in 90% of yield with almost 100% for purity. As the 5-bromoconiferyl alcohol **4** is not stable to long-term storage, it should be used immediately for the next coupling reaction.

For the synthesis of pinoresinol and syringaresinol, radical coupling of coniferyl alcohol and sinapyl alcohol catalyzed by peroxidase(s) in the presence of H_2O_2 are the traditional methods (Vermes et al., 1991; Davin et al., 1992; Zhang et al., 2003). In this study, for a better comparison purpose, coupling reactions of 5-bromoconiferyl alcohol **4** catalyzed by two different catalysts, peroxidase and $FeCl_3$, were studied. Quantitative ^{1}H NMR characterization showed that the yield of 5,5′-bromopinoresinol **5** catalyzed by peroxidase was 44.1%, which was much higher than that of coupling of coniferyl alcohol (at most 10–12%) (Vermes et al., 1991; Quideau and Ralph, 1994; Ricklefs et al., 2015). The 5,5′-bromopinoresinol **5** can be purified by TLC separation to give 30.4% isolation yield and by recrystallization in hexane/ethanol to give 24.6% crystal yield. For the radical coupling catalyzed by $FeCl_3$, the yield of 5,5′-bromopinoresinol was 30.1% from ^{1}H NMR, not 58% as reported previously (Brezny and Alfoldi, 1982). In this case, the isolated yield from TLC purification was 20%, accounting for about 66% of the total obtained 5,5′-bromopinoresinol, which was consistent with the case using peroxidase as catalyst.

By comparison, the yield of 5,5′-bromopinoresinol obtained via peroxidase-catalyzed radical coupling was higher, about 1.5 times, than that from $FeCl_3$ catalyzed coupling. Nevertheless, in contrast to sinapyl alcohol, the β-β′ bond formation was not the dominant radical coupling pathway for the coupling reaction of 5-bromoconiferyl alcohol. More side-reactions than expected still occurred even with the aromatic C-5 position blocked by bromine, such as β-O-4 dimer, etc. (see **Supplementary Figure 6**). Additionally, it is worth pointing out that, the molar equivalents of H_2O_2 used and the reaction time are two key variables in the radical coupling reactions. There will be no pinoresinol formed if H_2O_2 was omitted, whereas the product will be polymerized (deeply colored precipitates) with sharply decreased pinoresinol yields (lower than 10%) as reaction time increased once the H_2O_2 was overcharged. In this study, 1.1 equivalents (relative to the phenols) of H_2O_2 were used to ensure full conversion of 5-bromoconiferyl alcohol **4** but to avoid further coupling reactions beyond dimerization. The reaction was quenched after 45 min to minimize formation of oligomers. After the normal workup procedure, crystalline product 5,5′-bromopinoresinol **5** was easily obtained after column purification.

Debromination of 5,5′-Bromopinoresinol 5

In the last step, a mild and efficient one-pot method was modified and used for the hydrodebromination of 5,5′-bromopinoresinol **5** (Sajiki et al., 2002). The reaction proceeded at room temperature under catalytic hydrogenation conditions, which gave a nearly 100% yield of the required product. It is worth pointing out that the pinoresinol obtained after hydro-debromination was pure enough to crystalize without initial purification. No side-reactions occurred during the debromination, and the NMR spectra of the final product confirmed the near 100% purity of the pinoresinol.

CONCLUSION

In summary, we have developed a feasible method for the synthesis of pinoresinol with higher yield than that of previous studies. The formation of the β-β′ bond during radical coupling was greatly improved by using 5-bromoconiferyl alcohol, an aromatic compound in which the C-5 position is protected by bromine, over the conventional use of coniferyl alcohol. The yield of 5,5′-bromopinoresinol **5** (which can be quantitatively converted into pinoresinol) obtained via peroxidase-catalyzed radical coupling was much higher than that via an $FeCl_3$-catalyzed reaction. With the relatively higher yield, it provides

a feasible way to obtain pinoresinol on a large scale, which will benefit the various research activities on pinoresinol structural characterization in lignins, in human nutrition, and for pharmacological applications.

DATA AVAILABILITY STATEMENT

The original contributions presented in the study are included in the article/**Supplementary Material**, further inquiries can be directed to the corresponding authors.

AUTHOR CONTRIBUTIONS

FY designed, performed the synthesis and analysis, wrote the paper, and obtained funding in China. WL aided in the analysis and synthesized some starting compounds. FL designed the project and obtained funding in China. LZ and RS aided in the analysis. JR advised on experiments, aided in analysis, and obtained the funding in the US. All authors were involved in the writing and revisions.

FUNDING

The authors are grateful to the financial support for this work by the National Natural Science Foundation of China (31870560 and 21908072), Natural Science Foundation of Guangdong Province (2018A030313840), Guangxi Key Laboratory of Clean Pulp and papermaking and pollution control (KF201805-5), and the DOE Great Lakes Bioenergy Research Center (DOE BER Office of Science DE-SC0018409).

SUPPLEMENTARY MATERIAL

The Supplementary Material for this article can be found online at: https://www.frontiersin.org/articles/10.3389/fenrg.2021.640337/full#supplementary-material

REFERENCES

Brandt, P., Norrby, P. O., Martin, I., and Rein, T. (1998). A quantum chemical exploration of the Horner-Wadsworth-Emmons reaction. *J. Org. Chem.* 63, 1280–1289. doi: 10.1021/jo971973t

Brezny, R., and Alfoldi, J. (1982). Prins reaction in the synthesis of lignin model compounds: 3. Alternative synthesis of pinoresinol, coniferyl aldehyde and guaiacyl vinyl ketone. *Chem. Zvesti* 36, 267–276.

Davin, L. B., Bedgar, D. L., Katayama, T., and Lewis, N. G. (1992). On the stereoselective synthesis of (+)-pinoresinol in *Forsythia Suspensa* from its achiral precursor, coniferyl alcohol. *Phytochemistry* 31, 3869–3874. doi: 10.1016/S0031-9422(00)97544-7

Eberhardt, T. L., Bernards, M. A., He, L., Davin, L. B., Wooten, J. B., and Lewis, N. G. (1993). Lignification in cell suspension cultures of *Pinus taeda*: *in situ* characterization of a gymnosperm lignin. *J. Biol. Chem.* 268, 21088–21096. doi: 10.1016/S0021-9258(19)36897-8

Feng, S. M., Gan, Z. J., Zhai, X. F., Fu, P. F., and Sun, W. J. (2006). Content comparison of pinoresinol diglucoside in original and reborn bark of *Eucommia ulmoides*. *Zhong Yao Cai* 29, 792–794. doi: 10.3321/j.issn:1001-4454.2006.08.017

Feng, S. M., Ni, S. F., and Sun, W. J. (2007). Preparative isolation and purification of the lignan pinoresinol diglucoside and liriodendrin from the bark of *Eucommia ulmoides* Oliv. by high speed countercurrent chromatography. *J. Liq. Chromatogr. Relat. Technol.* 30, 135–145. doi: 10.1080/10826070601036324

Fukuhara, Y., Kamimura, N., Nakajima, M., Hishiyama, S., Hara, H., Kasai, D., et al. (2013). Discovery of pinoresinol reductase genes in sphingomonads. *Enzyme Microb. Technol.* 52, 38–43. doi: 10.1016/j.enzmictec.2012.10.004

Halls, S. C., Davin, L. B., Kramer, D. M., and Lewis, N. G. (2004). Kinetic study of coniferyl alcohol radical binding to the (+)-pinoresinol forming dirigent protein. *Biochemistry* 43, 2587–2595. doi: 10.1021/bi035959o

Jung, J. C., Kim, J. C., Moon, H. I., and Park, O. S. (2006). Stereoselective total synthesis of furofuran lignans through dianion aldol condensation. *Tetrahedron Lett.* 47, 6433–6437. doi: 10.1016/j.tetlet.2006.06.127

Kim, H. Y., Kim, J. K., Choi, J. H., Jung, J. Y., Oh, W. Y., Kim, D. C., et al. (2010). Hepatoprotective effect of pinoresinol on carbon tetrachloride-induced hepatic damage in mice. *J. Pharmacol. Sci.* 112, 105–112. doi: 10.1254/jphs.09234FP

Kim, J. C., Kim, K. H., Jung, J. C., and Park, O. S. (2006). An efficient asymmetric synthesis of furofuran lignans: (+)-sesamin and (-)-sesamin. *Tetrahedron Asymmetry* 17, 3–6. doi: 10.1016/j.tetasy.2005.11.007

Lewis, N. G., Kato, M. J., Lopes, N., and Davin, L. B. (1995). Lignans - diversity, biosynthesis, and function. *Chem. Amazon* 588, 135–167. doi: 10.1021/bk-1995-0588.ch013

Li, A. L., Li, G. H., Li, Y. R., Wu, X. Y., Ren, D. M., Lou, H. X., et al. (2019). Lignan and flavonoid support the prevention of cinnamon against oxidative stress related diseases. *Phytomedicine* 53, 143–153. doi: 10.1016/j.phymed.2018.09.022

Li, S. X., Shi, L. L., Wang, C., Yue, F. X., and Lu, F. C. (2020). Naphthalene structures derived from lignins during phenolation. *Chemsuschem* 13, 5549–5555. doi: 10.1002/cssc.202001693

Lin, B., Sun, L. N., Xin, H. L., Nian, H., Song, H. T., Jiang, Y. P., et al. (2016). Anti-inflammatory constituents from the root of Litsea cubeba in LPS-induced RAW 264.7 macrophages. *Pharm. Biol.* 54, 1741–1747. doi: 10.3109/13880209.2015.1126619

Maryanoff, B. E., and Reitz, A. B. (1989). The wittig olefination reaction and modifications involving phosphoryl-stabilized carbanions - stereochemistry, mechanism, and selected synthetic aspects. *Chem. Rev.* 89, 863–927. doi: 10.1021/cr00094a007

Milder, I. E., Arts, I. C., Van De Putte, B., Venema, D. P., and Hollman, P. C. (2005). Lignan contents of Dutch plant foods: a database including lariciresinol, pinoresinol, secoisolariciresinol, and matairesinol. *Br. J. Nutr.* 93, 393–402. doi: 10.1079/BJN20051371

Min, T. P., Kasahara, H., Bedgar, D. L., Youn, B. Y., Lawrence, P. K., Gang, D. R., et al. (2003). Crystal structures of pinoresinol-lariciresinol and phenylcoumaran benzylic ether reductases and their relationship to isoflavone reductases. *J. Biol. Chem.* 278, 50714–50723. doi: 10.1074/jbc.M308493200

Morreel, K., Ralph, J., Kim, H., Lu, F., Goeminne, G., Ralph, S. A., et al. (2004). Profiling of oligolignols reveals monolignol coupling conditions in lignifying poplar xylem. *Plant Physiol.* 136, 3537–3549. doi: 10.1104/pp.104.049304

Pare, P. W., Wang, H. B., Davin, L. B., and Lewis, N. G. (1994). (+)-Pinoresinol synthase - a stereoselective oxidase catalyzing 8,8′-lignan formation in *Forsythia-Intermedia*. *Tetrahedron Lett.* 35, 4731–4734. doi: 10.1016/S0040-4039(00)76953-X

Paska, C., Innocenti, G., Ferlin, M., Kunvari, M., and Laszlo, M. (2002). Pinoresinol from *Ipomoea cairica* cell cultures. *Nat. Prod. Lett.* 16, 359–363. doi: 10.1080/1057530290033123

Pellegrini, N., Valtuena, S., Ardigo, D., Brighenti, F., Franzini, L., Del Rio, D., et al. (2010). Intake of the plant lignans matairesinol, secoisolariciresinol, pinoresinol, and lariciresinol in relation to vascular inflammation and endothelial dysfunction in middle age-elderly men and post-menopausal women living in Northern Italy. *Nutr. Metab. Cardiovasc. Dis.* 20, 64–71. doi: 10.1016/j.numecd.2009.02.003

Quideau, S., and Ralph, J. (1992). Facile large-scale synthesis of coniferyl, sinapyl, and *p*-coumaryl alcohol. *J. Agr. Food Chem.* 40, 1108–1110. doi: 10.1021/jf00019a003

Quideau, S., and Ralph, J. (1994). A biomimetic route to lignin model compounds *via* silver (I) oxide oxidation. 1. Synthesis of dilignols and non-cyclic benzyl aryl ethers. *Holzforschung* 48, 12–22. doi: 10.1515/hfsg.1994.48.1.12

Ralph, J., Brunow, G., Harris, P. J., Dixon, R. A., Schatz, P. F., and Boerjan, W. (2008). "Lignification: Are lignins biosynthesized via simple combinatorial chemistry or via proteinaceous control and template replication?," in *Recent Advances in Polyphenol Research,* eds. F. Daayf, A. El Hadrami, L. Adam, and G.M. Ballance (Oxford: Wiley-Blackwell Publishing), 36–66.

Ralph, J., Helm, R. F., Quideau, S., and Hatfield, R. D. (1992). Lignin-feruloyl ester cross-links in grasses. Part 1. Incorporation of feruloyl esters into coniferyl alcohol dehydrogenation polymers. *J. Chem. Soc. Perkin Trans.* 1, 2961–2969. doi: 10.1039/P19920002961

Ralph, J., Lundquist, K., Brunow, G., Lu, F., Kim, H., Schatz, P. F., et al. (2004). Lignins: natural polymers from oxidative coupling of 4-hydroxyphenylpropanoids. *Phytochem. Rev.* 3, 29–60. doi: 10.1023/B:PHYT.0000047809.65444.a4

Ralph, J., Peng, J. P., Lu, F. C., Hatfield, R. D., and Helm, R. F. (1999). Are lignins optically active? *J. Agr. Food Chem.* 47, 2991–2996. doi: 10.1021/jf9901136

Ralph, S., Landucci, L., and Ralph, J. (2004). *NMR Database of Lignin and Cell Wall Model Compounds*. Available online at: https://www.glbrc.org/databases_and_software/nmrdatabase/

Ricklefs, E., Girhard, M., Koschorreck, K., Smit, M. S., and Urlacher, V. B. (2015). Two-step one-pot synthesis of pinoresinol from eugenol in an enzymatic cascade. *Chemcatchem* 7, 1857–1864. doi: 10.1002/cctc.201500182

Sajiki, H., Kume, A., Hattori, K., and Hirota, K. (2002). Mild and general procedure for Pd/C-catalyzed hydrodechlorination of aromatic chlorides. *Tetrahedron Lett.* 43, 7247–7250. doi: 10.1016/S0040-4039(02)01622-2

Saliu, F., Tolppa, E. L., Zoia, L., and Orlandi, M. (2011). Horseradish peroxidase catalyzed oxidative cross-coupling reactions: the synthesis of "unnatural" dihydrobenzofuran lignans. *Tetrahedron Lett.* 52, 3856–3860. doi: 10.1016/j.tetlet.2011.05.072

Schroeder, F. C., Del Campo, M. L., Grant, J. B., Weibel, D. B., Smedley, S. R., Bolton, K. L., et al. (2006). Pinoresinol: a lignol of plant origin serving for defense in a caterpillar. *Proc. Natl. Acad. Sci. U.S.A.* 103, 15497–15501. doi: 10.1073/pnas.0605921103

Self, M. F., Pennington, W. T., and Robinson, G. H. (1990). Reaction of diisobutylaluminum hydride with a macrocyclic tetradentate secondary amine–synthesis and molecular-structure of [Al(I-Bu)]2[C10h20n4][Al(I-Bu)3]2–evidence of an unusual disproportionation of (I-Bu)2alh. *Inorg. Chim. Acta* 175, 151–153. doi: 10.1016/S0020-1693(00)84819-7

Sih, C. J., Ravikumar, P. R., Huang, F. C., Buckner, C., and Whitlock, H. Jr. (1976). Letter: Isolation and synthesis of pinoresinol diglucoside, a major antihypertensive principle of Tu-Chung (*Eucommia ulmoides*, Oliver). *J. Am. Chem. Soc.* 98, 5412–5413. doi: 10.1021/ja00433a070

Suzuki, S., and Umezawa, T. (2007). Biosynthesis of lignans and norlignans. *J. Wood Sci.* 53, 273–284. doi: 10.1007/s10086-007-0892-x

Tamura, M., Tsuji, Y., Kusunose, T., Okazawa, A., Kamimura, N., Mori, T., et al. (2014). Successful expression of a novel bacterial gene for pinoresinol reductase and its effect on lignan biosynthesis in transgenic Arabidopsis thaliana. *Appl. Microbiol. Biotechnol.* 98, 8165–8177. doi: 10.1007/s00253-014-5934-x

Touchard, F. P. (2004). New and efficient conditions for the Z-selective synthesis of unsaturated esters by the Horner-Wadsworth-Emmons olefination. *Tetrahedron Lett.* 45, 5519–5523. doi: 10.1016/j.tetlet.2004.05.026

Umezawa, T. (2003). Diversity in lignan biosynthesis. *Phytochem. Rev.* 2, 371–390. doi: 10.1023/B:PHYT.0000045487.02836.32

Vermes, B., Seligmann, O., and Wagner, H. (1991). Synthesis of biologically-active tetrahydro-furofuranlignan-(syringin, pinoresinol)-monoglucosides and bisglucosides. *Phytochemistry* 30, 3087–3089. doi: 10.1016/S0031-9422(00)98258-X

Yue, F., Lu, F., Sun, R., and Ralph, J. (2012b). Synthesis and characterization of new 5-linked pinoresinol lignin models. *Chem. Eur. J.* 18, 16402–16410. doi: 10.1002/chem.201201506

Yue, F., Lu, F., Sun, R.-C., and Ralph, J. (2012a). Syntheses of lignin-derived thioacidolysis monomers and their uses as quantitation standards. *J. Agr. Food Chem.* 60, 922–928. doi: 10.1021/jf204481x

Zhang, L., Henriksson, G., and Gellerstedt, G. (2003). The formation of β-β structures in lignin biosynthesis—are there two different pathways? *Org. Biomol. Chem.* 1, 3621–3624. doi: 10.1039/B306434D

Zhao, C. K., Hu, Z. H., Shi, L. L., Wang, C., Yue, F. X., Li, S. X., et al. (2020). Profiling of the formation of lignin-derived monomers and dimers from *Eucalyptus* alkali lignin. *Green Chem.* 22, 7366–7375. doi: 10.1039/D0GC01658F

Conflict of Interest: The authors declare that the research was conducted in the absence of any commercial or financial relationships that could be construed as a potential conflict of interest.

Advantages of publishing in Frontiers

OPEN ACCESS
Articles are free to read for greatest visibility and readership

FAST PUBLICATION
Around 90 days from submission to decision

HIGH QUALITY PEER-REVIEW
Rigorous, collaborative, and constructive peer-review

TRANSPARENT PEER-REVIEW
Editors and reviewers acknowledged by name on published articles

Frontiers
Avenue du Tribunal-Fédéral 34
1005 Lausanne | Switzerland

Visit us: www.frontiersin.org
Contact us: frontiersin.org/about/contact

REPRODUCIBILITY OF RESEARCH
Support open data and methods to enhance research reproducibility

DIGITAL PUBLISHING
Articles designed for optimal readership across devices

FOLLOW US
@frontiersin

IMPACT METRICS
Advanced article metrics track visibility across digital media

EXTENSIVE PROMOTION
Marketing and promotion of impactful research

LOOP RESEARCH NETWORK
Our network increases your article's readership